Biomineralisation processes in the radula teeth of the chiton *Acanthopleura hirtosa* (Mollusca: Polyplacophora)

This thesis is presented for the degree of Doctor of Philosophy of Murdoch University, Western Australia
2007

Submitted by

Jeremy Albert Shaw, B.Sc. (Hons) Murd.

Murdoch University

I declare that this thesis is my own account of my research and contains, as its main content, work which has not previously been submitted for a degree at any tertiary institution.

Jeremy Albert Shaw
2007

Abstract

A detailed row-by-row investigation of major lateral tooth cusp mineralisation, together with the concomitant development of the superior epithelial tissue surrounding the teeth of the chiton *Acanthopleura hirtosa* has been undertaken using a combination of light microscopy, and scanning and transmission electron microscopy. A holistic approach has been adopted that encompasses observations over a range of spatial scales, from whole radula mineralisation processes to those occurring within individual tooth cusps at various stages of development. In addition, mineralisation in radulae from freshly collected animals has been compared to that of animals maintained for extensive periods within a newly developed iron-limited system, which restricts radula mineralisation without impeding the formation of the organic matrix.

An evaluation of the iron-limitation technique has revealed that maintaining specimens of *A. hirtosa* within an iron-poor environment results in a significant departure from the normal pattern of mineralisation in these animals. As a consequence of iron-limitation, there is an obvious increase in the number of unmineralised tooth rows in addition to associated alterations in structure and composition at all stages of tooth development.

In normal specimens of *A. hirtosa*, the onset of mineralisation in the tooth cusps occurs following the prior accumulation of iron at the junction zone and the sudden accumulation of iron-containing granules in the cusp epithelium at tooth row 13. The superior epithelium surrounding the tooth cusps undergoes a series of developmental changes leading up to, and following, the onset of mineralisation. In particular, the abundance of mitochondria within the apical cusp epithelium increases, presumably in order to provide the ideal conditions of pH, and thus solubility, needed for the supersaturation of iron and its nucleation at row 13. Once mineralisation has commenced, the microvilli attached to the cusps develop rapidly, and are suggested to

do so in order to facilitate the transport of iron, and thereby ensure that a high concentration gradient of this element into the cusps is maintained.

The delivery of iron into the cusps occurs from two fronts, the first from the superior epithelium via the posterior surface, and the second from the junction zone via an internal pathway situated along the lepidocrocite boundary between the magnetite and core regions of the tooth. The existence of a plume of elements between this internal mineralisation pathway and the junction zone, provides the first direct evidence that the junction zone is involved in the storage and release of elements for cusp mineralisation. Data from iron-limited radulae also indicate that iron continues to be deposited at the junction zone in preference to the superior epithelium or cusps, despite the disruption of mineralisation, highlighting the importance of this region in the mineralisation process.

Iron-reinstatement experiments have also shown that the internal pathways of iron delivery within the organic matrix remain viable, despite prolonged periods of iron-limitation. In addition, the reinstatement of iron has revealed that the plumes, situated between the junction zone and internal mineralising pathway of the cusp, stem from the centre of the plate-like junction zone, directly above the stylus canal, a tube-like cavity situated within the styli of each major lateral tooth.

An in-depth study of the stylus canal has revealed that cells within the canal are remarkably similar to those of the epithelium surrounding the cusps, suggesting that this structure may also be involved in the delivery of ions to the junction zone. The stylus canal is shown to be present in the major lateral tooth cusps of 38 chiton species distributed worldwide, and is therefore likely to be a feature common to all chitons. The presence of the canal, and indeed its absence from the bases of all remaining non iron-mineralised teeth, irrespective of chiton species, also points strongly to a functional relationship between the stylus canal and tooth cusp mineralisation.

Table of contents

Acknowledgements

My undergraduate and postgraduate experiences at Murdoch University have acquainted me with many people to whom I owe much for their help and friendship these past eight years. In particular, my PhD candidature has been a wonderful time and I have been fortunate to have been provided with so many rewarding experiences.

These experiences have in large part been due to the incredible support and friendship provided by my supervisors, Associate Professor David Macey, Dr Lesley Brooker and Dr Peta Clode. Their collective expertise, wisdom and above all passion for this research has motivated me more than my clumsy words could ever adequately express. I am also exceedingly grateful for the moral and financial support that they have all provided, which has made it possible for me to attend so many conferences during my candidature.

This commitment was not only undertaken by me but by my family, who have all had to make sacrifices in order for me to complete my studies. To my wife and best friend Nicole, thank you. Without your love, encouragement and patience this would not have been possible. To my daughters Emma and Evelyn, who have both had a student for a Dad since they were born, thank you for your love and for being so good. Also, a huge thank you to my Mum and Dad, Kate and John, and to my mother and father in-law, Kathryn and Ken, for your love and support, and for giving so selflessly of your time to look after the kids on so many occasions.

I must make special mention of my friend Garth Maker, who I have had the privilege of knowing for my entire university career and without whom I would no doubt have ever considered the path I have taken. My many thanks and best wishes. I was also incredibly fortunate in having had the opportunity to work with Professor Kenji Okoshi and his wife Dr Waka Okoshi, who both came to Perth from Japan in

2005. I owe many thanks to Kenji for his advice and guidance during his stay, which I will always fondly remember.

It has been my pleasure and privilege to work in this field with a number of professional colleagues, including Professor John Webb and Dr Alasdair Lee, whom I thank for their expertise, advice and friendship. I have also benefited from the technical and moral support provided by Gordon Thompson, Peter Fallon, Edd Stockdale, Rachel Binks and Richard Webb, who have assisted with various histological aspects of this thesis.

A number of individuals have also assisted at various times over the past three years, including my friend Mark Maddern, who helped to collect samples, Steven Goynich, Philip Good, Guiseppe Paccani, David Tunbridge, Claudia Mueller, Michael Taylor and Keith Brooker from Environmental Sciences and Biological Sciences at Murdoch University, John Murphy, Steve Parry and Guy Ben-Ary at the University of Western Australia and James and Renee Hockridge at the CSIRO.

This research was partially funded by an Australian Research Council Large Grant (# DP0559858). Many aspects of this study were carried out using facilities at the Centre for Microscopy and Microanalysis/Biomedical Image and Analysis Facility, The University of Western Australia, which are supported by University, State and Federal Government funding. We also acknowledge the technical, scientific and financial assistance from the NANO-MNRF. I am very grateful for the financial support provided in the form of an Australian Postgraduate Award Scholarship from Murdoch University. Financial support was also provided my Murdoch University for my attendance at the 9th International Symposium on Biomineralization, Pucon, Chile in 2005 and by the American Malacological Society (AMS) for attending the Joint Meeting of the AMS and Western Society of Malacologists, Seattle, USA in 2006. Student bursaries were obtained for attending the 2004 and 2006 Joint Meetings of the Western Australian Society for Electron Microscopy and Australian X-ray Analytical Association.

Chapter 1

General Introduction

1.1. Mollusca: Polyplacophora

1.1.1. *Chiton distribution*

Approximately 750 living species of chiton are known, with the class being well represented in the fossil record since the late Cambrian (Gowlett-Holmes, 1998; Kaas and Jones, 1998). Most species can be found grazing upon hard substrata in intertidal and subtidal regions of coastlines around the world (Figure 1.1), although a number of species can be found at depths of up to 8000 m (see for example: Ferreira, 1979; Eernisse *et al*., 1988; Saito and Okutani, 1990; Kaas and Jones, 1998). While chitons are mainly found on hard substrata, there are species that have adapted to living epiphytically on seagrasses, interstitially within sand, in the crypts of sponges and around hydrothermal vents (Saito and Okutani, 1990; Kaas and Jones, 1998).

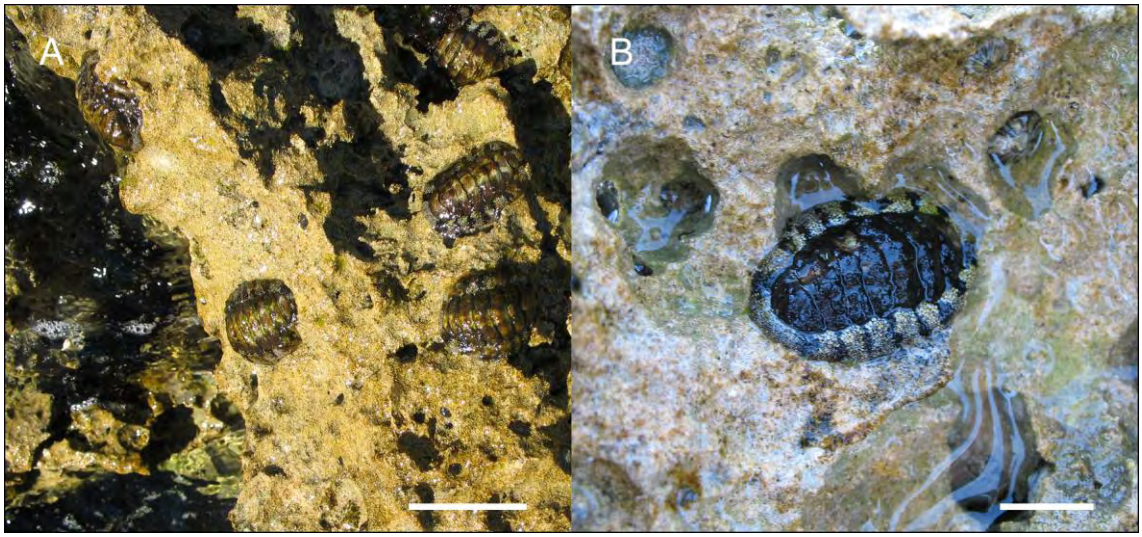

Figure 1.1. Specimens of the chiton *Acanthopleura hirtosa* living on hard limestone substrate within the mid-upper intertidal region at Woodman Point in the Perth metropolitan region in Western Australia.

Scale bars = (A) 5 cm and (B) 2 cm.

1.1.2. *Chiton anatomy*

Chitons are bilaterally symmetrical, dorso-ventrally flattened molluscs characterised by a series of eight dorsal, articulating shell plates (valves) that are embedded, to varying degrees, in a fleshy, muscular girdle (Kaas and Jones, 1998) (Figure 1.2). On the ventral surface, a simple head, without eyes or tentacles, is situated anteriorly to a large foot, which is separated laterally from the girdle by narrow pallial grooves that contain the gills (ctenidia). Chitons typically range in length from a few millimetres to 100 mm (Kaas and Jones, 1998), although the largest species, *Cryptochiton stelleri*, can reach lengths of up to 330 mm (Harbo, 2001).

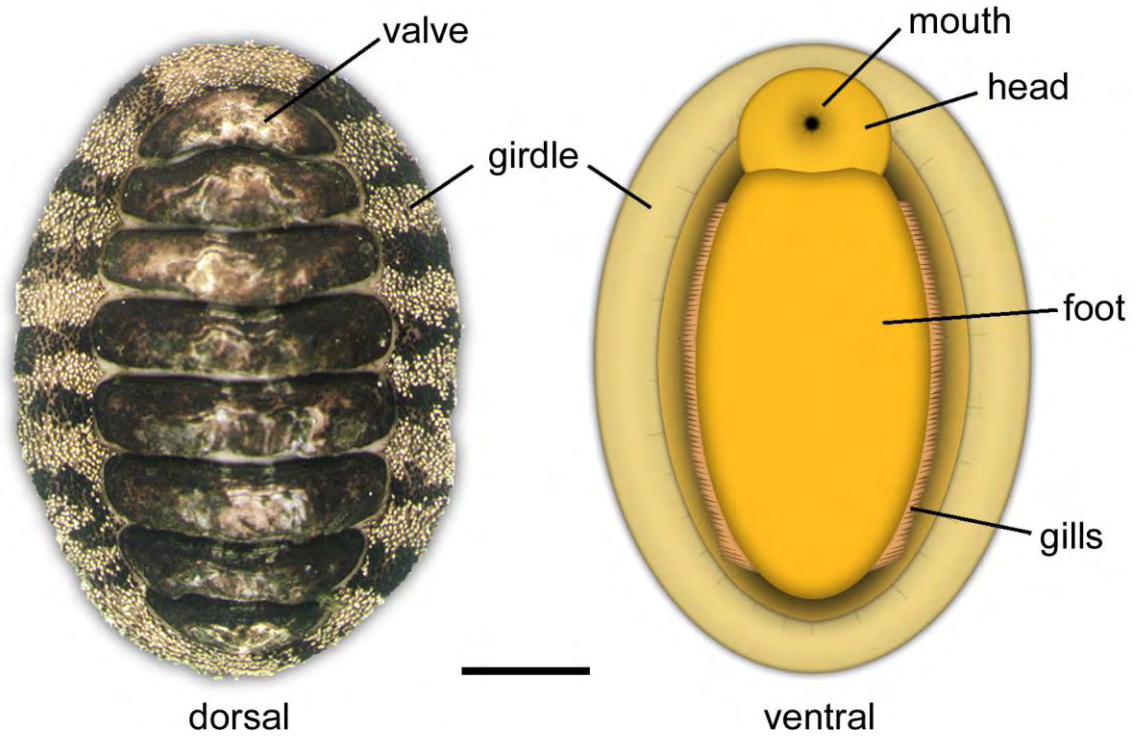

Figure 1.2. Light micrograph of the dorsal surface of the chiton *A. hirtosa* (left) and a diagrammatic representation of the ventral surface (right) highlighting the overall body plan of the Polyplacophora. Scale bar = 1 cm.

1.1.3. *Chiton diets*

Over the past two decades there have been a number of studies of Polyplacophoran diets (Steneck and Watling, 1982; Langer, 1983; Nishihama *et al*., 1986; Piercy, 1987; Black *et al*., 1988; Putman, 1990). Kaas and Jones (1998) describe most chitons as being generalist grazers on hard substrata, consuming mainly microflora, algae and small encrusting animals. Algal material seems to be a common dietary preference among chitons, and includes crustose corallines (Bell, 1994), leathery macrophytes (Steneck and Watling, 1982), filamentous algae, microalgae and diatoms (Piercy, 1987). Carnivory has also been observed within the Polyplacophora, with the majority feeding on sedentary animals such as sponges, bryozoans and coelenterates (Kaas and Jones, 1998). In addition, many chiton species have been determined to be omnivorous, supplementing the algal component of their diet with animal material such as worms, amphipods, barnacles, gastropods and bivalves (Nishihama *et al*., 1986; Piercy, 1987). It has been shown that the consumption of both plant and animal food types is often a selective process, although some incidental or opportunistic uptake of non-specific food items may also occur (Putman, 1990; Bell, 1994).

1.1.4. *The chiton radula*

The dietary diversity observed in chitons is a result of the flexible nature of the Polyplacophoran radula, which has been described as a "multi-purpose tool" (Steneck and Watling, 1982). In structure, it is considered to have parallels with both the excavating attributes of the docoglossan (limpet) radula, and the less abrasive motions of the rhipidoglossan radula with its copious, feathery marginal teeth (Steneck and Watling, 1982). In addition, the chiton radula is flexoglossate, which allows these animals to grasp and hold food items, a feature that has been linked to dietary diversity as it can prevent ingested food from moving back towards the mouth during radula retraction (Guralnick and Smith, 1999).

The radula is supported by a number of anatomical components including the odontophore and associated musculature (Figure 1.3). Together, these organs form the major tissue elements of the buccal mass, which lies within an expanded chamber within the head: termed the buccal cavity (Graham, 1973; Boyle, 1977). Lying above the odontophore/radula complex is the oesophagus, which links the buccal cavity to the stomach (Fretter, 1937). The oesophagus is separated from the radula by the radula diverticulum, a mobile structure whose movements help to pass food from the radula teeth into the oesophagus (Graham, 1973). In addition, the diverticulum prevents food from entering the radula sheath (sac) (Graham, 1973).

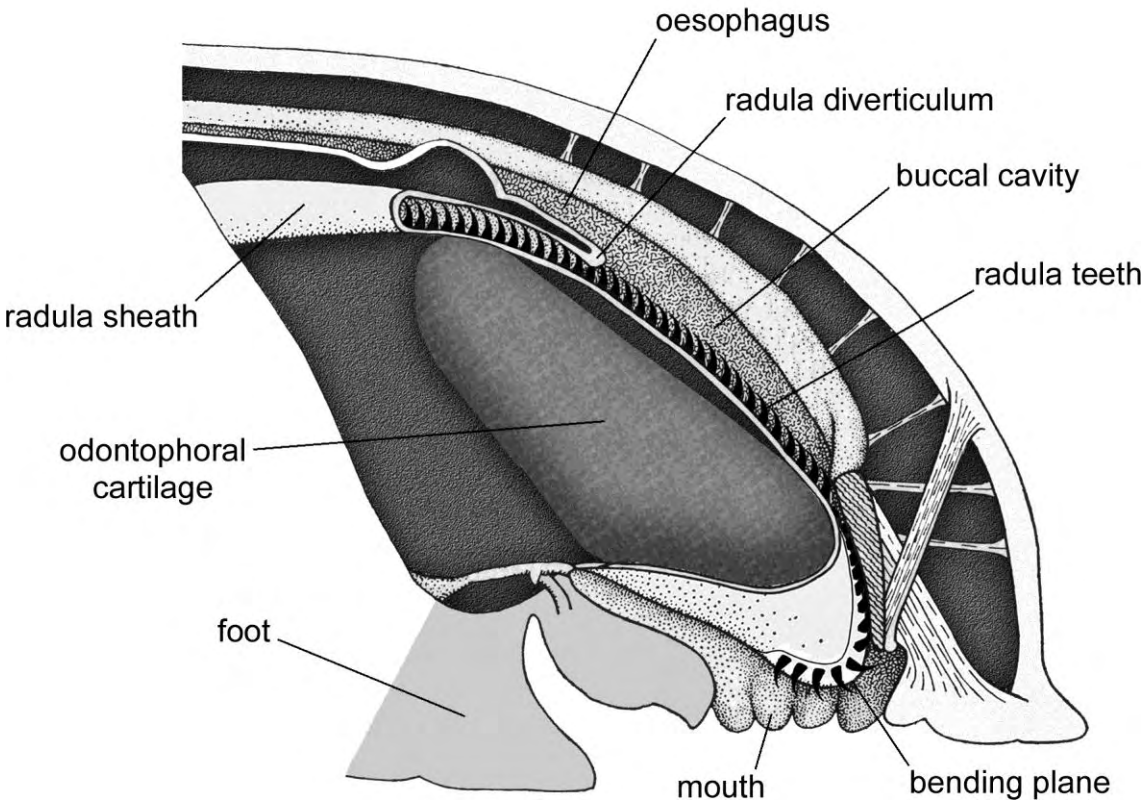

Figure 1.3. Sagittal section through the anterior head and foot of the prosobranch mollusc *Monodonta lineata* outlining the basic anatomy and orientation of the buccal mass, which is of similar configuration to that observed in chitons. (Adapted from Nisbet in Fretter and Graham, 1962).

The chiton radula is composed of a ribbon-like series of morphologically identical transverse tooth rows (Figure 1.4) whose production is achieved via a hemispherical cushion of epithelial cells, termed odontoblasts, and which are situated at the posterior end of the radula sheath (Figure 1.5) (see for example: Nesson, 1969; Nesson and Lowenstam, 1985; Eernisse and Kerth, 1988; Kim *et al*., 1989). Each transverse row is comprised of 17 teeth including a central (rachidian) tooth, which is flanked by lateral teeth with these, in turn, flanked by marginal teeth. In chitons, the prominent single pair of major laterals are the principal teeth that contact the substratum, where they are used to abrade the surface and thereby excavate the algae embedded in the rock. The major lateral teeth consist of a base, shaft (stylus) and cusp (Nesson and Lowenstam, 1985), which may possess from one, to as many as four, denticles (Brooker and Macey, 2001). The styli and bases commonly interlock with those of adjacent tooth rows, acting to distribute and transfer stress from the cutting edge of the major lateral cusps (Solem, 1972; Hickman, 1980), which are hardened with various biominerals during radula development (Figure 1.4).

In all radula bearing molluscs, tooth maturation is controlled by the superior epithelium, the cells of which are intimately attached to the teeth, and move in unison with the teeth at the same rate along the radula (Figure 1.5) (see for example: Fretter and Graham, 1962; Runham, 1963, Isarankura and Runham, 1968; Nesson and Lowenstam, 1985; Kim *et al*., 1989; Rinkevich; 1993; Shaw *et al*., 2002). Once fully mature, the teeth emerge from the superior epithelial tissue and, whilst being supported by the odontophore and radula musculature, are deployed in the feeding process, where they are worn down and eventually discarded (Figure 1.4) (Nesson and Lowenstam, 1985; Bullock, 1989; van der Wal *et al*., 2000). As such, the production and subsequent wear and replacement of the radula is in dynamic equilibrium, where the rate of teeth being produced posteriorly is balanced by the loss of teeth anteriorly as a result of the feeding process (Runham, 1963).

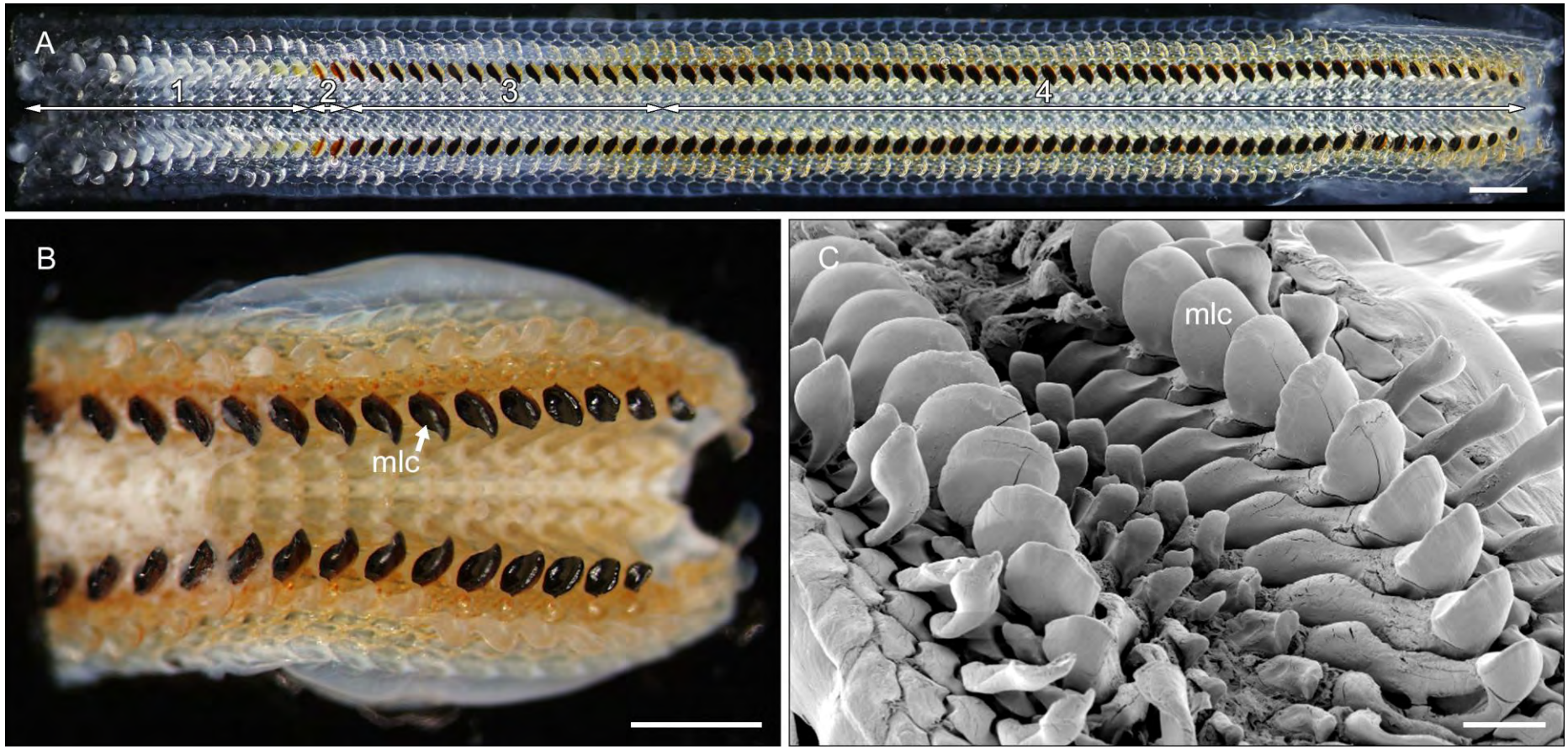

Figure 1.4. Radulae excised from the chiton *A. hirtosa* demonstrating the (A) ribbon-like series of transverse tooth rows, which develop sequentially in stages (1 – 4) from posterior to anterior (left to right). Once fully mature (B and C) the prominent major lateral cusps (mlc) become worn and abraded as a result of the feeding process. Scale bars = (A and B) 500 μm, (C) 200 μm.

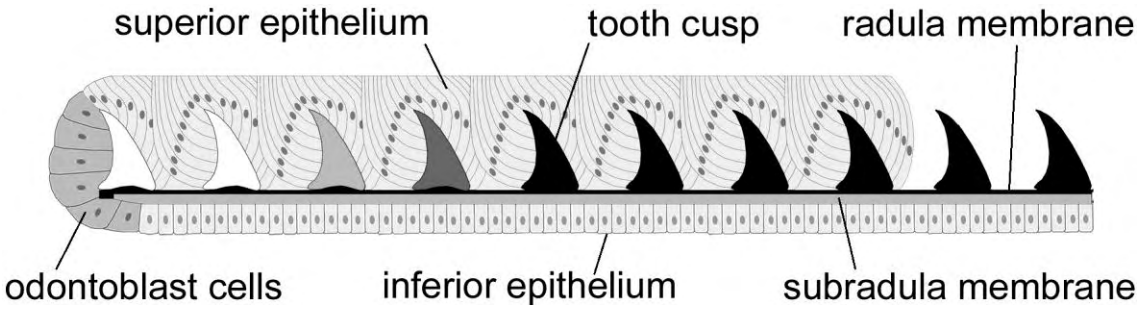

Figure 1.5. Diagrammatic representation of the radula sheath and the various tissue components responsible for radula production and development.

In flexoglossate radulae, such as is present in chitons, the teeth flex outwards laterally as they are pulled past the bending plane (Figure 1.3) during radula protraction, and then sweep inwards during retraction (Salvini-Plawen, 1988; Ponder and Lindberg, 1997). This action is made possible due to mechanical restrictions imposed by the flexible, but inelastic, subradula membrane, and its close association with the odontophoral cartilages (Guralnick and Smith, 1999). The end result is a feeding stroke that resembles a zipper-like licking motion as the radula teeth are protracted and retracted back and forth across the bending plane.

The feeding stroke is orchestrated by four main muscle groups, the odontophoral protractors and retractors, and the radula protractors and retractors (Figure 1.6) (Graham, 1973). These two pairs of antagonistic muscles, which possess a deep red colouration due to the presence of myoglobin (Manwell, 1958; Tergwilliger and Read, 1970; Smith *et al*., 1988), coordinate to achieve two main functions during the feeding process. Firstly, the gross forward and backward motion of the odontophore as a whole, and secondly, superimposed upon this, the protraction and retraction of the subradula membrane and hence the radula teeth. The radula retractor muscles are the largest and most powerful, as they are responsible for pulling the radula teeth against the hard substrate during feeding (Graham, 1973).

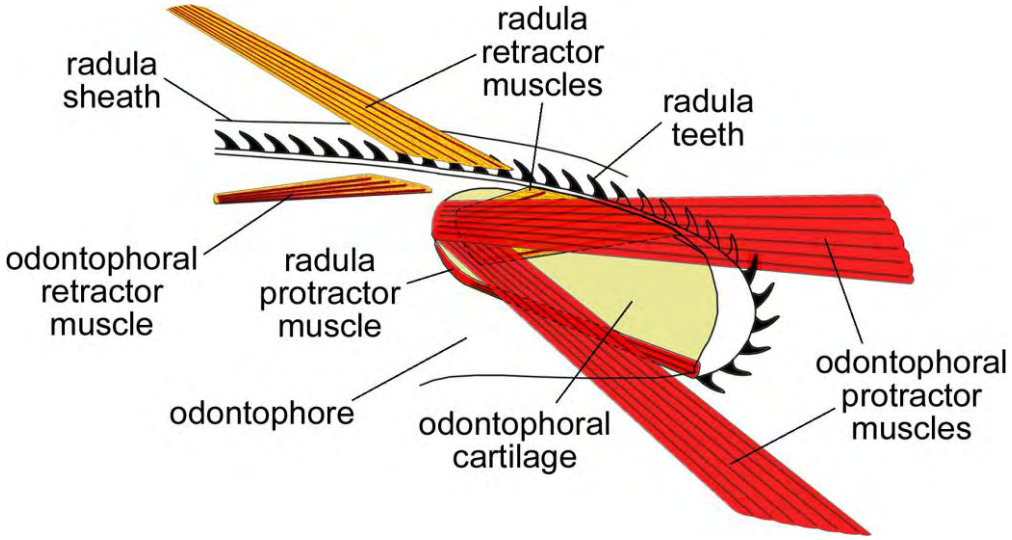

Figure 1.6. Diagrammatic representation of the major muscle groups of the molluscan buccal mass. Muscles displayed in red are responsible for protraction, and those in yellow for retraction, of the odontophore and radula.

1.2. Principals and processes of biomineralisation

Biomineralisation can be defined as the process by which inorganic solids are formed and deposited in biological systems (Mann, 2001). These biominerals often allow exploitation of specific ecological niches. Some of the more commonly recognised biomineralised structures include the vertebrate skeleton, mollusc shell and arthropod cuticle. In these instances, biomineralisation provides a robust framework for muscle attachment, which is fundamental to movement, and, in the case of molluscs and arthropods, it also provides protection from predation and adverse environmental conditions. While the biomineralisation strategy is used to great effect for movement and protection by a wide range of organisms, it is also employed for a range of other applications, such as reproduction, buoyancy, directional orientation, storage and feeding (Mann and Weiner, 1999; Mann, 2001).

Many biomineralisation processes occur under strict cellular control, where chemical conditions within the tissues can be regulated to create suitable environments for mineral precipitation (Mann, 2001). This may involve the synthesis of lipid or proteinaceous vesicles within the cell, which in turn form specialised intracellular

compartments with microenvironments suited for mineral deposition. A classic example of this so-called boundary-organised biomineralisation process is provided by magnetotactic bacteria, which precipitate chains of nano-sized magnetite crystals within specialised compartments termed magnetosomes (Scheffel *et al*., 2006). The magnetosomes are in turn anchored to the cytoskeleton by protein filaments in order to provide the maximum possible magnetic moment, thereby enabling the bacteria to navigate along the Earth's magnetic field (Scheffel *et al*., 2006).

However, this form of intracellular boundary-organised mineralisation is generally not conducive to the synthesis of large composite structures, such as teeth, shells or bone (Mann, 2001). For these purposes, organisms create an elaborate extracellular framework called the organic matrix, which provides the functional template for the fabrication of complex biomineralised structures. The organic matrix is a complex macromolecular scaffold comprised of both soluble and insoluble proteins and polysaccharides, which act in concert with the surrounding tissues to control extracellular biomineralisation (Addadi and Weiner, 1989; Lowenstam and Weiner, 1989; Simkiss and Wilbur, 1989; Weiner and Dove, 2003). The matrix provides the precise spatial delineation needed for the control of mineral deposition and the overall framework for growth of the final mineralised structure (Mann, 2001). Chemical control over biomineralisation is governed by both the cells surrounding the matrix and the matrix itself, which act to regulate the solution chemistry within the extracellular mineralising compartment (Mann, 2001). This includes factors such as pH, the solubility and supersaturation of inorganic salts and the presence of crystal inhibitors, all of which are crucial for creating favourable thermodynamic conditions for subsequent nucleation and the control of crystal growth.

The organic matrix provides a substrate that is chemically and structurally conducive to the control of heterogeneous nucleation (Mann, 2001). A two-component

model for the composition of the matrix has been proposed, which includes both hydrophobic framework macromolecules and hydrophilic acidic macromolecules, the later of which act as the nucleation surfaces for biomineralisation (Mann, 2001). The organic matrix also exerts some control over the initial orientation of nucleation and crystal growth (epitaxy) through structural matching at the inorganic-organic interface (Mann, 2001). However, nucleation and subsequent crystal growth are highly dependent on the degree of supersaturation of the mineralising ions within the extracellular compartment, which is, in turn, regulated by ion transport from the tissues and factors, such as pH and solubility, as outlined above. Importantly, the combined control exerted by cellular and matrix-mediated processes makes it possible for the organism to form specific mineral polymorphs. For example, calcium carbonate may be deposited as either aragonite or calcite in mollusc shell (Lowenstam and Weiner, 1989), or the iron oxides magnetite and lepidocrocite deposited in chiton teeth (Webb *et al*., 1989). In addition, the final mineral may arise from an initial amorphous precursor phase, such as in the formation of sea urchin spines, where calcite forms from an amorphous calcium carbonate intermediate (Politi *et al*., 2004). A similar amorphous precursor has also been proposed for shell formation in molluscs (Addadi *et al*., 2006).

1.3. Biomineralisation in chiton radulae

Chitons are able to significantly extend the working life of their major lateral teeth through the incorporation of various iron and calcium biominerals into the tooth cusps. In particular, the teeth are impregnated with the iron oxide magnetite, which, due to its extreme hardness, allows them to use their teeth for excavating and extracting the endolithic component of the substrate upon which they graze (Towe and Lowenstam, 1967; Lowenstam, 1967; Lowenstam and Weiner, 1989; Webb *et al*., 1989). It is this tooth mineralisation process, and in particular the formation of iron biominerals in the major lateral teeth, that is the major focus of this thesis.

Confirmation of the existence of biogenic magnetite (Fe_3O_4) and goethite (α-FeOOH) was first reported in chitons and patellid limpets respectively by Lowenstam (1962a; 1962b). Since this time, the radulae of these two mollusc groups have been studied extensively, providing valuable insights into many fundamental processes and mechanisms of biomineralisation. In both chitons and limpets, the various biominerals are formed upon an extracellular framework or organic matrix, which is composed of the support polysaccharide α-chitin (Evans *et al*., 1990; Liddiard *et al*., 2004). Thus, the iron mineralised teeth of these molluscs represent a classic example of matrix-mediated biomineralisation. In addition, as the radula is comprised of a sequential series of morphologically identical tooth rows at various stages of mineral development, it is possible to observe the entire process of biomineralisation in a single animal (Webb *et al*., 2001).

Although magnetite is the principal mineral found at the posterior cutting surface of major lateral teeth (Figure 1.7), other ferric oxide biominerals have also been found, including goethite and lepidocrocite (β-FeOOH) (Brooker *et al*., 2002), which have been suggested to be formed by phase transformation of ferrihydrite ($5Fe_2O_3{\cdot}9H_2O$) (Towe and Lowenstam, 1967; Mann, 2001). Maghemite (γ-Fe_2O_3) has also been reported (St Pierre *et al*., 1992), although its presence at the anterior end of the radula suggests that it may be formed by oxidative processes upon exposure of the teeth to seawater (Brooker *et al*., 2002). Advances have been made in determining the range of mineral types formed by these organisms, and their structural organisation within the cusps, using a range of techniques. For example, the use of Mössbauer spectroscopy and, in particular, *in situ* Raman spectroscopy have both proven useful for determining the mineral phases present in chiton and limpet teeth (see for example: St Pierre *et al*., 1986; Lee *et al*., 1998; Lee *et al*., 2003a; Lee *et al*., 2003b).

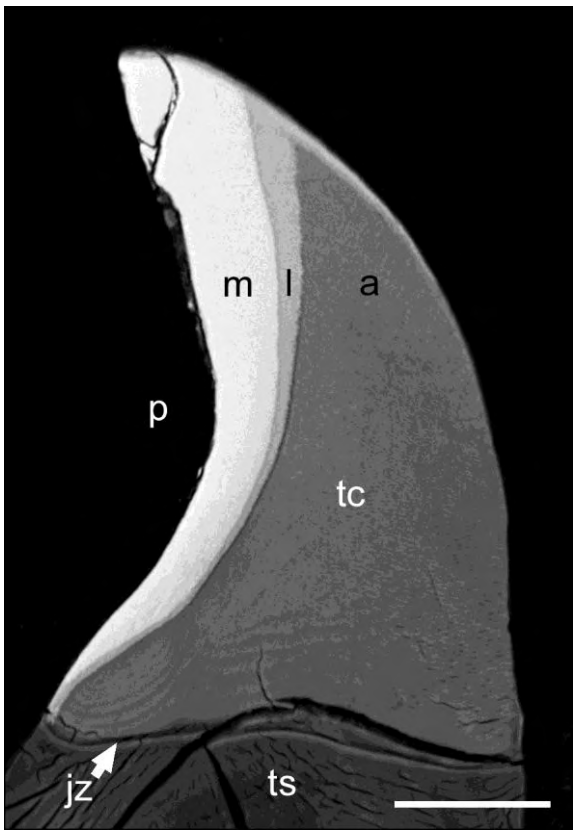

Figure 1.7. Back-scattered scanning electron micrograph of a major lateral tooth from the chiton *A. hirtosa* in sagittal section, highlighting the overall structure including the tooth base or stylus (ts), junction zone (jz) and tooth cusp (tc). In addition, the cusp is further divided into distinct mineral regions, which for *A. hirtosa* include magnetite (m), lepidocrocite (l) and apatite (a). p = posterior surface. Scale bar = 50 μm.

Chitons are conventionally described as exhibiting two broad mineralisation strategies with respect to the type and compositional arrangement of minerals within the major lateral tooth cusps (see for example: Lowenstam and Weiner, 1989; Brooker and Macey, 2001; Numako *et al*., 2006). In one strategy (henceforth referred to as strategy A), magnetite completely encloses the tooth core (typified by the genera *Cryptochiton* and *Cryptoplax*), while in the other strategy (henceforth referred to as strategy B), magnetite is primarily limited to the posterior surface of the cusps (typified by the

family Chitonidae) (Figure 1.8). In a number of genera exhibiting strategy B, magnetite also appears at the anterior tip of the cusp in the form of a distinct tab that is contiguous with the magnetite on the posterior surface, and is thought to contribute towards minimising tooth wear on the anterior surface (Lowenstam, 1967; Bullock, 1989; Brooker and Macey, 2001). In addition to the extent of magnetite coverage, differences also exist in the type of minerals formed within the tooth's core for each mineralisation strategy. The core of strategy A type teeth has been reported to contain amorphous hydrous ferric phosphate (Lowenstam, 1972; Lowenstam and Weiner, 1989), while the core of strategy B type teeth is bordered by a layer of lepidocrocite and contains various calcium phosphate mineral types, which may include either francolite ($Ca_5(PO_4)_3F$) (Lowenstam, 1967), dahllite ($Ca_5(PO_4,CO_3)_3OH$) (Lowenstam and Weiner, 1989), crystalline carbonated apatite (Lee *et al*., 2000) or carbonate and fluoride substituted apatite, as in *A. hirtosa* (Figure 1.8) (Evans *et al*., 1992; Lee *et al*., 1998).

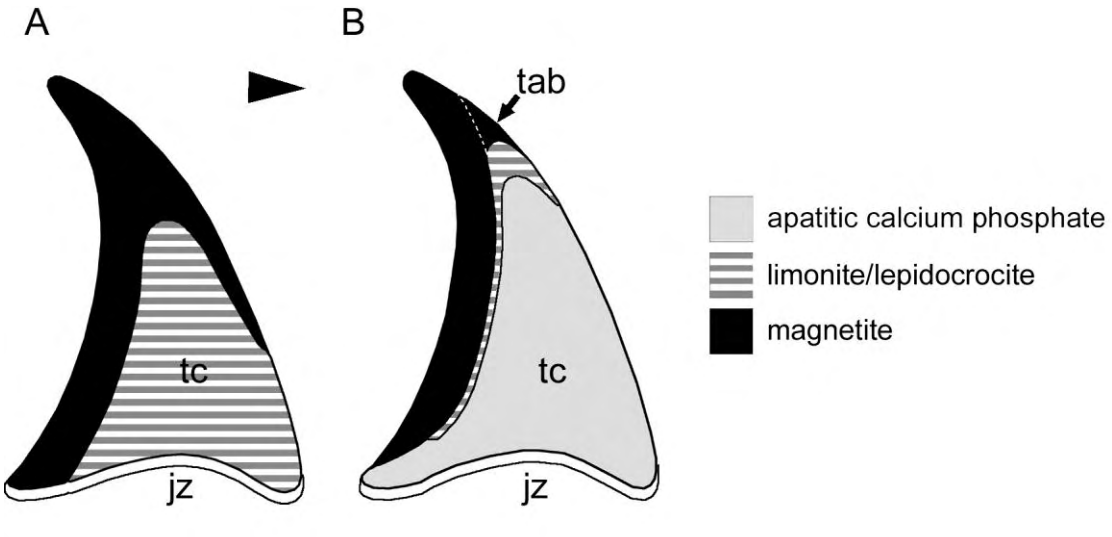

Figure 1.8. Diagrammatic representation of the general structure and composition of lateral teeth from (A) *Cryptochiton* and *Cryptoplax* and (B) Chitonidae (represented here by *A. hirtosa*) radulae. jz = junction zone, tc = tooth core. Arrowhead denotes anterior direction.

Recently however, new findings suggest that the two strategy model for core mineralisation may be far too generalised. For example, in the chiton *Plaxiphora albida*, which exhibits strategy A, a layer of the hydrated iron(III) oxide limonite has been described as separating the magnetite and core regions of the tooth (Lee *et al*., 2003a). In addition, the phosphorus within the core of this, and a number of other species, is not associated with a separate iron phosphate mineral as has been suggested previously (Lowenstam, 1972; Lowenstam and Rossman, 1975), and instead, the core contains a combination of limonite and lepidocrocite or apatite (Lee *et al*., 2003a; Lee *et al*., 2003b; Brooker *et al*., 2006b). It is therefore evident that further studies are needed to reveal the full extent of the various mineralisation strategies utilised by chitons.

Little is known about the fine structure of the organic matrix upon which the various biominerals are deposited in the teeth of chitons and limpets. In the chitons *Chiton olivaceus* and *A. echinata*, a rod and trough subunit structure, organised into sheets has been described (Figure 1.9) (van der Wal *et al*., 1989; Wealthall *et al*., 2005). Notably, at the border between mineral regions, such as lepidocrocite and apatite, both minerals have been shown to occupy a single subunit (Figure 1.9) (Wealthall *et al*., 2005). This suggests that the deposition of various minerals is not entirely controlled by the physical structure of the organic matrix, rather it is more dependent on the chemical composition of the matrix and/or the chemical environment during the various stages of mineralisation (Wealthall *et al*., 2005). The arrangement of the subunits into sheets appears to provide advantageous properties with respect to tooth wear, as their orientation dictates the fracture planes along which cracks will propagate (Wealthall *et al*., 2005). However, the differences in fine structure observed between unicuspid and tricuspid chiton species suggest that our understanding of cusp microarchitecture is also incomplete (van der Wal *et al*., 2000; Wealthall *et al*., 2005).

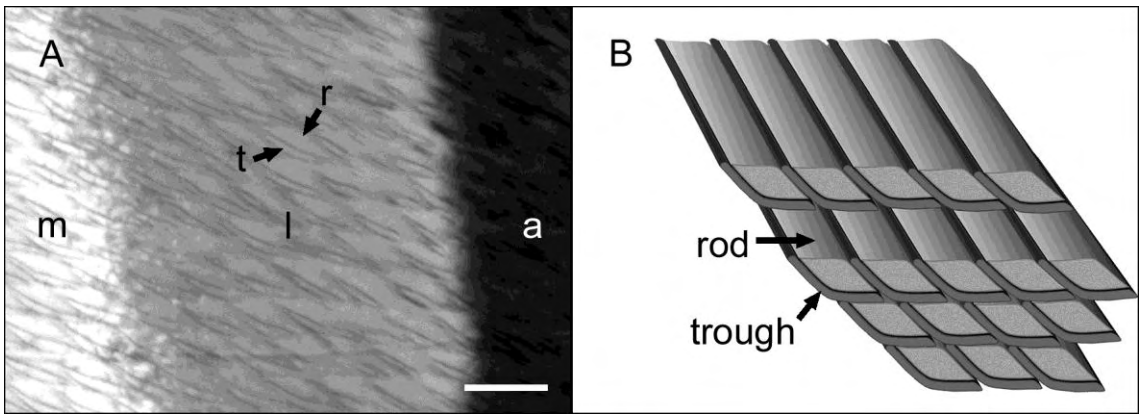

Figure 1.9. Fine structure of the mineralised teeth of the chiton *A. echinata* as observed using (A) back-scattered scanning electron microscopy, where the delineation between magnetite (m), lepidocrocite (l) and apatite (a) boundaries are not dictated by the rod (r) and trough (t) substructure. (B) Diagrammatic representation of the rod and trough system showing the organisation of subunits into sheets. (both images adapted from Weathall *et al*., 2005) Scale bar = 2 μm.

There has been a tendency for researchers to separate the various mineralisation events occurring along the radula into stages (Figure 1.4), which is justified considering the discrete order in which the minerals are deposited. Kirschvink and Lowenstam (1979) assigned four stages of radula development to the chitons *Cryptochiton stelleri* and *Chiton tuberculatus*. Stage 1 describes the newly formed colourless teeth at the posterior end of the radula, which are comprised of only the organic unmineralised tooth framework. In Stage 2 teeth, the colouration changes to reddish-brown, providing the first evidence for the onset of mineralisation. In chitons, this first mineral has been identified as ferrihydrite, which has been suggested to be an amorphous precursor that undergoes subsequent phase transformation to magnetite and the other intermediate iron oxide phases found in the teeth (Kirschvink and Lowenstam, 1979; Kim *et al*., 1989; Mann, 2001). Notably, a similar precursor phase has not been observed in limpets, which appear to precipitate goethite directly onto the organic matrix (Sone *et al*., 2007).

At Stage 3, the teeth take on a black appearance as a result of the phase transformation of ferrihydrite to magnetite, and over subsequent tooth rows (Stage 4), this magnetite layer thickens, and the tooth's core is eventually filled with a variety of other mineral types, which varies depending on the particular species involved.

The practice of assigning stages to the various mineralisation events along the radula has since been applied to studies involving a number of chiton and limpet species (see for example: Burford *et al*., 1986; Mann *et al*., 1986; St Pierre *et al*., 1986; Kim *et al*., 1989; Rinkevich, 1993; Macey *et al*., 1996), and provides an ideal framework upon which to base the linear progression of mineralisation events. However, these, and other subsequent studies, have revealed a number of additional developmental processes occurring along the radula that build on the original description of each stage provided by Kirschvink and Lowenstam (1979). For instance, it has been determined, in both chitons and limpets, that there is an initial influx of iron into the junction zone (Figures 1.7 and 1.8) well before the deposition of mineral at Stage 2, and this region has been proposed as a store of ions for later delivery into the tooth cusps (see for example: Macey and Brooker, 1996; Lee *et al*., 2000; Brooker and Macey, 2001; Brooker *et al*., 2003; Liddiard *et al*., 2004; Cruz and Farina, 2005; Sone *et al*., 2007).

1.4. Iron transport and storage

Iron biominerals are found in virtually all organisms from bacteria through to fungi, plants and animals (see for example: Bazylinski and Frankel, 2004; Scheffel *et al*., 2006; Beinfait, 1987; Eisenstein, 2000), and this derives from the basic need for life to both harness, and contend with, the fourth most abundant element in the Earth's crust (Aisen *et al*., 2001; Turner *et al*., 2001). Iron's ability to easily cycle between its two most common oxidation states, Fe^{2+} and Fe^{3+}, provides the basis for many redox driven reactions in metabolic processes (Allen and Hill, 1982; Aisen *et al*., 2001; Lewin *et al*., 2005). However, iron is also potentially toxic to cells, and so must be maintained in a

biologically available form, while simultaneously being prevented from its natural tendency to react with dioxygen, and thereby generate highly reactive, and highly damaging, hydroxyl radicals (Aisen *et al*., 2001; Lewin *et al*., 2005). As a result of the requirement for iron to be balanced against its potentially toxic effects, organisms have developed a number of specific transport and storage proteins for maintaining iron homeostasis (Sargent *et al*., 2005).

In mammals, iron absorption and transport is mediated by enterocytes within the epithelial layer of the duodenum, the cells of which express a number of proteins involved in the uptake and movement of iron into the body (Figure 1.10) (Trinder *et al*., 2002; Sargent *et al*., 2005). The currently accepted model for cellular iron metabolism involves multiple pathways of iron uptake, including separate routes for ferric (Fe^{3+}) and ferrous (Fe^{2+}) iron (see for example: Conrad *et al*., 2000; Gunshin *et al*., 2001; Mims and Prchal, 2005; Sargent *et al*., 2005). The two major pathways of uptake include the integral membrane transport protein, divalent metal transporter 1 (DMT1), and receptor-mediated endocytosis, which are both responsible for Fe^{2+} uptake into the cell (Figure 1.10).

By far the most work on iron metabolism has been performed on mammals, though many of the conclusions drawn from this group can also be extended to other vertebrate groups and even invertebrates. For example, DMT1 is highly conserved in evolution, with remarkable sequence homology between yeast, plant, fly and mammalian proteins (Cellier *et al*., 1995), and a form of the iron transport protein transferrin has been documented in insects (Locke and Nichol, 1992). In the case of vertebrates, receptor-mediated endocytosis involves the binding of the iron-laden protein transferrin (holo-transferrin) to transferrin receptors on the cell membrane, with the entire complex being subsequently endocytosed within a clathrin coated pit (Mims and Prchal, 2005). Although transferrin has not been documented in chitons, the process of endocytosis has been observed at the endothelial layer of the radula superior

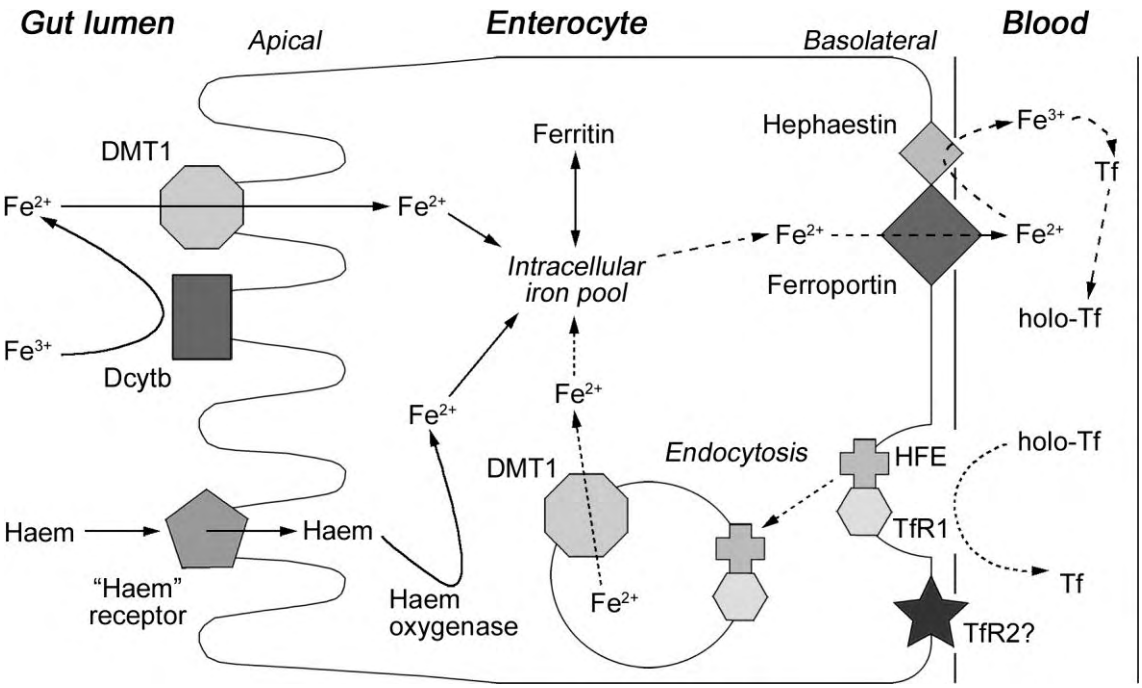

Figure 1.10. The presumptive mammalian model for the complex pathways, proteins and enzymes associated with iron absorption by the enterocyte cells. Non-haem iron within the lumen is reduced to Fe^{2+} by the membrane bound haem protein Dcytb prior to being transported into the cell by divalent metal transporter 1 (DMT1). The transport of haem iron is mediated by a haem receptor; this iron is then released from haem by haem oxygenase. Once inside the enterocyte, ferrous iron enters the intracellular iron pool, where it is either stored as ferritin or transferred out of the cell through the basolateral membrane by ferroportin. Extracellular ferrous iron is then oxidised by haephestin prior to being bound by plasma transferrin (Tf). Iron can return to the enterocyte via receptor-mediated endocytosis, where holo-transferrin (Holo-Tf) binds to the transferrin receptor 1 (TfR1)/haemochromatosis (HFE) protein complex within a clathrin coated pit. Iron within the endocytosed vesicles passes back to the intracellular iron pool via DMT1. A second transferrin receptor (TfR2) of unknown function has also been identified. (adapted from Trinder *et al*., 2002).

epithelium in chitons, where it has been suggested to be involved in the transport of iron to the major lateral teeth (Nesson and Lowenstam, 1985). However, given the importance of iron for the continued mineralisation of their tooth cusps, chitons and limpets are likely to also possess a divalent transport protein similar to DMT1. Once internalised within the cell, iron is either utilised, or stored in the form of the proteins ferritin or haemosiderin (Lewin *et al*., 2005; Sargent *et al*., 2005).

The iron storage and transport protein ferritin is another example of intracellular, boundary-organised biomineralisation, and is suggested to be a crucial precursor to the extracellular matrix-mediated mineralisation within the tooth cusps of chitons and limpets (Towe and Lowenstam, 1967; Nesson and Lowenstam, 1985; Kim *et al*., 1989). The iron-laden protein ferritin, and its iron-free counterpart apoferritin, consists of a spherical polypeptide cage, 2 nm in thickness and 8 nm in internal diameter (Figure 1.11) (Andrews, 1998; Stillman *et al*., 2001; Lewin *et al*., 2005). The protein forms spontaneously from a combination of 24 heavy (H) and light (L) subunits, that together act to bind and rapidly oxidise Fe^{2+}, depositing it within the core as a hydrous ferric oxide mineral (ferrihydrite ($Fe_2O_3{\cdot}nH_2O$)) with variable phosphate content (Lewin *et al*., 2005). Iron passes into the aqueous cavity of the core via molecular channels within the boundary of the protein shell, where it nucleates at the ferroxidase centre on the H-chain subunit prior to being transferred to carboxylate nucleation sites on the interior surface (Mann, 2001; Kidane *et al*., 2006). The mechanisms involved with the release of iron from the core are less well characterised, although recent studies have shown that the release of iron from ferritin is achieved by degradation through lysosomal proteolysis (Kidane *et al*., 2006).

The control of iron homeostasis is regulated at the genetic level by translation and post-translational modification, the latter of which involves iron regulatory proteins (IRPs) and iron responsive elements (IREs), which act to either promote or inhibit the

translation of various transport and storage proteins related to iron metabolism (Sargent *et al*., 2005). As with DMT1, ferritin is also highly conserved in nature, and exists in high concentrations within the hemolymph and radula tissues of chitons and limpets, where it has been proposed to act as an integral part of a high-capacity transport system, delivering large amounts of iron to the rapidly mineralising tooth cusps (Towe and Lowenstam, 1967; Webb and Macey, 1983; Burford *et al*., 1986; Kim *et al*., 1986a; Kim *et al*., 1986b; Webb *et al*., 1986; Kim *et al*., 1988).

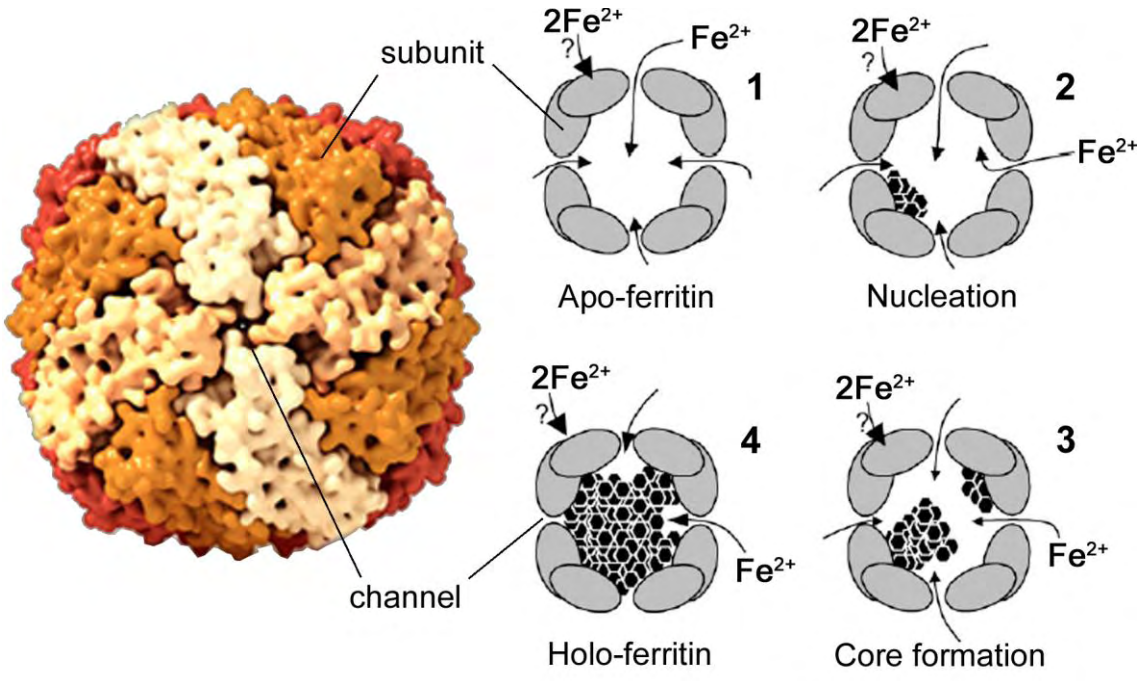

Figure 1.11. The spherical iron storage protein ferritin is composed of 24 individual subunits that form a protein cage that facilitates the nucleation of iron after its passage through molecular channels in the protein shell. Note: Arrows with question marks indicate the possibility of Fe^{2+} binding and oxidation at sites within the protein shell. Image on left adapted from United States National Library of Medicine (2007). Images on right adapted from Lewin *et al*. (2005).

1.5. Justifications

The interest in the developmental processes occurring along the length of chiton and limpet radulae is largely attributed to their ability to mineralise their teeth with a range of specific biogenic minerals. Chiton teeth are of particular interest due to the complex internal architecture of their major lateral cusps, where various minerals are deposited within discrete regions at precise stages of development (see for example: Kirschvink and Lowenstam, 1979; Lowenstam and Weiner, 1989; Kim *et al*., 1989; Macey *et al*., 1996). This exceptional display of control over mineral precipitation across various spatial scales is perhaps the most fascinating aspect of research into biomineralisation, and is epitomised in tooth formation in chitons.

As with all biomineralised structures, chiton teeth have evolved through the processes of random mutation and natural selection (Kirschvink and Hagadorn, 2000), the end result of which is a working and functionally efficient tool. The teeth of chitons exhibit a number of functional adaptations at a range of spatial scales, from the overall arrangement of minerals within the cusps (Figure 1.7) to the rod- and trough-like microarchitecture of the organic matrix (Figure 1.9). The properties of the final composite impart a high degree of mechanical strength and optimal wear characteristics, such that the tooth design has been used as a model for the fabrication of man-made industrial cutting devices (van der Wal *et al*., 2000). In addition, the high levels of iron metabolised by chitons and limpets (Kim *et al*., 1988), without any adverse effect from its toxicity, is of interest to studies related to human iron overload pathologies, such as thalassemia and hemochromatosis (Webb *et al*., 1989).

The study of biomineralisation requires a multidisciplinary approach, including expertise in biology, molecular biology, chemistry and physics, which is a direct result of the complex nature of the materials, and the techniques needed to investigate them. The chiton radula is no exception and, in terms of sample preparation, is perhaps one of the most difficult tissues to study, due to its intricate structure and its association with large amounts of solid material. Most sample preparation methods, whether chemical or

cryogenic, are impeded by the hard mineral deposits within the teeth, which inhibit tissue fixation, embedding and sectioning, making histological investigations incredibly difficult. As such, observations of the tissues surrounding the radula are primarily limited to the immature and early stages of tooth mineralisation (see for example: Nesson and Lowenstam, 1985; Kim *et al*., 1989). However, a number of methods have been developed that permit *in situ* observations of the radula teeth using a variety of analytical tools including light microscopy, scanning and transmission electron microscopy and energy dispersive, Raman and Mössbauer spectroscopy (see for example: Webb *et al*., 1989; Macey and Brooker, 1996; Lee *et al*., 1998).

Biomineralisation is of specific interest to the rapidly developing fields of nanotechnology and biomimetics, which aim to draw upon these biological processes to inspire the production of novel materials (Birchall, 1989). By replicating the processes of biomineralisation, it may be possible to synthesise new materials that are harder, stronger, lighter, resistant to chemical attack or high temperatures, or possess electronic or optical characteristics (Birchall, 1989). As such, the elegant, and yet sophisticated, way in which biology has refined and perfected its control over inorganic crystal growth is of vital importance to the future development of modern materials technologies.

1.6. Aims

Although a great deal is known about the chemical composition and distribution of minerals within the tooth cusps of chitons, both the cellular and matrix-mediated mechanisms involved in the controlled deposition of these minerals remains poorly elucidated. Recently, it was reported that tooth mineralisation in chitons and limpets could be suspended by maintaining animals in an iron-limited system, thus providing an exciting new avenue for further studies in this field (Shaw *et al*., 2005). The ability to selectively and reversibly control the extent of mineralisation in a living tissue offers the potential to answer key questions in regard to the processes of tooth biomineralisation in chitons.

In particular, while a small number of studies have documented the major ultrastructural components of the superior epithelium surrounding the tooth cusps, to date no study has attempted to observe the row-by-row development of this tissue, as it matures during the early stages of cusp mineralisation. In addition, information pertaining to the role of the junction zone in cusp mineralisation is extremely limited. The process whereby ions accumulate in this region, and how they are subsequently transferred to the mineralising fronts within the tooth, is unknown. The existence of the stylus canal (Nesson, 1969; Nesson and Lowenstam, 1985), a cell filled cavity located centrally within the major lateral tooth bases of chitons, provides one possible pathway for the delivery of ions to the junction zone. While the existence of the stylus canal has been recognised (Nesson, 1969; Nesson and Lowenstam, 1985), no attempts have been made to fully resolve its structure or function.

In order to fill these major gaps in our understanding of the tooth mineralisation process, a detailed study on the sequential development of the cusps and superior epithelium of the chiton *A. hirtosa* has been undertaken. After an initial evaluation of the iron-limitation technique first described by Shaw *et al*. (2005), this method has been employed to provide comparative information about radulae from normal animals and those maintained within the iron-limited system.

The aim of this thesis is to focus on fine scale processes at the individual tooth level, and to make observations on the overall processes and pathways of biomineralisation occurring along the radula. Radula development is discussed in the context of maintaining cellular control over the extracellular tooth compartment and the influences of the junction zone and organic matrix over mineral formation. In addition, for the first time, a detailed morphological study documenting the structure of the stylus canal and its associated tissue has been undertaken for the purpose of elucidating its role in the cusp mineralisation process.

Chapter 2

General Methods

2.1. Study site and sample collection

Specimens of the chiton *Acanthopleura hirtosa* were obtained from Woodman Point; an artificial limestone breakwater, situated in Jervoise Bay, within the Perth metropolitan region, on Australia's south-west coast (Lat. 32^{o}S, Long. 116^{o}E) (Figure 2.1). The Perth region experiences a 'Mediterranean' climate, with average air temperatures ranging from 18 to 29^{o}C in summer and 9 to 18^{o}C in winter (DEP, 1996). Water temperatures in the near-shore region of the coast range annually from 16 to 24^{o}C (Pearce *et al*., 1999). The region is within a micro-tidal zone, subject to a diurnal regime with spring tidal amplitudes of less than 1 m (DEP, 1996). The coastline is composed primarily of Tamala limestone, which is predominantly calcarenite with the inclusion of some lateritic materials (McArthur, 1991). Chitons were removed from their home scars by hammering a screwdriver into the substratum near the mantle of each animal. A portion of the substratum to which each animal was attached was then levered free of the rock surface, thereby minimising specimen damage. Once removed, animals were placed in fresh seawater and transported back to the laboratory for further study.

2.2. Dissections

Two dissection methods were employed for observations of the radula and its associated tissues. For the imaging of hard structures, radulae were excised and then cleaned using a fine water jet to remove the surrounding epithelial tissue (Figure 2.2). This method removed epithelial tissues without damage to the mineral or organic matrix and was thus used routinely as a replacement for chemical treatments, such as sodium hypochlorite and potassium hydroxide, which have been used for cleaning radulae in the past (for example see: Bullock, 1989; Rinkevich, 1993; Liddiard *et al*., 2004). Samples were then either observed fresh, or placed in fixative (see Section 2.3) for at least

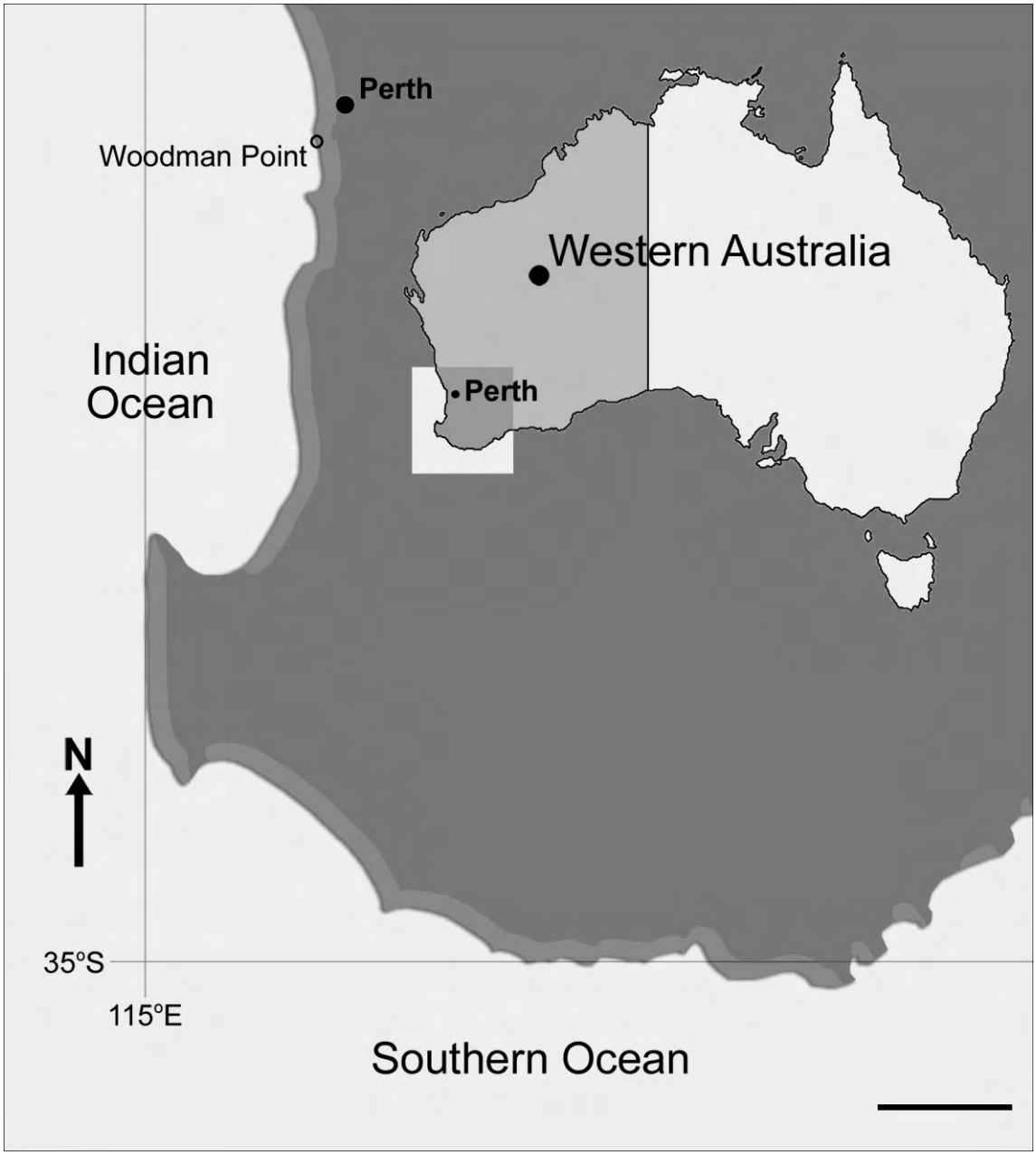

Figure 2.1. Location of the study site used for the collection of specimens of the chiton *A. hirtosa*. Scale bar = 50 km.

24 hours, prior to further processing for light microscopy (LM) or scanning electron microscopy (SEM), otherwise samples were transferred to 70% ethanol for storage. For the study of epithelial and other soft tissues using LM and transmission electron microscopy (TEM), freshly collected specimens were dissected by making incisions along both pallial grooves from the anus towards the head, thereby freeing the foot, visceral mass and buccal mass as a single entity from the shell plates and girdle. The visceral mass was then carefully removed to expose the radula sac, which was immediately bathed in fixative prior to separating the buccal mass, with radula intact, from the remainder of the animal. Radulae and associated tissues were then either fixed whole, or cut transversely into three or four segments, prior to fixation and further treatment.

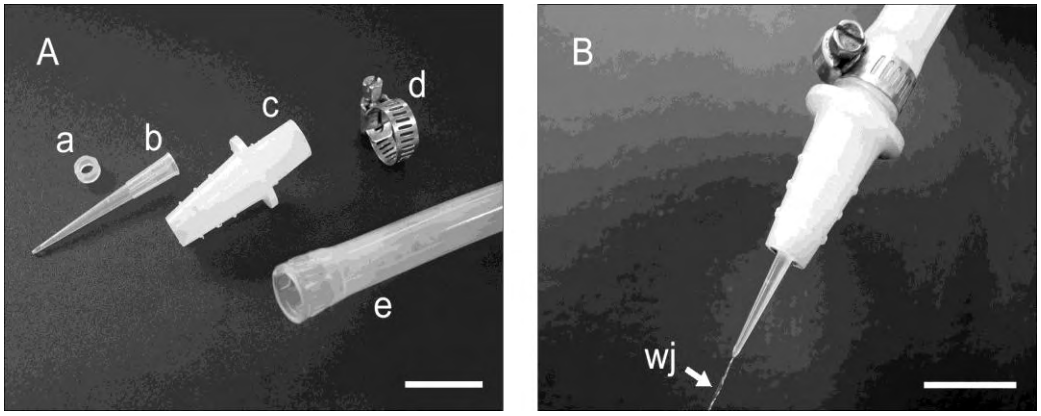

Figure 2.2. Images illustrating the (A) components of the cleaning apparatus and (B) assembled apparatus complete with water jet (wj) used for cleaning superior epithelial tissue from chiton radulae. a = washer, b = micropipette tip (200 μL), c = hose connector, d = hose clip, e = hose. Scale bars = 2 cm.

2.3. Sample preparation for LM and TEM

Both whole radulae and radula sections were fixed using 2.5% glutaraldehyde buffered in 0.1 M phosphate at pH 7.2, and adjusted to an osmolarity of 900 $mmol.kg^{-1}$ using sucrose (buffer A). After primary fixation, samples were rinsed in buffer A, post-fixed in 1% osmium tetroxide (OsO_4) in phosphate buffered saline (buffer B), then rinsed in buffer B before being dehydrated through a graded series of acetones and then infiltrated and embedded in Spurr's resin (Spurr, 1969). Samples were subsequently processed using either a conventional bench top protocol or a microwave oven protocol using a Pelco Biowave® with cold spot and vacuum chamber. A complete listing of processing schedules is given in Tables 2.1 and 2.2. Microwave tissue processing techniques are becoming more common in laboratories worldwide as they reduce processing times and the handling of toxic chemicals (see for example: Giberson and Demaree, 1999; Laboux *et al*., 2004). Note: a code describing the applicable processing method for each image will be present within individual figure descriptions throughout the thesis (CP = conventional protocol, MP = microwave protocol).

Table 2.1. Conventional processing schedules for the radula epithelial tissues of the chiton *A. hirtosa*.

Step	Medium	Concentration %	Conventional times
Fixation	glutaraldehyde (buffer A)	2.5	24 h
Rinse	buffer A		15 min x4
Post-fixation	OsO_4 (buffer B)	1	2 h
Rinse	buffer B		15 min x4
Dehydration	acetone	10, 30, 50, 75, 90, 100	15 min x2 each
Infiltration	Spurr's resin	5, 10, 20, 40, 60, 80, 100	8-12 h each
Polymerisation	Spurr's resin	100	conventional oven 60^{o}C overnight

Note: Spurr's embedding formulation = NSA (13g), ERL4206 (5g), DER (3g) and DMAE (0.2g)

Table 2.2. Microwave processing schedules for the radula epithelial tissues of the chiton *A. hirtosa*.

Step	Medium	Concentration %	Microwave times	Microwave wattage (W)
Fixation	glutaraldehyde (buffer A)	2.5	2x(2 ^{on}/2 ^{off}/2 ^{on}) (min) (v)	80
Rinse	buffer A		40 sec (v)	250
Post-fixation	OsO_4 (buffer B)	1	2x(2 ^{on}/2 ^{off}/2 ^{on}) (min) (v)	80
Rinse	buffer B		40 sec (v)	250
Dehydration	acetone	50, 75, 90, 100	40 sec each (100 x2)	250
Infiltration	Spurr's resin	50, 75, 90, 100	3 min each (100 x2) (v)	250
Polymerisation	Spurr's resin	100	conventional oven 60^{o}C overnight	

(v) = steps under vacuum, $^{on/off}$ denotes magnetron (irradiation) cycle.
Note: Spurr's embedding formulation is as stated in Table 2.1

Following polymerisation, resin blocks were trimmed and sectioned, using either a Sorval JB-4 or Reichert-Jung 2050 microtome, for observations at the LM level, and a Reichert Ultracut E ultramicrotome for observations at the TEM level. Sections were cut to a thickness of ~1 μm and ~100 nm for LM and TEM, respectively. 1% Methylene Blue + 1% Azur II (aqueous) (20 sec) was used for the staining of all LM sections, while double staining with uranyl nitrate (single crystal in one drop of 50% methanol) (10 min) and Sato's lead citrate (10 min) (Hanaichi *et al*., 1986) was used for all TEM sections.

Note that, due to the increasing degree of mineralisation along the radula, it was not possible to obtain information beyond tooth row 18. This is a direct result of cusp mineralisation, which causes chips to form in the glass and diamond knives used for producing sections for LM and TEM.

All experiments conducted during the study comply with the Australian Code of Practice for the Care and Use of Animals for Scientific Purposes - 7th Edition 2004.

2.4. Sample preparation for SEM

Two principle SEM techniques were used for examining the major lateral tooth cusps and styli. The first involved direct imaging and analysis of whole radulae, teeth and tooth fragments using secondary electrons (SE), and the second involved imaging of resin embedded and polished radulae using SE, back-scattered electrons (BS) and energy dispersive X-ray analysis (EDS).

For direct imaging, fixed radulae were dehydrated through a graded series of ethanols followed by amyl acetate, prior to being dried to the critical point of CO_2 (drier made by Balzers Union, Lichtenstein). Radula segments, individual teeth and tooth fragments (the latter two being obtained by dissection of intact radulae) were mounted on aluminium stubs using double-sided carbon tape and coated with 30 nm of gold prior to imaging.

For resin embedded radulae, samples were prepared as described by Macey and Brooker (1996), where radulae were fixed and dehydrated through a graded series of ethanols followed by propylene oxide, and then infiltrated and embedded using Procure-Araldite resin (Table 2.3). After polymerisation, sample blocks were trimmed using a microtome, such that the face of the block was made parallel to longitudinal section along the radula. Samples were then placed in aluminium ring moulds and re-embedded in 100% Procure-Araldite and polymerised. The ring embedded sample blocks were ground using a graded series of silicon carbide papers to 4000 grit to produce sagittal sections through the major lateral teeth along the length of the radula. Ring embedded blocks were then polished with 1 μm diamond paste on a Struers DP-10 polishing wheel, and then coated in 30 nm of carbon for SEM/EDS analysis. Note: To accurately determine the tooth row number and the stages of tooth development, radulae were photographed at the LM level prior to fixation and prior to being carbon coated (Table 2.4, Code B and Code A respectively).

Table 2.3. Processing schedule for hard structures of the radulae in the chiton *A. hirtosa* for imaging and energy dispersive spectroscopy in the scanning electron microscope.

Step	Medium	Concentration %	Times
Fixation	glutaraldehyde (buffer A)	2.5	24 h
Rinse	buffer A		15 min x4
Dehydration	ethanol	10, 30, 50, 75, 90, 100	15 min x2 each
Dehydration	propylene oxide	50, 100	15 min, 15 min x2
Infiltration	Procure-Araldite	5, 10, 20, 40, 80, 100	8-12 h each
Polymerisation	Procure-Araldite	100	60^{o}C overnight

Note: Procure-Araldite embedding formulation = Procure 812 (12.5g), Araldite 502 (10g), DDSA (27.5g) and BDMA (1.25g)

2.5. Microscopy

Due to changes in the availability of instrumentation, a range of dissecting and compound LM's, TEM's and SEM's were utilised during the course of the study (Tables 2.4 and 2.5). The microscope code given here for each instrument is provided either in text or within individual figure descriptions for LM and EM micrographs throughout the thesis. In addition, for many LM and SEM images, a series of micrographs were taken at high magnification and assembled digitally to produce a single composite image. Any composite images are denoted within the respective figure captions in each Chapter.

All qualitative elemental analyses were performed on a Zeiss 1555 (VP-FESEM) (Table 2.5, code H). The EDS system was calibrated with a copper standard prior to sample analysis, and at least 2 hourly thereafter. This system allows for the analysis of elements with an atomic number greater than 4, from within a sample volume approximating a 2 μm sphere.

Table 2.4. Optical and transmission electron microscope manufacturers, together with the code allowing figure identification, parameters and camera systems employed for the study of radula material from the chiton *A. hirtosa*.

Microscope type	Code	Manufacturer	Model	Operating voltage (keV)	Camera system
Optical dissecting	A	Olympus	SZH10	n/a	Olympus DP10 digital
Optical compound	B	Olympus	BX51	n/a	Olympus DP70 digital
TEM	C	Philips	CM100	80	Plate film
	D	JEOL	2000FX	80	Plate film
	E	JEOL	3000F-FEG	300	CCD digital

n/a = not applicable

Table 2.5. Scanning electron microscope manufacturers, parameters and analytical systems employed for the study of radula material from the chiton *A. hirtosa*.

Microscope type	Code	Manufacturer	Model	Operating voltage (keV)	Beam current (nA)	Working distance (mm)	Analytical system	Detector type
SEM	F	Philips	XL20	10	n/a	variable	n/a	Be window
	G	JEOL	6400	15	n/a	variable	n/a	Be window
	H	Zeiss	1555 VP-FESEM	20*	1	16*	Oxford Instruments INCAx-sight	Thin window

* Denotes values used during elemental analysis, otherwise variable. n/a = not applicable

Chapter 3

Iron-limited radula development

3.1. Introduction

Chitons rely on the continued production of new teeth to replace those worn away whilst feeding, and as such, there is a continual requirement for the elements involved in radula mineralisation (Nesson and Lowenstam, 1985; Shaw *et al*., 2002). The chiton *Acanthopleura hirtosa* has a radula production rate of 0.40 tooth rows.day^{-1} and thus requires ~3 μg of iron on a daily basis in order to continuously mineralise its teeth (see Appendix A). The formation of biominerals within the radula teeth of chitons is a highly complex and ordered process, occurring as a well defined series of depositional events (see for example: Kirschvink and Lowenstam, 1979; Kim *et al*., 1989). Although the distribution, and type, of minerals formed varies between species (Lee *et al*., 2003b; Brooker *et al*., 2006b), there is a high degree of uniformity exhibited within species (Nesson and Lowenstam, 1985; Brooker and Macey, 2001). In addition, the rate of radula formation also appears to be under strict control, with the rate of synthesis being maintained within a very limited range for any given species (see for example: Isarankura and Runham, 1968; Nesson, 1969; Padilla *et al*., 1996; Shaw *et al*., 2002).

This obligate requirement for mineral precursors for radula synthesis, and iron in particular, is likely to be met through the consumption of organic material such as algae and small microorganisms (Carefoot, 1965; Marigomez *et al*., 2002). In addition, iron may be extracted from the substrate, which can also form a significant fraction of a chiton's total dietary intake, as evidenced by the large quantities of inorganic material found in the faecal pellets of many species (Langer, 1983; Black *et al*., 1988; Macey *et al*., 1996). Tooth recycling and the direct uptake of iron from seawater have also been proposed as possible sources of iron for mineralisation (Nesson, 1969; Marigomez *et al*., 2002; Shaw, 2003). However, no study has thus far isolated which of the above

sources is the most utilised, and this remains a fundamental question with respect to chiton biology.

Following uptake, iron is contained within the major iron storage proteins ferritin and haemosiderin, which can be found within various tissues in the body (Towe and Lowenstam, 1967; Webb and Macey, 1983; Kim *et al*., 1986a; Kim *et al*., 1988). Aside from the radula and its associated tissues, the highest concentration of iron can be found within the hemolymph, with the chiton *A. hirtosa* possessing as much as 10 mg Fe/100 ml (~0.01% plasma iron by weight) (Webb and Macey, 1983), chiefly in the form of ferritin, suggesting that the hemolymph is the major route by which iron is transported around the body. While the concentrations of iron in major organs, such as the anterior and posterior intestine, hepatopancreas, stomach and gonad, are lower than that found in the blood, these tissues also contribute to the animals available iron pool (Kim *et al*., 1988). In the short term, these significant reserves of ferritin and haemosiderin provide an uninterrupted supply of iron to the radula tissue, which is ultimately responsible for iron delivery to the developing major lateral tooth cusps.

The practice of manipulating trace element availability is commonly used for determining metabolic function in animals, plants and bacteria (see for example: Russell-Hunter and Aldridge, 1983; Papathanassiou and King, 1984; Lane, 1986; Trivier and Courcol, 1996; Morse *et al*., 1999; Dupic *et al*., 2002). As iron is of primary importance to the maturation of the major lateral teeth in chitons, limiting the availability of this element is likely to disrupt the highly organised pattern of development expressed along the radula, which may allow aspects of the mineralisation process to be elucidated.

This study reports on the effects of iron-limitation on overall radula formation and mineralisation in the chiton *A. hirtosa*, with the aim of presenting a new technique for the study of biomineralisation in chitons.

3.2. Materials and methods

A total of 30 adult specimens (determined by size) of *A. hirtosa* were collected as outlined in Chapter 2.1 and were then plunged into fresh 4^{o}C seawater for a period of 48 hours. This cold-shock procedure can be used to determine radula production rates, since it creates a constriction anomaly in the developing radula, which progresses anteriorly due to the production of new radula material, and can be visualised and subsequently tracked following dissection (Isarankura and Runham, 1968; Shaw *et al*., 2002).

To observe the effects of iron-limitation on radula development, cold-shocked animals were placed in a 60 L aquarium divided into 1 'rock' and 1 'glass' treatment, where animals were allowed to graze only on either limestone freshly collected from the sub-tidal region (rock, n = 15), or on the glass walls of the aquarium (glass, n = 15). The rock and glass compartments were partitioned by water permeable plastic mesh to prevent the movement of animals between treatments, but to allow water flow, and all other parameters, to be equal. The aquarium had been prepared two months in advance to allow algae and bacteria to grow on the tank walls, which provided the sole food supply for the animals in the 'glass' treatment. The limestone used in the 'rock' treatment was collected from Woodman Point immediately prior to the introduction of animals to the tank, and was covered in various natural algae and encrusting organisms. In order to limit the availability of Fe required for radula mineralisation, and to maintain basic aquarium hygiene, one full water change was performed each month. The tanks were checked on a daily basis and any dead animals were removed when found.

Six individuals were removed from each of the rock and glass treatments at 125 days, and a further four and seven individuals at 234 days, respectively. For controls, 12 individuals were collected fresh from the wild in order to make comparisons with normal radula mineralisation. All animals were dissected according to the method for

observing hard structures (Chapter 2.2) and observed using light microscopy (Table 2.4, Code A). Four distinctive, and visually discrete features, were identified and recorded for each radula, which included the number of clear, yellow, orange and black major lateral tooth rows. In addition, for animals in the rock and glass treatments, the number of tooth rows occurring posterior to the cold-shock anomaly was determined. During the course of the study, feeding observations were made on animals within each of the two treatments, and each dissected radula was examined for tooth wear.

3.3. Results

Distinct changes from the normal pattern of iron mineralisation were observed in the radulae of animals subjected to iron-limitation (Figure 3.1). On average, freshly collected *A. hirtosa* radulae had a total of 73 transverse tooth rows (SD = 3.2, n = 12), divided into ten rows of clear immature teeth (SD = 0.6, n = 12), followed by three rows of yellow teeth (SD = 0.3, n = 12), which precede cusp mineralisation, invariably at row 14, where the posterior cutting face of a single tooth takes on a dark orange appearance (Figure 3.2). From this point the remaining 59 teeth appeared black (SD = 3.0, n = 12).

Following 125 days in the iron-limitation treatment, the total number of tooth rows had increased relative to the control from 73 to 84 and 87 in animals from the rock and glass treatments, respectively. This resulted from an increase in the number of tooth rows observed at all stages of development, except for yellow and orange. Notably, yellow tooth rows were absent in all iron-limited animals.

While a slight increase in the number of clear tooth rows was observed in animals from the rock treatment after 234 days, those in the glass treatment displayed a marked increase in the number of clear teeth compared to control animals. This was coupled with high variability in the number of orange teeth. For example, in certain individuals no orange teeth were observed, whilst as many as five rows of orange teeth were recorded in other animals. After 234 days, the number of black teeth in animals from both the rock and glass treatments returned to a figure slightly above that of the control.

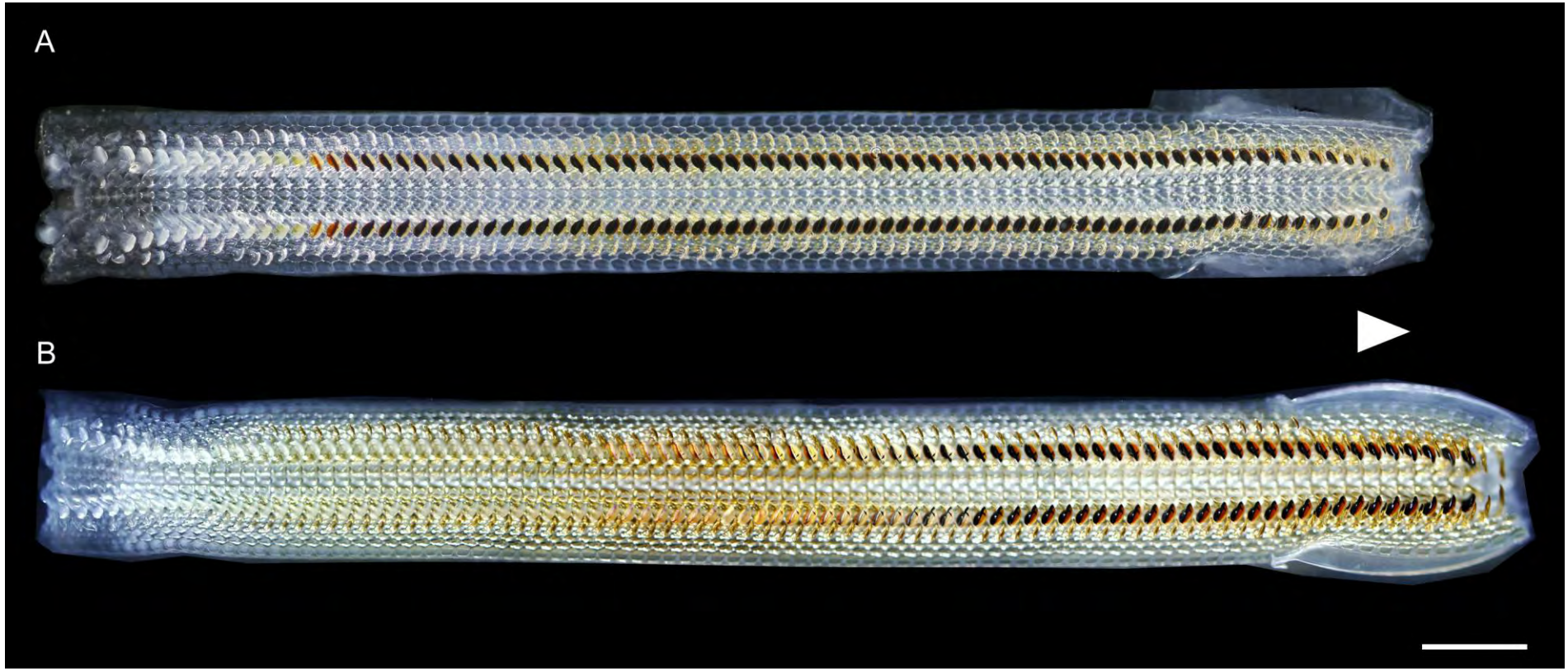

Figure 3.1. Radulae excised from *A. hirtosa*: (A) freshly collected; (B) iron-limited, showing a marked increase in the number of unmineralised tooth rows following iron-limitation for 234 days in the glass treatment. Arrowhead = anterior. Scale bar = 1 mm.

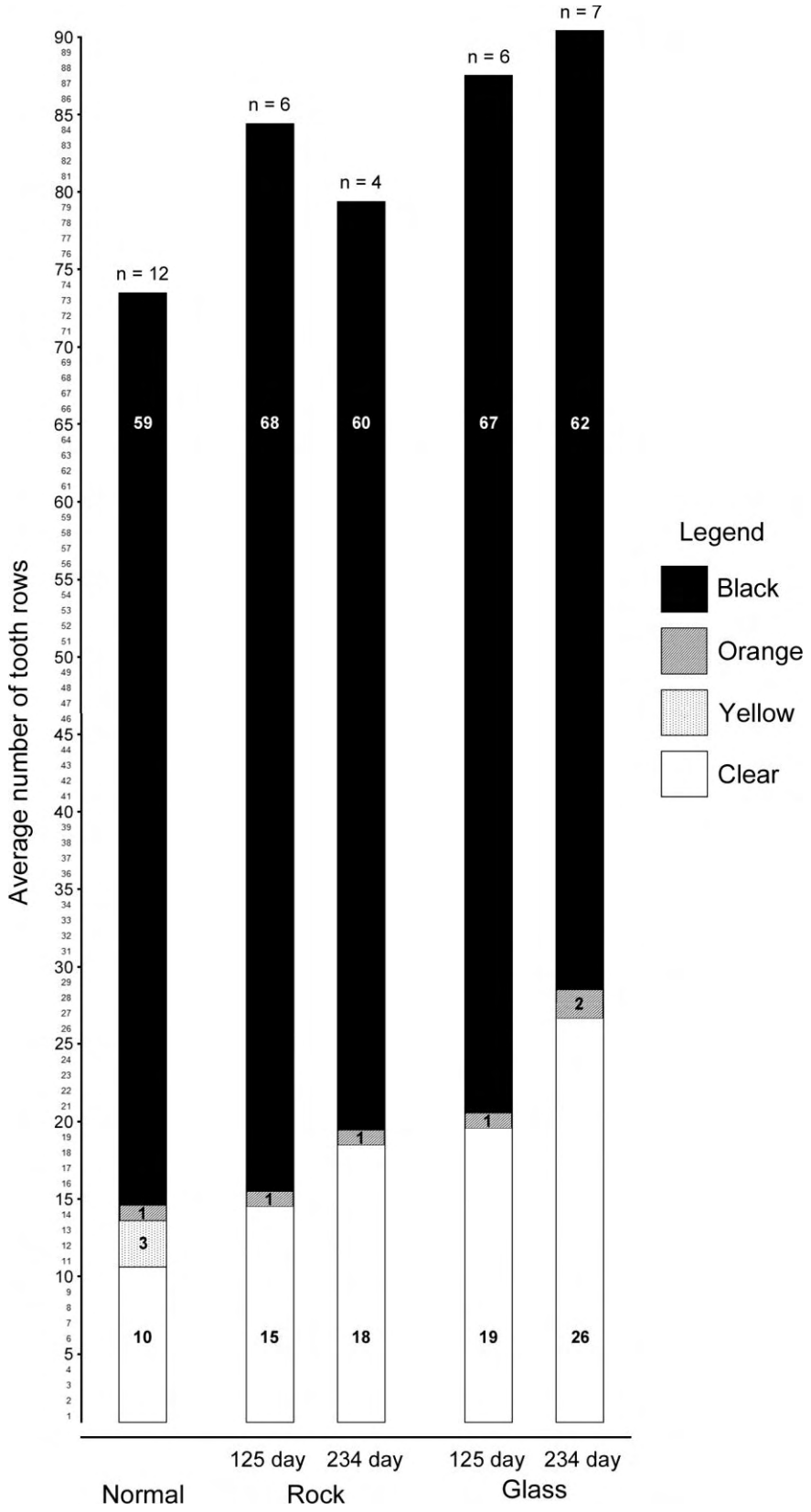

Figure 3.2. Changes to radula mineralisation in the chiton *A. hirtosa* after being maintained for 125 and 234 days in iron-limited rock and glass treatments.

Evidence of animals feeding during the course of the study was compiled from a combination of direct observation, the deposition of faecal pellets, and by the presence of tooth marks left in the algae covering the glass. The faecal pellets of animals in the rock treatment maintained their typical sandy colouration, while animals in the glass treatment produced green pellets. In addition, the anterior working teeth of animals within the rock treatment exhibited wear patterns similar to those of freshly collected animals, while the teeth of animals within the glass treatment showed no signs of wear. During the study period, five animals died in the rock treatment and two died in the glass treatment, with four of these deaths (two rock and two glass) occurring in the first week after the cold-shock.

At 125 days, radula production rates for animals in the rock and glass treatments were calculated at 0.38 (SD = 0.04, n = 6) and 0.35 tooth rows.day^{-1} (SD = 0.03, n = 6), respectively (Figure 3.3). After 234 days, animals within the rock treatment had completely replaced the entire radula through the secretion of new radula material, as evidenced by the total absence of any constriction anomaly; suggesting a minimum radula production rate of 0.34 tooth rows.day^{-1} (SD = 0.03, n = 4), based on the total number of tooth rows in each radula. After 234 days, the constriction anomaly remained clearly visible for animals within the glass treatment, and radula production had slowed to 0.27 tooth rows.day^{-1} (SD = 0.01, n = 7).

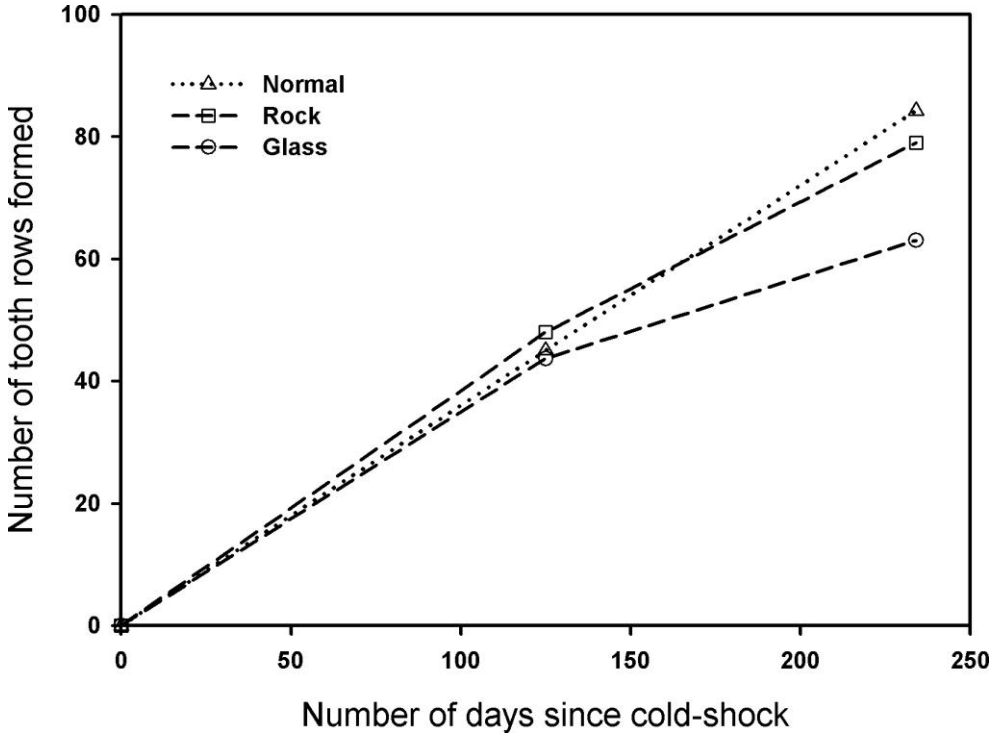

Figure 3.3. Radula production rates for the chiton *A. hirtosa* after maintenance for 125 and 234 days in rock and glass treatments. Note: Data for normal radula production in *A. hirtosa* is taken from Shaw *et al*. (2002).

3.4. Discussion

This study provides the first example of the effects of iron-limitation on radula production in a member of the Polyplacophora. Maintaining specimens of the chiton *A. hirtosa* within an iron-limited system resulted in atypical radula mineralisation and tooth formation. Specifically, a dramatic increase in the number of unmineralised/immature tooth rows was observed compared to freshly collected animals. In addition, the number of orange and black tooth rows also increased as a result of iron-limitation, while the yellow colouration of tooth rows prior to mineralisation was lost. Previous studies on chiton and limpet species suggest that biomineralisation is a highly regulated process, with little variation in the overall developmental stages between individuals of a given species

(Nesson and Lowenstam, 1985; Brooker and Macey, 2001; Liddiard *et al*., 2004). As such, the obvious changes observed in iron-limited specimens of *A. hirtosa*, especially those maintained within the glass treatment, can be regarded as a significant departure from the normal pattern of mineralisation. In addition to this distinctive visual change, concomitant and substantial alterations in structure and composition could be expected to have occurred at all stages of tooth development at various spatial scales.

Generally, the overall radula production rates calculated for animals in the rock and glass treatments remained very close to rates observed previously for this species (Shaw *et al*., 2002), suggesting that radula production may occur at a rate that is independent of the degree of tooth wear incurred as a result of grazing on the different substrate types. While the slightly depressed rate observed for animals in the glass treatment at 234 days may be due to reduced tooth wear, it is more likely to have resulted from the deterioration in the health of individuals as a direct result of prolonged captivity in the iron-limited system.

Notably, the number of unmineralised tooth rows that form due to iron-limitation does not match the radula production rate in any of the animals. The significant concentrations of ferritin and haemosiderin in the hemolymph and various other body tissues (Webb and Macey, 1983; Kim *et al*., 1988) are likely to be sufficient for maintaining radula mineralisation at normal levels for a substantial period. The increase in the number of unmineralised tooth rows at 125 days suggests that these reserves had been diminished. However, the production of unmineralised tooth rows in animals subjected to the longer period of iron-limitation did not progress at the same rate as radula production, which suggests that animals may have had some limited exposure to iron within the treatments.

Whilst iron was limited, as far as possible, for the duration of the experimental period, animals may have obtained some additional iron from a range of sources. For

animals grazing within the rock treatment, iron may have been acquired from the limestone, which is known to contain approximately 1 mg of iron per g substrate (Shaw, 2003). Animals within the glass treatment were often found on the bottom of the tank, where they would have the opportunity to ingest their own teeth, as evidenced by the presence of intact major lateral teeth in the animal's faecal pellets. In addition, the faecal pellets of *A. hirtosa*, which also accumulated on the bottom of the tank, normally contain a significant portion of inorganic material (presumably the substrate) ingested during the feeding process (Macey *et al.*, 1996). As such, it is likely that the more dramatic increase in the number of unmineralised tooth rows in the glass treatment resulted from preventing animals from consuming the limestone substrate, and, in turn, the eventual loss of this material in the faecal pellets.

Seawater has been discounted as a source of iron for radula mineralisation, as it is generally thought to exist in extremely low concentrations in its biologically available form as Fe^{2+} (Carefoot, 1965; Nesson, 1969). However, while the concentration of iron in the open ocean is certainly low ($0.02 – 2$ nmol L^{-1}), dissolved iron can reach levels of 300 nmol L^{-1} in various marine environments, including coastal regions and the pore waters of marine sediments (Turner *et al.*, 2001). In addition, the uptake of metals at the gills of molluscs has been shown to be enhanced by the synthesis of metal-binding proteins and chelating agents (Marigomez *et al.*, 2002). The narrow pallial grooves that contain the gills of chitons would provide an ideal environment for regulating chemical conditions, such as pH, salinity and redox potentials. Given that these animals remain clamped to the substrate for extended periods, it is not unreasonable to assume that such processes may be occurring. Iron may also have been sourced indirectly by feeding on algae, which had absorbed additional iron following water changes. Studies have also shown that ions such as calcium and magnesium can be mobilised from mollusc shell when in short supply

(Lane, 1986; Porcel *et al*., 1996). Although the pathways of iron uptake have not been elucidated in chitons, it is reasonable to suggest that iron could be sequestered from a range of sources, including the ingestion of substrate, algae, seawater and through the recycling of their teeth, and is clearly an area in need of further study.

The continual deposition of faecal pellets throughout the study provided evidence that animals were feeding in both treatments. The radulae of animals in the rock treatment had similar tooth wear patterns to those observed in freshly collected specimens, whereas radulae excised from animals in the glass treatment showed no signs of wear. As such, iron-limitation may have had a greater affect on animals within the glass treatment due to a reduction in the amount of abraded iron-containing tooth material that would normally be ingested while feeding. Notably, the obvious increase in the number of tooth rows for animals in the glass treatment indicates that, in *A. hirtosa*, the loss of teeth is a function of wear, rather than purely a growth-controlled process as has been suggested previously (van der Wal *et al*., 2000).

The yellow colouration of teeth typically observed just prior to the orange tooth row in normally mineralised radulae was not present in animals maintained within the iron-limited system. Previous researchers have attributed the presence of this yellow material to an influx of either protein or sulphur into the tooth cusp or junction zone (Evans *et al*., 1991; Brooker *et al*., 2003). From the growing body of evidence relating to the initial deposition of ions at the junction zone (see for example: Macey and Brooker, 1996; Brooker *et al*., 2003; Liddiard *et al*., 2004; Sone *et al*., 2007), it would appear likely that this yellow material results from the mass accumulation of iron and other elements in this region prior to mineralisation. Its absence from iron-limited teeth therefore suggests that this accumulation is insufficient to be observed under the light microscope.

The technique of maintaining chitons within an iron-limited system has the potential to significantly aid the understanding of biomineralisation in the major lateral teeth of

chitons. Importantly, chitons continue to produce new tooth rows despite the disruption to the supply of iron required for cusp mineralisation. This provides the opportunity to study the cells that control the mineralisation process in the absence of the iron normally found within the tissues surrounding the cusps. Information relating to the delivery of iron into the tooth cusps could be elucidated by observing differences in cell development between radula tissue from normal and iron-limited animals. Investigations on the structure of the organic matrix have been restricted as a direct result of the limitations imposed by the mineralisation process itself. As such, the ability to selectively control mineral deposition opens a host of opportunities for the further study of mineral deposition within the matrix. For example, observations of the matrix in teeth from iron-limited animals may reveal how chitons exert such fine control over the spatial organisation of the various minerals within the tooth cusps.

The chiton *A. hirtosa* has proven to be a resilient test subject, in withstanding long periods of time both exposed to laboratory conditions and without its normal dietary requirements. This is likely to be a direct consequence of the highly variable environmental conditions experienced by this species in the wild, which include large fluctuations in temperature, salinity and moisture. Such resilience may be useful for other long-term studies in which iron-limitation may be required. For example, molecular based studies may be able to resolve the genetic basis of biomineralisation by observing variations in gene expression between normal and iron-limited animals. In addition, experiments aimed at determining the major sources from which chitons obtain the large amounts of iron needed for tooth mineralisation, may also require the long-term maintenance of animals. However, designing experiments in which iron is excluded from either controls or treatments is problematic due to the difficulties associated with obtaining iron-free reagents and the natural abundance of iron in the environment.

Chapter 4

Major lateral tooth cusp mineralisation processes

4.1. Introduction

Radula development in chitons and limpets has historically been categorised into stages representing discrete mineralisation events that occur along the length of the radula ribbon (see Chapter 1.3 for review). These stages of mineralisation have been continually refined and redefined as a result of ongoing studies and the application of new techniques. For example, the advent of *in situ* methods for studying chiton and limpet radulae has expanded our understanding of the fine structure of the major lateral tooth cusps, and has revealed additional steps in the biomineralisation process, including the initial deposition of iron at the junction zone (see for example: Macey and Brooker, 1996; Liddiard *et al*., 2004; Wealthall *et al*., 2005). However, while advances in sample preparation and analysis have yielded many structural and compositional details regarding the tooth cusps, little information is available on the delivery and deposition of the elemental precursors required for cusp mineralisation.

In Chapter 3, it was demonstrated that, in the chiton *Acanthopleura hirtosa*, iron-limitation resulted in atypical radula development. The capacity to suspend radula mineralisation presents researchers with a unique opportunity to apply previously refined techniques in a dynamic and new environment. In addition, the daily requirement for elements involved in radula production has been accurately determined for *A. hirtosa* (Shaw, 2003, Appendix A), thereby providing the measure by which these elements can be reinstated following periods of iron-limitation. By manipulating the availability of the elements required for mineralisation, it may be possible to elucidate the pathways and processes of the delivery of elements to the tooth cusps.

For example, in addition to the obvious increase in the number of unmineralised tooth rows caused by iron-limitation, it is also likely that fine-scale changes have occurred, including disturbances in the distribution and type of minerals being deposited

along the radula, or an alteration of the structural and functional properties of the organic matrix. These changes could well provide valuable information with respect to understanding the processes of normal biomineralisation in these animals. As such, a detailed comparative study documenting radula development in normally mineralised animals, iron-limited and iron-reinstated animals has been undertaken using a combination of light microscopy (LM) and scanning electron microscopy (SEM) in conjunction with qualitative energy dispersive spectroscopy (EDS).

4.2. Materials and Methods

4.2.1. *Normal radula mineralisation*

The radulae excised from specimens of *A. hirtosa*, collected for the study outlined in Chapter 3, were also used for observations of normal mineralisation. In addition to the number of clear, yellow, orange and black major lateral tooth rows, the row at which the window region on the anterior surface of the major lateral cusps changes from clear to opaque was also documented. Six of these radulae were then processed using the resin embedding method outlined in Chapter 2.4. A further six animals were collected and dissected for additional LM observations of the superior epithelial tissues, as outlined in Chapters 2.1 and 2.2 respectively, and then processed using the microwave technique as per Chapter 2.3. Light microscope sections were stained for 15 min using a variation of the Perl's Prussian blue method for ferric iron (Culling, 1974), where resin sections were placed in a freshly prepared solution comprised of equal parts of potassium ferrocyanide and hydrochloric acid, each made to 4% in distilled water.

4.2.2. *Mineralisation in iron-limited and iron-reinstated radulae*

Two systems were used to produce iron-limited radulae. A closed iron-limited system was utilised in order to minimise the availability of iron for radula mineralisation and an open system was utilised in order to improve tank hygiene and maintain animal health.

In the closed system, a total of 58 specimens of *A. hirtosa* were collected, with equal numbers being placed into two identical 60 L glass aquaria, with aeration and fluorescent lighting (Gro-lux^{TM}) that had been prepared two months in advance to allow algae to grow on the tank walls. The findings detailed in Chapter 3 made it apparent that a limited amount of iron was still available to animals in the glass treatment. As such, plastic biomatting was installed at the bottom of each tank to reduce the likelihood of animals ingesting their own iron-impregnated teeth, or tooth remnants, which are often shed whilst feeding. Animals were maintained in this iron-limited system for a period of 190 days, and, with the exception of monthly water changes, no further inputs were supplied. The system was inspected several times each week, and animals were removed and dissected at regular intervals during the 190 day period to determine the degree of iron-limitation within the radulae. Any individuals found dead were removed upon discovery.

The open system consisted solely of a fibreglass tank reticulated by continuous fresh seawater pumped at a rate of ~3.4 L.min^{-1} from a subterranean bore situated 50 m offshore. A total of 84 animals were maintained upon the fibreglass walls of the tank for 313 days, with periodic dissections being performed to assess the degree of iron-limitation. Any changes in the pattern of radula mineralisation were documented.

After 190 days in the closed system, six iron-limited individuals were removed, with three being dissected for the observation of hard structures and three for observations on the superior epithelial tissues (Chapters 2.2). A supply of iron was then returned to the remaining individuals by detaching them from the aquarium walls and placing them onto algae covered limestone rocks that had been freshly collected from the Woodman Point study site. These animals were left to graze on the rocks for three days, after which six individuals were removed and dissected as above. This was repeated after a further five days, where four and three individuals were dissected for observations of hard structures and superior epithelial tissues, respectively. During this

iron-reinstatement period, a full seawater change was performed twice each day. Following dissection, visual information was documented as for normally mineralised radulae prior to processing, as described in Chapter 2.4. Radulae, dissected for observations on the superior epithelium, were processed using the microwave technique for LM as per Chapter 2.3 and stained using the Perl's Prussian blue method outlined in Chapter 4.2.1.

4.3. Results

4.3.1. *Normal radula mineralisation*

Radulae excised from freshly collected (*i.e.* normal) individuals of *A. hirtosa* exhibited a high degree of consistency with respect to the pattern of mineralisation of their major lateral tooth cusps. A typical *A. hirtosa* radula possesses an average of 10 rows of clear immature major lateral teeth, followed by 3 rows of yellow teeth, 1 orange tooth row and 59 black tooth rows (see Chapter 3.3) (Figure 4.1 A, B and C). With the exception of the infilling of the window on the anterior face of the cusps, which on average occurs at row 31 (SD = 1.2, n = 12), little additional direct visual information can be obtained from the teeth using optical microscopy.

An LM examination of radulae prior to the onset of mineralisation at row 14, revealed that the yellow colouration of teeth (Figure 4.2 A) corresponds to well defined, anteriorly intensifying bands at the plate-like junction zone region, seen using back-scattered electrons in the SEM (Figure 4.2 B). In addition, a thin band, extending from the junction zone to the cusp tip could also be observed approximately 30 μm from the posterior cusp surface at row 13, just prior to the orange tooth (Figure 4.2 B). Radula sections treated with Perl's Prussian blue stain strongly at the junction zone, confirming the presence of ferric iron from row 8 onwards (Figure 4.2 C). Perl's stain also highlights the presence of a thin band of iron between the junction zone and cusp tip at row 13; similar to that observed in the SEM. At the same tooth row, the Perl's

Figure 4.1. Light micrographs of a typical radula excised from the chiton *A. hirtosa* showing the various visual changes in tooth development as a consequence of the progressive mineralisation process.

A, Whole radula ribbon with clear immature major lateral teeth on the left (posterior) and worn mature teeth on the right (anterior). (Code: A), Scale bar = 500 μm.

B, Early stages of major lateral tooth development highlighting the transition from clear immature teeth to black magnetite mineralised teeth. Note the yellow colouration of the teeth prior to the onset of cusp mineralisation at row 14 (arrows). (Code: A), Scale bar = 200 μm.

C, Change in opacity of the window region on the anterior surface of the tooth cusp at tooth row 31 (arrow). (Code: A), Scale bar = 200 μm.

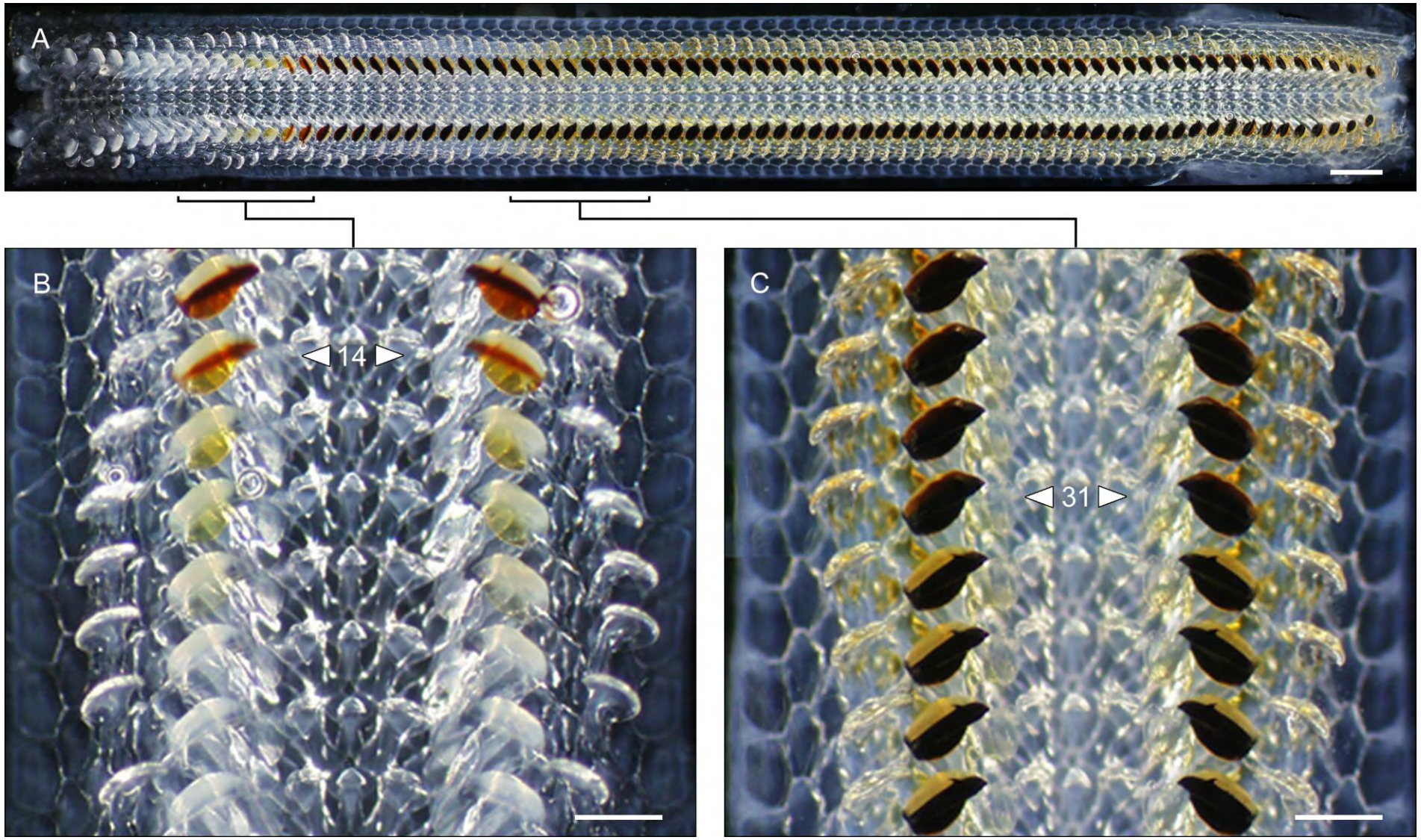
A
B
14
C
31

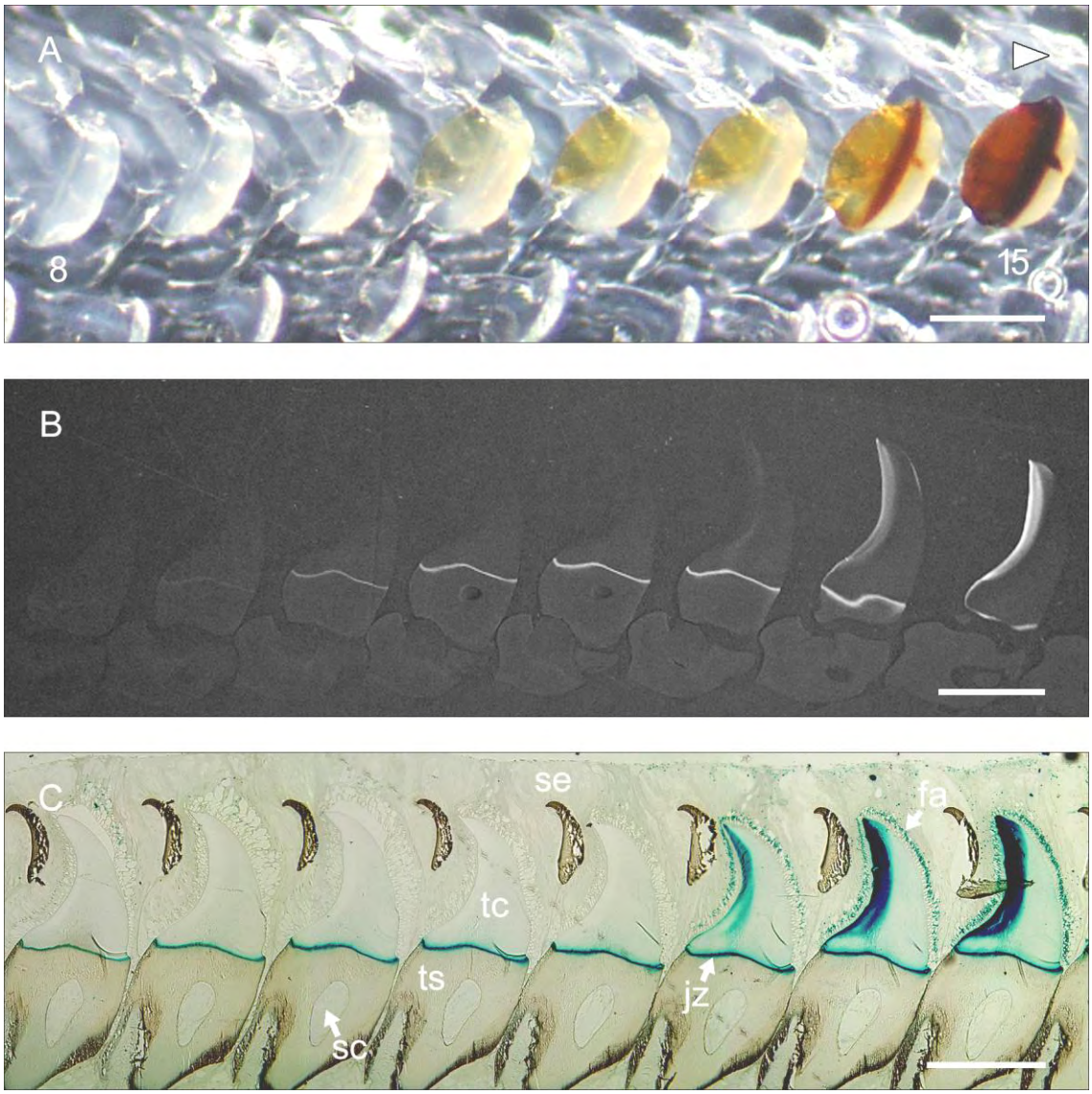

Figure 4.2. Light and electron micrographs of major lateral tooth development in the chiton *A. hirtosa* demonstrating deposition events at the junction zone and tooth cusps from tooth rows 8 to 15. (A) Anteriorward (arrowhead) changes in tooth colouration in a freshly excised radula and (B) the same radula in longitudinal section highlighting the presence of distinct bands, visible when imaged using back-scattered electrons, (C) which correspond to ferric iron in the junction zone and cusps as revealed with Perl's Prussian blue stain. Note: Image C is from a different radula. fa = ferritin aggregates, jz = junction zone, sc = stylus canal, se = superior epithelium, tc = tooth cusp, ts = tooth stylus (Codes: (A) A; (B) CP, G; (C) MP, B), Scale bars = 200 μm.

stain reveals a large accumulation of iron within the superior epithelial tissue surrounding the cusps, presumably in the form of ferritin. Perl's stained sections, EDS mapping (data not shown) and EDS spot analyses confirm that the distinct bands at the junction zone are primarily due to the presence of iron. Qualitative spectra from spot analyses, collected from the junction zone early in tooth development, indicate that sulphur is present at tooth row 7 followed by iron, phosphorous, calcium and magnesium at tooth row 8 (Figure 4.3). Spot analyses demonstrate that these elements are present at the junction zone in all subsequent tooth rows to row 13, and elemental maps indicate that iron, phosphorous and calcium persist at the junction zone to at least the developmental stage of tooth core mineralisation. Chlorine and silica, largely attributable to the epoxy resin used for embedding and the SiC polishing media respectively, is also present.

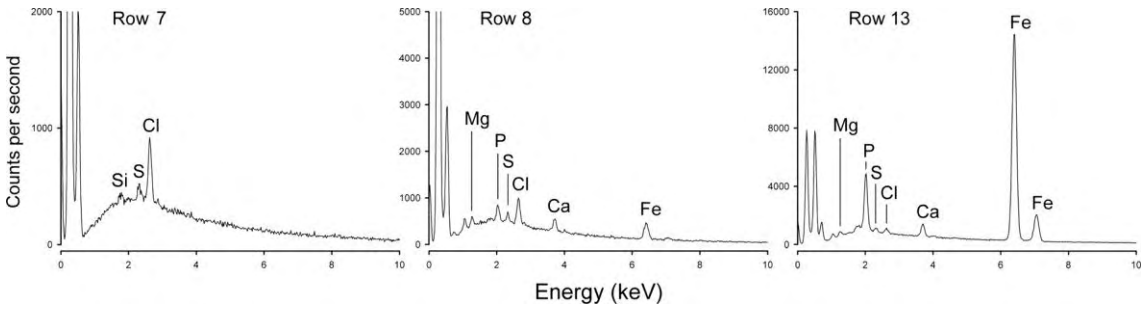

Figure 4.3. X-ray microanalytical (EDS) spectra demonstrating the presence of elements in the junction zone region at tooth rows 7, 8 and 13 from the radula of the chiton *A. hirtosa*. (Codes: CP, H)

The change in opacity of the window region on the anterior surface of each major lateral tooth cusp at row ~31 is due to the deposition of a thin layer of a high atomic number element that extends from the anterior boundary of the magnetite region to approximately midway down the anterior cusp surface (Figure 4.4). In subsequent tooth rows, EDS mapping revealed that the material on the anterior surface was iron (Figures 4.5 and 4.6). This event coincides with the formation of the lepidocrocite region, which forms a border between the magnetite region and tooth core in all subsequent tooth rows.

Mineralisation of the tooth core commences with the deposition of calcium and phosphorous at the apex of the core region at row ~37 (Figure 4.5). This mineralisation front subsequently migrates ventrally along the boundary of the iron-mineralised region and anterior cusp surface before progressively infilling the remainder of the core, which is predominantly in-filled by row ~43.

A previously undescribed feature, consisting of a ~25 μm wide plume composed primarily of iron, phosphorous and calcium, can be observed between the junction zone and iron-mineralised regions of the tooth (Figure 4.5 B-E). The plume is visible using back-scattered imaging and EDS, and can also be observed in sections stained with Perl's Prussian blue (see Chapter 5). This plume is evident in all teeth along the length of the radula, from the initial deposition of iron at row 14, to where the core becomes completely in-filled at row ~61. Notably, plumes appeared more intense, using the Perl's stain and back-scattered imaging, when sagittal orientations through the cusps were achieved (*ie.* directly above the stylus canal). Towards the anterior end of the radula, where the core becomes mineralised, there is a reversal in the relative atomic density between the core and the plume region, with the latter appearing as an area of relatively low atomic density. Further along the radula at row ~61 the plume region is finally in-filled with calcium and phosphorous minerals (Figure 4.6). Notably, there is a distinct discontinuity in the organic matrix above the junction zone in this plume region (Figure 4.7).

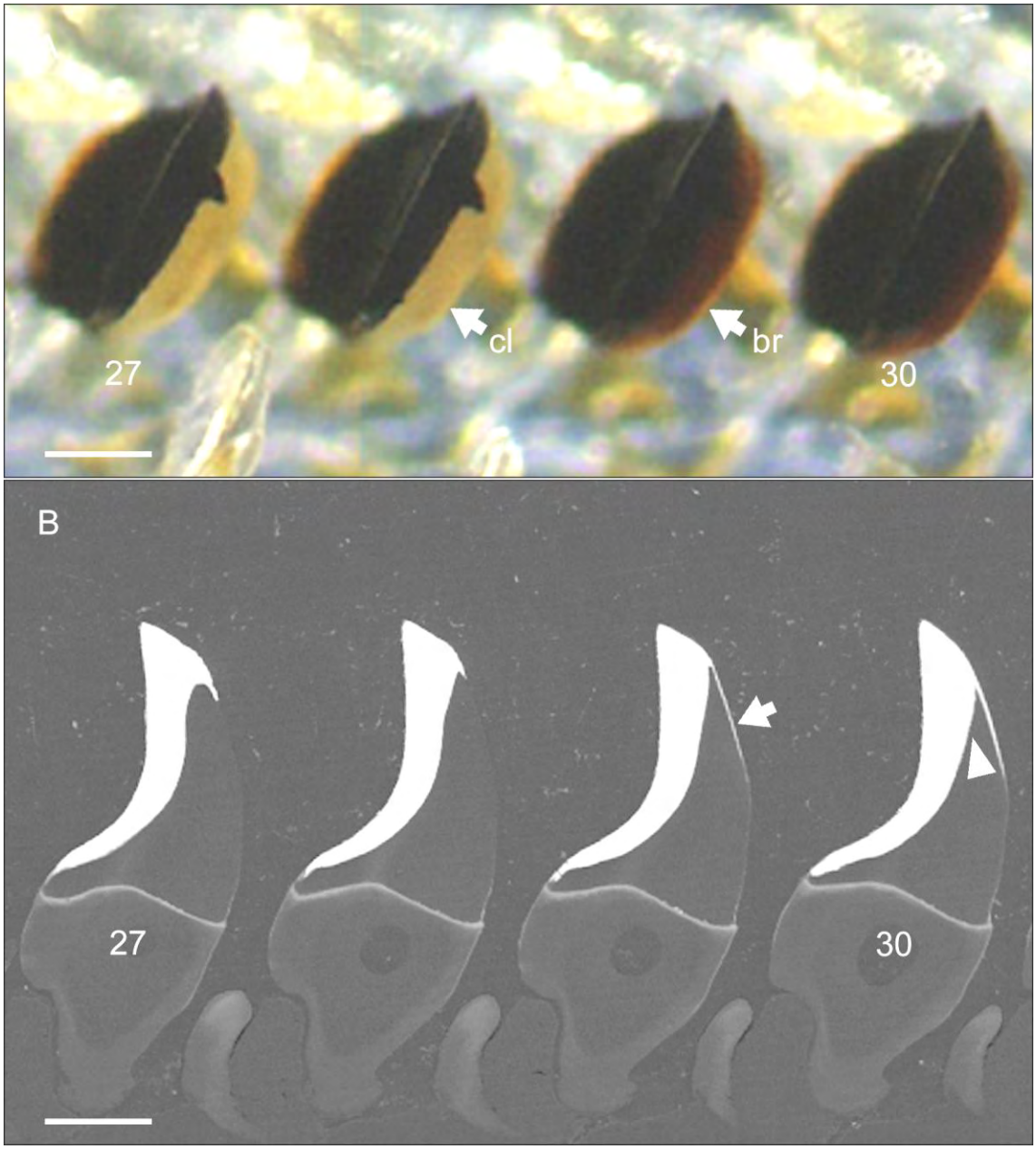

Figure 4.4. Developmental changes to the window region on the anterior surface of the major lateral tooth cusps of *A. hirtosa*. (A) Light micrograph showing the change in window colour from clear (cl) to brown (br) from tooth rows 28 to 29, respectively. (B) A longitudinally polished section of the same radula, imaged using back-scattered electrons in a SEM, indicates the appearance of high atomic number elements in this region at row 29 (arrow). Note the absence of this material at row 28 and the initial formation of the lepidocrocite region at row 30 (arrowhead). (Codes: (A) A; (B) CP, G), Scale bars = 100 μm.

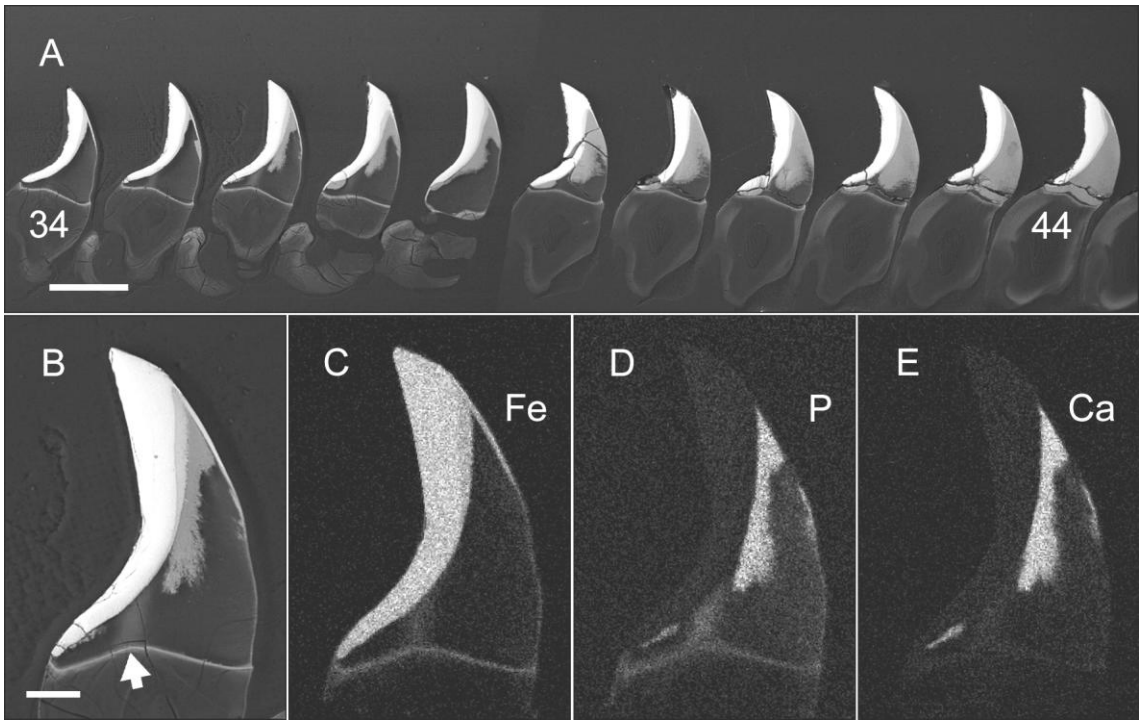

Figure 4.5. Back-scattered scanning electron micrographs demonstrating the deposition of phosphorous and calcium within the core region of the major lateral tooth cusps in *A. hirtosa*. (A) Core mineralisation is initiated at tooth row 35 and progressively fills over approximately nine tooth rows. (B) Back-scattered image highlighting the plume of high atomic number material at tooth row 36 situated between the junction zone and the boundary of the iron-mineralised region (arrow). Elemental mapping confirms this is comprised of (C) iron, (D) phosphorous and (E) calcium. (Codes: CP, H), Scale bars = (A) 200 μm, (B) 50 μm.

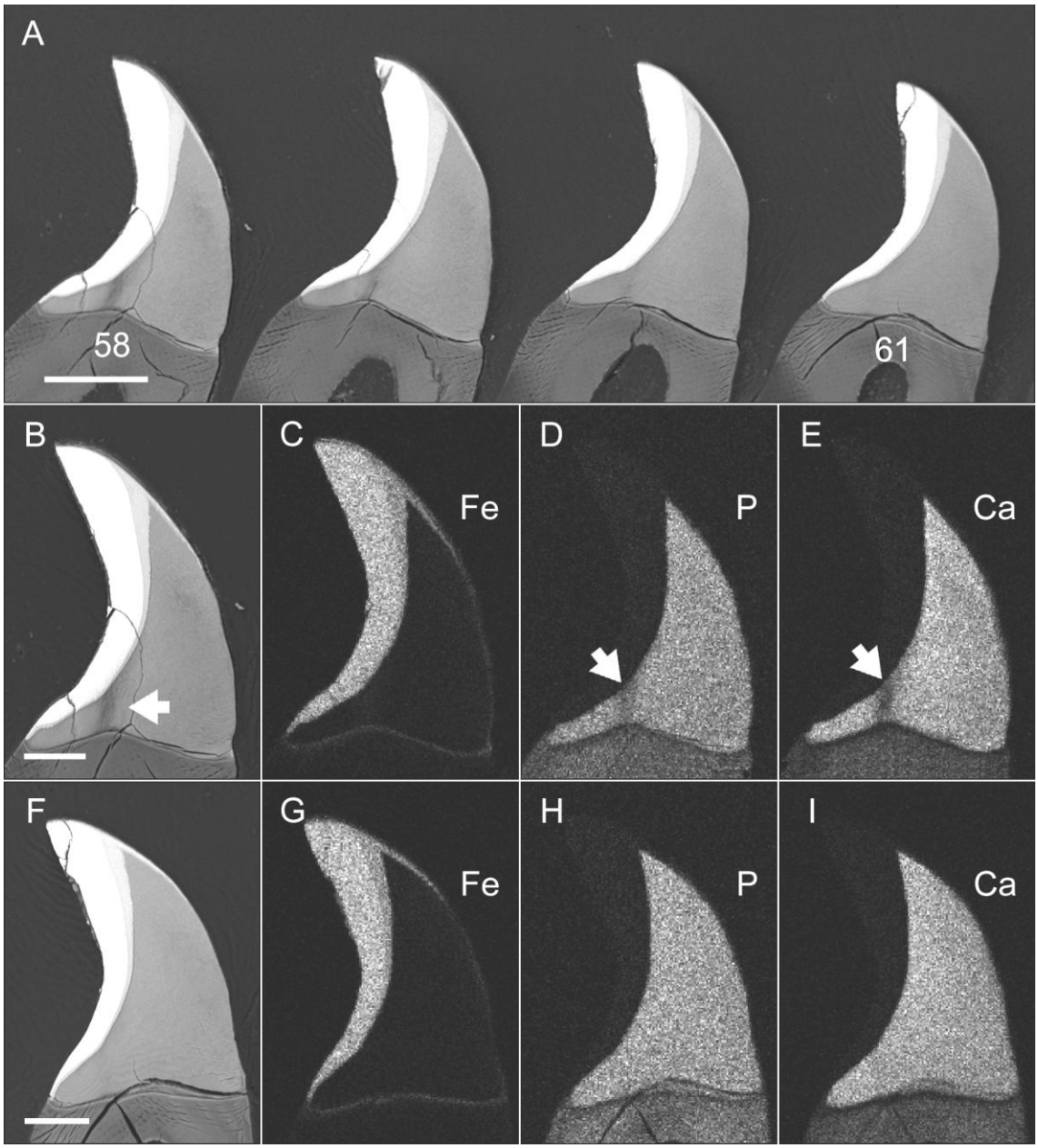

Figure 4.6. Back-scattered scanning electron micrographs of (A) heavily mineralised major lateral teeth from rows 58 to 61 at the anterior end of the radula from *A. hirtosa*, demonstrating (B-E) the absence of iron, phosphorous and calcium in the plume region relative to the remainder of the tooth core at row 58 and (F-I) the final in-filling of this region with phosphorous and calcium at row 61. (Codes: CP, H), Scale bars = (A) 100 μm, (B and F) 50 μm.

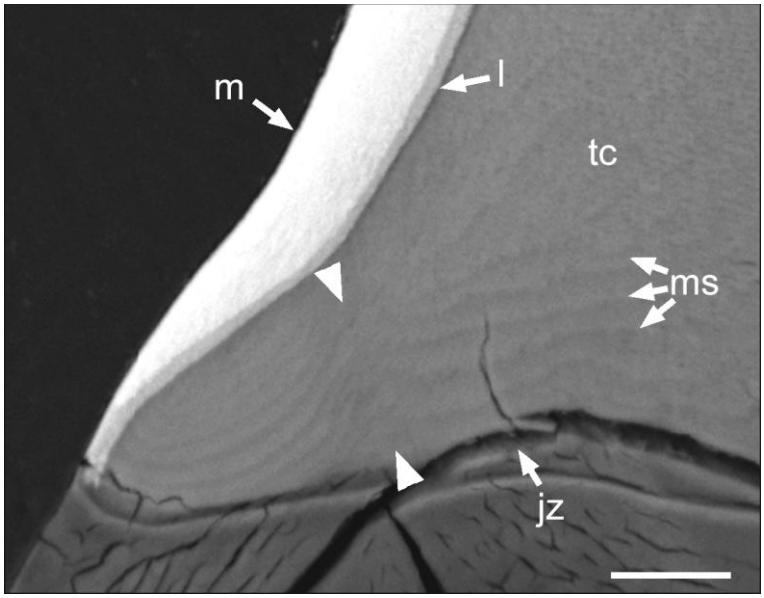

Figure 4.7. Back-scattered scanning electron micrograph demonstrating the discontinuity in the matrix structure (ms) within the plume region (arrowheads) at tooth row 61 in *A. hirtosa*. This appears as a break in the concentric bands situated within the tooth core (tc) between the junction zone (jz) and magnetite (m)/lepidocrocite (l) regions. (Codes: CP, H), Scale bar = 20 μm.

4.3.2. *Mineralisation in iron-limited and iron-reinstated radulae*

Of the 58 animals introduced to the closed iron-limited system, three animals were dissected and 36 animals died (62%) prior to iron-reinstatement. Of the 84 animals introduced to the open, flow-through iron-limitation system, 27 had died (32%) by the end of the 313 day study. The radulae of animals cultured in the closed iron-limited system for 190 days, and those in the closed system where iron was reinstated for periods of 3 and 8 days after iron-limitation, exhibited distinct differences in the number of tooth rows, and the visual appearance of various developmental stages, compared to normally mineralised radulae (Figure 4.8). In all cases, the number of unmineralised tooth rows increased and the yellow colouration of cusps disappeared from tooth rows prior to cusp mineralisation. Although a high degree of variability was evident between individuals, most 190 day iron-limited and iron-reinstated radulae exhibited either an increase in the number of cusps with orange colouration, or variation in colour at the cusp tip and anterior surface (Figures 4.8 and 4.9). In addition, atypical orange spots were present at the centre of the junction zone region above the stylus canal, which diminished in size posteriorly from the orange tooth row, and were most evident in iron-reinstated radulae. The spotting effect, observed in animals maintained within the closed system, was particularly evident in a number of animals within the open system (Figure 4.10). Despite the marked changes in mineralisation observed in certain individuals, the effects of iron-limitation within the open system were highly variable, and many radulae remained fully mineralised for the duration of the study. As such, the remaining results will focus on the animals maintained within the closed system.

Despite the suspension of iron deposition within the tooth cusps, 190 day iron-limited and all iron-reinstated individuals maintained iron deposition within the junction zone to within five tooth rows of normal deposition in this region (Figure 4.8). This was evidenced using both LM (Perl's Prussian blue) and SEM (back-scattered electrons), where ferric iron and high atomic weight elements were observed at the junction zone for iron-limited (Figure 4.11), and 8 day iron-reinstated radulae (Figure 4.12).

Figure 4.8. Diagrammatic representation of the major stages of cusp mineralisation in normal (n = 12), iron-limited and iron-reinstated *A. hirtosa* radulae (closed system). Due to the variability in iron-limitation observed between individuals, each bar represents the mineralisation stages from individual radulae excised from iron-limited and 3 and 8 day iron-reinstated animals. Number values represent the number of tooth rows in each developmental stage. Underlined values represent the number of tooth rows from the orange tooth to the change in window (w) opacity. The row at which iron is first observed at the junction zone (jz) and the deposition of calcium and phosphorous (c) in the tooth core are also indicated.

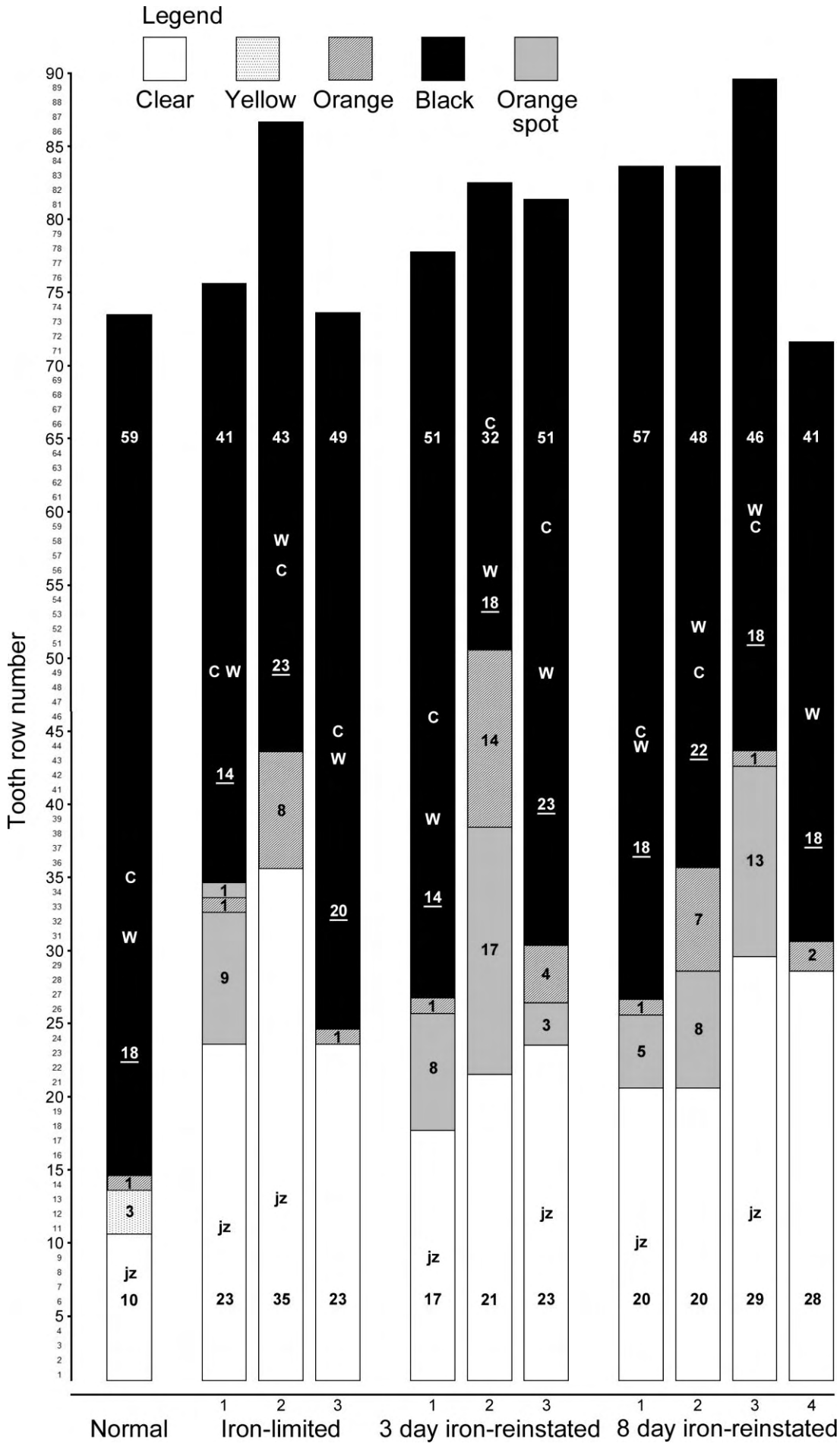
Legend
Clear
Yellow
Orange
Black
Orange spot
Tooth row number
Normal
Iron-limited
3 day iron-reinstated
8 day iron-reinstated
59
C
W
18
1
3
jz
10
41
C W
14
1
1
9
jz
23
43
W
C
23
8
jz
35
49
C
W
20
1
jz
23
51
C
W
14
1
8
jz
17
C
32
W
18
14
17
jz
21
51
C
W
23
4
3
jz
23
57
C
W
18
1
5
jz
20
48
W
C
22
7
8
jz
20
46
W
C
18
1
13
jz
29
41
W
18
2
jz
28

Figure 4.9. Composite LM images illustrating the differences between (A) a normally mineralised radula from *A. hirtosa* and (B) a 3 day iron reinstated radula, typical of changes shown in cusp colouration for iron-limited and iron-reinstated radulae. Note: radulae are aligned at the orange tooth row (lower row number and arrows), and the tooth row number at which there is a change in window opacity (upper row number and arrows) is also indicated. (Code: A), Scale bars = 200 μm.

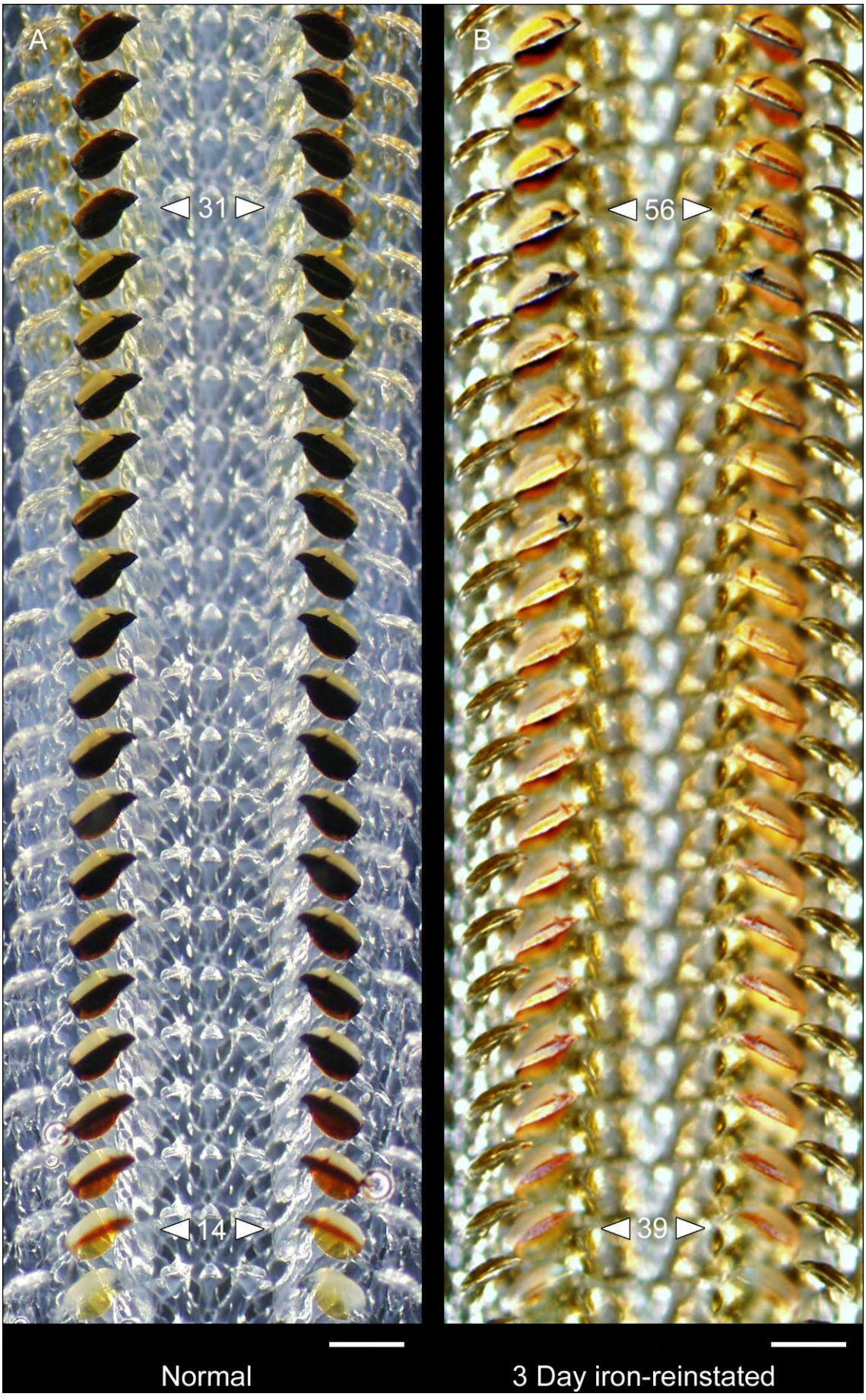
A
31
14
B
56
39
Normal
3 Day iron-reinstated

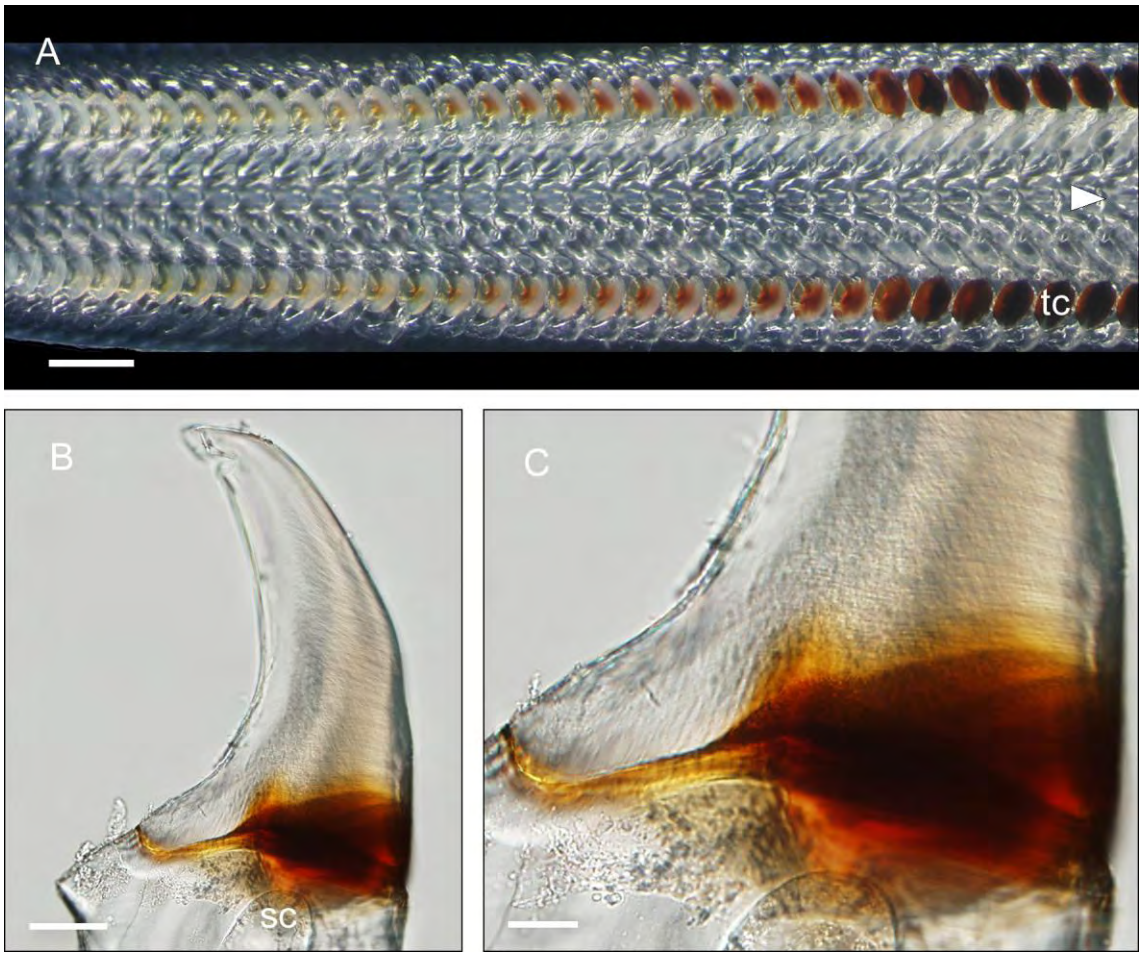

Figure 4.10. Light microscope image of an iron-limited radula excised from a specimen of *A. hirtosa*, maintained for 313 days in the iron-limited flow-through seawater system, demonstrating the presence of reddish-brown material within the core of the tooth cusp (tc), which appears to stem from the junction zone region. Note the (A) reduction in material towards the posterior end of the radula and the (A, B, C) positioning of the opaque material above the stylus canal (sc). Arrowhead = anterior. (Code: A), Scale bars = (A) 500 μm, (B) 50 μm, (C) 20 μm.

Figure 4.11. Composite LM and back-scattered SEM micrographs of major lateral tooth development in specimens of *A. hirtosa*, iron-limited for 190 days within the closed system, demonstrating deposition events at the junction zone (jz) and within the tooth cusps (tc). (A) Anteriorward (arrowhead) changes in tooth colouration in an iron-limited radula (rows 13-37). Longitudinal sections highlight the presence of (B) high atomic weight elements and (C) ferric iron in the junction zone (rows 14-43) and cusp (row 43) when imaged using back-scattered electrons and stained with Perl's Prussian blue, respectively. Note: Images A and B are taken from the same animal. (Codes: (A) A; (B) MP, H; (C) MP, B), Scale bars = 200 μm.

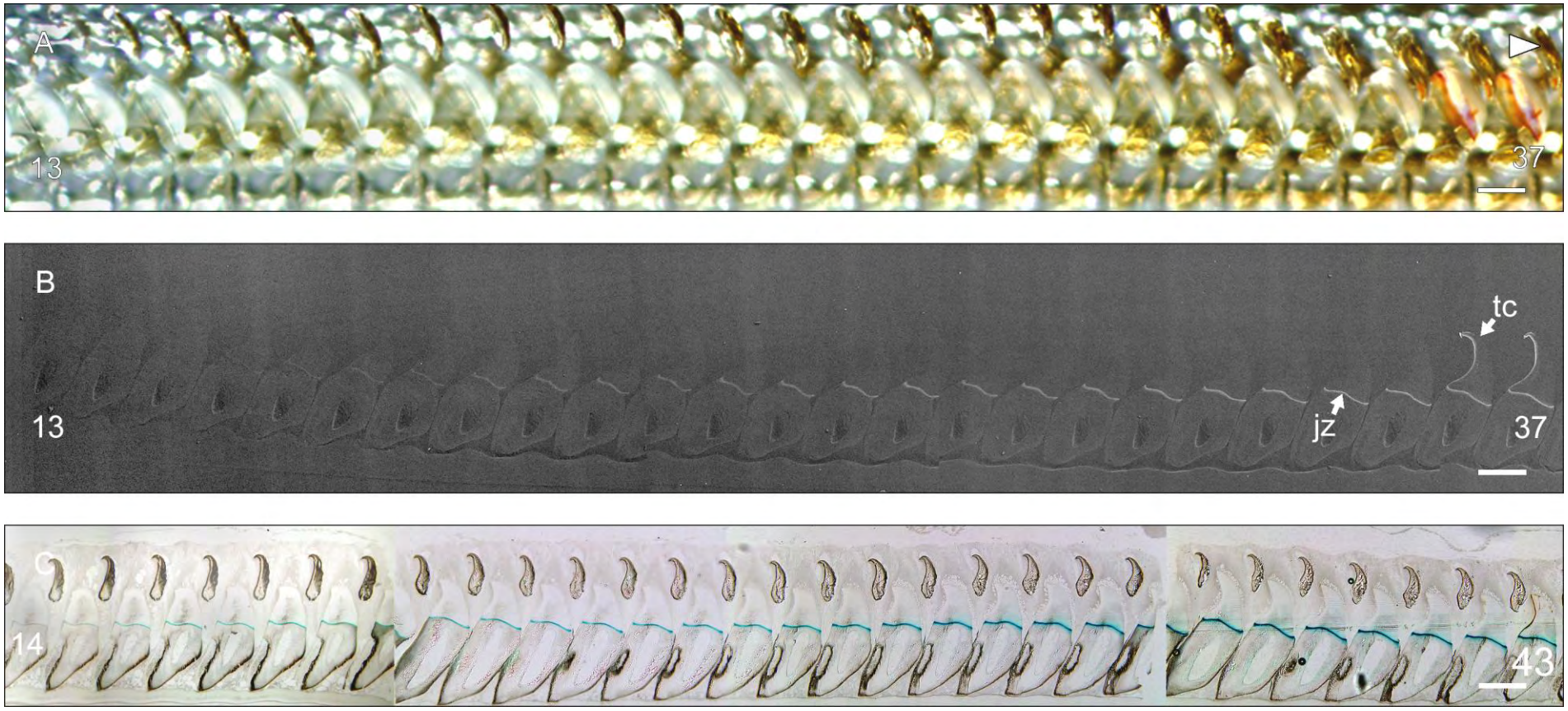
A
13
37
B
13
tc
jz
37
C
14
43

Figure 4.12. Light microscope and back-scattered SEM micrographs of major lateral tooth development in 8 day iron-reinstated specimens of *A. hirtosa* demonstrating deposition events at the junction zone (jz) and in the tooth cusps (tc). (A) Anteriorward (arrowhead) changes in tooth colouration, including orange spotting, in an 8 day iron-reinstated radula (rows 17-44). Longitudinal sections highlighting the presence of (B) high atomic weight elements both at and above the junction zone and (C) ferric iron in the junction zone and cusps (arrowheads) (rows 14-38) when imaged using back-scattered electrons and stained with Perl's Prussian blue, respectively. Note: Images A and B are taken from the same animal. (Codes: (A) A; (B) MP, H; (C) MP, B), Scale bars = 200 μm.

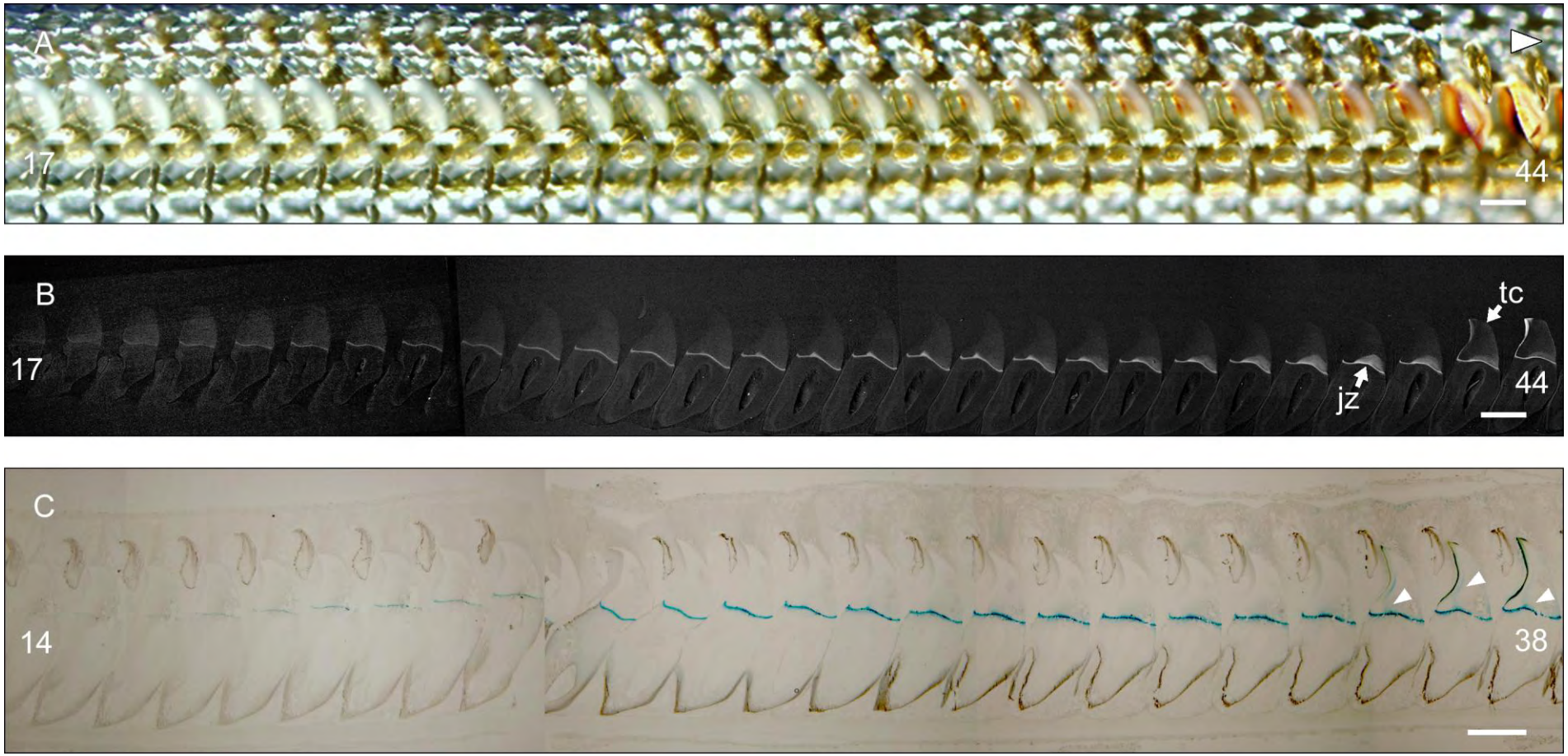
A
17
44
B
tc
17
jz
44
C
14
38

Qualitative X-ray microanalysis (EDS), performed using spot analyses, revealed that a similar range of elements to those normally found at the junction zone were present in 190 day iron-limited and 8 day iron-reinstated radulae. For iron-limited radulae, and 8 day reinstated radulae, detectable levels of iron, phosphorous, magnesium and sulphur first appear at the junction zone at tooth rows 13 and 12, respectively (Figure 4.13). Calcium also appears at row 13 in iron-limited radulae, but was detected earlier at row 11 for 8 day iron-reinstated radulae. In addition, data from these same radulae at the tooth row immediately prior to the first appearance of minerals in the cusps, also show that the junction zone contains similar elements to normal radulae, with the exception of potassium, which was not found in normal radulae but was detected in both the iron-limited and 8 day samples.

The plumes containing iron, phosphorous and calcium, observed in normally mineralised radulae, were rarely observed in iron limited radulae (Figure 4.11). However, plumes were always present, to varying degrees, in 3 day and 8 day iron-reintroduced radulae. For 3 day iron-reintroduced radulae, the plume appears to originate from the centre of the junction zone region and move upwards through the core, and along the boundary that would normally serve as the interface between the posterior iron-mineralised region and apatite mineralised core of each cusp (Figure 4.14). For 8 day iron-reintroduced radulae, the plumes manifested as a prominent up-welling from the junction zone into the tooth cusp directly above the stylus canal (Figure 4.15). Notably, plumes were found to coincide with the appearance of orange spotting in the centre of the junction zone region above the stylus canal (Figures 4.10 and 4.12).

The deposition of phosphorous and calcium in the core region of iron-limited and iron-reintroduced radulae, typically occurs over fewer tooth rows compared to normally mineralised radulae, and the transition from initial deposition to the infilling of the core is often abrupt (Figure 4.16). In addition, the lepidocrocite region, which, in normally mineralised radulae, forms prior to phosphorous and calcium deposition, loses its

Figure 4.13. X-ray microanalytical (EDS) spectra demonstrating the presence of elements in the junction zone region in normal, 190 day iron-limited and 8 day iron-reinstated *A. hirtosa* radulae. (Codes: MP, H).

* spectra taken at the junction zone in the tooth row prior to the detection of iron in this region.

** spectra taken at the junction zone in the tooth row where iron is first detected in this region.

*** spectra taken at the junction zone in the tooth row prior to the deposition of iron in the tooth cusps.

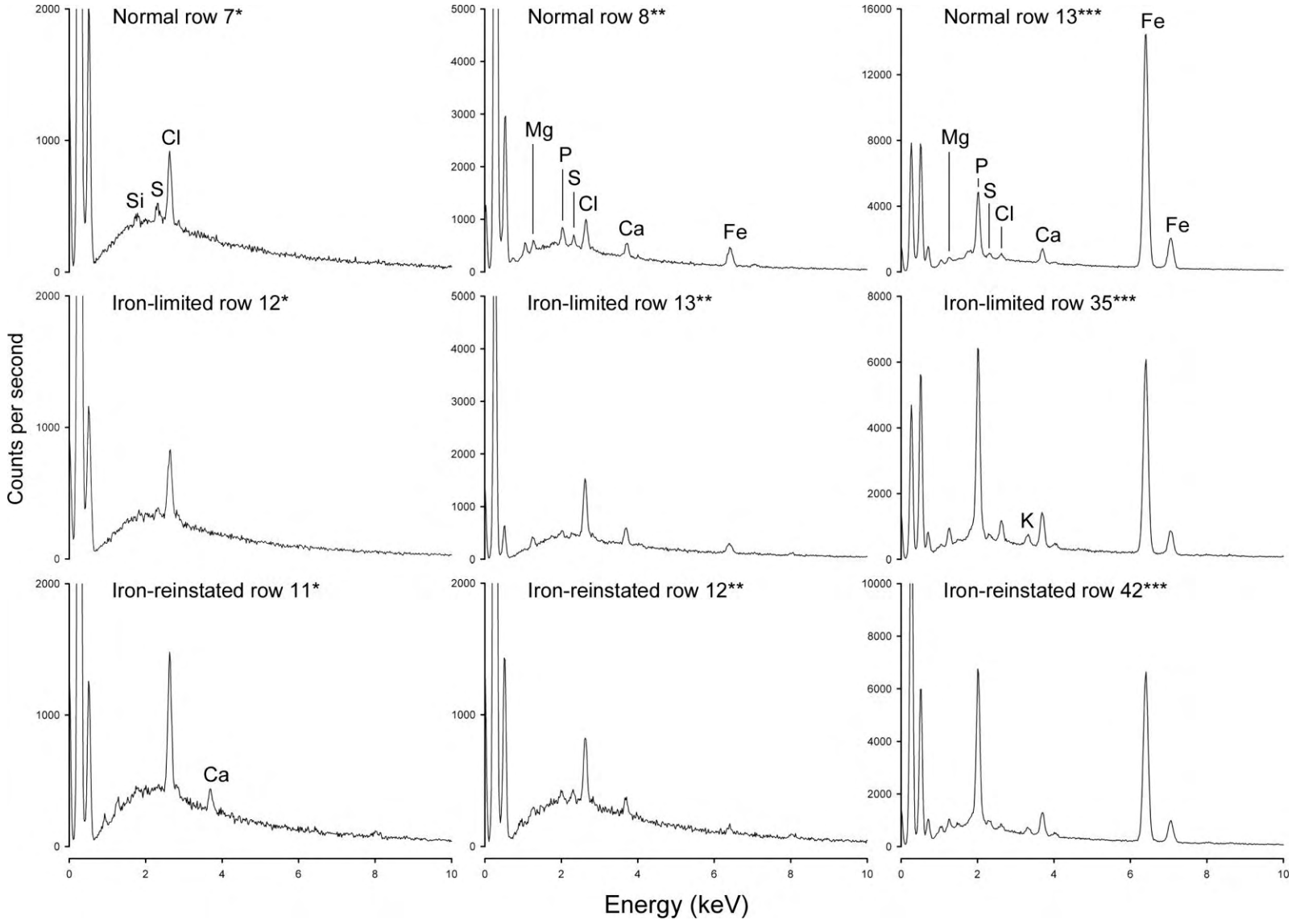
Normal row 7*
Si
S
Cl
Normal row 8**
Mg
P
S
Cl
Ca
Fe
Normal row 13***
Mg
P
S
Cl
Ca
Fe
Iron-limited row 12*
Iron-limited row 13**
Iron-limited row 35***
K
Iron-reinstated row 11*
Ca
Iron-reinstated row 12**
Iron-reinstated row 42***
Counts per second
Energy (keV)

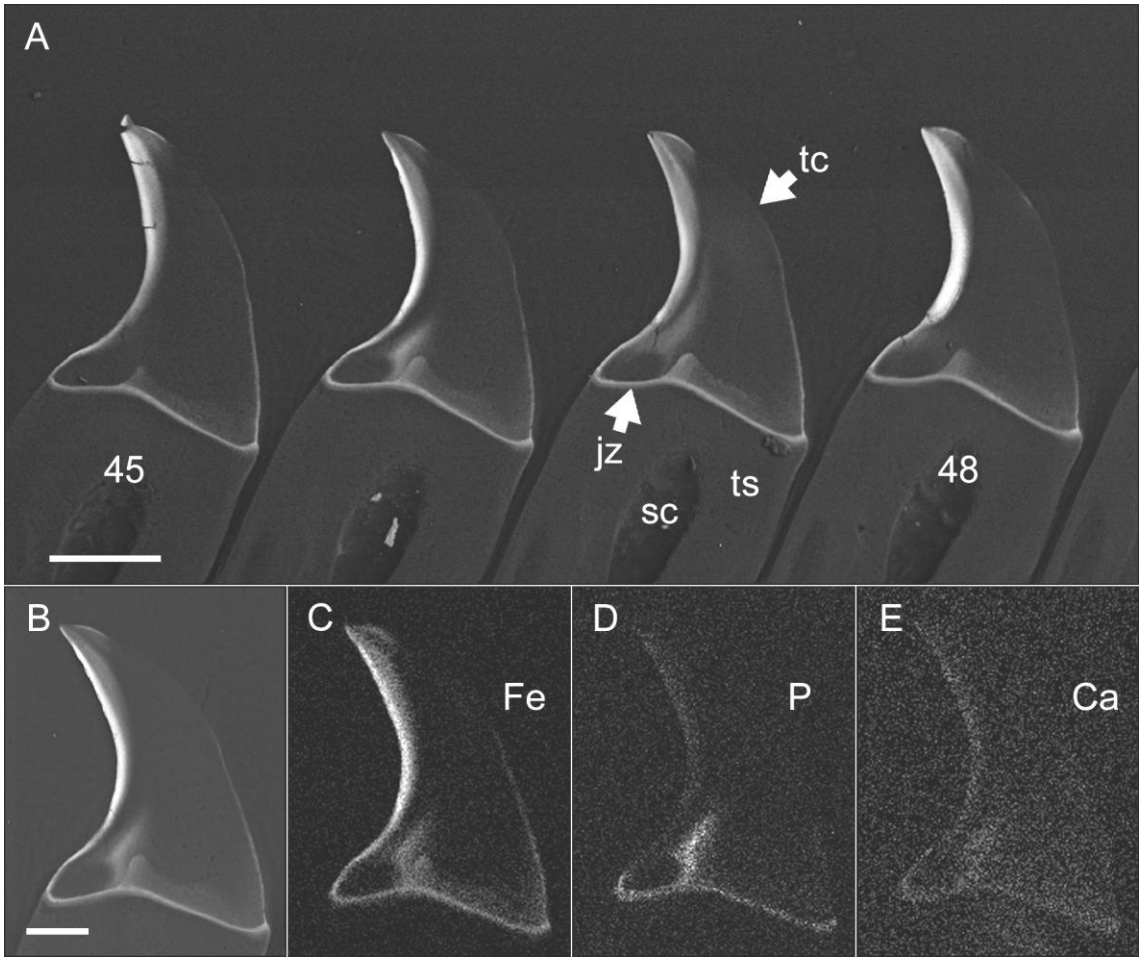

Figure 4.14. Back-scattered scanning electron micrographs of a 3 day iron-reinstated radula from (A) tooth rows 45 to 48 demonstrating the plume of high atomic weight material within the tooth cusp (tc) above the junction zone (jz) and stylus canal (sc). At tooth row 46, (B) a back-scattered image and (C, D, E) elemental maps reveal that the plume contains iron, phosphorous and calcium. ts = tooth stylus. (Codes: MP, H), Scale bars = (A) 100 μm, (B) 50 μm.

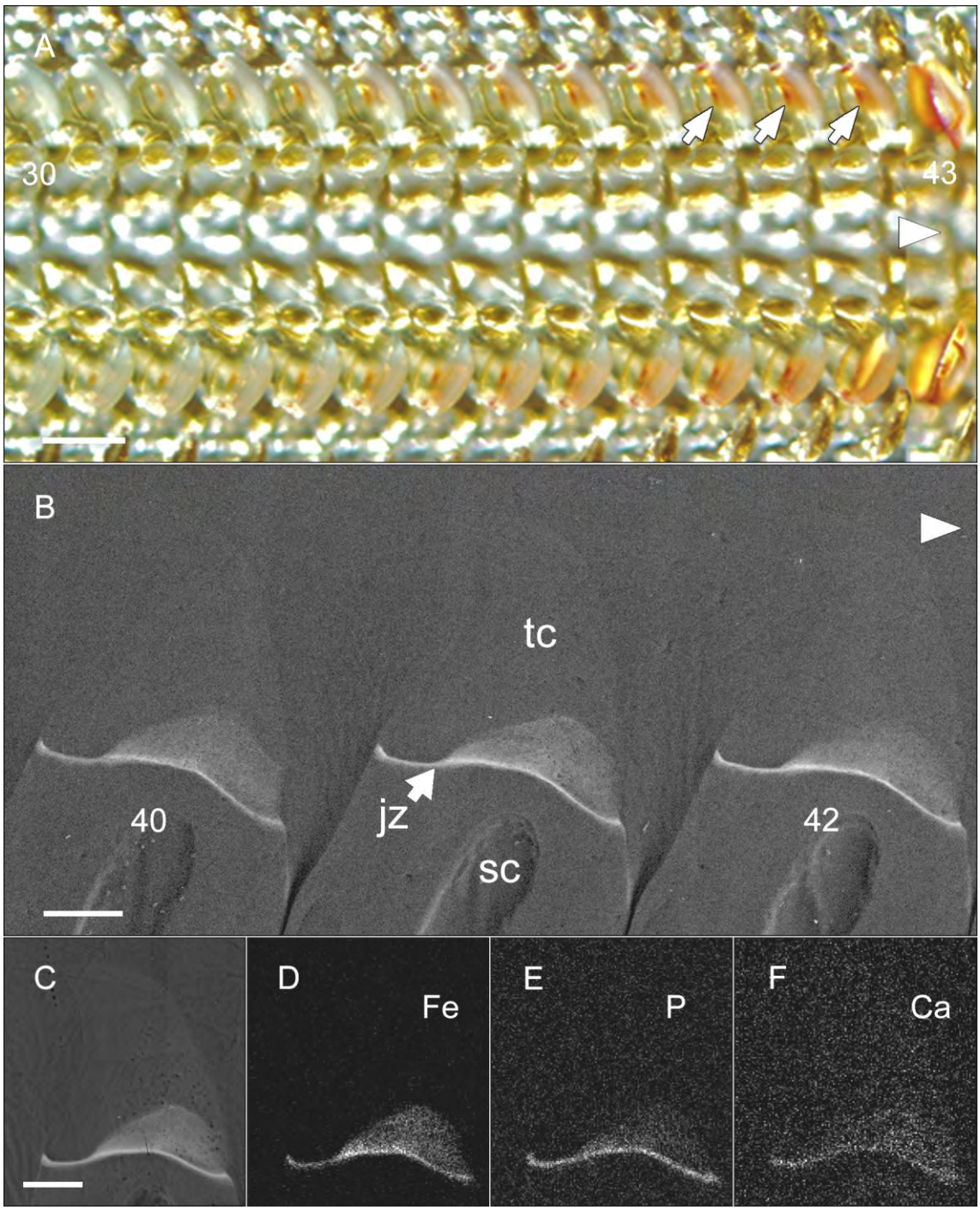

Figure 4.15. Light and back-scattered scanning electron micrographs of an 8 day iron-reintroduced radula, demonstrating plumes of material within the tooth cusps (tc) of *A. hirtosa*. (A) Orange spotting (arrows) is evident in the centre of the cusps between tooth rows 30-43 and corresponds to (B) up-welling from the junction zone (jz) above the stylus canal (sc). At tooth row 41, (C) the back-scattered image and (D, E, F) elemental maps reveal that the up-welling contains iron, phosphorous and calcium. (Codes: (A) A; (B – F) MP, H), Scale bars = (A) 200 μm, (B – F) 50 μm.

association with the change in window opacity, and does not become apparent until after the deposition of elements in the core is initiated. Notably, the average number of tooth rows from the orange tooth cusp to the point at which core mineralisation is initiated, and to where the anterior window region of the cusp becomes opaque, is similar for normal (core 21, SD = 1, n = 6) (window 18, SD = 1, n = 12), iron-limited and iron-reinstated animals (core 21, SD = 5, n = 10) (window 19, SD = 3, n = 10) (Figure 4.8).

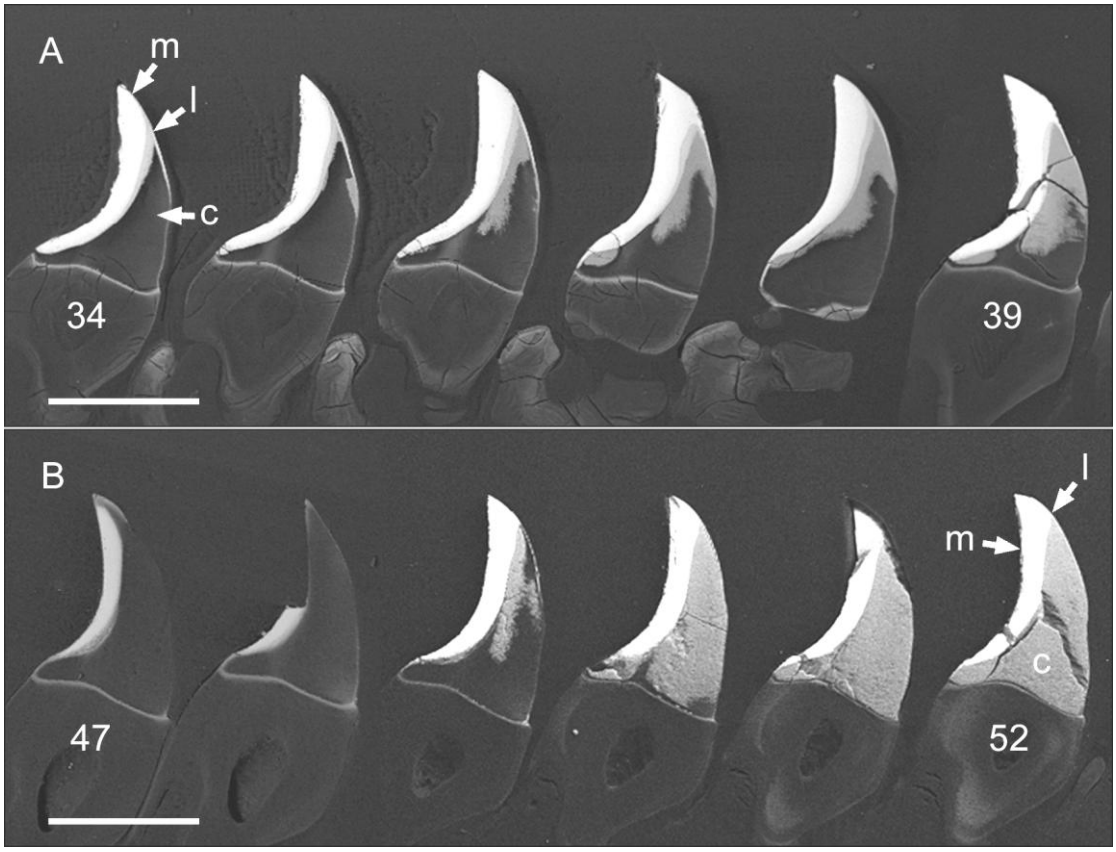

Figure 4.16. Back-scattered scanning electron micrographs comparing core (c) mineralisation in (A) a normal radula and (B) an iron-limited radula. Note the prominent layer of lepidocrocite (l) between the magnetite (m) region and the core of normally mineralised teeth and the absence of this region in rows 47-51 for the iron-limited radula. Also note the decrease in the number of rows over which the core is in-filled in the iron-limited radula compared to the normal radula. (Codes: (A) CP, H; (B) MP, H), Scale bars = 200 μm.

4.4. Discussion

This thesis shows that, in the chiton *A. hirtosa*, the initial deposition of elements required for tooth biomineralisation occurs at the junction zone, from where they are subsequently transferred, potentially via a plume of material, to the various mineralising fronts within the tooth cusp. Iron, phosphorous and calcium enter the junction zone six rows prior to the onset of mineralisation in the cusp. This finding is consistent with reports for the seven other chiton species that have been examined to date (see for example: Macey and Brooker, 1996; Lee *et al*., 2000; Brooker and Macey, 2001; Brooker *et al*., 2003). As such, the accumulation of elements at the junction zone appears to be a critical step prior to the formation of all mineral types in the teeth of these animals. Sections stained with Perl's Prussian blue confirm that iron is present in the posterior region of the tooth cusps at row 13, just prior to the orange tooth. Notably, this also coincides with the appearance of large quantities of ferritin in the cusp epithelium at tooth row 13, and the formation of a previously undescribed plume above the junction zone. As such, row 13 would appear to be the point at which the mass transfer of iron into the tooth cusp from both the junction zone and superior epithelium is initiated, thereby triggering the iron mineralisation process in normal animals.

Iron-limitation and reinstatement experiments have revealed further valuable evidence in relation to the importance of the junction zone in tooth cusp mineralisation. Perhaps the most significant finding is the continued presence of mineralising elements within the junction zone in both iron-limited and iron-reinstated individuals, despite an increase in the number of unmineralised tooth rows. This preferential deposition suggests that elements supplied to the junction zone are delivered via an alternative pathway to that of the cusps. This was also proposed by Nesson (1969), who used Fe^{59} to reveal that the tooth bases of the chiton *Mopalia muscosa* have a higher specific activity for iron compared to the cusps. However, it is difficult to determine whether

Nesson's analysis resulted from iron being deposited at the junction zone or the tooth bases, as the junction zone material may have remained attached to the bases after fracturing away the cusps.

It is likely that the preferential delivery of iron to the junction zone is due to the presence of one or more proteins with higher binding potentials for this element relative to the remainder of the tooth. By acting as a reservoir for elements, the junction zone is therefore able to facilitate the attainment of a critical density of iron and other elements needed to trigger the precipitation of ions and the onset of mineralisation in the cusps. In effect, the plate-like junction zone provides a platform for the delivery of elements into the cusps; working in concert with the external surfaces in contact with the superior epithelium. Maintaining control over each of the surfaces bordering the extracellular compartment of the tooth cusp may assist in regulating the solution chemistry within the macromolecular framework of the cusps. Control over properties of the mineralising environment, such as solubility, pH and ion supersaturation, is crucial for regulating mineral precipitation (Mann, 2001).

In the present study, the plume of iron, phosphorous and calcium within the tooth core establishes a direct link between the junction zone and a second mineralisation front. Detailed observations of normally mineralised *A. hirtosa* radulae indicate that cusp mineralisation, at row 14, is initiated following an influx of iron from the junction zone along a boundary layer situated between the magnetite and core regions of the tooth at row 13. The magnetite region is rapidly mineralised, and this seems to occur simultaneously on two fronts from both this boundary layer and the posterior cusp face.

The boundary layer situated between the magnetite and core regions of the tooth, appears to correspond to the position of the lepidocrocite region, which forms just prior to the onset of core mineralisation. For this boundary layer to serve as a route for the delivery of elements, it is likely that the organic matrix fibres within this region are

structurally distinct from the remainder of the cusp. Previous studies on the organic matrix in *A. hirtosa* show that fibres in the lepidocrocite region are tightly interwoven and the mineral contained within is resistant to acid treatment, suggesting that this region possesses different physical and/or chemical properties to the rest of the tooth (Evans *et al*., 1990; Evans *et al*., 1994). In addition, immature and demineralised *A. hirtosa* tooth cusps were shown to retain ferritin in this region in preference to other regions of the cusp (Evans *et al*., 1994). It has also been suggested that the lepidocrocite region provides a high density of nucleation sites, which subsequently allows the rapid precipitation of carbonated apatite in the tooth core (Lee *et al*., 2000). Previously, the structure of the fibres in the lepidocrocite region have been proposed to act in preventing crack propagation during the feeding process (van der Wal *et al*., 1989, 2000; Evans *et al*., 1994). However, the different fibre structure in this boundary layer may also be due to its role in iron transport and may, in part, be responsible for controlling the formation of this particular mineral polymorph within this region of the cusp.

In addition to the presence of plumes, the discontinuity in organic matrix structure within the plume region also suggests that this area of the tooth cusp is the main transport pathway for elements between the junction zone and the remainder of the cusp. Evidence for multiple-front mineralisation has been established in the major lateral teeth of *A. echinata*, where the concentration of iron in the magnetite region at the onset of mineralisation was found to be well in excess of that observed after mineralisation had commenced (Brooker *et al*., 2003). It was also demonstrated that iron concentrations were higher on the internal mineralising front compared to that at the cusp face, suggesting that iron transferred internally through the cusp from the junction zone may be the dominant transport process (Brooker *et al*., 2003).

Until recently, the formation of minerals within the tooth was thought to result solely from the delivery of elements by the superior epithelium, which covers the anterior and posterior surfaces of the cusps (Nesson and Lowenstam, 1985; Webb *et al*., 1989) (but see Brooker *et al*., 2003). While the superior epithelium remains a crucial pathway for the delivery of elements into the cusps, a second delivery mechanism supplying elements directly into the tooth core from below would provide a number of advantages. Not only would it assist in rapidly achieving supersaturation and maintaining finer control over mineral formation, but it may also permit the variety in mineral composition, and complexity, observed in chiton teeth.

A supply of mineralising elements from the junction zone would assist in the continued delivery of Fe, Ca and P into the tooth core once transport from the superior epithelium becomes inhibited due to mineral formation in the cusps. Prior to the onset of mineral deposition within the core region, a thick layer of magnetite is already in place between the tooth core and the posterior superior epithelium. This would prevent the movement of elements across the entire posterior cusp surface. In addition, the passage of elements across the anterior face of the cusp may also be limited by the mineral partially covering this surface. It has been demonstrated that the region where the plume extends is the last area of the core to become mineralised. This process could only be facilitated by a supply of elements from the junction zone. As such, the composite nature of the tooth cusp, with its various mineral regions, can be attributed to the supply of elements delivered not only by the superior epithelium, but also from the junction zone.

In addition to the major mineralising elements (iron, calcium and phosphorous), magnesium, sulphur and potassium were also detected at the junction zone. These elements have been reported previously in the major lateral teeth of chitons (see for example: Macey and Brooker, 1996; Okoshi and Ishii, 1996; Brooker *et al*., 2003).

Although the exact role of these elements has not been elucidated, it is likely that some are related to the biomineralisation process. For example, magnesium is known to inhibit the conversion of amorphous calcium phosphate to crystalline hydroxyapatite (Lowenstam and Weiner, 1989), while sulphur has been associated with the tanning of the organic matrix (Macey *et al*., 1997) and is also suggested to influence phase transformations in the iron oxide/hydroxide-mineralisation system (Cornell and Schneider, 1989).

The presence of orange spotting in iron-reinstated animals has also highlighted the point of plume origin, which would have otherwise been masked by the rapid onset of mineralisation in normal animals. Orange spotting is always located at the centre of the junction zone plate directly above the distal terminus of the stylus canal, which strongly suggests that this tube-like conduit situated within the major lateral tooth stylus is also involved in cusp mineralisation (see Chapter 6). In addition, the diminishing size of the orange spots toward the posterior end of the radula suggests that the elements involved in cusp mineralisation are supplied from the anterior end of the radula. In support of this, Nesson and Lowenstam (1985) suggested that an anteriorly located branch of the cephalic blood sinus, which transports hemolymph to the radula musculature, is likely to supply blood to the dorsal sinus (see Chapter 5). The anteriorward progression of new radula material, and posteriorward supply of elements, is analogous to various counter-current physiological systems observed in nature (for example see: Randall *et al*., 1997).

Importantly, in iron-reinstated animals, iron first reappears at the internal mineralising front, and in plumes at, or near, the first black teeth, and not at the posterior end at row 14, as in normally mineralised radulae. This indicates that although mineral formation in normal radulae occurs in sequence over well defined stages, these stages are not limited to discrete regions, but instead, the cusps are capable of becoming

mineralised at any point along the entire length of the radula. In addition, because plumes were far more apparent in normal and iron-reinstated animals compared to iron-limited individuals, it is likely that the release of iron stored at the junction zone is dependent on the levels of iron available elsewhere within the radula. The sequential nature of mineralisation events occurring along the radula, and the control exhibited in the face of iron-limitation, both hint at the underlying influence of the cells surrounding the tooth cusps, and their importance in mediating tooth mineralisation at the molecular level.

The initiation of phosphorous and calcium deposition within the core region of the tooth also occurs at a precise point along the radula, and appears to coincide with the completion of iron deposition, which is consistent with studies of mineralisation in other species (see for example: Macey and Brooker, 1996; Lee *et al*., 2000; Brooker and Macey, 2001; Brooker *et al*., 2003). Once the lepidocrocite region is formed, phosphorous and calcium begin to flow from the junction zone into the tooth core. Apatite forms firstly at the top of the core, after which the mineralising front progressively moves downward, leaving the plume region as the last area to become mineralised. A similar pattern of core mineralisation occurs in the chiton *A. echinata* (Lee *et al*., 2000). However, in this species, the final stage of mineral deposition in the core was observed towards the anterior tooth surface, above the junction zone. It is possible that the presence, and therefore infilling, of the plume region in *A. echinata* was missed due to differences in sample orientation, as the teeth must be aligned such that the sagittal plane of the cusp is exposed (ie. directly above the distal tip of the stylus canal). It is unclear how the transport of elements along the boundary layer switches from iron to calcium and phosphorous. It is likely that this switch is made at the junction zone, which would, in turn, be under molecular control from either the cusp epithelium or the stylus canal tissue. The complexity of this region is evident, and

warrants further study to elucidate both its structural and functional role in cusp mineralisation.

Of interest is the consistent number of tooth rows occurring between the first row of black teeth and the onset of calcium and phosphorous mineralisation within the core, which was similar for normal, iron-limited and iron-reintroduced radulae. If core mineralisation was maintained during the iron-limitation treatment, the number of tooth rows between the first black row and the onset of core mineralisation would be expected to decline. As this was not the case, core mineralisation must also be suspended as a result of the iron-limitation procedure. However, a number of cusps may be sufficiently mineralised with iron such that core mineralisation continues for a short period following the suspension of iron mineralisation. This is made evident in iron-limited and iron-reinstated animals where core formation commenced despite the absence of the lepidocrocite layer. For this to occur, it is likely that core mineralisation continued briefly, despite the fact that the delivery of iron from the junction zone had ceased. This is also supported by the presence of only a thin layer of iron on the posterior cusp surface of iron-limited and iron-reinstated animals, suggesting that mineralisation had occurred from only a single front via the superior epithelium. As suggested, it is likely that the triggers for various mineralisation events along the radula are driven by proteins that are, in turn, regulated by the levels of elements in the tissues and tooth cusps. Iron-limitation may therefore be a useful tool for molecular studies aimed at isolating the proteins associated with tooth mineralisation, and for determining their regulation and expression.

A relatively abrupt shutdown of mineralisation as a result of iron-limitation is also supported by the sudden appearance of phosphorous and calcium in the core, which, in normally mineralised radulae, occurs gradually over a number of tooth rows. Preliminary results, using quantitative X-ray analysis (EDS), also show that a similar

effect occurs for iron in the magnetite region. Once cusp mineralisation is discontinued, the only remaining active pathway seems to be the delivery of elements to the junction zone, which once again emphasises the fundamental importance of this region in cusp mineralisation.

Chapter 5

The Superior Epithelium: Development and Iron Delivery

5.1. Introduction

While significant progress has been made in elucidating the structure and composition of the iron-mineralised tooth cusps of chitons and limpets, the cellular basis for biomineralisation remains poorly understood. This is particularly true of the extent to which chemical control is exerted by the tissues involved in the manufacture of biomineralised structures, and how they influence processes such as solubility, supersaturation and nucleation. Maintaining control over these three factors is crucial for regulating inorganic precipitation onto the organic matrix, and subsequent crystal growth (Mann, 2001).

An excellent description of the superior epithelial tissues, in the chitons *Lepidochitona hartwegii* and *Mopalia muscosa*, has been provided by Nesson and Lowenstam (1985), which includes a detailed summary of the principle findings made in Nesson's Ph.D. (1969). A number of researchers have since made further observations on the superior epithelium of chitons (including that of *Acanthopleura hirtosa*) and limpets, with particular emphasis on the iron-containing granules within the tissues, and the various stages of mineral deposition within the cusps (see for example: Mann *et al*., 1986; Kim *et al*., 1989; Rinkevich, 1993). However, the nature of the physiological mechanisms by which the cells exert control over mineral deposition remains a fundamental question with respect to the biomineralisation processes in these animals.

In order to address this current gap in our understanding, a detailed LM and TEM study of the tissue surrounding the major lateral teeth of the chiton *A. hirtosa* has been undertaken, with particular focus on the row-by-row development of the apical region of the cusp epithelium and the tooth organic matrix. In addition, the iron-limitation

technique utilised in Chapters 3 and 4 has been employed in a comparative study of the apical cusp epithelium, and organic matrix, of radulae from normal, iron-limited and iron-reinstated animals. Detailed observations on the sequential development of the various organelles contained within the apical epithelium have been made, and are discussed with reference to their role in mediating the deposition of minerals within the extracellular compartment of the tooth cusp.

5.2. Materials and Methods

5.2.1. *Normal epithelial development*

Specimens of *A. hirtosa* were collected fresh from the study site and processed for LM and TEM using either conventional bench-top, or microwave-assisted, protocols (Chapter 2.3). Due to the incorporation of hard mineral deposits into the tooth cusps, it is not possible to obtain sections from tooth rows 19 onwards, as such, this study focuses on epithelial development from tooth rows 10 to 18, which encompass four tooth rows anterior and posterior to the orange tooth at row 14.

For energy-filtered TEM imaging and analysis (see for example, Thomas and Midgley, 2002), 100-120 nm thick resin sections were cut on a diamond knife (Diatome™), and mounted on formvar-filmed or holey-carbon-filmed copper grids. All imaging and analyses were conducted at 300 kV in a JEOL 3000F Field Emission TEM fitted with a Gatan Image Filter (GIF). Elastic-filtered images were acquired by centring the GIF's energy-selecting slit on the zero-loss peak of the EELS spectrum, with a slit width of 40 eV. Iron elemental maps were obtained using the iron K-edge and generated using the conventional three-window method (see for example, Brydson, 2001). The pre-edge (background) images were acquired at energies of 643 eV and 683 eV, and the post-edge Fe K peak image at 728 eV. A slit width of 40 eV and acquisition time of 30 s was used for all images. All energy-filtered TEM data were acquired from sections that were unstained.

5.2.2. *Iron-limited and iron-reinstated epithelial development*

Five specimens of *A. hirtosa*, which had been maintained for a period of 143 days in the iron-limited system outlined in Chapter 4.2.2, were prepared for observations at the LM and TEM level. In addition, the three specimens of *A. hirtosa* removed for the study of epithelial tissues in Chapter 4.2.2, which had been iron-limited for a period of 190 days, and three further specimens, removed following 8 days of iron-reinstatement, were also examined for changes in epithelial development at the LM level.

5.2.3. *Observations of the organic matrix*

Observations of the organic matrix were made on sections prepared for TEM from normally mineralised and 143 day iron-limited animals.

5.3. Results

5.3.1. *Normal epithelial development*

Light microscopy of the radula superior epithelium from the chiton *A. hirtosa* highlights the intense staining of the cusp epithelium, the cells of which originate from the dorsal sinus and terminate on both the anterior and posterior surfaces of each major lateral tooth cusp (Figure 5.1). The minor epithelium, which stains less intensely, also stems from the dorsal sinus but instead terminates on the surfaces of the minor teeth and major lateral tooth styli. Numerous vesicles can commonly be observed, situated within the apical region of the cusp epithelium of all cells terminating on both the anterior, and posterior, surfaces of each tooth. However, whilst these vesicles can be seen surrounding the entire cusp surface, they tend to be more prominent, and occur most frequently, on the anterior surface of the cusp tip (Figures 5.1 and 5.2). These vesicles can be either abundant, or virtually absent, at the same stage of tooth development in different animals; a pattern consistent for samples prepared using either conventional bench-top or microwave-assisted methods (see Appendix B).

In the vast majority of specimens, cusp mineralisation is initiated at row 14, where the posterior face of the tooth cusp takes on an orange appearance due to the formation of ferrihydrite (Figure 5.1). However, sections stained with Perl's Prussian blue for ferric iron show that large quantities of iron, presumably in the form of ferritin, are present at the basal and apical poles of the cusp epithelium at row 13 (Figure 5.2). Perl's stain also indicates that some iron is present in the cusp epithelium as early as tooth row 7 and is always present at the junction zone from at least tooth row 8 onwards. In addition, the dramatic accumulation of iron, which appears in the cusp epithelium at row 13, coincides with the appearance of iron at the posterior cusp face, along with the formation of a plume of iron in the tooth core that seems to flow from the junction zone to an internal front parallel to the posterior surface of the cusp (also see Chapter 4).

High resolution TEM images reveal that many of the granules in the cusp epithelium at row 14 are comprised of aggregations of circular material of low electron density. These are approximately 12 nm in diameter, with an electron dense core approximately 8 nm in diameter (Figure 5.3A). Such dimensions are consistent with the iron storage protein ferritin. Elemental mapping, by EFTEM, conclusively verifies that these aggregations contain iron, presumably in the form of microcrystalline ferrihydrite (Figure 5.3B). Particles of similar size can be observed within the cytoplasm in close proximity to the ferritin aggregates (siderosomes), and these are likely to be individual ferritin molecules in the process of joining, or being released from, the main granule (Figure 5.4). While numerous granules are visible within the cusp epithelium, high resolution TEM and direct elemental mapping have also revealed the presence of granules with a more amorphous internal structure that do not contain iron (Figure 5.5). In addition, some granules exhibit internal variation in electron density due to the presence of a mixture of iron-containing and amorphous material (Figure 5.6). For the purposes of this thesis, all future reference made to the presence of granules in the cusp epithelium refers to all of the above mentioned granule types.

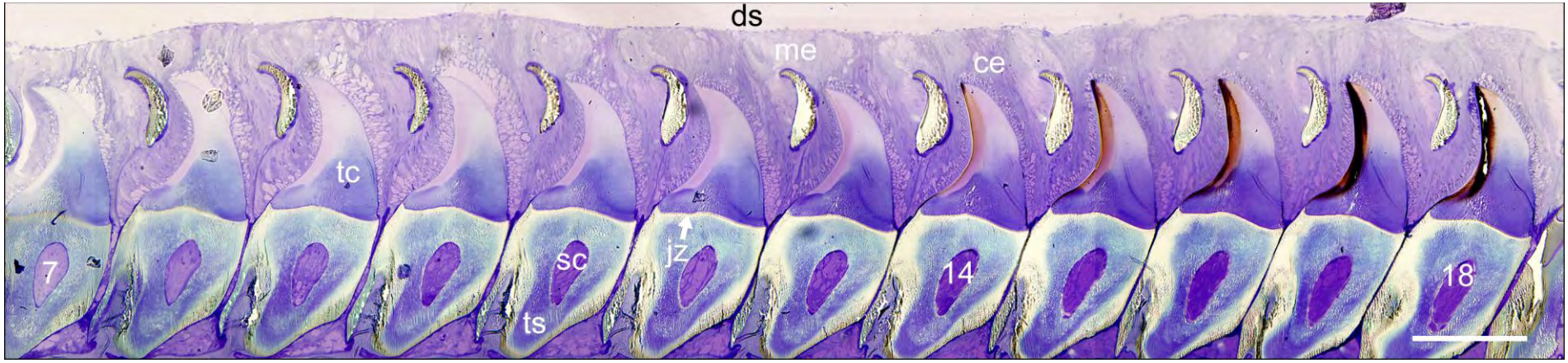

Figure 5.1. Light micrograph of tooth rows 7 to 18 from the radula of *A. hirtosa* orientated longitudinally, with the major lateral tooth cusps in medial section. The four main components of each major lateral tooth, including the tooth cusp (tc), tooth stylus (ts), stylus canal (sc) and junction zone (jz), are clearly represented, together with the intensely staining cusp epithelium (ce), and the lighter staining minor epithelium (me), which both stem from the dorsal sinus (ds) and terminate on the major lateral tooth cusps or minor teeth and tooth styli, respectively (stained with methylene blue and azur II). The onset of mineralisation is apparent at tooth row 14, where the posterior face of the cusp becomes orange in colouration and is subsequently blackened as the cusps become progressively mineralised with magnetite. (Codes: MP, B), Scale bar = 200 μm.

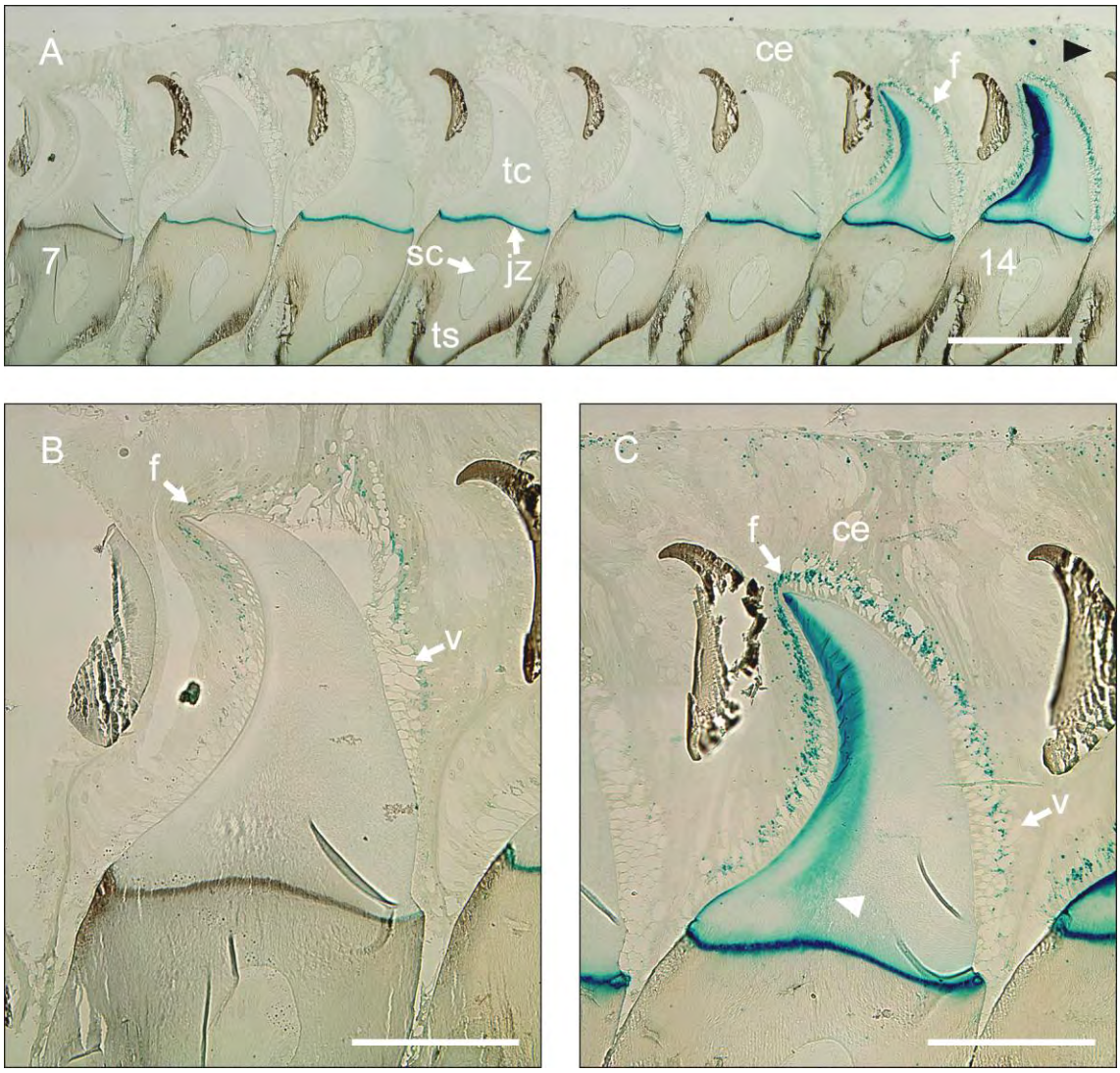

Figure 5.2. Light micrograph of the same radula as in 5.1 stained with Perl's Prussian blue for ferric iron, showing (A) the distribution of ferric iron in the cusp epithelium (ce), tooth cusp (tc) and junction zone (jz). Aggregations of iron containing granules (f), identified as ferritin, are evident within the cusp epithelium at (B) tooth row 7 and (C) later at tooth row 13, where heavy iron accumulation occurs prior to the orange tooth at row 14. Also note the (B) vesicles (v) distributed over the anterior and posterior cusp surfaces, the (C) presence of iron in the posterior region of the cusp, and the associated plume formation (white arrowhead) at row 13. Black arrowhead in A = anterior direction. (Codes: MP, B), Scale bars = (A) 200 μm and (B and C) 100 μm.

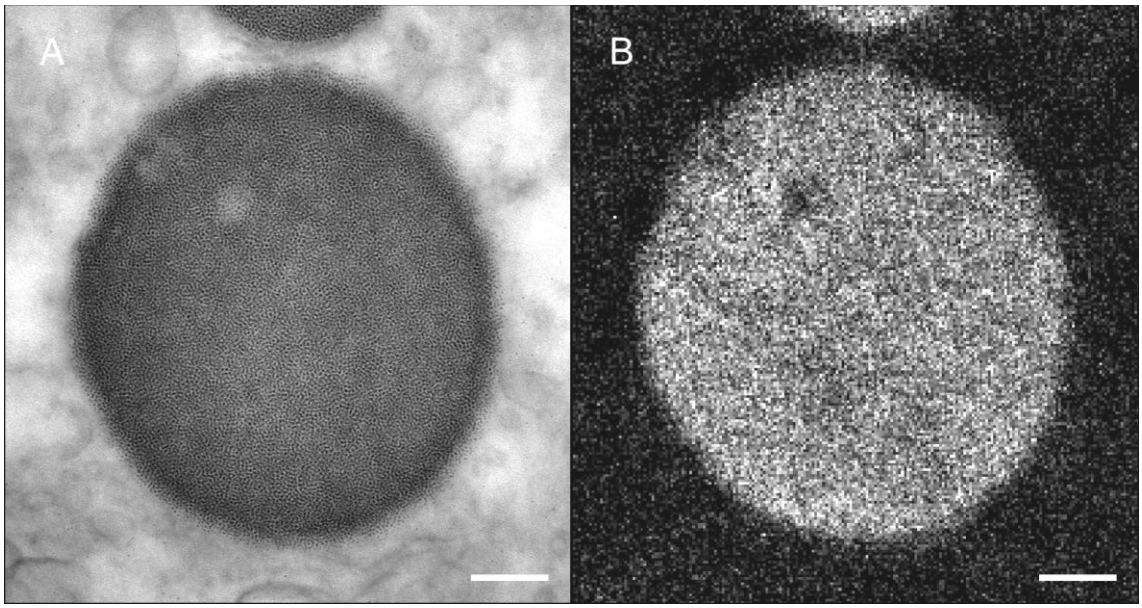

Figure 5.3. TEM micrographs of a typical ferritin granule (siderosome) from the cusp epithelium at tooth row 14 in *A. hirtosa*, highlighting (A) the substructure of electron dense microcrystallites, and (B), the presence of iron as revealed in the associated EFTEM Fe map. (Codes: MP, E), Scale bars = 20 nm.

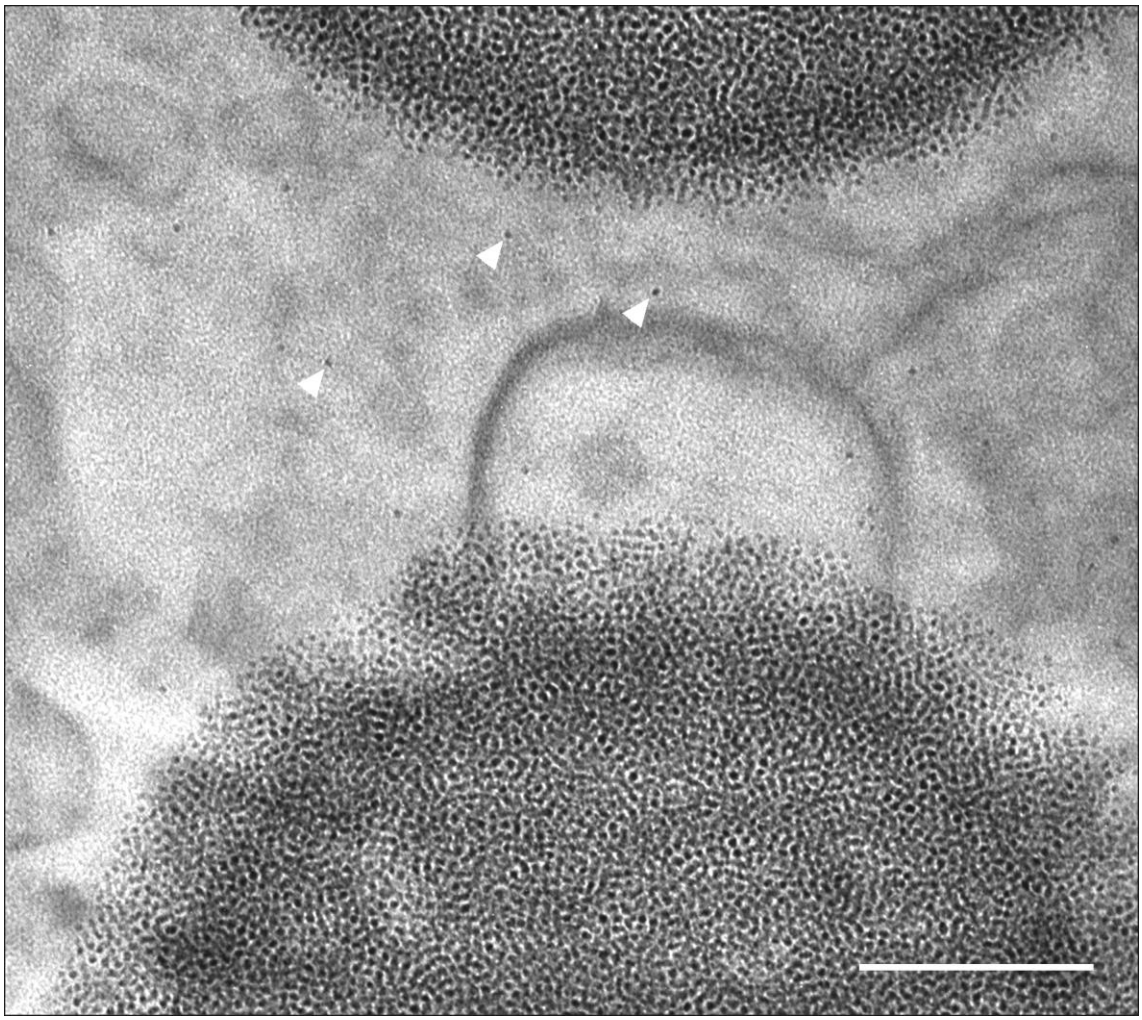

Figure 5.4. TEM micrograph highlighting isolated 8 nm electron dense microcrystallites (arrowheads) between two ferritin siderosomes within the cytoplasm of the cusp epithelium at tooth row 14 in *A. hirtosa*. (Codes: MP, E), Scale bar = 200 nm.

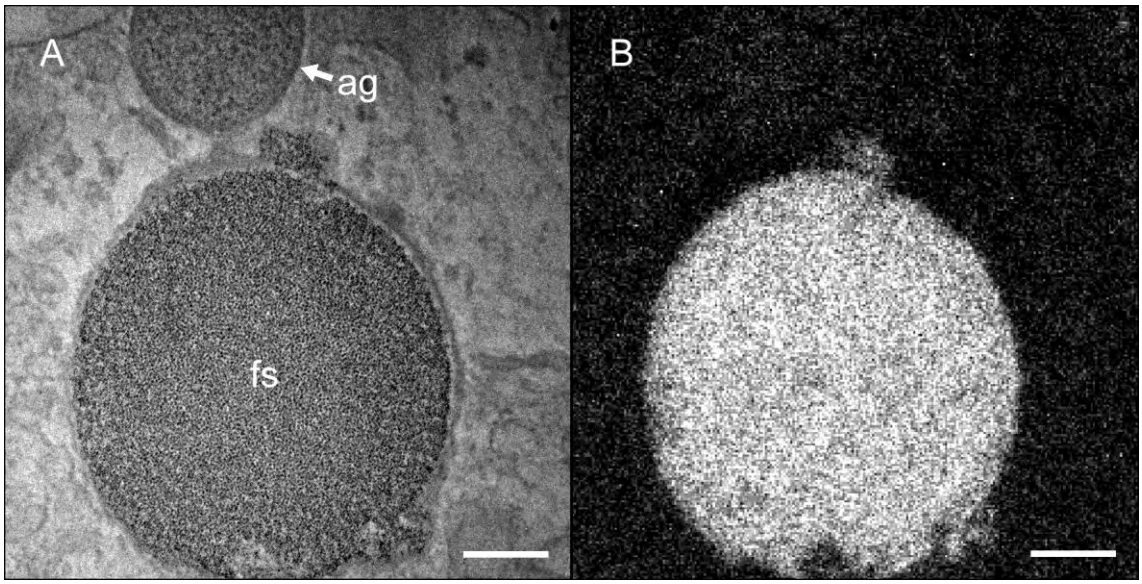

Figure 5.5. TEM micrographs of (A) a ferritin siderosome (fs), and an amorphous granule (ag), together in the cytoplasm of the cusp epithelium at tooth row 14 in *A. hirtosa*, and the (B) corresponding iron map, highlighting the difference in elemental composition between the two granules. (Codes: MP, E), Scale bars = 200 nm.

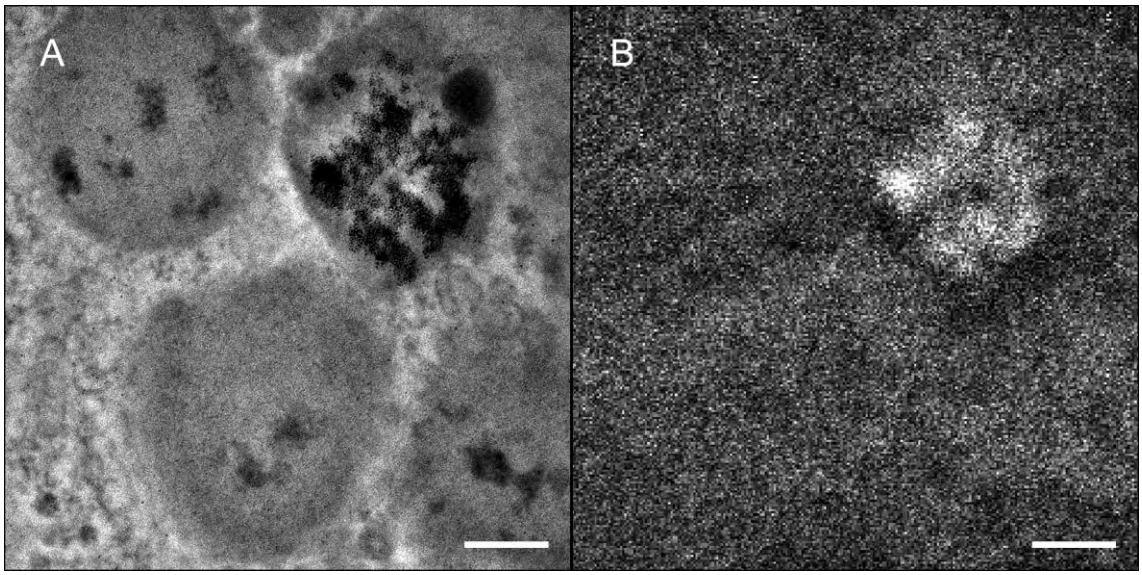

Figure 5.6. TEM micrographs of granules within the cusp epithelium at tooth row 14 in *A. hirtosa*, showing (A) variations in electron density within individual granules that, in the case of the upper right granule, is due to (B) the presence of iron as evidenced by the Fe map. (Codes: MP, E) Scale bars = 200 nm.

The cusp epithelium surrounding the major lateral teeth of *A. hirtosa* is columnar, and contains organelles that are typical of other epithelia bordering extracellular compartments. A prominent nucleus is located towards the apical half of the central region of each cell, such that the nuclei form a distinct band 40-50 μm from the cusp surface. The apical end of each cell, which can be defined as the area between the nucleus and the cusp surface, can be divided into a number of distinct regions, some of which undergo change as tooth maturation progresses (Figure 5.7). The first of these regions lies directly apically to the nucleus of each cell, and contains a system of well developed rough and smooth endoplasmic reticulum, together with a number of Golgi bodies. The next region is comprised of numerous electron dense granules, within which the various iron containing, and amorphous, granules described above aggregate. The final region contains numerous mitochondria that are situated in close proximity to microvilli, which are, in turn, attached to the anterior and posterior surfaces of the tooth cusps and project, to varying degrees, into the apical cytoplasm. The limit of cusp epithelial attachment can easily be distinguished by the presence of the microvilli region, which abruptly disappears at the junction zone (Figure 5.8).

At tooth row 10, four rows prior to the onset of mineralisation, relatively few granules are present within the cusp epithelium, and the microvilli are relatively undeveloped, appearing as small interdigitating membranes extending only 1-2 μm into the cell cytoplasm (Figure 5.9). Junctional complexes, common to epithelial cells, are present, as evidenced by the presence of zonula adherens, and which are situated approximately 2 μm from the apical terminus of each cell membrane (Figure 5.10). Notably, the organic matrix fibres within the tooth cusp can also be observed, and are consistently orientated towards the cusp tip at an angle of approximately 60^{o} relative to the posterior surface of the tooth. At tooth row 11 the cusp epithelium remains similar to the previous row in terms of the number of granules and the development of the

Figure 5.7. TEM micrograph of the apical cusp epithelium between the nuclei (n) and the surface of the tooth cusp (tc), illustrating the general cell ultrastructure in the chiton *A. hirtosa*. Three distinctive regions are present, the first of which contains well developed endoplasmic reticulum (er) and Golgi apparatus (gl). Further towards the tooth cusp is a region that contains numerous granules (g) (depending on the stage of cusp development) of varying electron density and iron content. The region closest to the tooth cusp contains a system of microvilli (mv) that change in appearance as tooth maturation progresses, and are surrounded by varying numbers of mitochondria (mt). (Codes: CP, C), Scale bar = 5 μm.

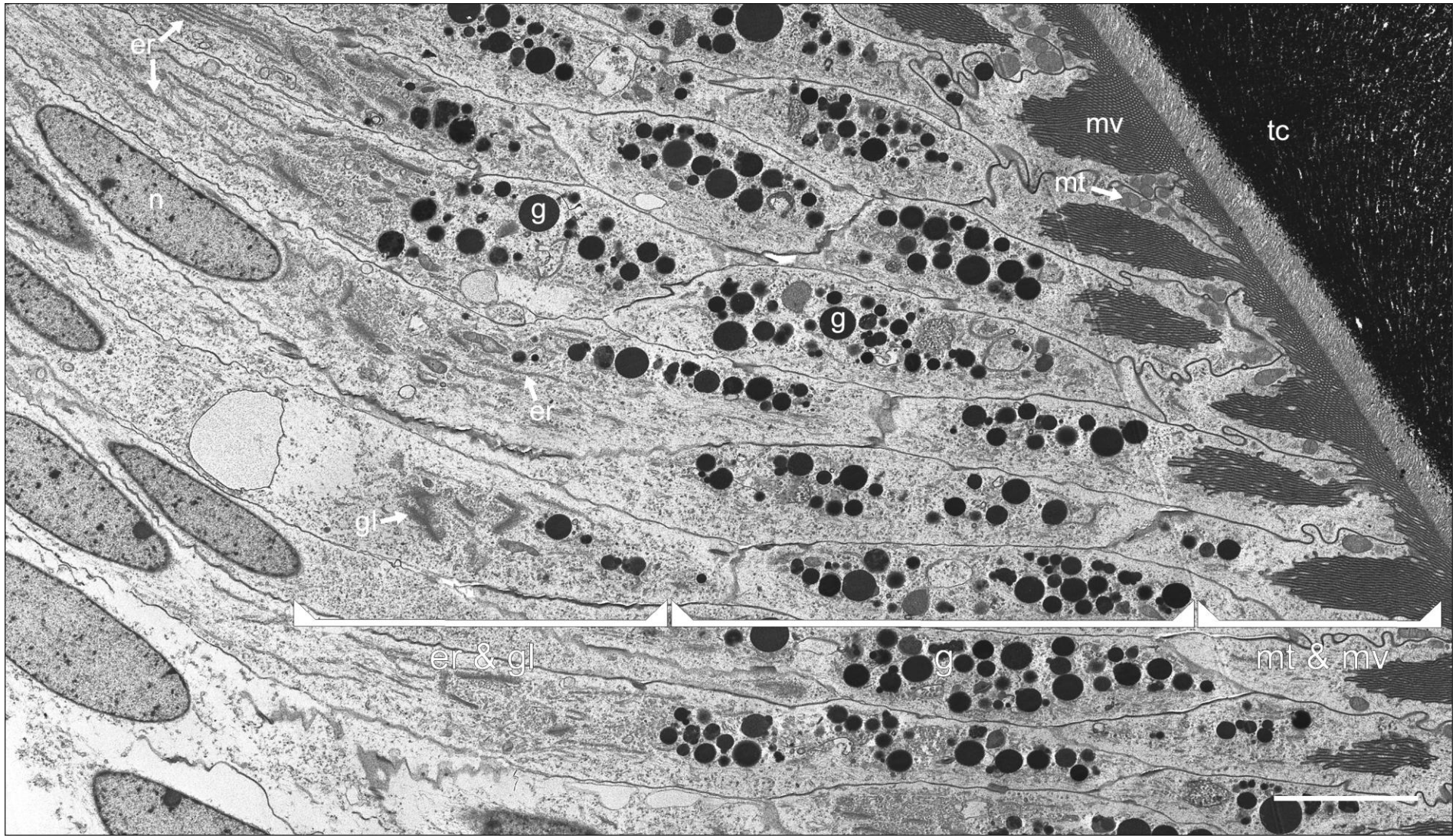
er
n
g
mv
tc
mt
g
er
gl
er & gl
g
mt & mv

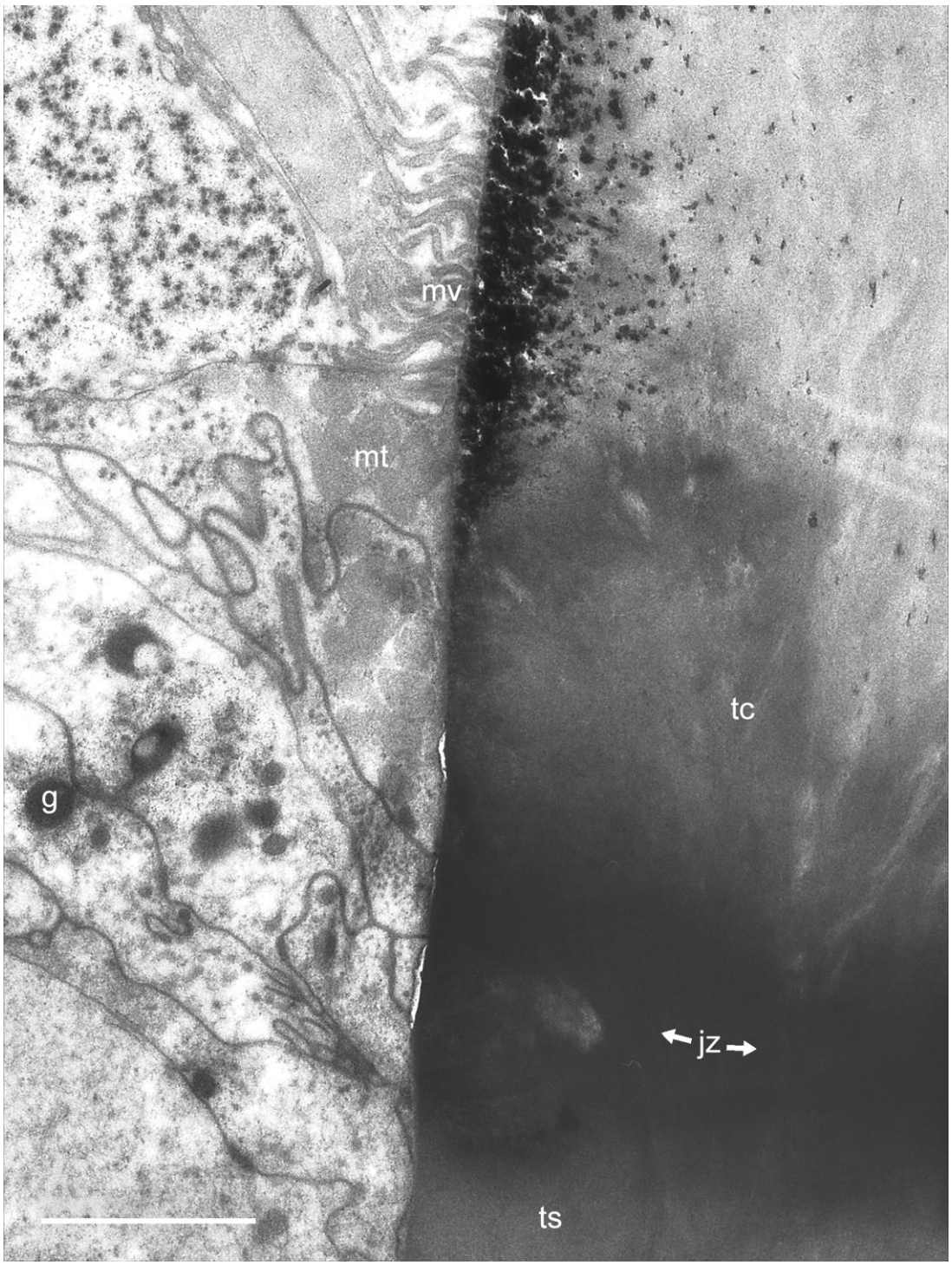

Figure 5.8. TEM micrograph of the posterior surface of a major lateral tooth cusp (tc) from *A. hirtosa* at row 14 where it joins to the tooth stylus (ts) at the junction zone (jz). Note that the microvilli (mv) associated with the deposition of iron into the cusps do not extend to the junction zone region. g = granule, mt = mitochondria. (Codes: MP, D), Scale bar = 2 μm.

Figure 5.9. TEM micrograph demonstrating the appearance of the cusp epithelium at tooth row 10, four rows prior to the onset of mineralisation in *A. hirtosa*. Only a small number of granules (g) are apparent within the tissue and the microvilli (mv) are relatively undeveloped. mt = mitochondria, n = nucleus, tc = tooth cusp. (Codes: CP, C), Scale bar = 20 μm.

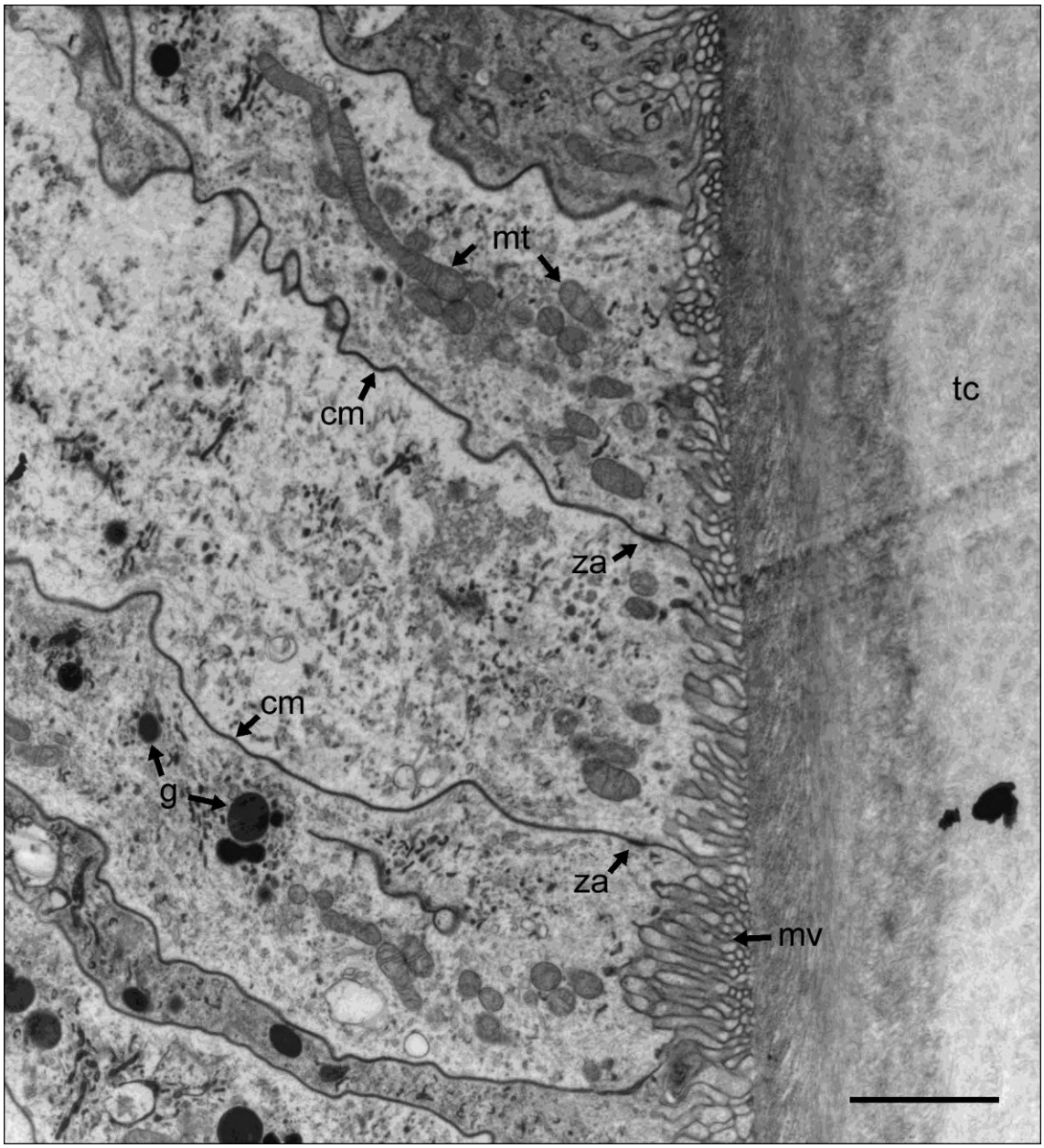

Figure 5.10. TEM micrograph of the apical region of the cusp epithelium at tooth row 10 highlighting the various components of the epithelial cells in *A. hirtosa*, including the presence of zonula adherens (za), which occur approximately 2 μm from where the cell membrane (cm) terminates on the surface of the tooth cusp (tc). Granules (g), mitochondria (mt) and relatively undeveloped microvilli (mv) are also evident. Also note the orientation of organic matrix fibres within the outer layer of the cusp surface, and which appear to extend towards the cusp tip at an angle of approximately 60^{o}. (Codes: CP, C), Scale bar = 2 μm.

microvilli. However, an increasing number of mitochondria can be observed above the microvilli, particularly towards the cusp tip (Figures 5.11 and 5.12). Development of the cusp epithelium at tooth row 12 is again similar to that of previous rows, although Figure 5.13 highlights the presence of prominent vesicles. The vesicles appear to displace, and disrupt, the normal configuration of organelles and cell membranes within the apical region. The vesicles contain varying amounts of granular material and ground substance, but otherwise have little recognisable structure. By tooth row 13, just prior to the orange tooth, developmental changes begin to occur in the microvilli region, with an increase in both the length, and number, of interdigitating membranes within each cell (Figure 5.14). There is also a dramatic increase in the number of granules and mitochondria within the apical cytoplasm (Figure 5.2 and 5.14).

Evidence of mineral precipitation at nucleation sites is also apparent, with numerous small mineral deposits forming in association with the fibres of the organic matrix (Figure 5.15). These appear to diminish in size further into the tooth cusp. Mineralisation develops rapidly at tooth row 14 and is marked by extensive ferrihydrite formation, giving the tooth its characteristic orange colouration at the LM level (see Chapter 3 and 4). There is also a striking change in the development of the microvilli, which increase to approximately 6 μm in length, and are surrounded by numerous mitochondria (Figures 5.1, 5.2 and 5.16). In addition, there is a further increase in the number of granules within the apical cytoplasm (Figures 5.16 and 5.17). Notably, although mineral formation upon the organic matrix begins at tooth row 14, an approximately 1 μm wide unmineralised border can be observed, which extends along the periphery of the posterior surface of the cusp (Figure 5.16). Crystal formation beyond this border region appears to follow the 60^{o} orientation of the matrix fibres observed in earlier tooth rows. Figures 5.14 to 5.17 also highlight the superior preservation of cell ultrastructure achieved when using microwave-assisted sample

Figure 5.11. TEM micrograph showing the appearance of the cusp epithelium in *A. hirtosa* at tooth row 11, three rows prior to the onset of mineralisation. The tissue is similar in appearance to that of the previous row, with only a small number of granules (g) and undeveloped microvilli (mv). mt = mitochondria, n = nucleus, tc = tooth cusp. (Codes: CP, C), Scale bar = 10 μm.

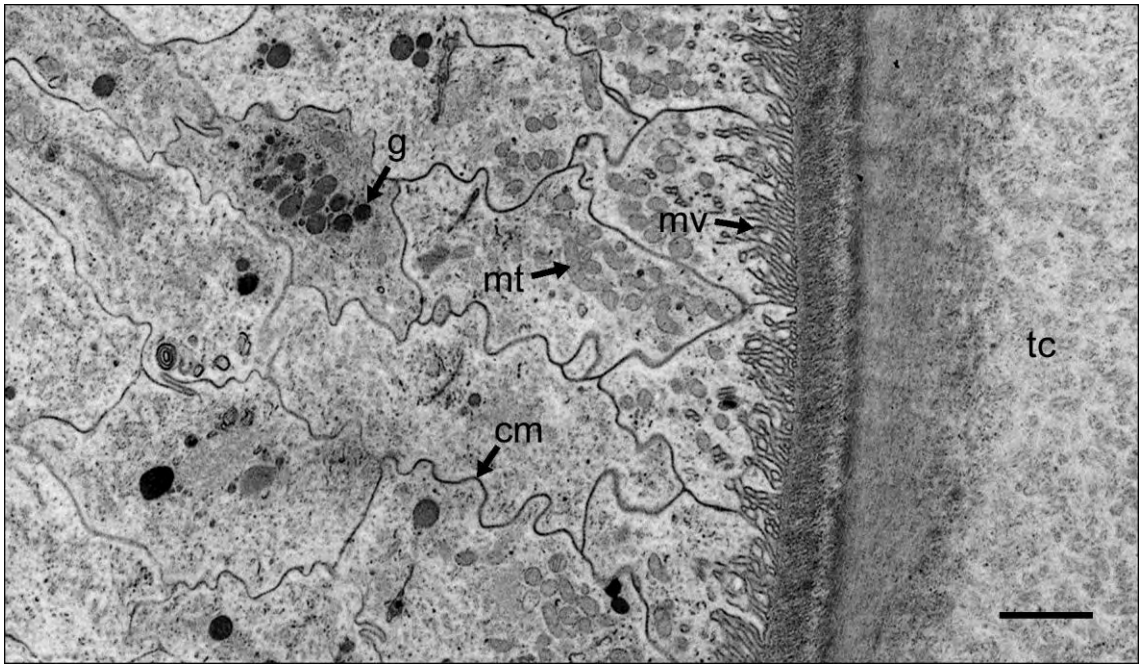

Figure 5.12. Higher magnification TEM micrograph of the same tooth row in *A. hirtosa* as in 5.11 showing the appearance of the apical region of the cusp epithelium at tooth row 11. Note the ~60^{o} orientation of the organic matrix fibres near the cusp surface. cm = cell membrane, g = granule, mt = mitochondria, mv = microvilli, tc = tooth cusp. (Codes: CP, C), Scale bar = 2 μm.

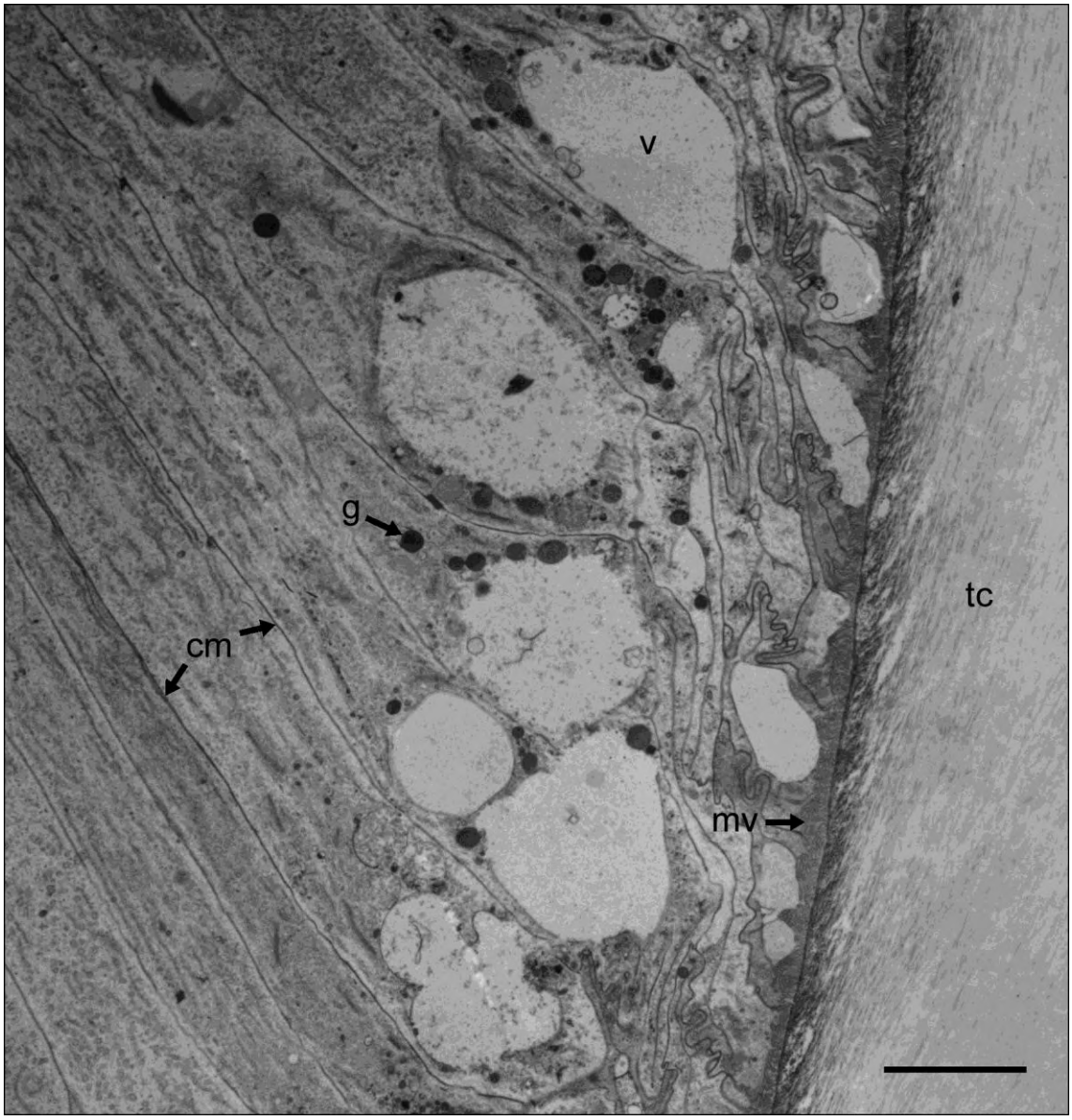

Figure 5.13. TEM micrograph showing the appearance of the cusp epithelium at tooth row 12, two rows prior to the onset of mineralisation in *A. hirtosa*. Large vesicles (v), which are often observed on the anterior and posterior surfaces of cusps at all stages of development, are present, and appear to disrupt the normal configuration of the apical region. Cell membranes (cm) are particularly distorted where vesicles are present. g = granule, mv = microvilli, tc = tooth cusp. (Codes: CP, C), Scale bar = 5 μm.

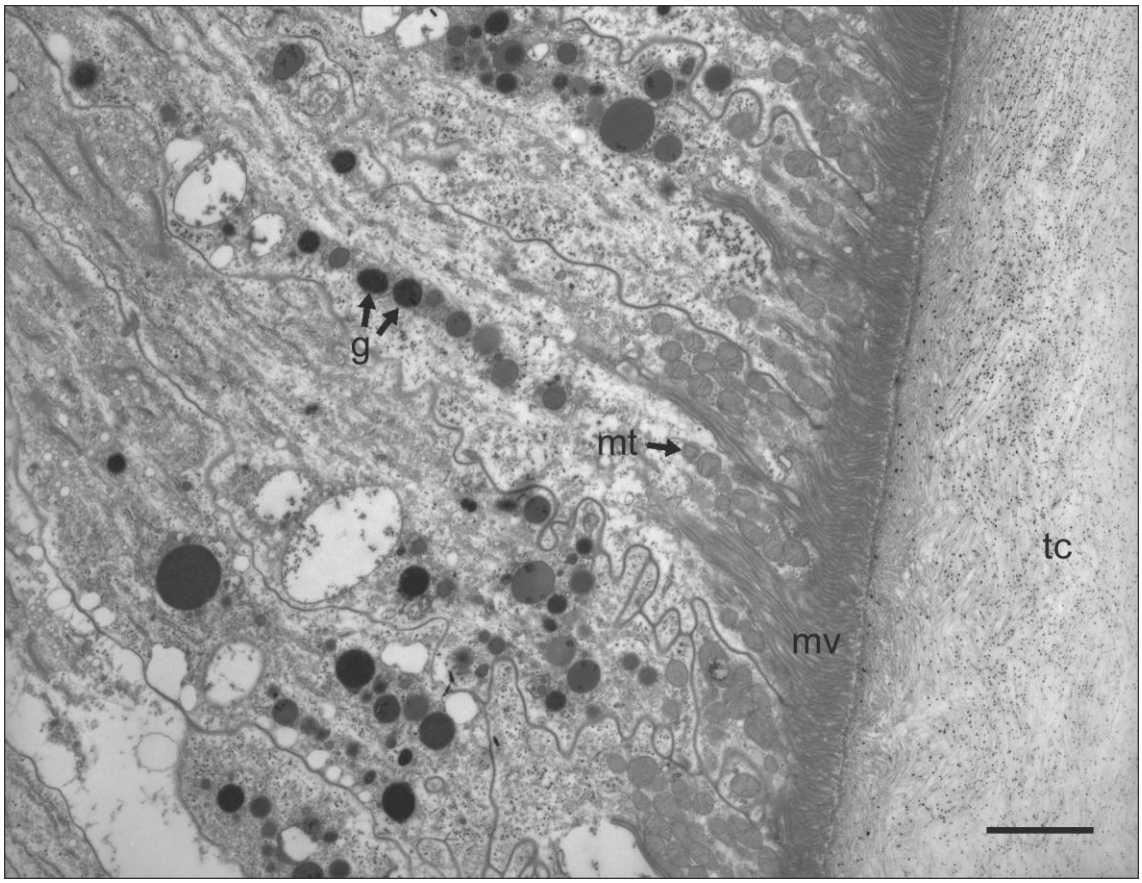

Figure 5.14. TEM micrograph showing the appearance of the cusp epithelium at tooth row 13, one row prior to the onset of mineralisation in *A. hirtosa*. There is a distinct increase in both the number of granules (g) within the apical region and the length and number of microvilli (mv) within each cell. mt = mitochondria, tc = tooth cusp. (Codes: MP, D), Scale bar = 2 μm.

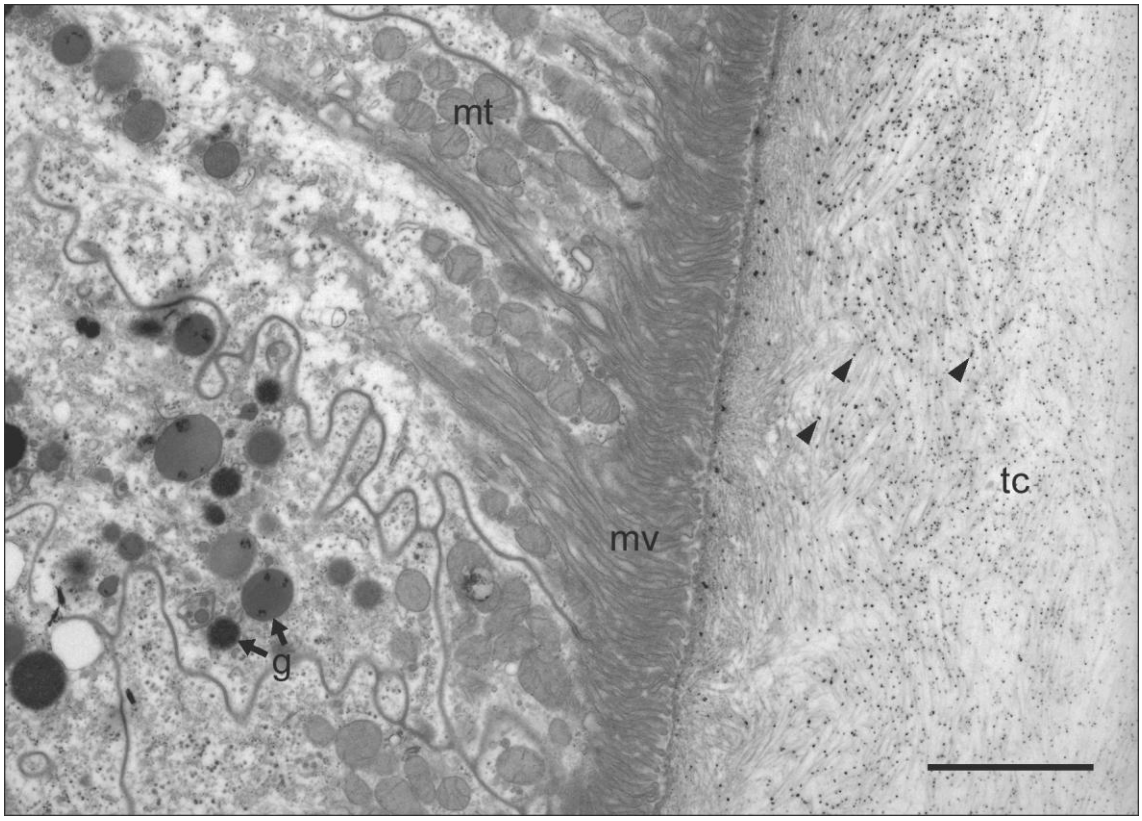

Figure 5.15. High magnification TEM of the cusp epithelium at tooth row 13 showing the initial deposition of mineral at nucleation sites within the organic matrix (arrowheads) in *A. hirtosa*. Note that each of the mineral deposits forms in association with the matrix fibres and appear to become smaller with increasing distance from the cusp surface. g = granule, mt = mitochondria, mv = microvilli, tc = tooth cusp. (Codes: MP, D), Scale bar = 2 μm.

Figure 5.16. TEM micrograph showing the appearance of the cusp epithelium at the onset of cusp mineralisation at tooth row 14 in *A. hirtosa*. There is a dramatic increase in the length of the microvilli (mv), the number of mitochondria (mt) and a further increase in the number of granules (g). Note the preservation of polysomes (p) as a result of microwave-assisted fixation of the tissue, which are not observed in conventional bench-top preparations. Also note the largely mineral-free border region at the cusp surface and the formation of mineral behind this layer within the tooth cusp (tc), where crystal growth appears to follow the ~60^{o} angle of the organic matrix fibres observed in earlier tooth rows. (Codes: MP, D), Scale bar = 2 μm.

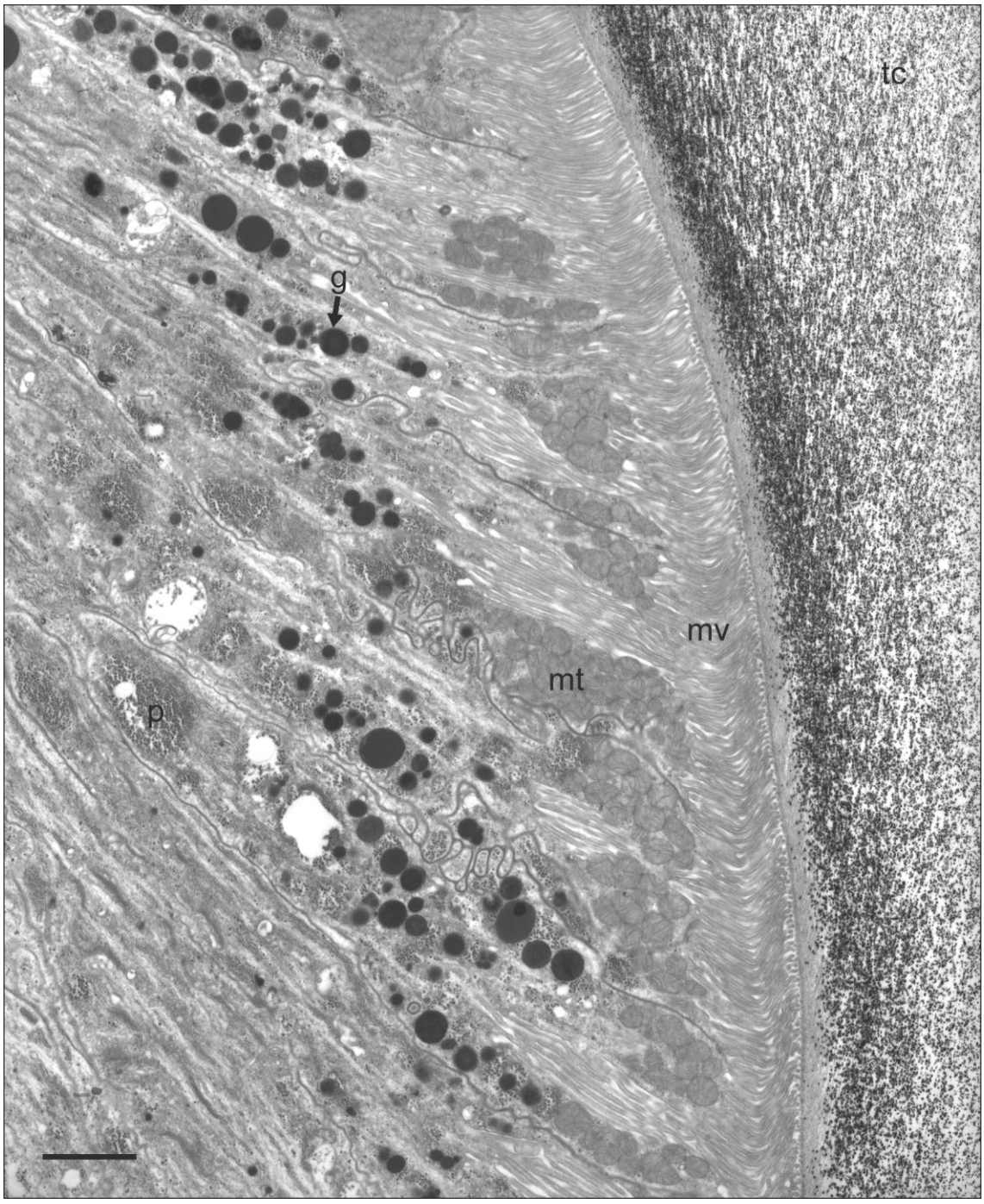
tc
g
mv
mt
p

Figure 5.17. High magnification TEM micrograph of the apical region at the onset of mineralisation at tooth row 14 in *A. hirtosa*, highlighting the developing microvilli (mv), prolific mitochondria (mt) and numerous granules (g). The excellent preservation of the tissue is again made evident by the retention of dense aggregations of polysomes (p), rough endoplasmic reticulum (rer) and the cristae within the mitochondria. cm = cell membrane, tc = tooth cusp. (Codes: MP, D), Scale bar = 2 μm.

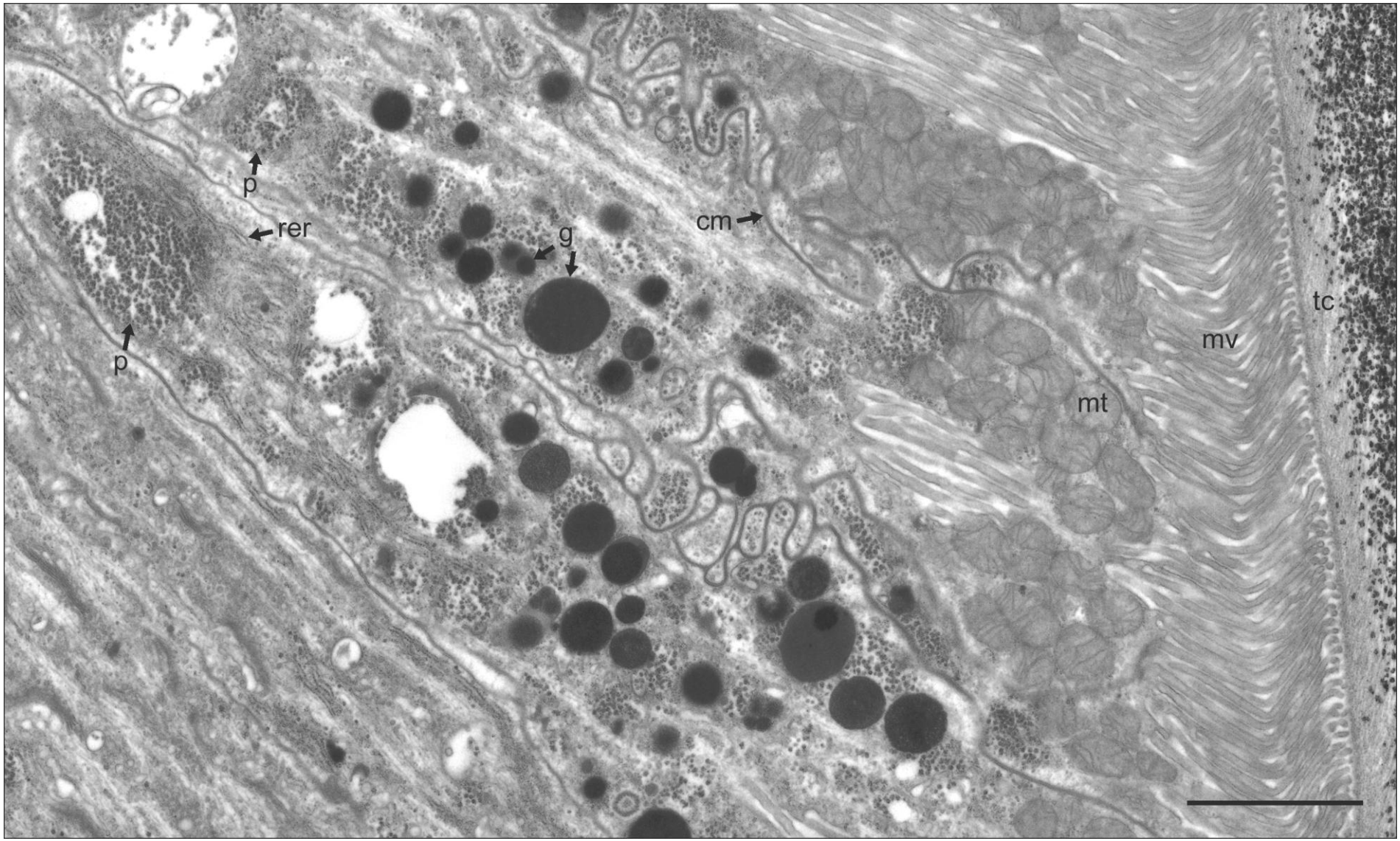
p
rer
p
g
cm
mv
tc
mt

preparation techniques over conventional bench top methods. Microwave prepared tissue has retained numerous aggregations, which are likely to be ribosomal material, or possibly glycogen, situated within the granule zone (see Appendix B). These structures have not been reported previously in the cusp epithelium of chitons.

By tooth row 15, an increasing number of granules can be observed in the apical region (Figures 5.18 and 5.19). The microvilli also continue to develop and extend to between 5 and 8 μm from the cusp surface into the apical cytoplasm. Conversely, there is a decrease in the number of mitochondria near the microvilli at row 15 compared to the number observed at the onset of mineralisation at row 14. Structures resembling lysosomes are also apparent, occurring approximately 15 μm from the cusp surface in each cell (Figure 5.19). The appearance of the cusp epithelium at tooth rows 16 and 17 is similar to that of row 15 in terms of the presence of granules, the development of the microvilli, which are now prominent structures extending well into the cytoplasm, and the number of mitochondria in the microvilli region (Figures 5.20, 5.21 and 5.22). Notably, the cusp epithelium is equally developed on the anterior surface of the tooth cusp as on the posterior surface (Figure 5.21). Although some evidence of crystal formation is present within the border region, especially towards the base of the cusp (Figure 5.20), this region remains relatively free of mineral compared to the remainder of the posterior cusp face at tooth rows 16 and 17. At tooth row 18 the posterior surface of the cusp is heavily impregnated with iron, and the appearance of the cusp epithelium is consistent with that observed for tooth rows 16 and 17 (Figure 5.23). Notably, by row 18, mineralisation within the border region on the posterior surface of the cusp now appears more extensive compared to that observed in previous rows (Figures 5.23 and 5.24).

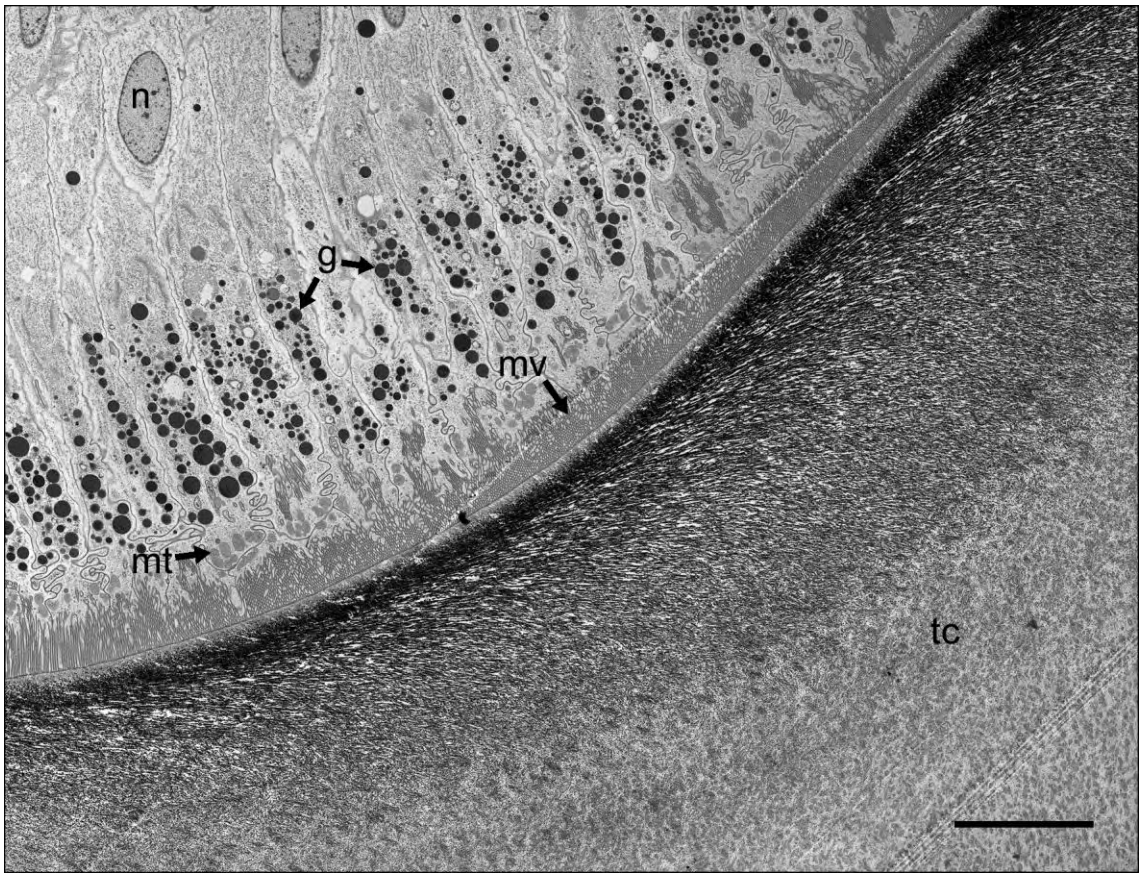

Figure 5.18. TEM micrograph showing the appearance of the cusp epithelium at tooth row 15, one row past the onset of cusp mineralisation in *A. hirtosa*. There is a further increase in the length of the microvilli (mv) and the number of granules (g). However, there is a decrease in the number of mitochondria (mt) surrounding the microvilli compared to the previous tooth row. Note that the border region at the cusp surface is still present, and crystal growth continues to form along the predefined orientation of the organic matrix fibres at approximately 60^{o} relative to the cusp surface. n = nucleus, tc = tooth cusp. (Codes: CP, C), Scale bar = 10 μm.

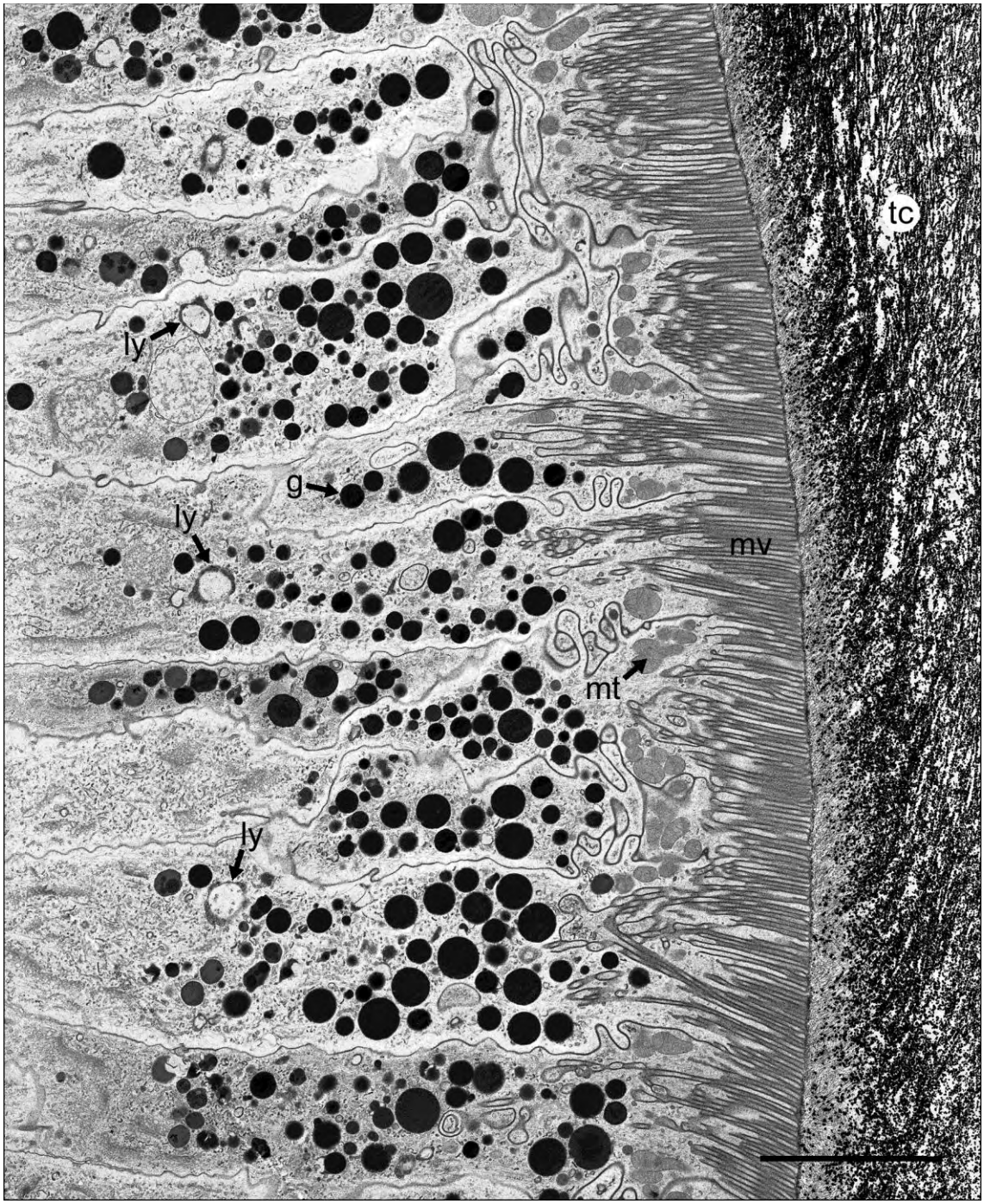

Figure 5.19. Higher magnification TEM micrograph of the cusp epithelium within the apical region at tooth row 15 in *A. hirtosa*. Note the presence of lysosomes (ly), which occur in similar positions within each cell behind the granule (g) region. mt = mitochondria, mv = microvilli, tc = tooth cusp. (Codes: CP, C), Scale bar = 5 μm.

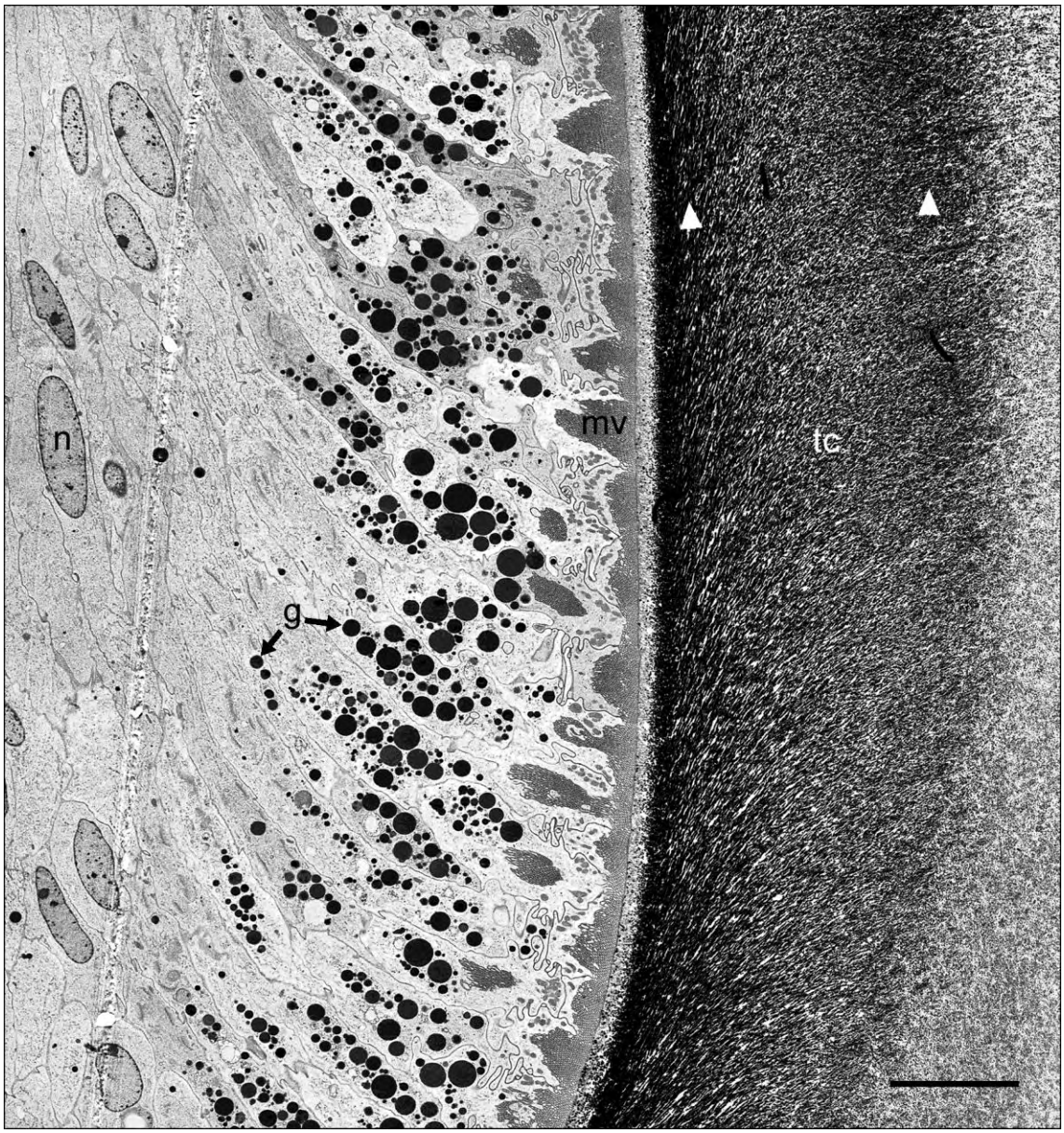

Figure 5.20. TEM micrograph of the cusp epithelium in *A. hirtosa* at tooth row 16, two rows past the onset of cusp mineralisation. The appearance of the epithelial tissue is similar to the previous row, with prominent microvilli (mv) and granule (g) regions. Note the border region at the cusp surface and the two particularly electron dense regions (arrowheads) running parallel to the tooth cusp (tc). n = nucleus. (Codes: CP, C), Scale bar = 10 μm.

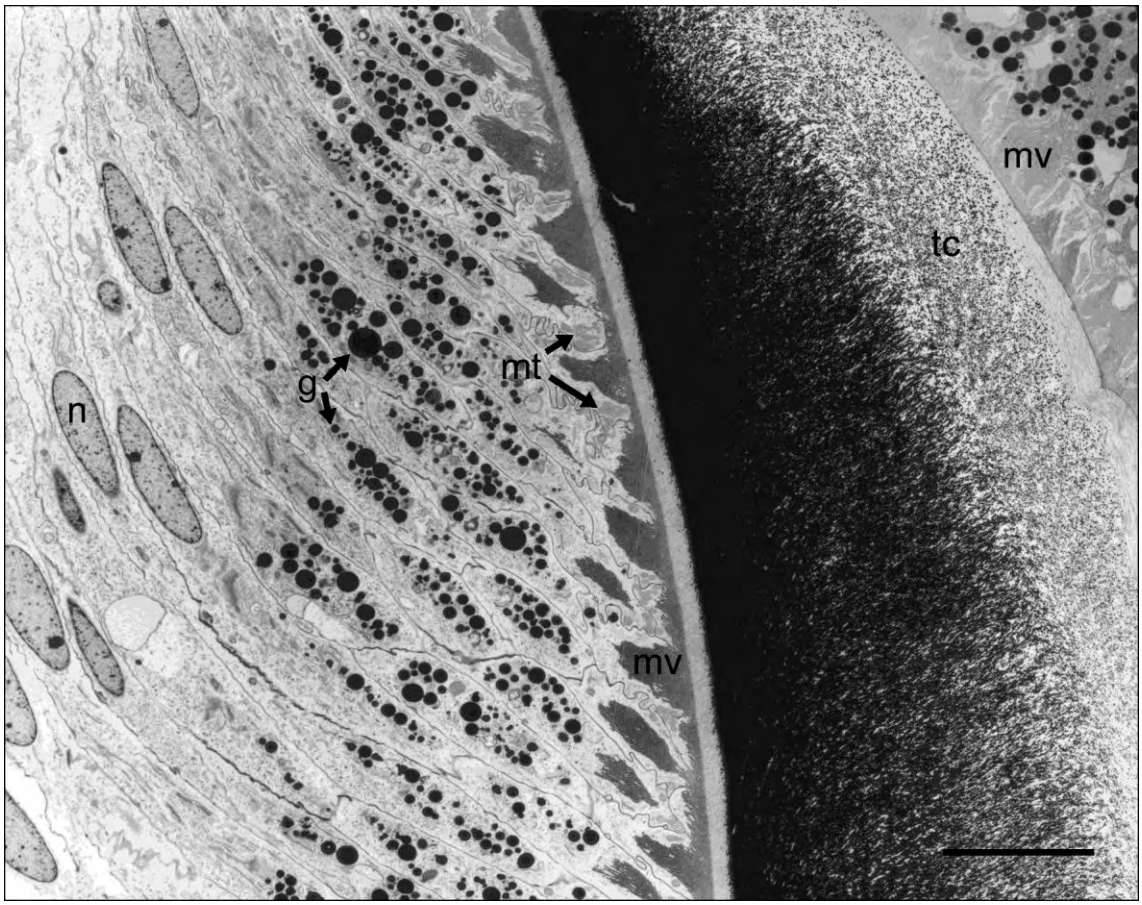

Figure 5.21. TEM micrograph of the cusp epithelium in *A. hirtosa* at tooth row 17, three rows past the onset of cusp mineralisation. Again, the appearance of the epithelial tissue is similar to that of the previous row, with prominent microvilli (mv) and granule (g) regions. Note the distinct border region at the surface of the tooth cusp (tc) and the presence of well developed microvilli on the opposite side of the tooth, highlighting the equally developed cusp epithelium on the anterior surface. mt = mitochondria, n = nucleus. (Codes: CP, C), Scale bar = 10 μm.

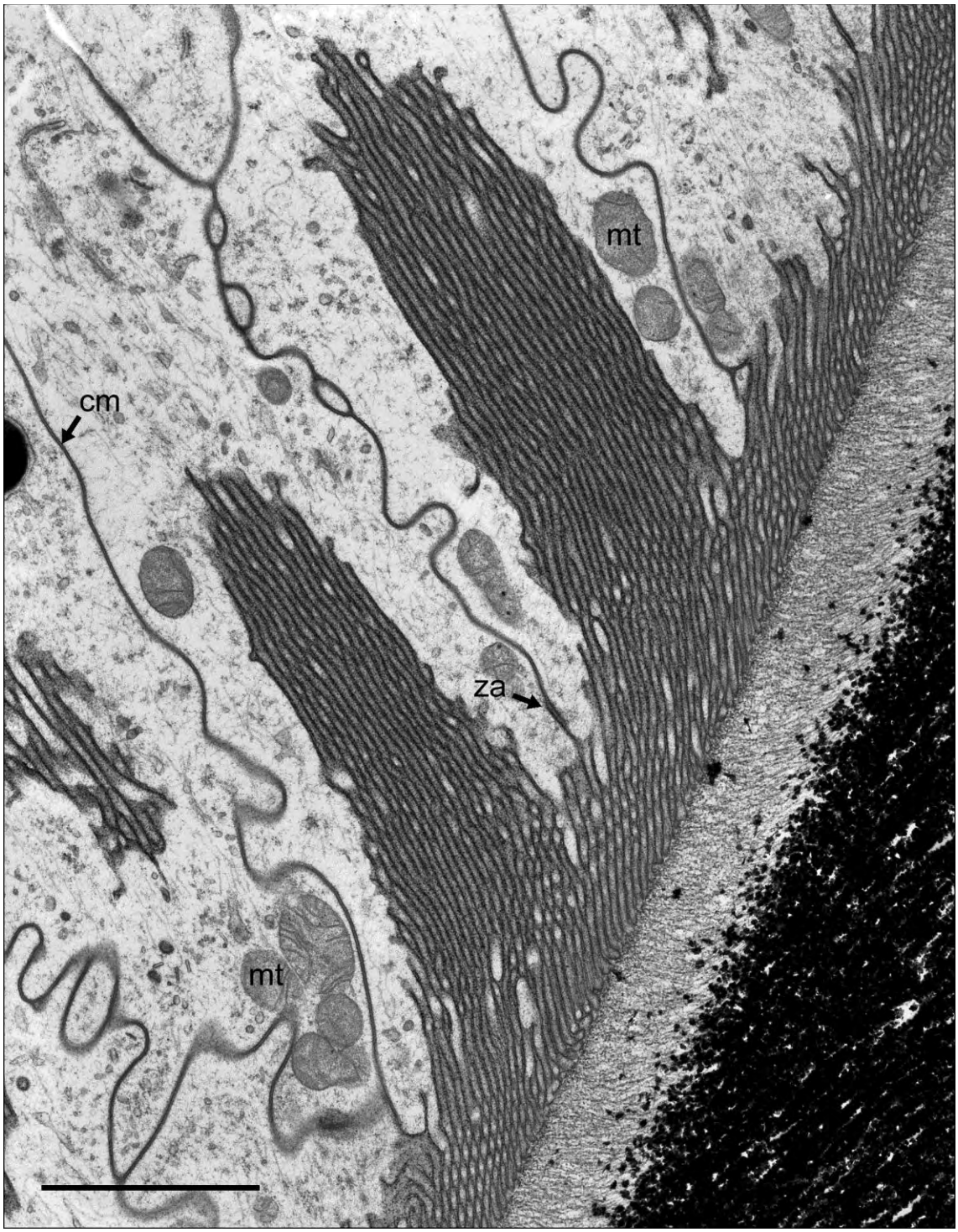

Figure 5.22. High magnification TEM micrograph of tooth row 17 in *A. hirtosa*, showing the well developed microvilli penetrating deeply into the apical cytoplasm. The border region is again clearly evident, forming a distinct ~1 μm boundary between the epithelium and the mineralised region. cm = cell membrane, mt = mitochondria, za = zonula adherens. (Codes: CP, C), Scale bar = 2 μm.

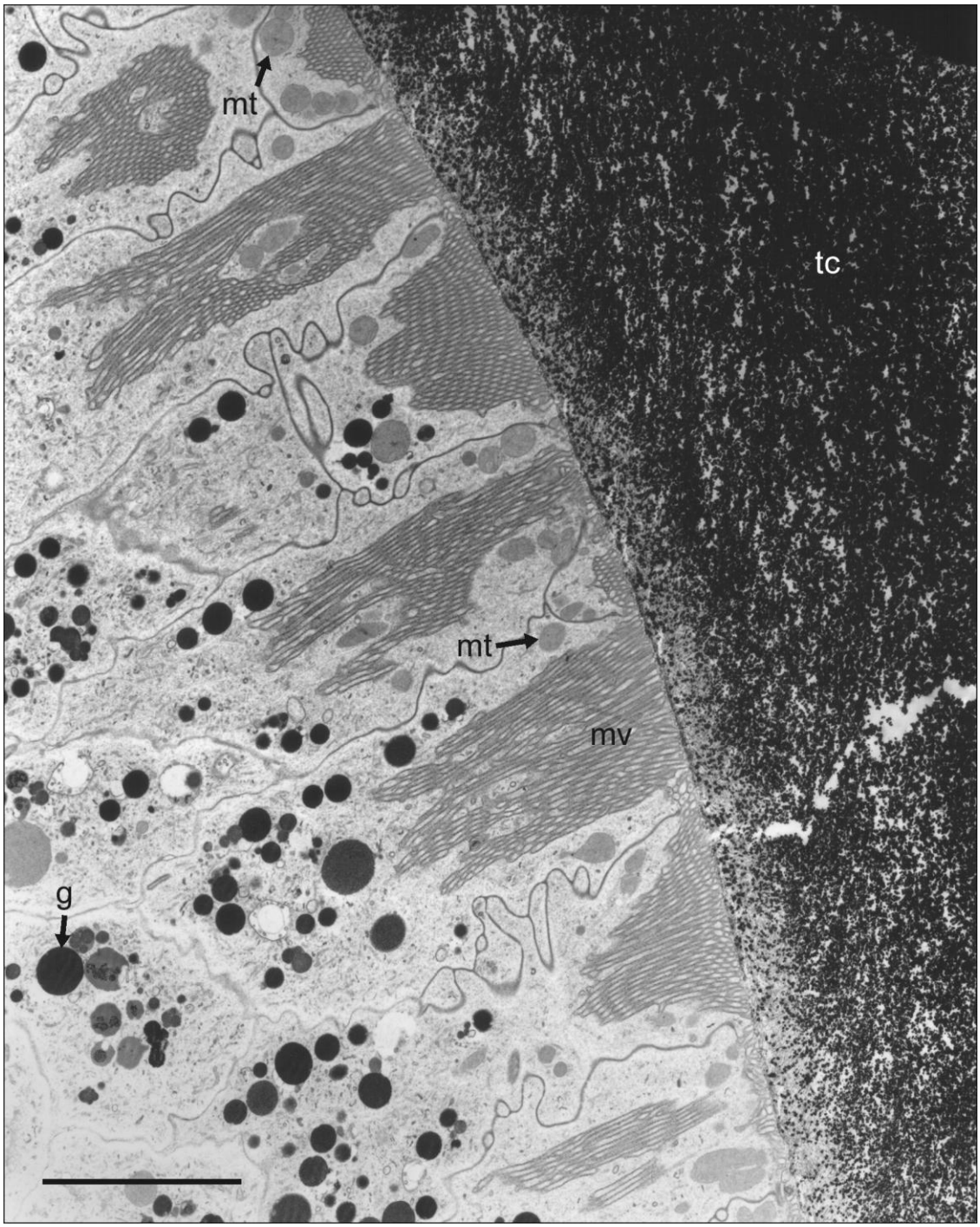

Figure 5.23. TEM micrograph of the cusp epithelium at tooth row 18, four rows past the onset of cusp mineralisation in *A. hirtosa*. The appearance of the tissue is similar to the previous row, with prominent microvilli (mv) and granule (g) regions. Note that the border region at the surface of the tooth cusp (tc) appears to contain considerable crystal growth compared to the previous tooth row. mt = mitochondria. (Codes: CP, C), Scale bar = 5 μm.

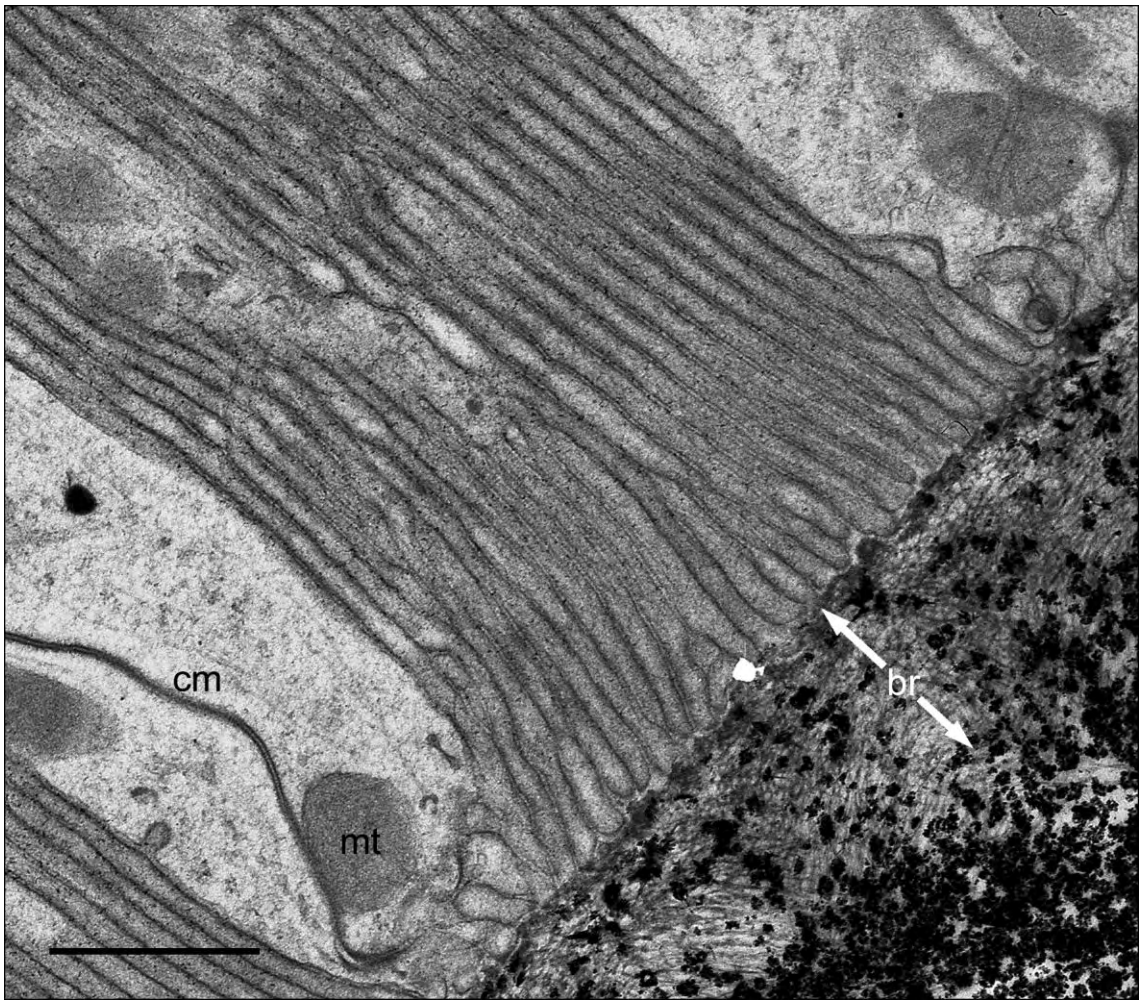

Figure 5.24. TEM micrograph of the microvilli region at tooth row 18, highlighting the formation of mineral within the border region (br) of the tooth cusp in *A. hirtosa*. cm = cell membrane, mt = mitochondria. (Codes: CP, C), Scale bar = 1 μm.

5.3.2. *Iron-limited and iron-reinstated epithelial development*

With the exception of the distribution of iron within the tissues, the overall structure of the superior epithelium, in iron-limited and iron-reinstated animals, at the LM level, was similar to that of normal individuals (Figure 5.25). This includes the respective alternating dark and light staining of the cusp and minor epithelium, and the presence of vesicles bordering the major lateral tooth cusps. While sections stained with Perl's revealed that ferric iron was clearly present at the junction zone of teeth in individuals that had been iron-limited for 190 days, almost no iron was detected in the cusp epithelial tissue. However, in animals reinstated with iron for 8 days following the 190 day iron-limitation period, iron was evident in the cusp epithelium from tooth rows 35 onwards, particularly at the basal poles bordering the dorsal sinus. In addition, these sections also revealed plumes of iron within the tooth core, the same as those present in normal animals, and which appear to flow from the junction zone to an internal mineralising front in the posterior region of the cusps.

However, at the EM level, by tooth row 13, the cusp epithelium in individuals that have been iron-limited for 143 days, exhibit considerable differences compared to that in the same row in normal animals (Figure 5.26). Fewer granules are present, and the microvilli remain undeveloped, such that the tissue more closely resembles epithelia from tooth rows 10-12 in normal animals. Notably, there is an abundance of mitochondria within the apical region of the cells close to the undeveloped microvilli. Further along the radula at tooth row 20, the number of granules, and the appearance of the microvilli, continues to resemble the undeveloped epithelia at row 13, however the number of mitochondria increased (Figure 5.27 and 5.28).

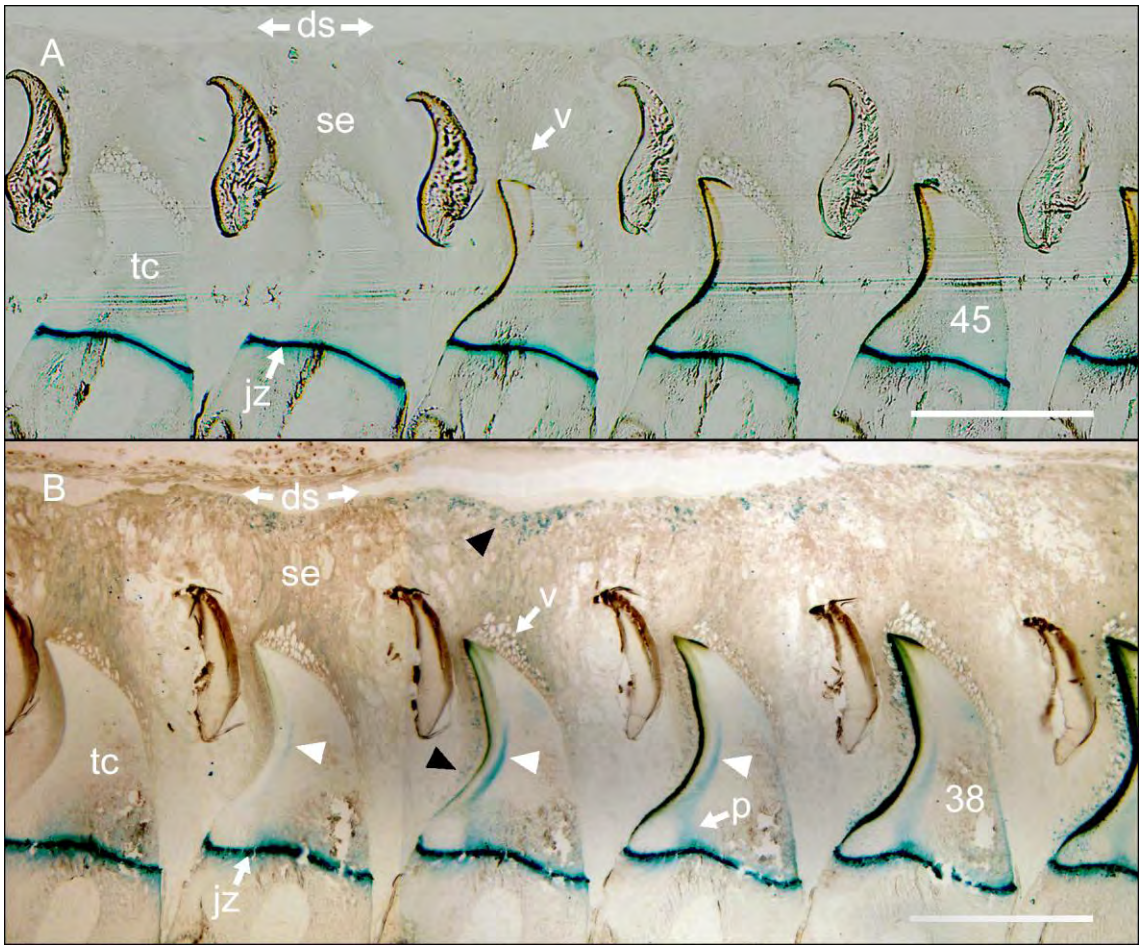

Figure 5.25. Light micrographs of Perl's Prussian blue stained, longitudinally orientated, radula sections from specimens of *A. hirtosa* (A) iron-limited for 190 days and (B) subsequently reinstated with iron for 8 days, where iron can be observed at the basal pole of the superior epithelium (se) bordering the dorsal sinus (ds) and adjacent to the posterior surface of the tooth cusps (tc) (black arrowheads). jz = junction zone, p = plumes, v = vesicles. White arrowheads denote the internal mineralising fronts. Note: numbers indicate the tooth row number. (Codes: MP, B), Scale bars = 200 μm.

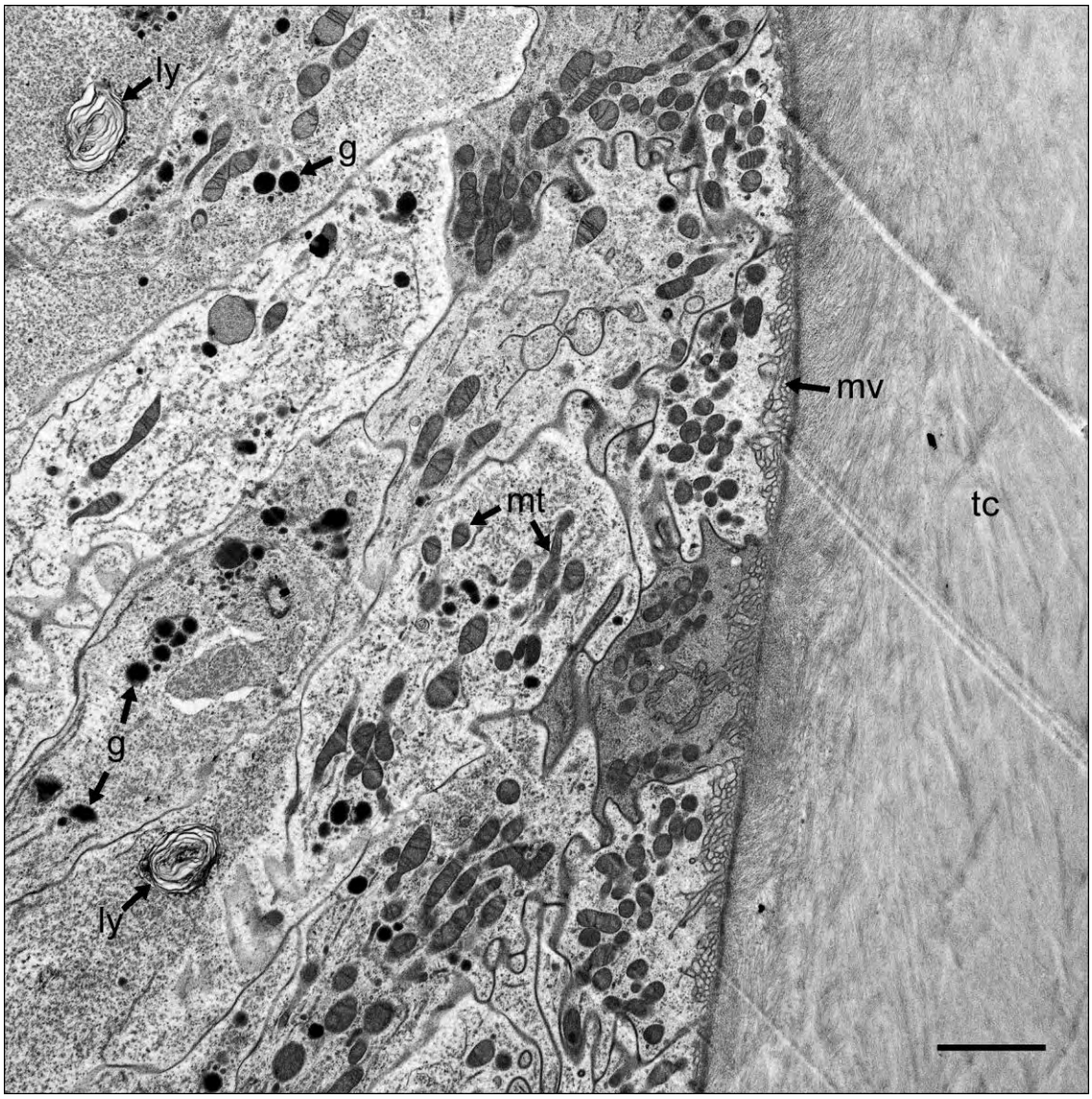

Figure 5.26. TEM micrograph of the apical region of the cusp epithelium at tooth row 13 from a specimen of *A. hirtosa* iron-limited for 143 days. The tissue appears normal, with the exception of the undeveloped microvilli (mv), which closely resemble those in the tissues of normal individuals at rows 10-12. g = granules, ly = lysosomes, mt = mitochondria, tc = tooth cusp. (Codes: CP, D), Scale bar = 2 μm.

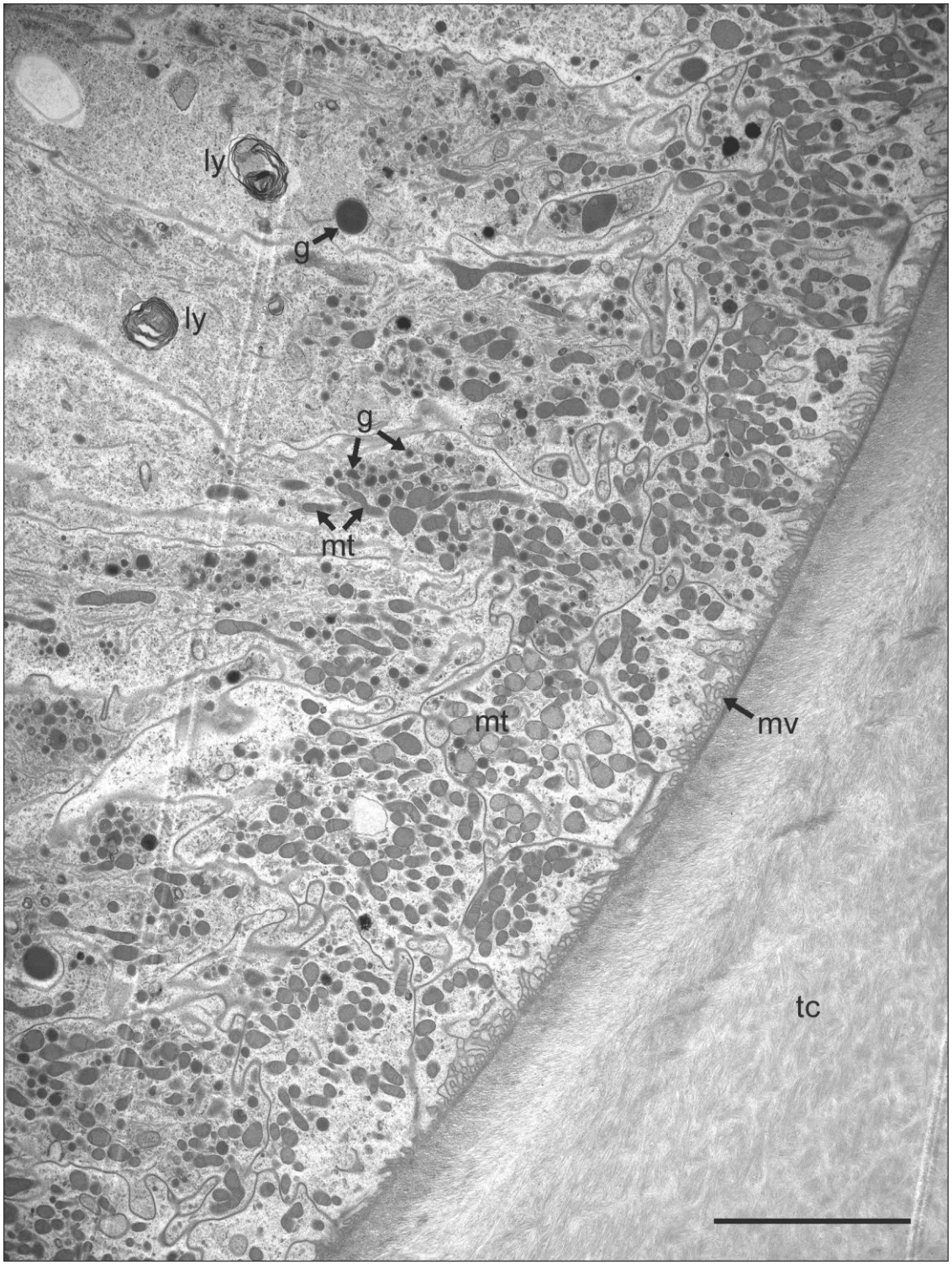

Figure 5.27. TEM micrograph of the cusp epithelium at tooth row 20 from the same 143 day iron-limited specimen of *A. hirtosa* in 5.26. Notice that there has been little change in the appearance of the apical region since row 13, with the exception of the presence of a large number of mitochondria (mt). g = granules, ly = lysosomes, mv = microvilli, tc = tooth cusp. (Codes: CP, D), Scale bar = 5 μm.

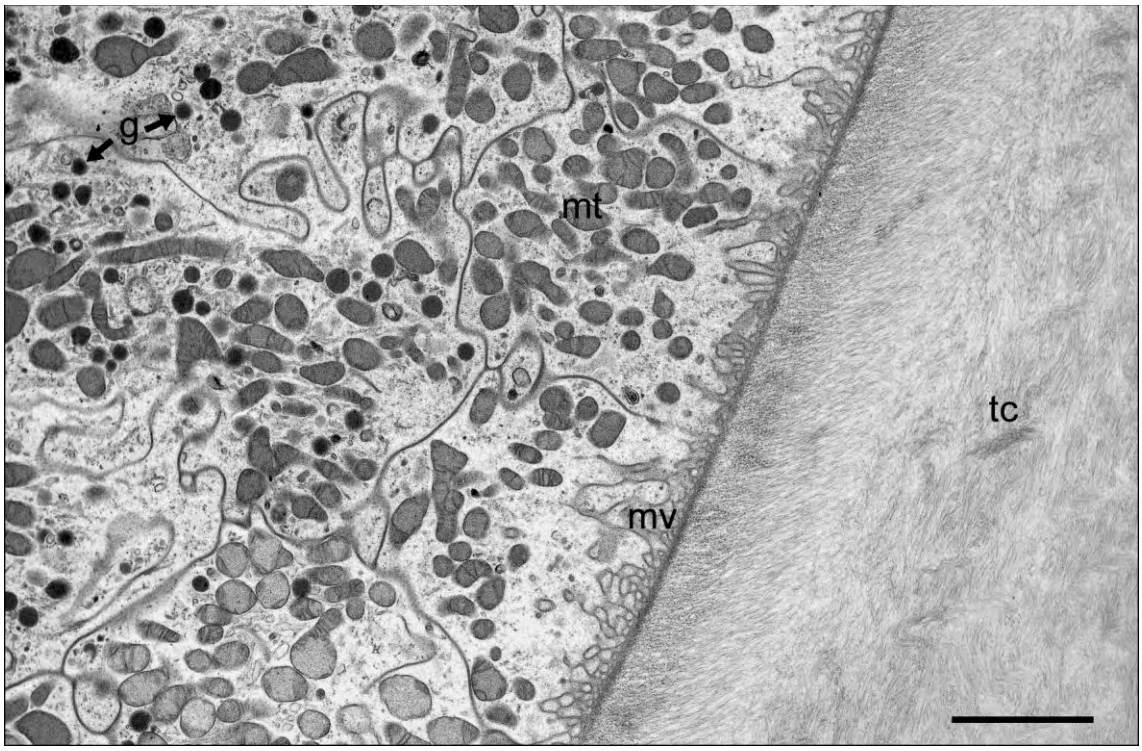

Figure 5.28. TEM micrograph of the apical region of the cusp epithelium at tooth row 20 from the same 143 day iron-limited specimen of *A. hirtosa* in Figure 5.27 highlighting the undeveloped nature of the microvilli (mv) and the large number of mitochondria (mt). g = granules, tc = tooth cusp. (Codes: CP, D), Scale bar = 2 μm.

5.3.3. *Observations of the organic matrix*

At tooth row 11, three rows prior to the onset of mineralisation, the organisation of the organic matrix fibres varies considerably within the posterior (magnetite mineralised) region of the tooth cusp. A layer of fibres, approximately 1 μm wide, runs upwards towards the cusp tip at an angle of approximately 60^{o} relative to the cusp surface (Figure 5.29). This border of fibres coincides with the mineral-free layer observed in teeth at rows 14-18. These fibres continue at this angle for approximately 3-4 μm before giving way to a region where the fibres take on a basket weave appearance and finally a more open structure of circular fibres. This trend can be observed in all immature teeth prior to the onset of mineralisation at tooth row 14 (Figures 5.10, 5.12, 5.13 and 5.14).

Transmission electron micrographs, taken at the onset of mineralisation at tooth row 14 and of subsequent mineralisation within the magnetite region over the next four rows, highlight the directional growth of magnetite crystals as they follow the ~60^{o} orientation of fibres near the cusp surface (Figures 5.16, 5.18, 5.19, 5.20, 5.21 and 5.23). Notably, at tooth rows 16 and 17 there is evidence of a second internal mineralising front, as evidenced by the presence of two electron dense regions bordering a region of relatively lower electron density running parallel to the cusp surface (Figures 5.20 and 5.29). Iron deposition within the magnetite region obscures the basket weave and circular fibre structure within the cusp, although some evidence of the circular fibres is still apparent within the internal mineralising front (Figure 5.29). Notably, at tooth row 20, the organic matrix fibres in iron-limited individuals are similar in appearance to the matrix in normal individuals prior to the onset of mineralisation (Figures 5.29 and 5.30).

Figure 5.29. TEM micrographs showing the orientation of organic matrix fibres within the posterior region of the major lateral tooth cusps in *A. hirtosa* at (A) tooth row 11 and (B) tooth row 17 in normally mineralised radulae and (C) tooth row 20 from an individual iron-limited for 143 days. Note the distinctive border at the cusp surface at tooth row 11, which coincides with the ~1 μm mineral-free layer at tooth row 17. In addition, note the arrangement of fibres within the first 2-4 μm, which appear to angle towards the cusp tip at approximately 60^{o} relative to the cusp surface. The overall appearance of the matrix at tooth row 11 in the normal cusp is similar to the matrix in the iron-limited cusp at row 20, where the densely packed 60^{o} fibres give way to a basket weave appearance followed by an open circular arrangement (black arrowheads). Notably, similarly spaced circular structures are still evident within an internal mineralising front three tooth rows after the onset of mineralisation at row 17 (white arrowheads). mv = microvilli. (Codes: (A and B) CP, C, (C) CP, D), Scale bars = 2 μm.

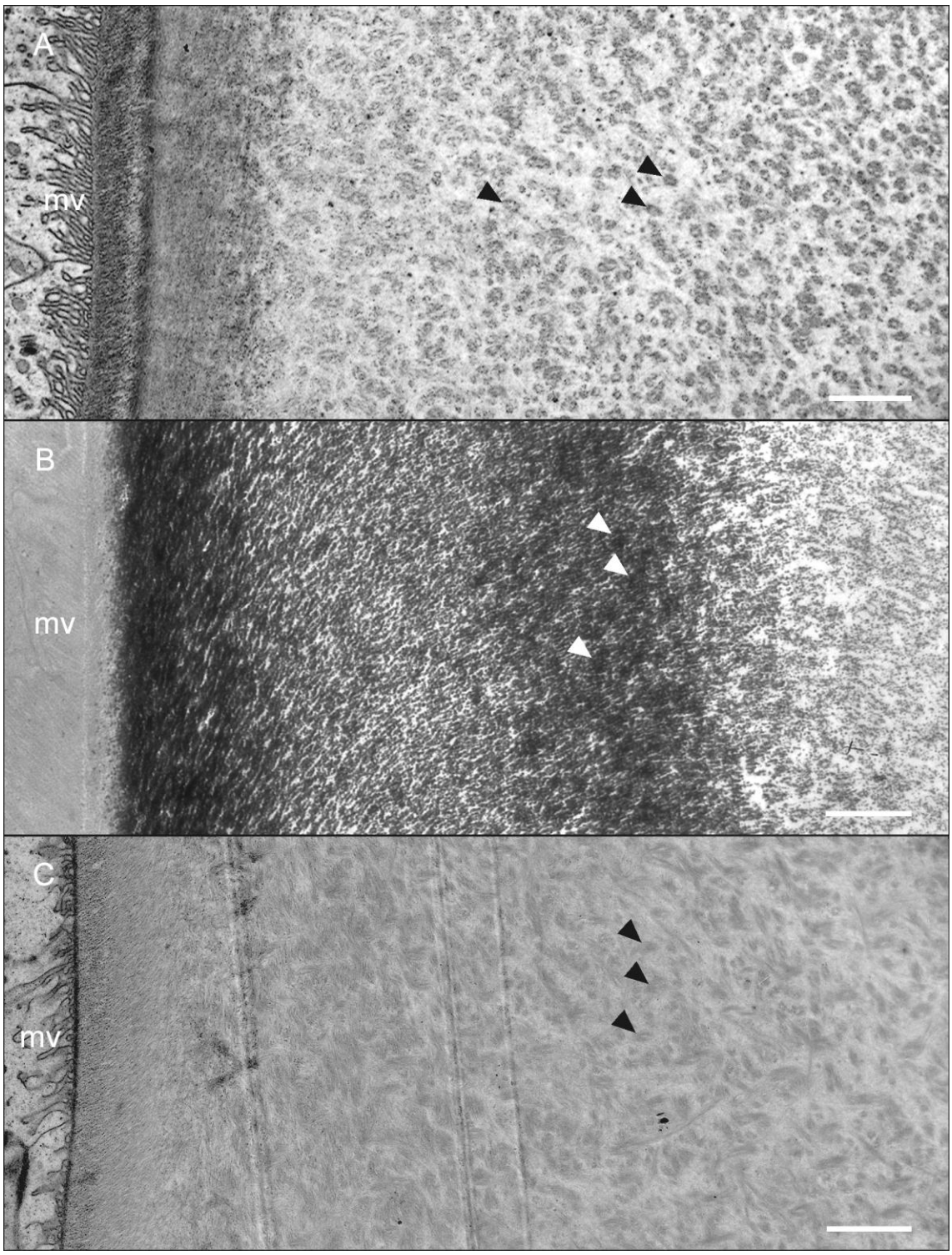
A
mv
B
mv
C
mv

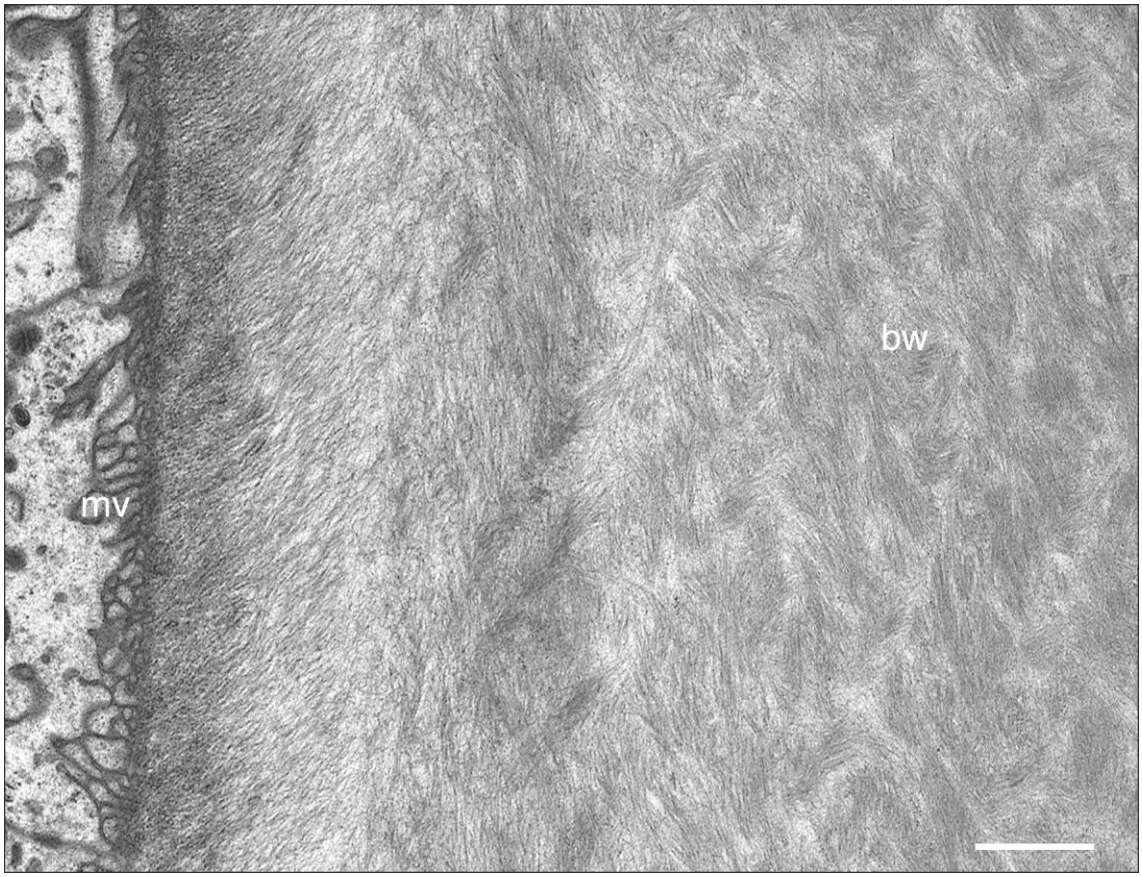

Figure 5.30. TEM micrograph showing the orientation of organic matrix fibres within the posterior region of the major lateral tooth cusps at tooth row 20 from a specimen of *A. hirtosa* iron-limited for 143 days. Note the ~60^{o} orientation of matrix fibres within the first 2 μm near the cusp surface, which eventually take on a basket weave (bw) appearance further into the cusp. mv = microvilli. (Codes: CP, D), Scale bar = 1 μm.

5.4. Discussion

The ultrastructure of the cusp epithelium surrounding the major lateral teeth of the chiton *A. hirtosa* undergoes a series of developmental changes that are intimately linked to the onset of tooth mineralisation and subsequent mineral deposition within the cusps. In particular, microvilli within the apical region of the cusp epithelium extend substantially at the onset of mineralisation, and their growth appears to be synchronised with the proliferation of iron containing granules within the tissues. In addition, this development coincides with the coordinated appearance of iron within the posterior tooth face, together with a plume of iron stemming from the junction zone, which follows an internal pathway to the mineralising cusp face. These events strongly suggest that many of the processes are predominantly occurring at tooth row 13, immediately prior to the orange tooth cusp, and are pivotal for creating the conditions necessary for mineral precipitation.

In contrast to the rapid extension of the microvilli surrounding the tooth cusp at row 13, which is likely to occur in response to the sudden influx of iron into the tissues, the increase in the number of mitochondria does not appear to be iron driven. The presence of numerous mitochondria prior to, and during the onset, of mineralisation in the tissue of normal animals suggests there is another trigger. In addition, the number of mitochondria within the apical region appears to decline from rows 15 to 18, despite the continued extension of the microvilli and the build up of iron. The cusp epithelium of iron-limited radulae was also observed to contain large numbers of mitochondria, despite poor microvilli development, an absence of iron containing granules, and the lack of mineral within the teeth. Microvilli have long been recognised as being responsible for the transport of iron from the apical region of the cusp cells to the extracellular compartment of the tooth in chitons (Nesson and Lowenstam, 1985; Kim *et al*., 1989). In addition, mitochondria are thought to be responsible for providing the

energy required for the active transport of solubilised iron through the microvilli and into the tooth cusp (Nesson and Lowenstam, 1985; Kim *et al*., 1989). While this is likely to be the case, the above mentioned patterns of mitochondrial accumulation in normal and iron-limited tissues suggests that the role of these organelles is not limited to energy production.

Mitochondria are responsible for cellular respiration, where electron-driven proton pumps, located in the inner mitochondrial membrane, generate a proton-motive force consisting of a pH gradient and a transmembrane electric potential (Stryer, 1999). The supply of electrons, derived from the NADH and $FADH_2$ formed in glycolysis, are donated to molecular oxygen, thereby liberating the free energy necessary for pumping the protons, in the form of hydrogen ions, out of the mitochondrial matrix. These protons flow back into the matrix via the transmembrane protein ATP synthase, which catalyses the production of ATP. As such, the consumption of molecular oxygen, and the high concentration of hydrogen ions outside the mitochondrial matrix results in a reductive, and acidifying, environment surrounding the organelle. The production of ATP, and the chemical environment created by the mitochondria, would be critical for driving the release of iron from ferritin, and maintaining iron in a soluble form as it is passed through the microvilli and into the tooth cusp. Furthermore, these activities may also influence the solution chemistry at the site of mineralisation, in particular, Fe solubility and supersaturation, which are both key elements for controlling the thermodynamic conditions for mineral precipitation (Mann, 2001).

The role of mitochondria in mediating solution chemistry within the extracellular tooth compartment, provides an explanation for the large accumulation of these organelles prior to, and their decline subsequent to, the onset of mineralisation at tooth row 14. On reaching some critical point of supersaturation, nucleation is initiated, which, in turn, provides the impetus for stable and continued crystal growth. Under

these conditions the cusp epithelium no longer needs to maintain as strong a reducing environment, and as such may be the reason for the decline in mitochondrial numbers within the tissues. However, some mitochondria are still required to provide the energy needed, and the conditions necessary, to facilitate the transport of iron into the tooth cusps in order to maintain crystal growth.

The very formation of mineral within the tooth cusps may explain the further extension of the microvilli as mineralisation progresses, given that the cells would need to compensate for the increasing resistance to transport brought about by the formation of mineral along the posterior surface of the cusp. Microvilli extension may also be linked to the decreasing concentration gradient between the cusp epithelium and the teeth as increasing amounts of iron are transported into the cusps. The increased surface area provided by the continued growth of the microvilli presumably facilitates a greater rate of transport across the apical border, in addition to maintaining a greater degree of control over the extracellular compartment of the cusp. A similar process of microvilli extension has been observed in the Malpighian tubules of crickets following exposure to secretion-stimulating hormone (Clode, pers. comm., 2007). In this instance, it is thought that microvilli growth allows for additional proton pumps in the membrane to rapidly alter the pH, thereby increasing acidification.

Maintaining a reducing environment in the superior epithelial tissues of chitons may also be assisted by the radula musculature, which is known to contain the oxygen transport pigment myoglobin, and gives the muscles their characteristic deep red colouration (Manwell, 1958; Tergwilliger and Read, 1970; Smith *et al*., 1988). These discrete narrow bands of muscle are also bathed in blood haemocyanin within the cephalic haemocoel, and it has been suggested that the presence of both respiratory pigments constitutes an oxygen transport system for these muscles (Boyle, 1977). In addition, an unusual feature of the radula muscle myoglobin in chitons is that it is

composed of both dimeric and monomeric components (Tergwilliger and Read, 1970), which has been suggested to have evolved due to the need for oxygen-binding systems optimised for both aquatic and aerobic conditions (Suzuki and Imai, 1998). The presence of these muscles at the anterior end of the radula, which has been proposed as the location for the main arterial blood supply for the dorsal sinus (Nesson and Lowenstam, 1985; Chapter 4), would aid in scavenging oxygen from the tissues in the buccal region, which are exposed to the environment when feeding.

The sudden development of the cusp epithelium, together with the coordinated release of iron from the junction zone at row 13, suggests that this particular tooth row is pivotal in the normal cusp mineralisation process. For a number of chiton species the concentration of iron at the junction zone has been shown to peak just prior to the onset of mineralisation, and then drop sharply before reaching a plateau over subsequent tooth rows (Macey and Brooker, 1996; Brooker and Macey, 2001; Brooker *et al*., 2003). This spike in iron concentration is likely to be the point at which large amounts of iron enter the cusp epithelium from the dorsal sinus, thereby triggering the mass influx of iron into the tooth from both the tissues and the junction zone. The flow of iron into the cusp, which is presumably driven and maintained by the strong ionic gradient created by the mitochondria, would quickly reach supersaturation within the reducing environment of the extracellular tooth compartment, and in so doing, create appropriate conditions for mineral precipitation, nucleation and crystal growth.

In *A. hirtosa*, the small crystal deposits, observed within the posterior cusp surface at tooth row 13, demonstrate that nucleation of ferrihydrite must also occur at this tooth row. The association of these initial deposits with the fibres of the organic matrix has been described previously for *A. hirtosa* (Kim *et al*., 1989; Evans *et al*., 1990; Evans *et al*., 1994), and for a number of other chiton and limpet species (see for example: Towe and Lowenstam, 1967; Nesson and Lowenstam, 1985; Sone *et al*., 2007). The

importance of the chitin framework in the mineralisation process has been demonstrated for the limpet *Patella caerulea*, where it has been shown that deposits of goethite nucleate on the chitin fibres, thereby controlling the initial orientation of the crystals (Sone *et al*., 2005; Sone *et al*., 2007). However, in these same studies it was observed that biological control over subsequent crystal growth is limited, as evidenced by the varied habit of goethite crystal morphologies within the cusp. As a result of this normal growth habit, the goethite crystals push aside, or engulf, the matrix fibres within the cusps. As there are many parallels in the processes of mineral formation between chitons and limpets it would seem reasonable to suggest that a similar pattern of crystal growth occurs in the teeth of *A. hirtosa*.

The exact mechanism triggering the initial nucleation of ferrihydrite on the matrix fibres is unknown, although its influence appears to be directed from the posterior cusp surface towards the tooth core. This is evidenced by the gradual reduction in crystal size from the posterior surface towards the tooth interior at row 13. This gradient in crystal size indicates that growth is initiated from the cusp face towards the core, with the youngest, and therefore most newly formed crystals, occurring further into the cusp. In addition, evidence for an internal mineralising front is provided by the heavily mineralised layer running parallel to the posterior surface at the boundary between the magnetite region and the tooth core; as observed at row 16 (also see Chapter 4). It is assumed, from the larger size of the crystals in this region, that nucleation must occur along this boundary at a similar time to that of the cusp face. The internal mineralising front, observed in *A. hirtosa*, has also been documented for the chiton *A. echinata* (Brooker *et al*., 2003), and in the limpet *P. caerulea* (Sone *et al*., 2007). It is uncertain whether nucleation in these regions is triggered by variations in the chemical composition of the organic matrix or the chemical environment within the tooth, or a combination of both.

The outermost periphery of the posterior cusp face remains largely free of mineral for a number of tooth rows following the onset of mineralisation. The organic matrix fibres in this region are uniformly orientated, running parallel to each other and perpendicular to the cusp face before giving way to a "basket weave" appearance approximately 2 μm in from the tooth surface. This structurally distinct layer is evident in a number of chiton species (see for example: Nesson and Lowenstam, 1985; Bullock, 1989; van der Wal *et al*., 1989; Evans *et al*., 1990; Evans *et al*., 1994; Brooker *et al*., 2003), and in mature teeth has been shown to be mineralised with ferrihydrite; where it has been suggested to act in protecting the magnetite region from oxidation once the tooth is exposed to seawater (Brooker *et al*., 2003). The ability of this discrete boundary layer to selectively remain free of mineral, despite nucleation within the remainder of the magnetite region, and then to mineralise ferrihydrite specifically, suggests that the chemical, and/or structural, characteristics of the matrix fibres in this region maintain a significant degree of control over nucleation rather than the chemical environment per se.

Although the organic matrix may not interfere with the crystal's natural formation habit (Sone *et al*., 2007), the overall orientation of crystal growth in *A. hirtosa* is obviously controlled by the organisation of the matrix fibres, which, in the magnetite region, are orientated at an angle of approximately 60^{o} from the posterior surface towards the cusp tip. This angle is a structural feature typical of that documented for a number of chiton and limpet species, where it has been suggested to assist in reducing tooth wear and the prevention of crack propagation (van der Wal *et al*., 1989; 2000; Macey *et al*., 1996; Wealthall *et al*., 2005). The structure of the organic matrix in this region, and for the tooth as a whole, appears to be similar for both iron-limited and normally mineralised radulae. Most importantly, the organic matrix appears to remain viable in its role in mediating mineralisation, despite prolonged periods of

iron-limitation, as evidenced by the return of plumes to the core region following the reinstatement of iron. Although experiments relating to the full recovery of mineralisation have not yet been conducted, these initial findings show that the main pathways for the delivery of elements, and the template for mineral formation, persist and remain functional.

Notably, there has been little emphasis placed on the cusp epithelium attached to the anterior surface of the major lateral teeth, which undergoes the same developmental changes as the cells on the posterior surface, including the large accumulation of iron containing granules. The iron within the anterior cusp epithelium is likely to be used for mineralising the tab region, which extends a short way down the anterior cusp surface from the tooth's tip. In addition, these cells are likely to be responsible for depositing the thin veneer of iron that covers the top half of the anterior tooth surface as described in Chapter 4. However, the abundance of iron within the anterior and posterior cusp epithelia appear to be similar, despite the obvious preferential deposition of iron within the posterior cusp region. Although the transfer of iron from the anterior epithelium through the organic matrix to the posterior side of the cusp may occur, the findings of this Chapter, and those provided in Chapter 4, suggest that the major pathways of iron transport to the magnetite region are via the posterior cusp surface and the junction zone. Preliminary experiments have revealed that iron containing granules are still present in *A. hirtosa's* cusp epithelium at tooth row 35, which is well beyond the point at which iron delivery from the posterior surface has ceased. As such, it would appear that the concentration of iron aggregated within the cusp epithelium is above that needed for tooth mineralisation. This would presumably aid in creating/maintaining a concentration gradient from the tissue to the cusp and thus ensure that supersaturation is readily achieved and maintained.

Following nucleation and the initial formation of ferrihydrite, the large amount of iron in the tissues would also aid in promoting continued phase transformation of ferrihydrite to magnetite over subsequent tooth rows. As these two mineral forms differ in their Fe to O ratios (Ferrihydrite = Fe_2O_3, Magnetite = Fe_3O_4), additional iron is required to drive the conversion of the amorphous precursor ferrihydrite to magnetite. Notably, preliminary studies on iron-limited radulae, using Raman spectroscopy, have revealed the formation of the hydrated iron(III) oxide mineral limonite (Lee, pers. comm., 2006), which has not been reported previously in the teeth of *A. hirtosa*. In addition, the amount of limonite was found to increase as a proportion of the total iron mineral with increasing periods of iron-limitation. This suggests that if there is insufficient iron in the tissues and cusps to drive the transformation of iron through to the desired end product magnetite, the intermediate limonite phase remains.

Chitons possess a large surplus of iron, as evidenced by the long period over which mineralisation is maintained once animals are transferred into an iron-limited system (see Chapter 3). Previous studies on *A. hirtosa* show that the radula and hemolymph contain, by far, the highest concentration of iron compared to the other major tissue types of the body (Webb and Macey, 1983; Kim *et al*., 1988). As such, in addition to their role in mineralisation, the radula tissues, together with the hemolymph ferritin, may constitute the principal sites for iron storage in chitons. With the cusp epithelium already structured for iron storage, large amounts could be retained within this tissue and then recycled into the hemolymph within the dorsal sinus upon reaching the anterior end of the radula.

The accumulation of iron containing granules around the major lateral tooth cusps first occurs at tooth row seven, a finding that is contrary to earlier studies on *A. hirtosa* where iron was not observed until immediately prior to the onset of mineralisation (Kim *et al*., 1989). However, the amount of iron in the cusp epithelium does not seem to rise

appreciably over subsequent tooth rows, and levels appear to remain static until the dramatic influx of iron into the cusp epithelium at row 13. The reason for the presence of iron in these tissues early in tooth development is unclear, although, the coinciding accumulation of iron at the junction zone in these tooth rows suggests that this iron may pass from the cusp epithelium to the junction zone region for later use. However, the absence of microvilli bordering the tooth surface at the junction zone would appear to refute this suggestion, as it is assumed that the microvilli are required for such transport. The exact process of element delivery to the junction zone remains unresolved, and whether the source of elements is derived from the cusp epithelium, or an alternative pathway, such as the stylus canal (see Chapter 6), is, as yet, unknown.

Direct elemental mapping has demonstrated that the electron dense granules within the cusp epithelium are not solely comprised of ferritin siderosomes, but are instead a mixture of both iron and non iron-containing granules. Similarly, individual granules also contain iron and non iron components. The detailed study of granule types in the chiton *Lepidochitona hartwegii*, by Nesson and Lowenstam (1985), also noted this variation in electron density both between, and within, granules, and suggested that the less ordered, amorphous material was composed of ferrihydrite bound to the iron storage protein hemosiderin. While the iron containing granules within the cusp epithelium may be in the form of either ferritin or haemosiderin, the composition of the amorphous material in *A. hirtosa* is unknown. At the onset of mineralisation, iron is likely to be liberated from the protein fraction of the ferritin molecule prior to being transported into the tooth cusp, thus leaving large amounts of the apoferritin protein shell within the cell. As such, the amorphous granules and granule components may be comprised of apoferritin that has aggregated following the release of the iron core, where it could then be recycled or reused for further iron storage. Whilst elucidating the exact nature of this amorphous material is outside the scope of this study, a preliminary

high resolution investigation has revealed that granules within the stylus canal tissue (see Chapter 6), similar to those within the cusp epithelium, are ordered in structure and may be aggregations of crystalline apoferritin.

The presence of large vesicles within the cusp epithelium surrounding the major lateral teeth remains a problematic issue with respect to whether they are truly represented features, or artefacts resulting from sample processing. These structures have been observed using both conventional and microwave-assisted fixation methods (see Appendix B), where they can be either abundant or virtually absent at the same stage of tooth development in different animals. In addition, similar vesicles can be observed in micrographs taken of both chitons and limpets by other researchers (see for example: Nesson and Lowenstam, 1985; Lu *et al*., 1995). It must be noted that, with the exception of Figure 5.13, which demonstrates the presence of these vesicles at tooth row 12, this study has focused on tissues in which the vesicles were absent. When present, the vesicles tend to be more prominent on the anterior surface at the cusp tip, although they can occur at any point along the cusp periphery, and in most cases they cause displacement of the surrounding tissues and organelles. It would seem likely that these structures are artefacts resulting from inadequate fixation. However, their association with the microvilli surrounding the cusps supports the earlier suggestion that the environment created by the mitochondria is highly reductive and acidic, which may exacerbate the breakdown of cellular material within the apical region.

Chapter 6

The Stylus Canal

6.1. Introduction

To date, research into tooth biomineralisation in chitons has focused mainly on the cusps of the major lateral teeth and their overlying superior epithelial tissue. This tissue has traditionally been accepted as being the sole delivery route for the elements involved in tooth cusp mineralisation (Towe and Lowenstam, 1967; Nesson and Lowenstam, 1985; Kim *et al*., 1989). However, very little work has been performed on the major lateral tooth bases (also referred to as the stylus in many anatomical manuscripts), which each contain a curious tube-like cavity filled with tissue. While this structure within the stylus is often visible in diagrams and photographs (see for example: Evans *et al*., 1991; Macey and Brooker, 1996; Webb *et al*., 2001), its existence has only been acknowledged for the chitons *Lepidochitona hartwegi* and *Mopalia muscosa* by Nesson (1969) and Nesson and Lowenstam (1985). These authors described the cavity as a canal, filled with cells that are connected to the minor epithelium via a pore on the medial surface of each tooth stylus. In addition, the distal end of the canal is mentioned to terminate in the vicinity of the junction zone. Thus far, no attempt has been made to determine the function of this so called "stylus canal", or whether the presence of the canal is a feature unique to all chiton species.

In the major lateral teeth of chitons, the elements involved in the biomineralisation process are first recorded in a region referred to as the junction zone, which occurs between the tooth cusp and the tooth stylus (Macey and Brooker, 1996; Brooker and Macey, 2001; Brooker *et al*., 2003; Chapter 4). The means by which elements are first transported to the junction zone remain unclear, as it does not appear to have any connection with the superior epithelium (Macey and Brooker, 1996; Chapter 5). The existence of a second mechanism for the delivery of

elements to the tooth cusps from the stylus canal, via the junction zone, has the potential to significantly enhance our understanding of the biomineralisation pathways in chiton teeth. To address this distinct lack of knowledge concerning the stylus canal, a histological investigation was undertaken to determine both the overall morphology of the canal itself, and the structure of the canal cells in the chiton *Acanthopleura hirtosa*. In addition, the major lateral teeth from a number of other chiton species were observed to determine whether the canal is a feature common to this group.

6.2. Materials and methods

Specimens of *A. hirtosa* were collected and dissected for the examination of either hard structures or soft tissues (Chapter 2). For LM and TEM, longitudinal and transverse sections of the radula were obtained that provided orientations at the distal end of the canal near to the junction zone and through the canal pore, respectively. The presence of the stylus canal was directly investigated in a further 19 species (Table 6.1), in addition to evidence collected from personal communications and previous literature.

Table 6.1. Species list from which direct observations were made for the presence of the stylus canal. Note: Specimens provided by Brooker (2007).

Species	Collection Site	Latitude	Longitude
Leptochiton liratus (H. Adams & Angas, 1864)	Cottesloe Reef, Perth, W.A.	31°60'S	115°45'E
Callochiton crocinus (Reeve, 1847)			
Ischnochiton cariosus Carpenter in Pilsbry, 1892			
Ischnochiton contractus (Reeve, 1847)			
Ischnochiton torri Iredale & May, 1916			
Ischnochiton verconis Torr, 1911			
Plaxiphora matthewsi Iredale, 1910			
Rhyssoplax torriana Hedley & Hull, 1910			
Cryptoplax burrowi (E.A. Smith, 1884)			
Cryptoplax iredalei Ashby, 1923			
Cryptoplax striata (Lamarck, 1819)			
Plaxiphora albida (de Blainville, 1825)	Woodman Point, Perth, W.A.	32°03'S	115°44'E
Acanthopleura hirtosa (de Blainville, 1825)			
Acanthochitona johnstoni Ashby, 1923			
Acanthopleura gemmata (de Blainville, 1825)	Port Headland, W.A.	20°18'S	118°36'E
Acanthopleura spinosa (Bruguière, 1792)			
Onithochiton quercinus (Gould, 1846)	Rottnest Is., W.A.	31°59'S	115°32'E
Ischnochiton thomasi Bednall, 1897	Hamelin Bay, Cape Leeuwin, W.A.	34°11'S	115°01'E
Cryptochiton stelleri (Middendorff, 1847)	Monterey Bay, Califoria, USA	36°45'N	122°0'W

6.3. Results

The major lateral tooth cusps of *A. hirtosa* are supported by a tooth base (or stylus) measuring ~540 μm in length and ~360 μm in height (Figure 6.1), which is embedded in the radula membrane. When excised from this membrane and strongly illuminated under the light microscope, the stylus canal can be clearly seen within the tooth stylus (Figure 6.1). Located centrally on the medial surface of the stylus, a teardrop-shaped canal pore, 100 μm across, opens into the stylus canal (Figure 6.2), extends ~280 μm into the stylus towards the distal end of the tooth and ends blindly ~25 μm below the junction zone (Figures 6.1 and 6.2). The stylus canal also extends ~125 μm towards the proximal end of the tooth. The distal arm of the canal tapers from ~75 μm at the pore opening to ~25 μm near the junction zone region.

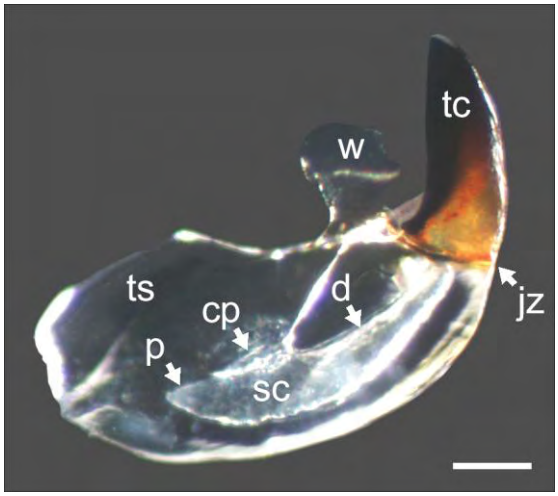

Figure 6.1. Light micrograph of the medial surface of a major lateral tooth freshly dissected from the chiton *A. hirtosa* highlighting the distal (d) and proximal (p) arms of the stylus canal (sc), which stem from the canal pore (cp) on the medial face of the tooth stylus (ts). tc = tooth cusp, jz = junction zone, w = major lateral wing. (Code: A), Scale bar = 100 μm.

Light microscopy of transversely sectioned radulae shows the stylus canal and the canal pore, both of which are clearly filled with, and contiguous to, strands of epithelial tissue. This tissue appears similar to that surrounding the major lateral teeth and the remaining minor teeth (Figure 6.3).

In normally mineralised radulae, sections reveal that the cusp and stylus change from a smooth and even appearance at row five, to becoming ropey and fragmented at row six (Figure 6.4). In particular, the region between the stylus canal and junction zone often exhibits variable sectioning properties caused by inadequate resin infiltration. Transmission electron micrographs show that there is a degree of interconnection in the fibres of the organic matrix between the tooth stylus, junction zone and tooth cusp in the region above the distal end of the canal (Figure 6.5). A layered pattern in the structure of the organic matrix can also be observed at the posterior base of the cusp (similar to that observed in the plume region in Figure 4.7, Chapter 4), which does not appear to penetrate across the region of fibres connecting the stylus, junction zone and cusp.

Longitudinal sections through the radula in this immature region confirm that the stylus canal is filled with cellular material, resembling that of columnar type epithelial tissue (Figure 6.4). Nuclei are clearly visible within the canal tissue approximately 30 μm from the apical pole of each cell. Dark staining granules are also present within the canal tissue (Figure 6.4), which appear as electron dense bodies when observed under the TEM (Figure 6.6). At tooth rows seven and eight the granules appear to aggregate approximately 8 μm from the apical pole of each cell and co-occur with numerous mitochondria. High resolution TEM images reveal variations in granule structure and electron density, with certain granules either containing dense inclusions or an outer layer of dense material, whilst others appear to be membrane bound (Figure 6.7).

Figure 6.2. Scanning electron micrographs of whole and fractured major lateral teeth from the chiton *A. hirtosa*. cp = canal pore, tc = tooth cusp, ts = tooth stylus. (Code: CP, F).

A, two left major lateral teeth cleaned and left *in situ* on the radula showing the relative position of the canal pore on the medial surface of the tooth stylus. Arrowhead denotes anterior direction. Scale bar = 100 μm.

B, medial tooth surface, highlighting the central position of the canal pore on the tooth stylus. Arrow denotes a fracture at the junction zone. Scale bar = 100 μm.

C and **D**, higher magnification images of the canal pore. Scale bars = (C) 50 μm and (D) 25 μm.

E, lateral surface of stylus fractured to expose the distal arm of the stylus canal and highlighting the close proximity of the canal to the junction zone region (arrow). Note: The tooth cusp was removed from the stylus during processing. Scale bar = 100 μm.

F, alternate view of the same tooth as shown in E highlighting the tubular nature of the canal and the location of the junction zone (arrow). Note the opposing surface of the canal in the tooth fragment (on left). Scale bar = 100 μm.

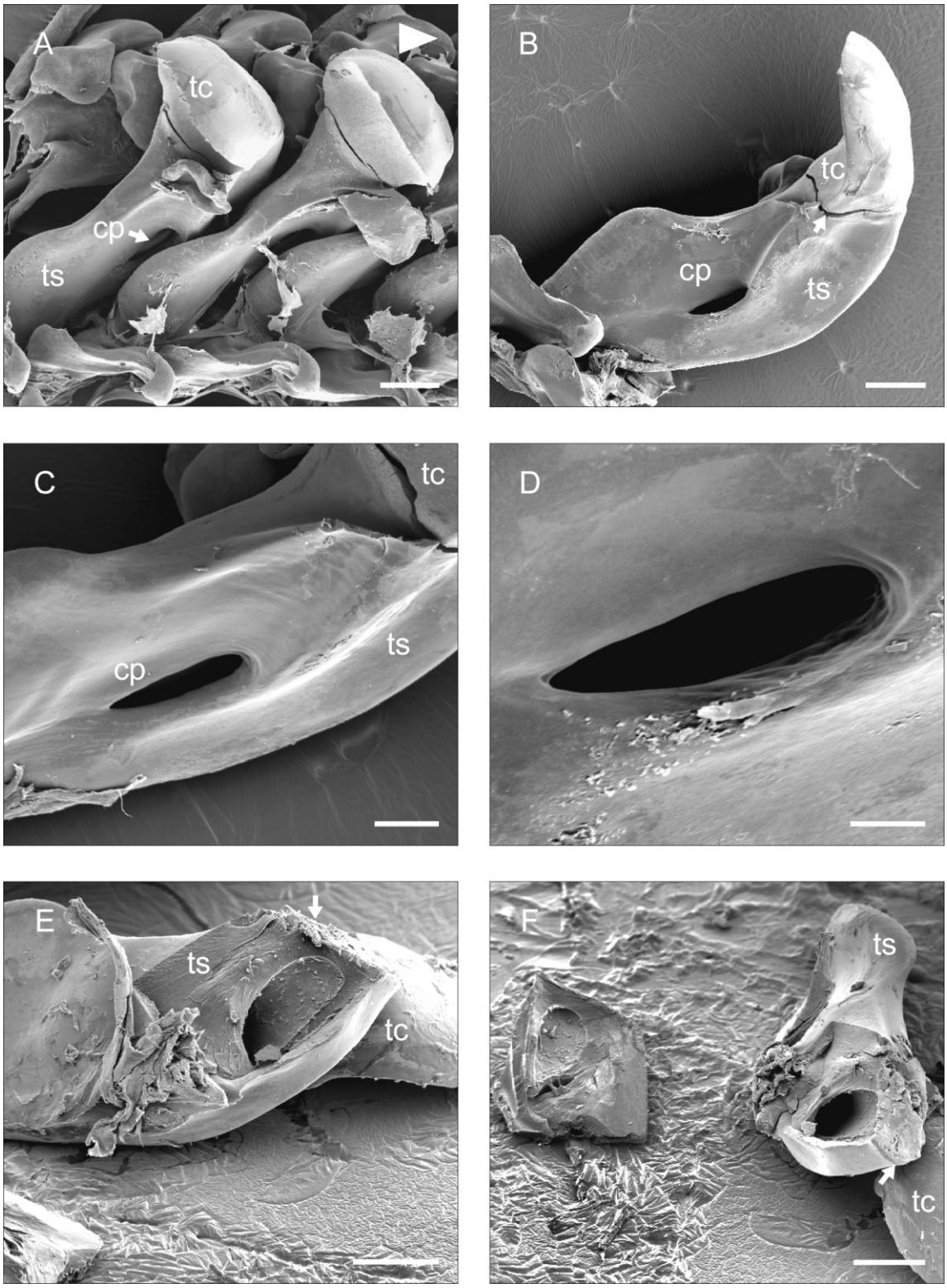
A
tc
cp
ts
B
tc
cp
ts
C
tc
ts
cp
D
E
ts
tc
F
ts
tc

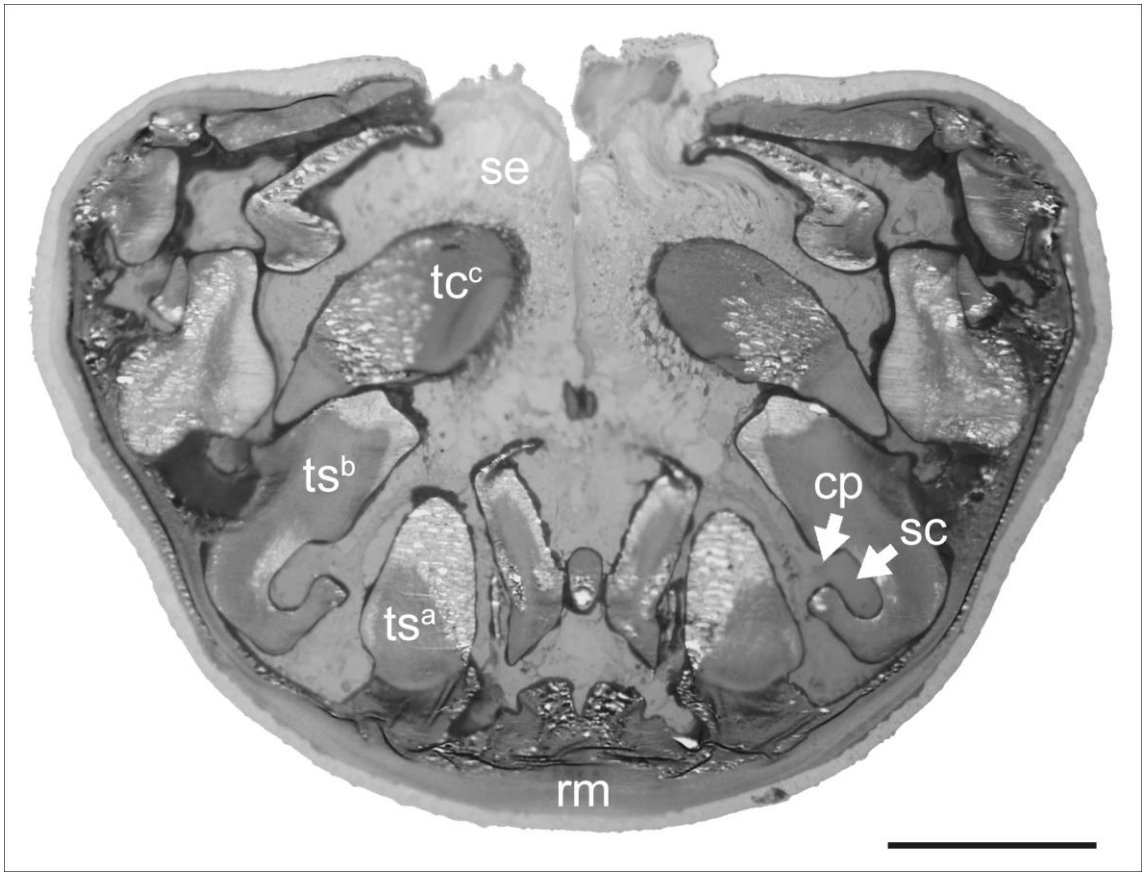

Figure 6.3. Transverse section through the radula of *A. hirtosa*, at approximately row 10, encompassing three major lateral tooth rows (a), (b) and (c). The tooth stylus (ts) at row (b) shows the canal pore (cp) opening into the stylus canal (sc), which is filled with epithelial tissue. Note: Due to the overlapping and interlocking nature of each tooth row, three separate major lateral teeth are sectioned simultaneously in a single transverse section. rm = radula membrane, se = superior epithelium, tc = tooth cusp. (Code: MP, B), Scale bar = 200 μm.

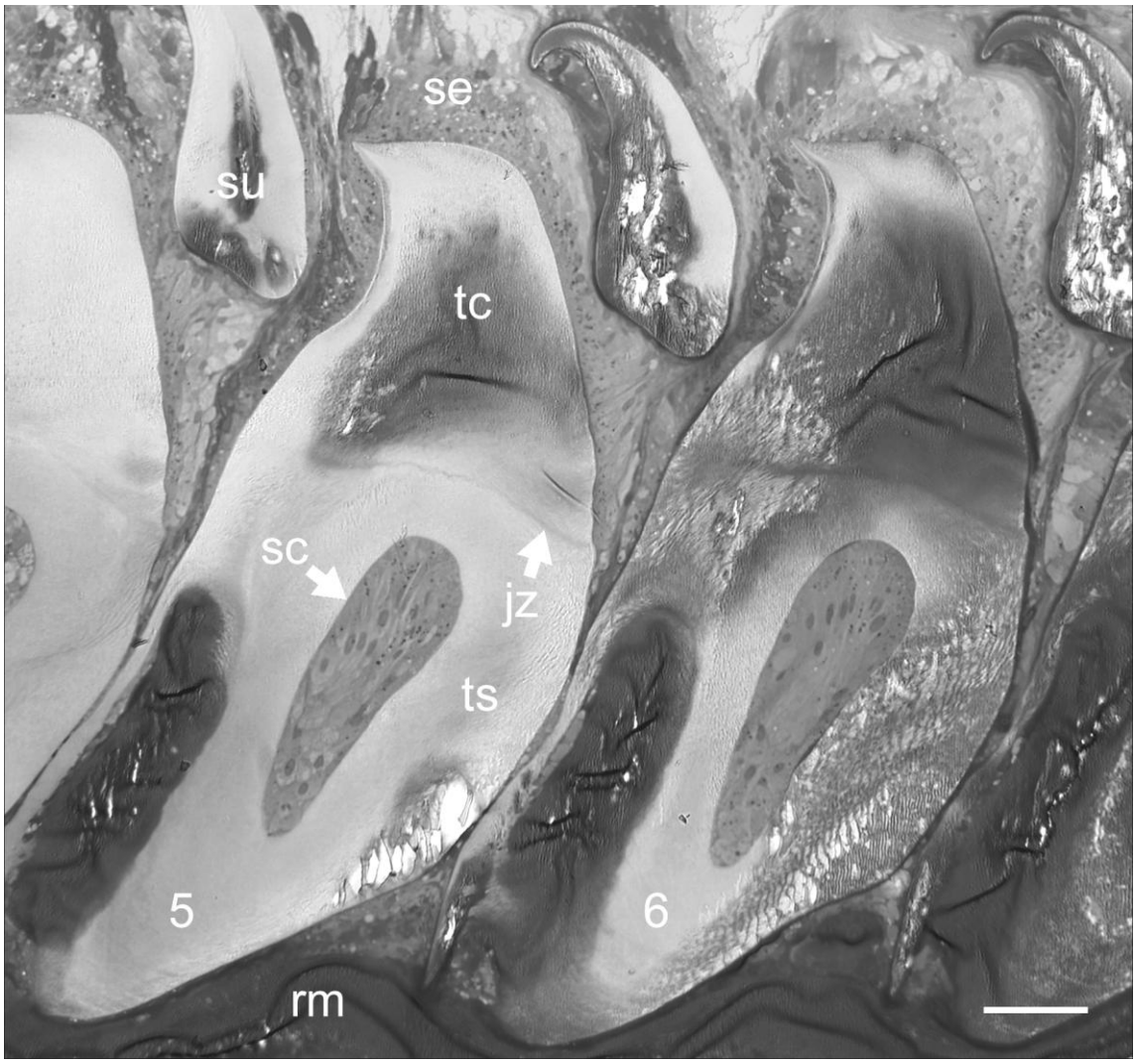

Figure 6.4. Light micrograph of a microwave prepared radula from *A. hirtosa*, sectioned longitudinally through major lateral tooth rows 5 and 6. Note the sectioning differences between the cusp (tc) and stylus (ts) above the canal (sc), especially in row six. jz = junction zone, rm = radula membrane, se = superior epithelium, su = spatulate uncinal tooth. (Code: MP, B), Scale bar = 50 μm.

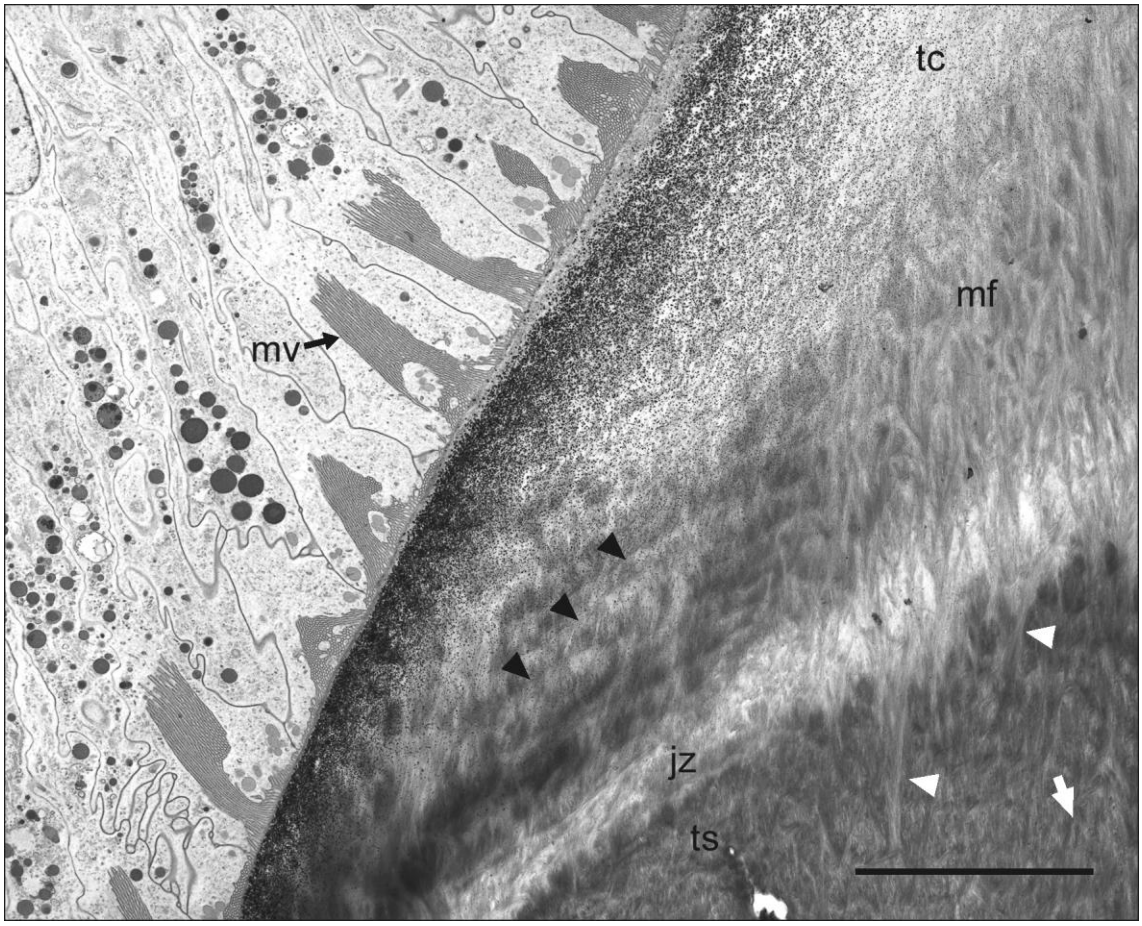

Figure 6.5. Major lateral tooth from the chiton *A. hirtosa* at row 17, three rows after the onset of mineralisation, highlighting the continuity of matrix fibres (mf and white arrowheads) between the tooth stylus (ts), junction zone (jz) and tooth cusp (tc) in the region above the stylus canal (arrow denotes direction of the canal). Note the layers in the structure of the organic matrix (black arrowheads), which run parallel to the junction zone from the posterior surface of the cusp but do not pass across the fibres connecting the stylus, junction zone and cusp. mv = mirovilli. (Code: CP, C), Scale bar = 10 μm.

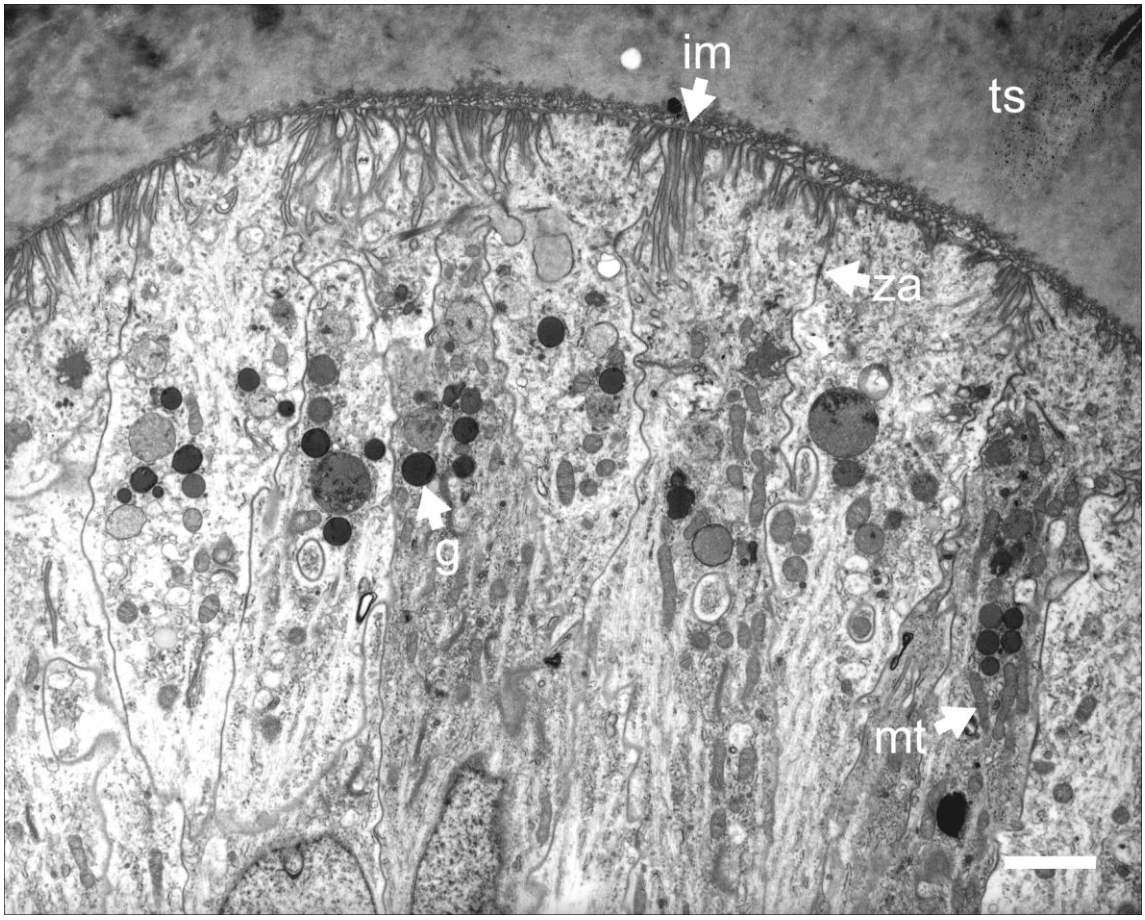

Figure 6.6. Stylus canal cells within the major lateral tooth stylus (ts) of *A. hirtosa* at row 8. Electron dense granules (g), interdigitating membranes (im), zonula adherens (za) and mitochondria (mt) are all present within the apical pole region. (Code: MP, D), Scale bar = 2 μm.

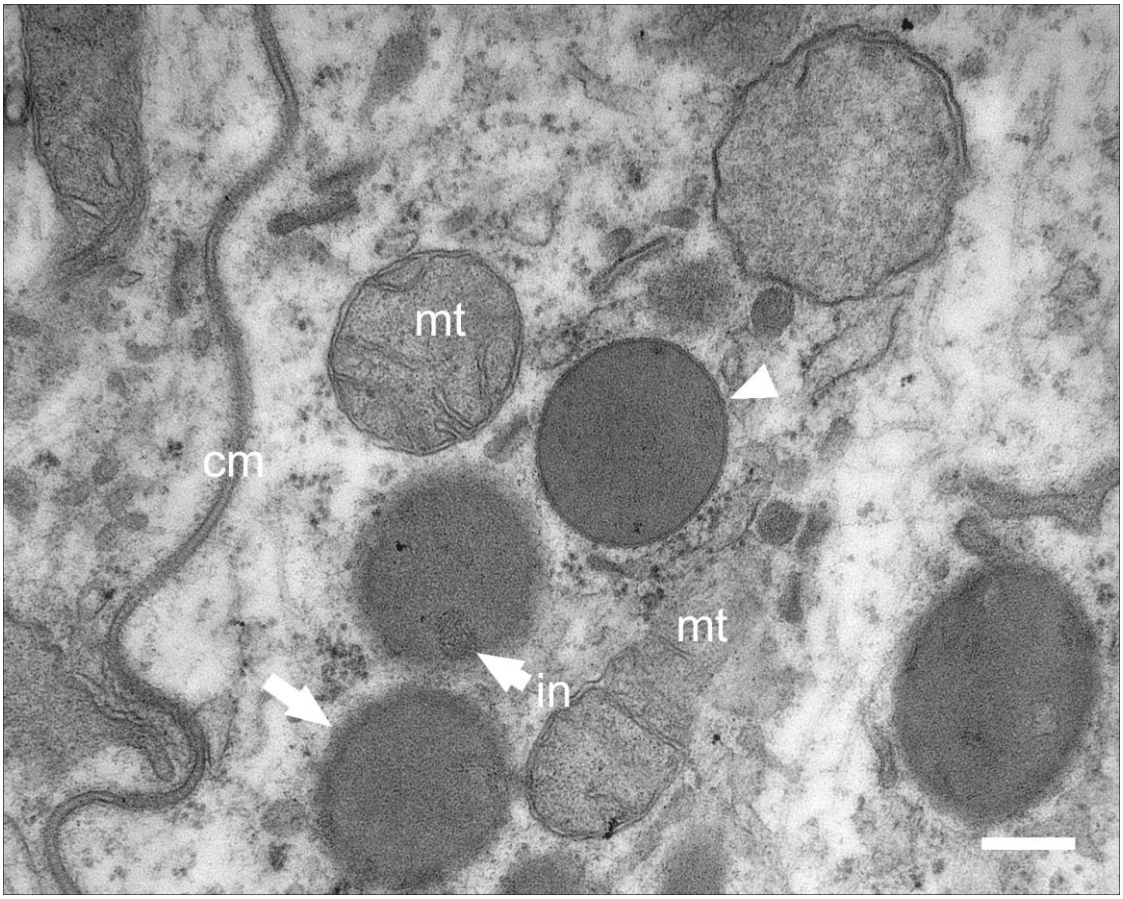

Figure 6.7. Electron dense granules within the apical region of the stylus canal cells in *A. hirtosa*, with variations in structure, including granules with membranes (arrowhead), dense inclusions (in) and dense borders (arrow). cm = cell membrane, mt = mitochondria. (Code: MP, D), Scale bar = 200 nm.

Other features within the apical region of the canal cells include interdigitating membranes that project into the apical cytoplasm from the distal surface of the canal (Figure 6.6 and 6.8). Notably, the interdigitating membranes of the canal epithelium are found only in the distal region of the canal, where the cells abut the surface closest to the junction zone. Junctional complexes, common to epithelial cells, are evident due to the presence of zonula adherens, which can be observed in the cell membrane near the apical terminus of each cell. In addition to the structures already mentioned, numerous organelles are present within the cytoplasm between the apical pole and the nuclei of each canal cell, including rough and smooth endoplasmic reticulum, Golgi apparatus and lysosomes (Figure 6.9).

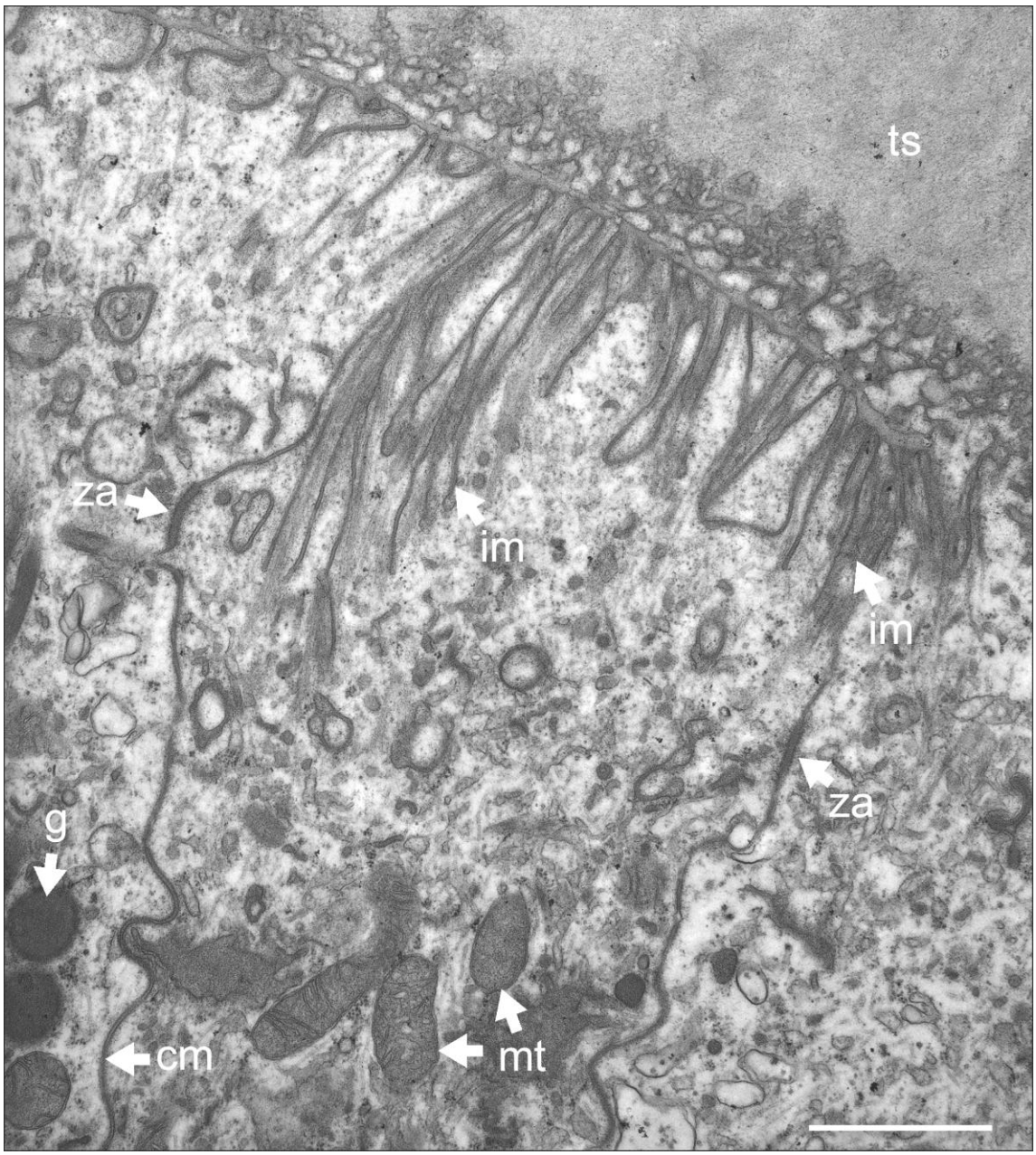

Figure 6.8. Cellular ultrastructure of the apical pole region of the stylus canal cells of *A. hirtosa* below the junction zone region at tooth row 8. Interdigitating membranes (im) are in contact with the tooth stylus (ts) and zonula adherens (za), typical of epithelial tissue, are present in the cell membranes (cm). Mitochondria (mt) and electron dense granules (g) are also present. (Code: MP, D), Scale bar = 1 μm.

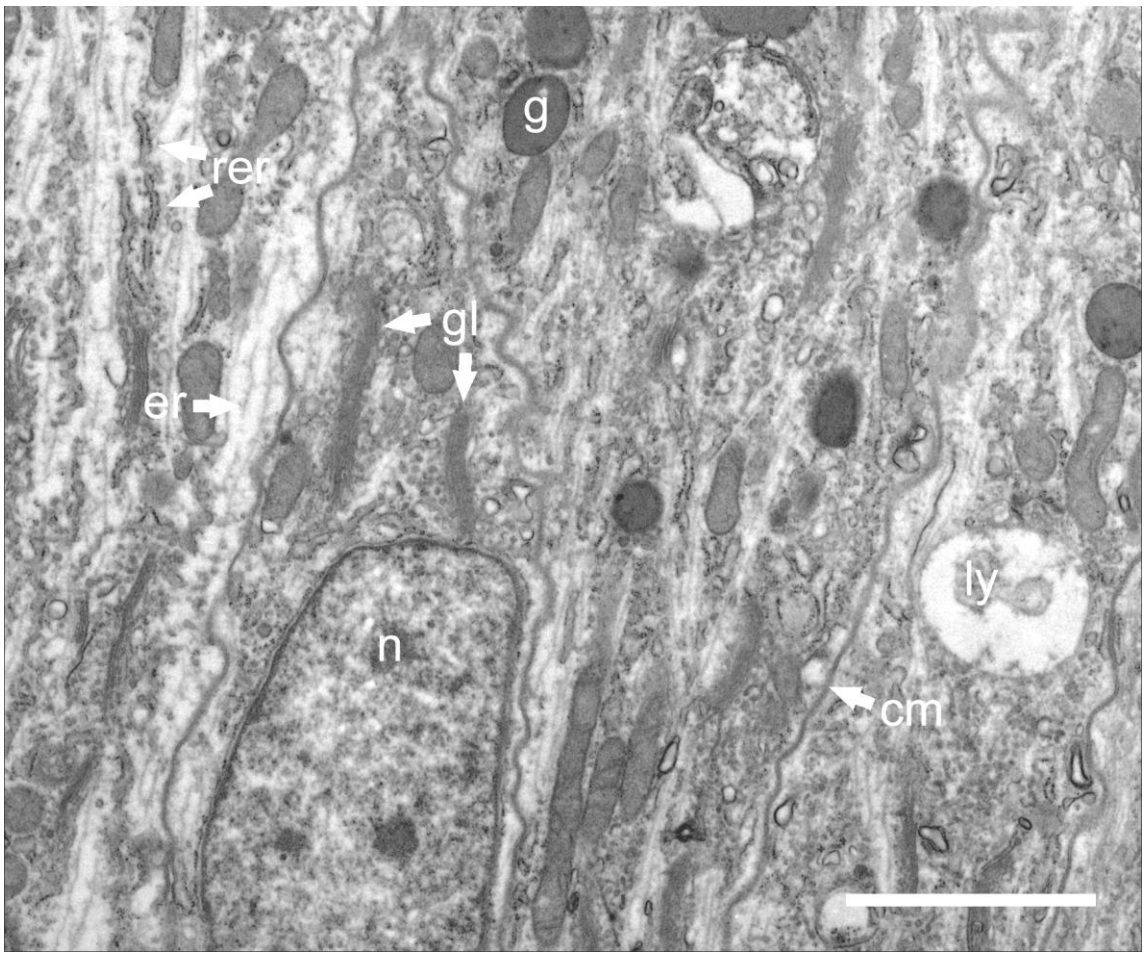

Figure 6.9. Organelles within the cytoplasm between the apical poles and nuclei of the stylus canal cells of *A. hirtosa* at tooth row 7. cm = cell membrane, er = endoplasmic reticulum, g = granule, gl = golgi apparatus, ly = lysosome, n = nucleus, rer = rough endoplasmic reticulum. (Code: MP, D), Scale bar = 2 μm.

The stylus canal was present in all species examined (see Table 6.1), and whilst some variation in the dimensions of the canal occurred relative to the respective size of the tooth cusps, the overall structure of the canal in each species closely resembled that described for *A. hirtosa*. In addition, personal communications and previous literature have confirmed that the stylus canal is present in a further 19 species sourced from various geographic locations worldwide (Table 6.2).

Table 6.2. Species from which the presence of the stylus canal has been confirmed by personal communication and previous literature.

Species	Geographic region	Reference
Acanthopleura vaillantii (Rochebrune, 1882)	Egypt	Personal communication (Brooker, 2007)
Acanthopleura haddoni (Winckworth, 1927)	Oman	
Acanthopleura testudo (Spengler, 1797)	Gulf of Aden Red Sea	
Acanthopleura granulata (Gmelin, 1791)	America (East Coast)	
Acanthopleura echinata (Barnes, 1824)	Peru Chile	
Acanthopleura brevispinosa (Sowerby, 1840)	Seychelles Africa (East Coast)	
Acanthopleura tenuispinosa (Leloup, 1939)	Japan	
Acanthopleura japonica (Lischke, 1873)	Hong Kong Japan	
Acanthopleura gaimardi (Blainville, 1825)	Australia (East Coast)	
Acanthopleura arenosa Ferrerira, 1986	Australia (East Coast)	
Acanthopleura loochooana (Broderip & Sowerby, 1829)	Japan	
Acanthopleura nigra (Barnes, 1824)	Peru	
Acanthopleura araucariana (Hedley, 1898)	New Caledonia Tonga	
Acanthopleura curtisiana (Smith, 1884)	Australia (West Coast)	
Acanthopleura miles (Carpenter in Pilsbry, 1893)	Australia (West Coast) West Java Philippines North Borneo Sri Lanka Indonesia	
Acanthopleura rehderi Ferreira, 1986	Cook Is.	
Ischnochiton australis (Sowerby, 1840)	Australia (East Coast)	
Lepidochitona hartwegii (Carpenter, 1855) *Mopalia muscosa* (Gould, 1846)	America (West Coast)	(Nesson and Lowenstam, 1985)

6.4. Discussion

This is the first study directed at resolving the structure and function of the stylus canal in the major lateral teeth of chitons. The columnar epithelial configuration of the cells, and distal position of the interdigitating membranes within the canal, exactly parallels that of the superior epithelium (for details see Chapter 5), and strongly suggests that, in *A. hirtosa*, the stylus canal is involved in the delivery of elements for the process of tooth biomineralisation. This finding challenges the long standing view that the transport of elements for tooth mineralisation occurs only via the superior epithelial tissue surrounding the cusps (see for example: Towe and Lowenstam, 1967; Nesson and Lowenstam, 1985; Kim *et al*., 1989; Webb *et al*., 1989), and supports the

growing body of evidence that suggests mineralising elements are transported into the cusp via the junction zone (see for example: Macey and Brooker, 1996; Brooker and Macey, 2001; Brooker *et al*., 2003; Chapters 4 and 5).

The stylus canal terminates directly below the centre of the junction zone, the plate-like interface between the stylus and cusp, where iron is first deposited prior to its appearance in the tooth cusps of chitons (see for example: Macey and Brooker, 1996; Brooker and Macey, 2001; Brooker *et al*., 2003; Chapter 4). Although the precise mechanism of iron delivery to the junction zone is unknown, the stylus canal is conveniently positioned to provide a pathway for the indirect delivery of iron and other mineralising elements to this region, and subsequently into the tooth cusp proper.

The junction zone has previously been proposed to act as a source of iron for an internal mineralising front within the magnetite region in the chiton *A. echinata* (Brooker *et al*., 2003). The formation of this region has been shown to occur simultaneously from two fronts, the first of which forms along the posterior surface of the cusp, and the second forms in parallel to the first approximately 20 - 30 μm further into the cusp (Chapters 4 and 5). While the supply of iron for this multiple-front mineralisation is likely to, in part, derive from the epithelium on the anterior and posterior cusp surfaces, this model does not fully explain the later deposition of other minerals, such as apatite, into the core region, which only occurs after iron deposition is complete (Brooker *et al*., 2003). In addition, certain chiton species, such as *Ischnochiton australis* and *Plaxiphora albida*, deposit magnetite over both the anterior and posterior surfaces of the tooth cusp prior to core mineralisation, leaving only a small window for the passage of mineralising elements on the anterior face of the cusp near the junction zone (Macey *et al*., 1996; Brooker and Macey, 2001). This envelope of crystalline magnetite would severely limit the further delivery of elements, from either the anterior or posterior cusp epithelium, into the core region of the cusp. As such, the

stylus canal may not only play a significant role in the initial delivery of iron to the junction zone, but may also be responsible for the delivery of elements to the core region during later stages of cusp development.

Despite the relatively short distance of only approximately 25 μm between the stylus canal and the junction zone, the precise mechanism of element transfer through this region is unclear. The structural organisation of the tooth's organic matrix is complex, consisting of fibres of variable size and orientation that vary in their arrangement depending on the species (Evans *et al*., 1990, 1991; Macey *et al*., 1996). Notably, there is a degree of continuity between the organic matrix fibres in the region above the distal tip of the canal between the cusp, junction zone and stylus. Although the extent of this interconnection has not been fully explored, the accumulation of iron at the junction zone, prior to mineralisation, is always limited to a discrete band at the interface between the cusp and stylus. As such, there must be an, as yet, undetermined structural property of the matrix at the junction zone that is different to that of the cusp and stylus. This property not only limits iron movement, thereby allowing it to be stored in this region, but also facilitates the controlled release of iron at the onset of mineralisation.

The changes in the sectioning quality of the teeth prior to mineralisation are likely to be the result of developmental processes, such as tanning, that correspond to the maturation of hard elements along the radula. The progressive hardening of the teeth reduces chemical fixative and resin infiltration, resulting in the deterioration of tissue preservation and sectioning properties. As such, adequate fixation of the stylus canal tissue was only achieved in the immature region of the radula to approximately row 13. Notably, there is a tendency for the integrity of sections to be better preserved above the stylus canal, which suggests that the region between the canal and junction zone may be more porus, thereby improving resin infiltration.

Direct and anecdotal evidence indicates that the stylus canal is a structure unique to polyplacophoran molluscs. It has been found in all chiton species examined to date, while an equivalent structure has not been documented in any other molluscan group (Fretter and Graham, 1962; Hickman, 1977; Messenger and Young, 1999). Indeed, the bases of gastropod teeth are solid in structure (Hickman, pers. comm., 2006). The canal is present in adult chiton teeth, regardless of the size of the species, or the size of their radula teeth. For instance, it is found in small species, such as *Acanthochiton johnstoni*, whose major lateral teeth are approximately 260 μm in length, and in large species, such as *Cryptochiton stelleri*, whose major laterals can reach 1.1 mm in length (Shaw unpublished data). This suggests that it plays a major functional role in all species. Conversely, the absence of a canal in the bases of all remaining non iron-mineralised teeth, irrespective of chiton species, also points strongly to a functional relationship between the stylus canal and tooth cusp mineralisation.

In support of this, preliminary investigations have revealed that the stylus canal is absent in *A. hirtosa* juveniles two days after metamorphosis, even though specimens possess iron mineralised tooth cusps at this early age (data not shown). It is unlikely that these teeth, which are no larger than 2 μm in diameter, support the same architectural complexity as observed in adult specimens, and would therefore not require the same level of control for mineral deposition. In addition, their smaller size would make it easier for mineralising elements to diffuse into the teeth. Further studies on tooth development from juvenile to adult may correlate stylus canal formation with increasing compositional and structural complexity within the cusp.

Serial sections have not revealed the location of the basal pole of the canal cells in *A. hirtosa*, which have been reported to exist at the lateral margins of the dorsal sinus for the chitons *Lepidochitona hartwegi* and *Mopalia muscosa* (Nesson, 1969). For *A. hirtosa*, which is similar in overall size to *M. muscosa* (Piercy, 1987), the distance

from the apical pole of the canal cells to the lateral margins of the dorsal sinus is approximately 800 μm, a distance that is unlikely to be controlled by a single cell (see Figure 6.3). The closest point of contact between the apical poles and the dorsal sinus occurs centrally along the radula, although this is still a distance of approximately 700 μm. Studies aimed at locating the basal poles of the canal cells are required in order to further elucidate the pathways involved in the delivery of mineralising elements to the cusps.

Iron is known to enter the cusp epithelium by endocytotic uptake at the basal cell membrane (Nesson, 1969; Nesson and Lowenstam, 1985). However, multiple pathways of iron uptake may exist, including membrane transport proteins such as Divalent Metal Transporter 1 (Eisenstein, 2000; Sargent *et al*., 2005). Such a protein may explain the presence of ferritin molecules within the minor cells despite the absence of endocytotic uptake at the cell membrane by the minor epithelium, as observed by Nesson (1969) and Nesson and Lowenstam (1985). Notably, Nesson (1969) observed higher concentrations of iron molecules in the minor cells terminating on the inner and outer surfaces of the major lateral tooth stylus, than in the cells of other minor teeth. In addition, through radioactive labelling experiments using Fe^{59}, Nesson (1969) determined higher specific activity of iron in the tooth styli compared to the cusps, and concluded that iron deposition in the styli occurred via a different pathway and kinetics to that of cusp mineralisation. As such, the stylus canal cells, although characteristic of other radula epithelia, may form a third tissue type, with a distinctly separate function to the cusp and minor epithelial tissues.

Preliminary observations on the tooth styli of the limpet *Patelloida alticostata* have revealed an opening similar to the canal pore in *A. hirtosa*. However, serial sections through *P. alticostata* radulae have not confirmed the presence of a prominent canal structure directly below the junction zone. The existence of a canal-like structure

in limpets would suggest some connection between the presence of this feature and iron mineralisation. Although limpets mineralise their tooth cusps with the iron oxide goethite rather than magnetite, as in chitons, the initial influx of iron still occurs at the junction zone, where it has also been proposed to act as a reservoir for elements prior to the onset of mineralisation in the cusps (Liddiard *et al*., 2004; Sone *et al*., 2007). While similar in the overall process of development, the structure and composition of limpet teeth is distinctly different from that of chitons. Limpets rely on silica in the form of hydrated amorphous opal ($SiO_2 \cdot nH_2O$) to mineralise the stylus and to provide support to the goethite cusps (Jones *et al*., 1935; Runham *et al*., 1969; Liddiard *et al*., 2004). However, silica deposition in limpets is far less ordered when compared to the highly organised tooth structure of chitons, where various minerals are formed within architecturally discrete compartments (Mann *et al*., 1986; Liddiard *et al*., 2004).

Chapter 7

General Discussion and Conclusions

7.1. Summary

This thesis presents, for the first time, a comparative view of the major lateral tooth cusp mineralisation process, including the effects of iron limitation, together with a precise, row-by-row, investigation of the concomitant development of the superior epithelial tissue surrounding the teeth of the chiton *Acanthopleura hirtosa*. A holistic approach has been adopted, which encompasses observations over a range of spatial scales, from whole radula mineralisation processes to those occurring within, and around, individual tooth cusps at various stages of development. Previous studies on radula development and mineralisation have made observations on either the cusps or tissues in isolation, and while this has provided a wealth of structural and compositional information, the mechanisms of mineral deposition remain poorly resolved (see for example: Nesson and Lowenstam, 1985; Kim *et al*., 1989).

By following the development of the superior epithelium with that of the tooth cusps during the early stages of mineralisation, this study has elucidated a number of key aspects related to the cellular basis of biomineralisation in the major lateral teeth. Cusp mineralisation would appear to be under strict cellular control, where the chemical environments surrounding, and within, the extracellular compartment of the tooth are highly regulated, providing optimum conditions required for transport, mineral precipitation and crystal growth. Strong evidence is also provided to suggest that both the superior epithelium and cusp organic matrix coordinate to control the precise series of depositional events along the radula, delivering elements to the cusps in sequence, thereby permitting the high level of structural and compositional complexity demonstrated previously (see for example: Nesson and Lowenstam, 1985; Kim *et al*.,

1989; Lowenstam and Weiner, 1989; Webb *et al*., 1989; van der Wal *et al*., 1989; Evans *et al*., 1990; Lee *et al*., 1998; Brooker *et al*., 2003).

Importantly, this thesis highlights the stylus canal as a structure that is crucial in our wider understanding of the cusp mineralisation processes in chitons. Evidence for the canal's involvement in mineralisation stems from a number of findings established in this study. The canal is a feature that appears to be limited to chitons, suggesting that it may have evolved in synchrony with the cusp mineralisation process. In addition, the cells within the canal are almost identical in structure to the superior epithelium, and terminate only 25 μm below the centre of the junction zone, the initial site of element storage for cusp mineralisation. Indirectly, the absence of microvilli in the epithelium attached to the cusp surface at the junction zone, suggests that elements are not transported to the junction zone via this route. The interdigitating membranes or microvilli in the canal cells suggest that the transport of elements to the junction zone occurs by way of the stylus canal. Perhaps the strongest factor linking the stylus canal to cusp mineralisation is the presence of plumes, stemming from the junction zone in normal and iron-reinstated animals, which are situated directly above the distal terminus of the canal. Taken together, this evidence suggests that the stylus canal forms a major route for the delivery of iron, and other mineralising elements, into the tooth cusps.

7.2. Whole radula mineralisation processes

The progression of major lateral cusp development in normal radulae from the chiton *A. hirtosa* can be divided into seven key stages involving the cusps, junction zone and the surrounding tissue, and which encompass the underlying processes leading to mineralisation as well as the actual mineral deposition events. While the convention has been to consider these stages as discrete linear events, the new information provided by this study, together with the growing amount of literature pertaining to cusp development (see for example: Evans *et al*., 1994; Macey and Brooker, 1996; Brooker

et al., 2003 Numako *et al*., 2006), requires a more complex overlapping model, as outlined in Table 7.1. For the first time, it is also possible to integrate the stages of tissue development in the superior epithelium surrounding the cusps during the initial onset of mineralisation. It must be noted that where the duration of Stages II, V, VI and VII in Table 7.1 have been indicated as continuing to maturity (i.e. becomes ready for feeding), the exact point at which each stage "matures" has not been determined. In the case of the junction zone, elements passing from this region to the tooth core are likely to do so until the core is completely filled. The iron mineralised regions of the teeth may be considered fully mature following the complete conversion of ferrihydrite to magnetite or lepidocrocite, depending on the region; a process that, in *A. echinata*, has been shown to stop only just prior to the teeth emerging from the superior epithelium (Lee, 2000).

In *A. hirtosa*, the onset of mineralisation occurs at tooth row 13, following the coordinated influx of iron into the cusps from the cells of the superior epithelium and from the pool of iron at the junction zone, a region previously suggested as being important in cusp mineralisation (Macey and Brooker, 1996; Lee *et al*., 2000; Brooker *et al*., 2003), and now shown to be critical in the overall mineralisation strategy. The prior accumulation of elements at the junction zone is one of a number of processes that are required for nucleation and subsequent crystal growth to occur. These include the dramatic changes in cell development, such as the increasing abundance of mitochondria in the apical cusp epithelium, which is likely to create the correct conditions of pH and solubility required for iron to reach supersaturation within the cusp prior to nucleation. Following the onset of mineralisation, the dramatic elongation of the microvilli would vastly increase the surface area for both active and passive transport processes of materials into, and out of, the cusps. In addition, the high levels of iron in the tissues surrounding the cusps, together with this increased diffusion surface, would ensure the continued movement of iron along its concentration gradient into the cusp.

Table 7.1. The seven stages of major lateral tooth cusp development, together with the concomitant development of the apical region of the cusp epithelium, in normally mineralised radulae from the chiton *A. hirtosa*.

Stage		Row number	Location	Process	Description
Stage I	**A**	1-12	cusp	development of organics	Immature tooth cusps composed primarily of α-chitin
	B	*10-12	cusp epithelium	development of cells	Some ferritin present within the cusp epithelium. The abundance of mitochondria increases creating a reductive and acidic enviroment in the apical region and cusp.
Stage II		8-12	junction zone	element storage	Elements accumulate in this region, possibly via delivery from the stylus canal
Stage III	**A**	13	cusp epithelium	iron delivery	Large amounts of ferritin appear in the cusp epithelium. Microvilli develop, transporting iron into the cusp.
	B	13	posterior cusp	nucleation	Onset of cusp mineralisation. Iron passes into the cusps from the superior epithelium and junction zone. Supersaturation of iron is reached and nucleation is initiated
Stage IV	**A**	14	cusp epithelium	iron delivery	Iron transport and deposition progresses. Microvilli continue to develop and large amounts of ferrtin persist in the apical region, which maintains the concentration gradient of iron into the cusp.
	B	14	posterior cusp	mineral formation	Orange tooth row. First visual evidence of mineral formation in the form of the amorphous precursor mineral ferrihydrite
Stage V	**A**	15-18*	cusp epithelium	iron delivery (post nucleation)	Fall in abundance of mitochondria as the requirement for maintaining iron as Fe^{2+} within the cusp is reduced following nucleation. Iron transport and delivery continues.
	B	15 to maturity	posterior cusp	mineral formation	Black tooth rows. Phase transformation of ferrihydrite to magnetite
Stage VI		31 to maturity	magnetite/core boundary and anterior surface	mineral formation	Lepidocrocite deposition at the boundary layer between the magnetite and core region and over the anterior cusp surface towards tip.
Stage VII		37 to maturity	core region	mineral formation	The core is progressively infilled with apatitic calcium phosphate from the core tip to the junction zone

* Denotes the lower and upper limit of tooth rows observed during the study on the epithelium.

Notably, the various processes involved in preparing the teeth for mineralisation appear to be dependent on the iron status of the tissues. In normal animals, the presence of iron at the junction zone, and the formation of mitochondria, microvilli and iron-containing granules within the apical epithelium, follow the developmental pattern as outlined in Table 7.1. However, this pattern changes in animals for which the availability of iron has been severely limited. In particular, mitochondria continue to accumulate within the apical region of the cells in iron-limited animals, while the microvilli remain in a similar state to that observed in the cusps prior to the onset of mineralisation. This suggests that mitochondrial accumulation is important for preparing the cusps for mineralisation, and occurs independently to the levels of iron within the epithelial tissues. Conversely, microvilli development appears to depend on the arrival of large amounts of iron immediately prior to mineralisation.

It has been demonstrated for the first time that the cellular processes associated with particular mineralisation "stages" are not limited to static regions along the radula. While iron-limitation has been shown to suspend mineralisation, the cusps and tissues of the partially mineralised and additional teeth, formed during this period, are capable of resuming the transport and delivery of iron upon its reinstatement. However, this transport and delivery does not return to the normal point of deposition at row 13, and instead, iron returns to the tissues and cusps in the region where mineralisation was suspended towards the anterior end of the radula.

This is suggested to occur because the iron is being delivered along the dorsal sinus to the first available teeth from an anteriorly situated supply of hemolymph. This is evidenced by the reappearance of iron in the superior epithelial tissues of these anteriorly situated cusps, and also the diminishing size of plumes seen above the junction zone, which become smaller in the posterior direction, following iron-reinstatement. Although iron-limitation is unlikely to occur for long periods in

nature, this property of the superior epithelium would ensure that the concentration gradient of iron in the anterior most teeth remains high. This would also ensure the continued formation of magnetite, and that it remains in the cusps once delivered.

7.3. Cusp mineralisation processes

The discovery of what appears to be a well defined delivery pathway for iron, and presumably other elements, within the major lateral tooth cusps of normal and iron-reinstated *A. hirtosa* radulae, suggests that the delivery of mineralising elements to the extracellular compartment of the cusp may be under far greater control than previously considered (Figure 7.1). In addition to the epithelial tissue surrounding the cusps, this internal pathway, situated initially between the magnetite and lepidocrocite regions, and subsequently between the lepidocrocite and apatite regions of the tooth, appears to provide a further route for the delivery of elements to the mineralising fronts within the cusp. The evidence provided in this thesis strongly suggests that these pathways may be supplied from the reservoir of elements stored at the junction zone, and are responsible for the sequential delivery of elements to the various mineral regions of the cusp mentioned above. Various studies have reported on the unique structural and compositional properties of the boundary between the magnetite and core regions of the tooth cusp (van der Wal *et al*., 1989; Evans *et al*., 1990; Evans *et al*., 1994; Brooker *et al*., 2003). The organic matrix in this area seems to possess properties that not only mediate the formation of lepidocrocite, thereby contributing to the structural attributes of the cusp, but also play a major transport role in delivering mineralising elements to the cusps.

This internal delivery pathway also provides supporting evidence for the recently discovered process of multiple front mineralisation, where the formation of magnetite has been observed to first occur at the anterior and posterior margins of this region

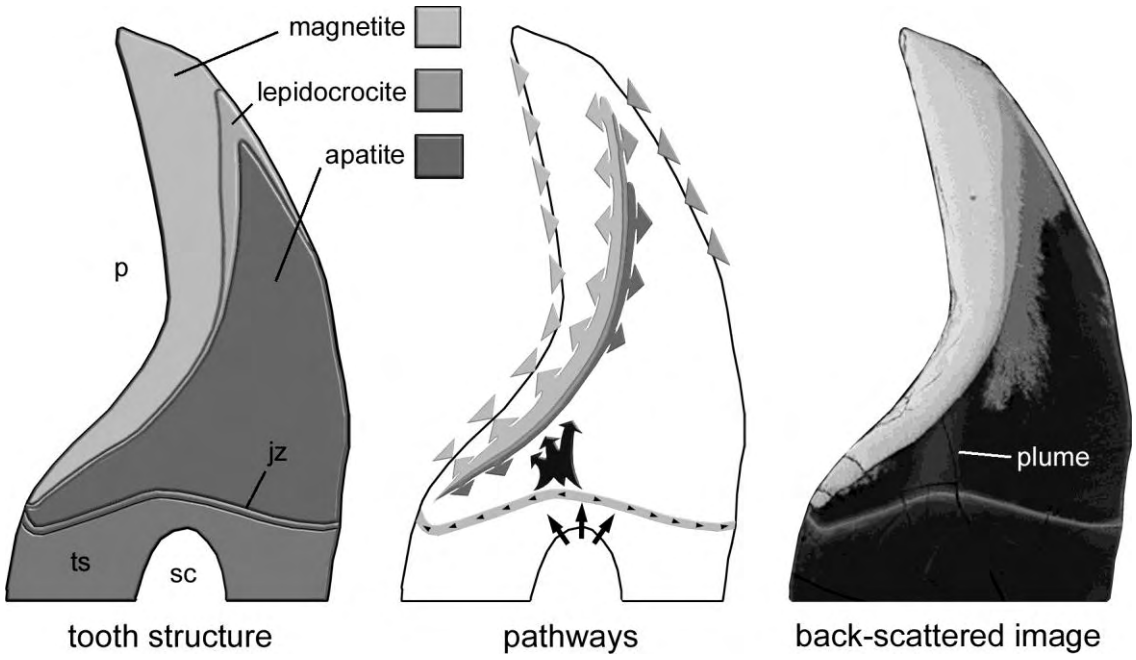

Figure 7.1. Diagrammatic representation of the proposed system of pathways responsible for delivering elements to the various mineralising regions within the major lateral teeth of the chiton *A. hirtosa*. The black arrows within the stylus canal (sc) represent the unknown mechanism responsible for the transfer of elements from the canal to the junction zone (jz). Elements are then distributed and stored within the junction zone (small black arrowheads) prior to being transferred to the various mineralising regions of the cusp. This transfer occurs via a plume within the tooth core, where elements are then delivered along a major mineralisation pathway situated between the magnetite and core regions of the cusp. Arrowheads on the anterior surface of the cusp represent the cellular delivery of iron from the anterior cusp epithelium, which may be responsible for lepidocrocite formation in this region. Arrowheads on the posterior (p) surface of the cusp represent the delivery of iron to the magnetite region by the cusp epithelium. ts = tooth stylus.

(Brooker *et al*., 2003). Such a mineralisation strategy would be advantageous for rapidly achieving the critical density of iron needed to reach supersaturation; thereby creating the conditions needed for nucleation. Multiple front mineralisation is supported by TEM evidence, which indicates that nucleation and subsequent crystal growth are initiated from both the posterior surface and an internal front. A supply of iron from two fronts would also be more suitable for maintaining a high concentration gradient of iron to this region, thereby ensuring the full transformation of ferrihydrite to magnetite, especially in light of the self limiting nature of mineral formation.

The complexity of the organic matrix is perhaps the most fascinating aspect of tooth mineralisation in chitons. In concert with the chemical environment created by the superior epithelial tissue, the organic matrix provides the overall structural framework for the tooth, the foundation for crystal nucleation and dictates the particular mineral polymorphs that form within the cusp. In addition, regions of the organic matrix have been suggested to direct or facilitate the movement of elements along defined pathways to the various mineralising fronts within the cusp. This ability to selectively distribute elements in particular directions suggests that there may be organic barriers within the cusp, the structure and/or composition of which effectively limits the movement of elements to isolated regions of the cusp. This selectively permeable barrier would be advantageous as it would break the cusp into smaller subregions, as has been suggested previously (Evans *et al*., 1994), thereby making it easier to control the conditions required for reaching supersaturation and initiating nucleation.

7.4. Further studies

This thesis presents the first example of the use of iron-limitation as a technique for resolving biomineralisation processes in chitons. The ability to perform comparative studies of mineralisation events in normal, iron-limited and iron-reinstated animals

provides a valuable new foundation upon which a wide range of studies can be undertaken.

Iron-limitation may prove useful for studies aimed at resolving the mechanisms involved in sequestering mineralising elements from the environment, and their subsequent transport and delivery to the teeth. In particular, the source from which chitons obtain the iron necessary for radula mineralisation remains unresolved. The possible candidates for such uptake include their algal food source, the incidental ingestion of rock substrate, seawater and the recycling of their own chipped and worn teeth. Experiments utilising iron-limitation and isotope labelling could be performed in conjunction with new techniques such as nanoscale secondary ion mass spectrometry (NanoSIMS); a system that is capable of mapping the precise distribution of selected ions returning to both the teeth and tissues of the radula.

The ability to suspend the deposition of minerals within the tooth cusps also provides a new approach for the study of the organic matrix, the properties of which remain poorly understood. Once mineralised, the extreme hardness of the tooth cusps prevents the use of techniques such as TEM, and the large amounts of deposited mineral effectively mask the presence of the matrix in more mature teeth. In the past, studies of the matrix have utilised harsh chemical demineralising techniques to remove the mineral component of the cusps (see for example: van der Wal *et al*., 1989; Evans *et al*., 1990; Evans *et al*., 1994), treatments that are likely to introduce artifactual information. Although the effects of the iron-limitation process may compromise aspects of matrix formation, this thesis shows that the internal mineralisation pathways within the cusp at least remain viable. Iron-limitation studies may therefore be used to study the structure and composition of the matrix in a mature unmineralised state.

Another fundamental step in the study of these animals is the use of molecular techniques for identifying the unique genes and proteins that are responsible for the

formation of the various biominerals in chiton radulae. Such studies have already commenced, where a list of candidate genes associated with specific biomineralisation events along the radula has been compiled (Brooker *et al*., 2006a; Brooker, pers. comm., 2007). By comparing the expression levels of these genes between radulae from normal and iron-limited animals it may be possible to establish their role in the pathways associated with specific biomineralisation events. The detailed account of the various stages of biomineralisation in *A. hirtosa* provides an excellent basis upon which to frame such future studies.

It is increasingly evident that the structural and functional properties of both the organic matrix and junction zone are highly complex. This study has shown that discrete pathways exist within the cusps, where elements are selectively transferred to the various mineralising regions of the cusp. In addition, despite the apparent continuity of fibres between the cusp, junction zone and tooth stylus, the junction zone appears to be able to retain high concentrations of elements and then release them into the cusp on a selective basis. The structural or biochemical mechanisms controlling the passage of elements within the matrix and junction zone must be elucidated in order to gain a full understanding of tooth mineralisation processes in these animals.

While the mineral composition and structure within the major lateral teeth varies depending on the species, recent studies suggest that, in addition to magnetite, many chitons posses a narrow band of either lepidocrocite or limonite between the magnetite and core regions of the cusp (Brooker and Macey, 2001; Lee *et al*., 2003a). The chiton *A. rehderi* is unusual in that it possesses a very limited magnetite region across the tip of its' four tooth denticles and an, as yet, unidentified mineral between the magnetite and core region (Lee *et al*., 2003b). A close examination of the internal pathways in chitons with different minerals in the boundary and core regions to that of *A. hirtosa*, such as

that of *A. rehderi*, may provide further insights into the cusp mineralisation strategies of these animals.

Further studies aimed at elucidating the role of the stylus canal in cusp mineralisation are critical. Although the evidence provided in this thesis strongly supports a link between the canal and cusp mineralisation, the transport mechanism for elements through the 25 μm section between the tooth stylus and junction zone has not been identified. Once again, techniques such as NanoSIMS, or molecular techniques such as *in situ* hybridisation, could be used to confirm the existence of a transport pathway in this region. In addition, the possibility of the existence of a canal-like structure in limpets needs to be confirmed. The presence of the junction zone in limpets (Liddiard *et al*., 2004; Cruz and Farina, 2005; Sone *et al*., 2007) suggests that this region is extremely important for cusp mineralisation in both mollusc groups. Further studies on chitons and limpets are needed to determine whether the mechanisms involved in the transport of elements to this region differ between these groups.

References

Addadi, L., Joester, D., Nudelman, F., and Weiner, S. (2006). Mollusk Shell Formation: A Source of New Concepts for Understanding Biomineralization Processes. *Chemistry a European Journal* **12,** 980-987.

Addadi, L., and Weiner, S. (1989). Stereochemical and structural relations between macromolecules and crystals in biomineralization. *In: Biomineralization: Chemical and Biochemical Perspectives* (S. Mann, J. Webb, and R. J. P. Williams, Eds.), pp. 133-156. VCH Verlagsgesellschaft, Weinheim.

Aisen, P., Enns, C., and Wessling-Resnick, M. (2001). Chemistry and biology of eukaryotic iron metabolism. *The International Journal of Biochemistry & Cell Biology* **33,** 940-959.

Allen, H., and Hill, O. (1982). Iron: An Element Well-Fitted for its Task? *In: The Biological Chemistry of Iron* (B. H. Dunford, D. Dolphin, K. N. Raymond, and L. Sieker, Eds.), Vol. 89, pp. 3-12. D. Reidel Publishing Company, Dordrecht.

Andrews, S. C. (1998). Iron storage in bacteria. *Advances in Microbial Physiology* **40,** 281-351.

Bazylinski, D. A., and Frankel, R. B. (2004). Magnetic Iron Oxide and Iron Sulfide Minerals within Microorganisms: Potential Biomarkers. *In: Biomineralization, Progress in Biology, Molecular Biology and Application* (E. Bäuerlein, Ed.), pp. 17-43. Wiley-VCH, Weinheim.

Bell, J. K. (1994). Ecology of chitons on Cottesloe Reef, Western Australia, with a focus on feeding ecology. Honours. Biological Sciences and Biotechnology. pp. 111. Murdoch University, Perth.

Bienfait, F. (1987). Biochemical Basis of Iron Efficiency Reactions in Plants. *In: Iron Transport in Microbes, Plants and Animals* (G. Winkelmann, D. van der Helm, and J. B. Neilands, Eds.), pp. 339-349. VCH Verlagsgesellschaft, Weinheim.

Birchall, J. D. (1989). The importance of the study of biominerals to materials technology. *In: Biomineralization* (S. Mann, J. Webb, and R. J. P. Williams, Eds.), pp. 491-509. VCH Verlagsgesellschaft, Weinheim.

Black, R., Lymbery, A., and Hill, A. (1988). Form and function: size of radular teeth and inorganic content of faeces in a guild of grazing molluscs at Rottnest Island, Western Australia. *Journal of Experimental Marine Biology and Ecology* **121,** 23-35.

Boyle, P. R. (1977). The physiology and behaviour of chitons (Mollusca: Polyplacophora). *Oceanography Marine Biology Annual Review* **15,** 461-509.

Brooker, L. R. (2007). Faculty of Science, Health and Education. University of the Sunshine Coast, Sippy Downs, Queensland, Australia, (Private Communication).

Brooker, L. R., Gardner, L., Macey, D. J., and Elizur, A. (2006a). Genes and biomineralisation in the radular teeth of chitons. Joint meeting of the American Malacological Society and the Western Society of Malacologists, Seattle, USA, 29 July – 3 August.

Brooker, L. R., Lee, A. L., Macey, D. J., and Webb, J. (2002). Marine Teeth (and Mammal Teeth). *In: Encyclopedia of Materials: Science and Technology* (P. Calvert, Ed.), pp. 5186-5189. Elsevier Science.

Brooker, L. R., Lee, A. P., Macey, D. J., van Bronswijk, W., and Webb, J. (2003). Multiple-front iron-mineralisation in chiton teeth (*Acanthopleura echinata*: Mollusca: Polyplacophora). *Marine Biology* **142,** 447-454.

Brooker, L. R., Lee, A. P., Macey, D. J., Webb, J., and van Bronswijk, W. (2006b). *In situ* studies of biomineral deposition in the radula teeth of chitons of the suborder Chitonina. *Venus* **65,** 71-80.

Brooker, L. R., and Macey, D. J. (2001). Biomineralization in chiton teeth and its usefulness as a taxonomic character in the genus *Acanthopleura* Guilding, 1829 (Mollusca: Polyplacophora). *American Malacological Bulletin* **16,** 203-215.

Brydson, R. (2001). *Electron Energy Loss Spectroscopy*. Springer-Verlag, Telos.

Bullock, R. C. (1989). Mechanical wear of radula denticle caps of *Acanthopleura granulata* (Gmelin, 1791) (Polyplacophora: Chitonidae). *American Malacological Bulletin* **7,** 13-19.

Burford, M. A., Macey, D. J., and Webb, J. (1986). Hemolymph ferritin and radula structure in the limpets *Patelloida alticostata* and *Patella peronii* (Mollusca: Gastropoda). *Comparative Biochemistry and Physiology* **83A,** 353-358.

Carefoot, T. H. (1965). Magnetite in the radula of the polyplacophora. *Proceedings of the Malacological Society of London* **36,** 203-212.

Cellier, M., Prive, G., A., B., Kwan, T., Rodrigues, V., Chia, W., and Gros, P. (1995). Nramp Defines a Family of Membrane Proteins. *Proceedings of the National Academy of Sciences of the United States of America* **92,** 10089-10093.

Clode, P. L. (2007). Centre for Microscopy, Characterisation and Analysis, University of Western Australia, Perth, (Private Communication).

Conrad, M. E., Umbreit, J. N., Moore, E. G., Hainsworth, L. N., Porubcin, M., Simovich, M. J., Nakada, M. T., Dolan, K., and Garrick, M. D. (2000). Separate pathways for cellular uptake of ferric and ferrous iron. *American Journal of Physiology-Gastrointestinal and Liver Physiology* **279,** G767-G774.

Cornell, R. M., and Schneider, W. (1989). Phase transformations in the ferrihydrite/cysteine system. *Polthedron* **8,** 2829-2836.

Cruz, R., and Farina, M. (2005). Mineralization of major lateral teeth in the radula of a deep-sea hydrothermal vent limpet (Gastropoda:Neolepetopsidae). *Marine Biology* **147,** 163-168.

Culling, C. F. A. (1974). *Handbook of Histopathological and Histochemical Techniques (including museum techniques)*. Butterworths, London.

Department of Environmental Protection (1996). South Metropolitan Coastal Waters Study (1991-1994), pp. 15. Department of Environmental Protection, Perth, Western Australia.

Dupic, F., Fruchon, S., Bensaid, M., Loreal, O., Brissot, P., Borot, N., Roth, M. P., and Coppin, H. (2002). Duodenal mRNA expression of iron regulated genes in response to iron loading and iron deficiency in four strains of mice. *Gut* **51,** 648-653.

Eernisse, D. J., and Kerth, K. (1988). The initial stages of radular development in chitons (Mollusca: Polyplacophora). *Malacologia* **28,** 95-103.

Eernisse, D. J., Terwilliger, N. B., and Terwilliger, R. C. (1988). The red foot of a lepidopleurid chiton: Evidence for tissue hemoglobins. *The Veliger* **30,** 244-247.

Eisenstein, R. S. (2000). Iron Regulatory Proteins and the Molecular Control of Mammalian Iron Metabolism. *Annual Review of Nutrition* **20,** 627-662.

Evans, L., A., Macey, D. J., and Webb, J. (1991). Distribution and composition of matrix protein in the radula teeth of the chiton *Acanthopleura hirtosa*. *Marine Biology* **109,** 281-286.

Evans, L. A., Macey, D. J., and Webb, J. (1990). Characterization and structural organization of the organic matrix of the radula teeth of the chiton *Acanthopleura hirtosa*. *Philosophical Transactions of the Royal Society London Series B* **329,** 87-96.

Evans, L. A., Macey, D. J., and Webb, J. (1992). Calcium biomineralization in the radular teeth of the chiton, *Acanthopleura hirtosa*. *Calcified Tissue International* **51,** 78-82.

Evans, L. A., Macey, D. J., and Webb, J. (1994). Matrix heterogeneity in the radular teeth of the chiton *Acanthopleura hirtosa*. *Acta Zoologica* **75,** 75-79.

Ferreira, A. J. (1979). The family Lepidopleuridae (Mollusca: Polyplacophora) in the eastern Pacific. *The Veliger* **22,** 145-165.

Fretter, V. (1937). Structure and function of the alimentary canal of some species of Polyplacophora (Mollusca). *Transactions of the Royal Society of Edinburgh* **59,** 119-164.

Fretter, V., and Graham, A. (1962). *British Prosobranch Molluscs, Their Functional Anatomy and Ecology*. Ray Society, London.

Giberson, R. T., and Demaree, R. S. J. (1999). Microwave processing techniques for electron microscopy: a four-hour protocol. *Methods in Molecular Biology* **117,** 145-158.

Gowlett-Holmes, K. L. (1998). Class Polyplacophora: Natural History (Biogeography), Fossil Record. *In: Mollusca: The Southern Synthesis. Fauna of Australia* (P. L. Beesley, G. J. B. Ross, and A. Wells, Eds.), Vol. Part A, pp. 161-177. CSIRO Publishing, Melbourne.

Graham, A. (1973). The anatomical basis of function in the buccal mass of prosobranch and amphineuran molluscs. *Journal of Zoology London* **169,** 317-348.

Gunshin, H., Allerson, C. R., Polycarpou-Schwarz, M., Rofts, A., Rogers, J. T., Kishi, F., Hentze, M. W., Rouault, T. A., Andrews, N. C., and Hediger, M. A. (2001). Iron-dependent regulation of the divalent metal ion transporter. *FEBS Letters* **509,** 309-316.

Guralnick, R., and Smith, K. (1999). Historical and biomechanical analysis of integration and dissociation in molluscan feeding, with special emphasis on the true limpets (Patellogastropoda : Gastropoda). *Journal of Morphology* **241,** 175-195.

Hanaichi, T., Sato, T., Iwamoto, T., Malavasi-Yamashiro, J., Hoshino, M., and Mizuno, N. (1986). A Stable Lead by Modification of Sato's Method. *Journal of Electron Microscopy* **35,** 304-306.

Harbo, R. M. (2001). *Shells & Shellfish of the Pacific Northwest*. Harbour Publishing, Madeira Park.

Hickman, C. S. (1977). Integration of electron scan and light imagery in study of molluscan radulae. *The Veliger* **20,** 1-8.

Hickman, C. S. (1980). Evolution and function of asymmetry in the archeogastropod radula. *The Veliger* **23,** 189-194.

Hickman, C. S. (2006). Department of Intergrative Biology, University of California, Berkeley, USA, (Private Communication).

Isarankura, K., and Runham, N. W. (1968). Studies on the replacement of the gastropod radula. *Malacologia* **7,** 71-91.

Jones, E. I., McCance, R. A., and Shackleton, L. R. B. (1935). The role of iron and silica in the structure of the radular teeth of certain marine molluscs. *Journal of Experimental Biology* **12,** 59-64.

Kaas, P., and Jones, A. M. (1998). Class Polyplacophora: Morphology and Physiology. *In: Mollusca: The Southern Synthesis. Fauna of Australia* (P. L. Beesley, G. J. B. Ross, and A. Wells, Eds.), Vol. Part A, pp. 163-174. CSIRO Publishing, Melbourne.

Kidane, T. Z., Sauble, E., and Linder, M. C. (2006). Release of iron from ferritin requires lysosomal activity. *American Journal of Physiology and Cell Physiology* **291,** 445-455.

Kim, K.-S., Burford, M. A., Macey, D. J., and Webb, J. (1988). Iron concentrations and characterisation of the major iron binding proteins in the tissues of the chiton *Clavarizona hirtosa*. *Comparative Biochemistry and Physiology* **91B,** 159-164.

Kim, K.-S., Webb, J., and Macey, D. J. (1986a). Properties and role of ferritin in the hemolymph of the chiton *Clavarizona hirtosa*. *Biochimica et Biophysica Acta* **884,** 387-394.

Kim, K.-S., Webb, J., Macey, D. J., and Cohen, D. D. (1986b). Compositional changes during biomineralization of the radula of the chiton *Clavarizona hirtosa*. *Journal of Inorganic Biochemistry* **28,** 337-345.

Kim, K. S., Macey, D. J., Webb, J., and Mann, S. (1989). Iron mineralization in the radula teeth of the chiton *Acanthopleura hirtosa*. *Proceedings of the Royal Society London* **B237,** 335-346.

Kirschvink, J. L., and Hagadorn, J. W. (2000). A grand unified theory of biomineralization. *In: The Biomineralisation of Nano- and Micro-Structures* (E. Bäuerlein, Ed.), pp. 139-150. Wiley-VCH Verlag GmbH, Weinheim.

Kirschvink, J. L., and Lowenstam, H. A. (1979). Mineralization and magnetization of chiton teeth: Paleomagnetic, sedimentologic and biologic implications of organic magnetite. *Earth Planetry Sci. Lett.* **44,** 193-204.

Laboux, O., Dion, N., Arana-Chavez, V., Ste-Marie, L.-G., and Nanci, A. (2004). Microwave Irradiation of Ethanol-fixed Bone Improves Preservation, Reduces Processing Time, and Allows Both Light and Electron Microscopy on the Same Sample. *Journal of Histochemistry and Cytochemistry* **52,** 1267-1275.

Lane, J. M. (1986). Allometric and biochemical studies on starved and unstarved clams, *Rangia cuneata* (Sowerby, 1831). *Journal of Experimental Marine Biology and Ecology* **95,** 131-143.

Langer, P. D. (1983). Diet analysis for three subtidal coexisting chitons sfrom the Northwestern Atlantic. *The Veliger* **25,** 370-377.

Lee, A. P. (2000). *In situ* Raman Spectroscopic Studies of the Iron and Calcium Containing Biominerals in Chiton Teeth. Ph.D. Biological Sciences and Biotechnology, pp. 220. Murdoch University, Perth.

Lee, A. P. (2006). Department of Applied Chemistry, Curtin University, Perth, Western Australia, (Private Communication).

Lee, A. P., Brooker, L. R., Macey, D. J., van Bronswijk, W., and Webb, J. (2000). Apatite mineralization in teeth of the chiton *Acanthopleura echinata*. *Calcified Tissue International* **67,** 408-415.

Lee, A. P., Brooker, L. R., Macey, D. J., Webb, J., and van Bronswijk, W. (2003a). A new biomineral identified in the cores of teeth from the chiton *Plaxiphora albida*. *Journal of Biological and Inorganic Chemistry* **8,** 256-262.

Lee, A. P., Brooker, L. R., van Bronswijk, W., Macey, D. J., and Webb, J. (2003b). Contribution of Raman Spectroscopy to identification of biominerals present in teeth of *Acanthopleura rehderi*, *Acanthopleura curtisiana,* and *Onithochiton quercinus*. *Biopolymers (Biospectroscopy)* **72,** 299-301.

Lee, A. P., Webb, J., Macey, D. J., van Bronswijk, W., Savarese, A., and De Witt, C. (1998). In situ Raman spectroscopic studies of the teeth of the chiton *Acanthopleura hirtosa*. *Journal of Biological and Inorganic Chemistry* **3,** 614-619.

Lewin, A., Moore, G. R., and Le Brun, N. E. (2005). Formation of protein-coated iron minerals. *Dalton Transcripts,* 3597-3610.

Liddiard, K. J., Hockridge, J. G., Macey, D. J., Webb, J., and van Bronswijk, W. (2004). Mineralisation in the teeth of limpets *Patelloida alticostata* and *Scutellastra laticostata* (Mollusca: Patellogastropoda). *Molluscan Research* **24,** 21-31.

Locke, M., and Nichol, H. (1992). Iron economy in insects: Transport, Metabolism, and Storage. *Annual Review of Entomology* **37,** 195-215.

Lowenstam, H. A. (1962a). Goethite in radular teeth of recent marine gastropods. *Science* **137,** 279-280.

Lowenstam, H. A. (1962b). Magnetite in denticle capping in recent chitons (Polyplacophora). *Bulletin of the Geological Society of America* **73,** 435-438.

Lowenstam, H. A. (1967). Lepidocrocite, an apatite mineral, and magnetite in the teeth of chitons (Polyplacophora). *Science* **156,** 1373-1375.

Lowenstam, H. A. (1971). Opal precipitation by marine gastropods (Mollusca). *Science* **171,** 487-490.

Lowenstam, H. A. (1972). Phosphatic hard tissues of marine invertebrates: their nature and mechanical function, and some fossil implications. *Chemical Geology* **9,** 153-166.

Lowenstam, H. A., and Rossman, G. R. (1975). Amorphous, hydrous, ferric phosphate phosphatic dermal granules in *Molpadia* (Holothuroidea): physical and chemical characterization and ecological implications of the bioinorganic fraction. *Chemical Geology* **15,** 15-51.

Lowenstam, H. A., and Weiner, S. (1989). *On Biomineralization*. Oxford University Press, Oxford.

Lu, H.-K., Huang, C.-M., and Li, C.-W. (1995). Translocation of ferritin and biomineralization of geothite in the radula of the limpet *Cellana toreuma* Reeve. *Experimental Cell Research* **219,** 137-145.

Macey, D. J., and Brooker, L. R. (1996). The junction zone: Initial site of mineralization in radula teeth of the chiton *Cryptoplax striata* (Mollusca: Polyplacophora). *Journal of Morphology* **230,** 33-42.

Macey, D. J., Brooker, L. R., and Cameron, V. C. (1997). Mineralisation in the teeth of the gastropod mollusc *Nerita atramentosa*. *Molluscan Research* **18,** 33-41.

Macey, D. J., Brooker, L. R., Webb, J., and St. Pierre, T. G. (1996). Structural organization of the cusps of the radular teeth of the chiton *Plaxiphora albida*. *Acta Zoologica* **77,** 287-294.

Mann, S. (2001). *Biomineralization, Principals and Concepts in Bioinorganic Materials Chemistry*. Oxford University Press, Oxford.

Mann, S., Perry, C. C., Webb, J., Luke, B., and Williams, R. J. P. (1986). Structure morphology composition and organization of biogenic minerals in limpet teeth. *Proceedings of the Royal Society London* **227,** 179-190.

Mann, S., and Weiner, S. (1999). Biomineralization: Structural questions at all length scales. *Journal of Structural Biology* **126,** 179-181.

Manwell, C. (1958). The oxygen-respiratory pigment equilibrium of the hemocyanin and myoglobin of the amphineuran mollusc *Cryptochiton stelleri*. *Journal of Cellular and Comparative Physiology* **52,** 341-352.

Marigomez, I., Soto, M., Cajaraville, M. P., Angulo, E., and Giaberini, L. (2002). Cellular and Subcellular Distribution of Metals in Molluscs. *Microscopy Research and Technique* **56,** 358-392.

McArthur, W. M. (1991). Reference soils of South-Western Australia. *In* "Australian Society of Soil Science Inc." pp. 23-29. State Printing Division W.A., Perth.

Messenger, J. B., and Young, J. Z. (1999). The radular apparatus of cephalopods. *Philosophical Transactions of the Royal Society London Series B* **354,** 161-182.

Mims, M. P., and Prchal, J. T. (2005). Divalent metal transporter 1. *Hematology* **10,** 339-345.

Morse, A. C., Beard, J. L., and Jones, B. C. (1999). A genetic developmental model of iron deficiency: biological aspects. *Proceedings of the Society for Experimental Biology and Medicine* **220,** 147-152.

Nesson, M. H. (1969). Studies on radula tooth mineralization in the polyplacophora. Ph.D. Zoology, pp. 250. California Institute of Technology, California, Pasadena.

Nesson, M. H., and Lowenstam, H. A. (1985). Biomineralization processes of the radula teeth of chitons. *In: Magnetite biomineralization and magnetoreception in organisms* (J. L. Kirshvink, D. S. Jones, and B. J. MacFadden, Eds.), pp. 333-361. Plenum press, ny.

Nishihama, S., Nojima, S., and Kikuchi, T. (1986). Distribution, diet and activity of a chiton *Liolophura japonica* (Lischkel), in Amakusa, west Kyushu. *Publications Amakusa Marine Biological Laboratory* **8,** 113-123.

Numako, C., Tsukiyama, Y., and Koto, K. (2006). Characterization of Iron Components in the Radula of the Japanese Chiton *Acanthopleura japonica*. *Venus* **65,** 153-163.

Okoshi, K., and Ishii, T. (1996). Concentrations of elements in the radular teeth of limpets, chitons and other marine mollusks. *Journal of Marine Biotechnology* **3,** 252-257.

Padilla, D. K., Dittman, D. E., Franz, J., and Sladek, R. (1996). Radula production rates in two species of *Lacuna* Turton (gastropoda: Littorinidae). *Journal of Molluscan Studies* **62,** 275-280.

Papathanassiou, E., and King, P. E. (1984). Effects of starvation on the fine structure of the hepatopancreas in the common prawn *Palaemon serratus* (Pennant). *Comparative Biochemistry and Physiology Part A* **77,** 243-249.

Pearce, A., Rossbach, M., Tait, M., and Brown, R. (1999). Sea temperature variability off Western Australia 1990 to 1994. *In: Department of Fisheries Research Report*, pp. 1. Department of Fisheries, Perth, Western Australia.

Piercy, R. D. (1987). Habitat and food preferences in six Eastern Pacific chiton species (Mollusca: Polyplacophora). *The Veliger* **29,** 388-393.

Politi, Y., Arad, T., Klein, E., Weiner, S., and Addadi, L. (2004). Sea urchin spine calcite forms via a transient amorphous calcium carbonate phase. *Science* **306,** 1161-1164.

Ponder, W. F., and Lindberg, D. R. (1997). Towards a phylogeny of gastropod molluscs: an analysis using morphological characters. *Zoological Journal of the Linnean Society* **119,** 83-265.

Porcel, D., Bueno, J. D., and Almendros, A. (1996). Alterations in the digestive gland and shell of the snail *Helix aspersa* Muller (Gastropoda, Pulmonata) after prolonged starvation. *Comparative Biochemistry and Physiology Part A* **115,** 11-17.

Putman, B. F. (1990). The diet and feeding selectivity of the chiton *Stenoplax heathiana* Berry, 1946 (Mollauca: Polyplacophora). *The Veliger* **33,** 372-374.

Randall, D., Burggren, W., and French, K. (1997). "Animal Physiology: Mechanisms and Adaptations." W. H. Freeman and Company, New York.

Rinkevich, B. (1993). Major primary stages of biomineralization in radula teeth of the limpet *Lottia gigantea*. *Marine Biology* **117,** 269-277.

Runham, N. W. (1963). A study of the replacement mechanism of the pulmonate radula. *Quarterly Journal of Microscopial Science* **104,** 271-277.

Runham, N. W., Thornton, P. R., Shaw, D. A., and Wayte, R. C. (1969). The mineralization and hardness of the radular teeth of the limpet *Patella vulgata* L. *Zeitschrift fur Zellforschung und mikroskopische Anatomie* **99,** 608-626.

Russell-Hunter, W. D., and Aldridge, D. W. (1983). Oxygen uptake and nitrogenous excretion rates during over winter de growth conditions in the pulmonate snail *Helisoma trivolvis*. *Comparative Biochemistry and Physiology Part A* **74,** 491-498.

Saito, H., and Okutani, T. (1990). Two new chitons (Mollusca: Polyplacophora) from a hydrothermal vent site of the Iheya Small Ridge, Okinawa Trough, East China Sea. *Venus* **49,** 165-179.

Salvini-Plawen, L. v. (1988). The structure and function of molluscan digestive systems. *In: The Mollusca, Form and Function* (E. R. Trueman and M. R. Clark, Eds.), Vol. 11. Academic Press, Orlando.

Sargent, P. J., Farnaud, S., and Evans, R. W. (2005). Structure/Function overview of proteins involved in iron storage and transport. *Current Medicinal Chemistry* **12,** 2683-2693.

Scheffel, A., Gruska, M., Faivre, D., Linaroudis, A., Plitzko, J. M., and Schüler, D. (2006). An acidic protein aligns magnetosomes along a filamentous structure in magnetotactic bacteria. *Nature* **440,** 110-114.

Shaw, J. A. (2003). Studies on the radula and feeding mechanisms in three species of intertidal mollusc. Honours. School of Biological Science and Biotechnology, pp. 139. Murdoch University, Perth.

Shaw, J. A., Brooker, L. R., and Macey, D. J. (2002). Radular tooth turnover in the chiton *Acanthopleura hirtosa* (Blainville, 1825) (Mollusca: Polyplacophora). *Molluscan Research* **22,** 93-99.

Shaw, J. A., Macey, D. J., Brooker, L. R., Lee, A. P., Clode, P. L., and Stockdale, E. J. (2005). A comparative analysis of the teeth and epithelial tissue in natural and iron starved specimens of the chiton *Acanthopleura hirtosa* (Mollusca: Polyplacophora). 9th International Symposium on Biomineralization, Pucon, Chile, 6-9 December.

Simkiss, K., and Wilbur, K. M. (1989). *Biomineralization: Cell Biology and Mineral Deposition*. Academic Press, San Diego.

Smith, S. E., Brittain, T., and Wells, R. M. G. (1988). A kinetic and equilibrium study of ligand binding to the monomeric and dimeric haem-containing globins of two chitons. *Biochemical Journal* **252,** 673-678.

Solem, A. (1972). Malacological applications of Scanning Electron Microscopy II Radular structure and functioning. *The Veliger* **14,** 327-336.

Sone, E. D., Weiner, S., and Addadi, L. (2005). Morphology of goethite crystals in developing limpet teeth: Assessing biological control over mineral formation. *Crystal Growth & Design* **5,** 2131-2138.

Sone, E. D., Weiner, S., and Addadi, L. (2007). Biomineralization of limpet teeth: A cryo-TEM study of the organic matrix and the onset of mineral deposition. *Journal of Structural Biology*.

Spurr, A. R. (1969). A low-viscosity epoxy resin embedding medium for electron microscopy. *Journal of Ultrastructural Research* **26,** 31.

St. Pierre, T. G., Evans, L. A., and Webb, J. (1992). Non-Stoichiometric Magnetite and Maghemite in the Mature Teeth of the Chiton *Acanthopleura hirtosa*. *Hyperfine Interactions* **71,** 1275-1278.

St. Pierre, T. G., Mann, S., Webb, J., Dickson, D. P. E., Runham, N. W., and Williams, R. J. P. (1986). Iron oxide biomineralization in the radula teeth of the limpet *Patella vulgata*; Mössbauer spectroscopy and high resolution transmission electron microscopy studies. *Proceedings of the Royal Society London* **228,** 31-42.

Steneck, R. N., and Watling, L. (1982). Feeding capabilities and limitation of herbivorous molluscs: A functional group approach. *Marine Biology* **68,** 299-319.

Stillman, T. J., Hempstead, P. D., Artymiuk, P. J., Andrews, S. C., Hudson, A. J., Treffry, A., Guest, J. R., and Harrison, P. M. (2001). The high-resolution X-ray crystallographic structure of the ferritin (EcFtnA) of Escherichia coli; comparison with human H ferritin (HuHF) and the structures of the Fe^{3+} and Zn^{2+} derivatives. *Journal of Molecular Biology* **307,** 587-603.

Stryer, L. (1999). *Biochemistry*. W. H. Freeman and Company, New York.

Suzuki, T., and Imai, K. (1998). Evolution of myoglobin. *Cellular and Molecular Life Sciences* **54,** 979-1004.

Terwilliger, R. C., and Read, K. R. H. (1970). The radula muscle myoglobins of the amphineuran molluscs, *Katharina tunicata* Wood, *Cryptochiton stelleri* Middendorf, and *Mopalia muscosa* Gould. *International Journal of Biochemistry* **1,** 281-291.

Thomas, P. J., and Midgley, P. A. (2002). An introduction to energy-filtered transmission electron microscopy. *Topics in Catalysis* **21,** 109-138.

Towe, K. M., and Lowenstam, H. A. (1967). Ultrastructure and development of iron mineralization in the radular teeth of *Cryptochiton stelleri* (Mollusca). *Journal of Ultrastructure Research* **17,** 1-13.

Trinder, D., Fox, C., Vautier, G., and Olynyk, J. K. (2002). Molecular pathogenesis of iron overload. *Gut* **51,** 290-295.

Trivier, D., and Courcol, R. J. (1996). Iron depletion and virulence in *Staphylococcus aureus*. *FEMS Microbiology Letters* **141,** 117-27.

Turner, D. R., Hunter, K. A., and De Baar, H. J. W. (2001). Introduction. *In: The Biogeochemistry of Iron in Seawater* (D. R. Turner and K. A. Hunter, Eds.), Vol. 7, pp. 1-7. John Wiley & Sons, Chichester.

United States National Library of Medicine. (2007). Genetics home reference handbook, Vol. 2007. National Institute of Health. http://ghr.nlm.nih.gov/handbook/illustrations/ferritin;jsessionid=01449032B7751BAB3BFC90E363777726 (Accessed: 26.5.07).

van der Wal, P., Giesen, H., and Videler, J. (2000). Radular teeth as models for the improvement of industrial cutting devices. *Materials Science & Engineering C: Biomimetic Materials, Sensors & Systems* **7,** 129-142.

van der Wal, P., Videler, J. J., Havinga, P., and Pel, R. (1989). Architecture and chemical composition of the magnetite-bearing layer in the radula teeth of *Chiton olivaceus* (Polyplacophora). *In: Origin, Evolution, and Modern Aspects of Biomineralization in Plants and Animals* (R. E. Crick, Ed.), pp. 536. Plenum Press, New York.

Wealthall, R. J., Brooker, L. R., Macey, D. J., and Griffin, B. J. (2005). Fine structure of the mineralized teeth of the chiton *Acanthopleura echinata* (Mollusca: Polyplacophora). *Journal of Morphology* **265,** 165-175.

Webb, J., Brooker, L. R., Lee, A. P., Hockridge, J. G., Liddiard, K. J., Macey, D. J., and van Bronswijk, W. (2001). Biomineralization-controlled microarchitecture in the radula teeth of chitons and limpets. *Australian Journal of Chemistry* **54,** 611-613.

Webb, J., and Macey, D. J. (1983). Plasma ferritin in *Polyplacophora* and its possible role in the biomineralization of iron. *In: Biomineralization and Biological Metal Accumulation* (P. Westbroek and E. W. de Jong, Eds.), pp. 423-427. Reidel, Dordrecht, Holland.

Webb, J., Macey, D. J., and Mann, S. (1989). Biomineralization of iron in molluscan teeth. *In: Biomineralization* (S. Mann, J. Webb, and R. J. P. Williams, Eds.), pp. 345-387. VCH Verlagsgesellschaft, Weinheim.

Webb, J., Mann, S., Bannister, J. V., and Williams, R. J. P. (1986). Biomineralization of iron: Isolation of ferritin from the hemolymph of the limpet *Patella vulgata*. *Inorganica Chimica Acta* **124,** 37-40.

Weiner, S., and Dove, P. M. (2003). An overview of biomineralization processes and the problem of the vital effect. *In: Biomineralization* (P. M. Dove, J. J. De Yoreo, and S. Weiner, Eds.), Vol. 54, pp. 1-29. The Mineralogical Society of America, Washington.

Appendix A:

Paper submitted to The Journal of the Marine Biological Association of the United Kingdom: Accepted.

Radula synthesis by three species of iron mineralizing mollusc: production rate and elemental demand

Jeremy A. Shaw, David J. Macey, Lesley R. Brooker

ABSTRACT

A cold-shock technique was used to determine radula production rates for the chitons *Acanthopleura hirtosa* and *Plaxiphora albida*, and for the limpet *Patelloida alticostata*, which replaced their radular teeth at rates of 0.40, 0.36 and 0.51 rows.day^{-1}, respectively. These rates are far slower than those determined previously for non iron-mineralising molluscs, suggesting that the improved working life of the teeth afforded by iron-mineralisation acts to significantly reduce replacement rates. In addition, ICP-AES has been used to determine the quantity of iron and other elements comprising the radula of each species. These data, used in conjunction with the radula production rates, reveal that *A. hirtosa*, *P. albida* and *Pa. alticostata* have daily radula mineralisation requirements for iron of 3.06, 4.12 and 0.55 μg, respectively. Such information is vital for continuing studies related to the cellular delivery of ions and subsequent biomineralisation of the tooth cusps in chitons and limpets.

INTRODUCTION

The radula is the principal feeding organ of many molluscan species. It comprises an elongated array of transverse tooth rows that are carried forwards in a conveyor belt manner (Lowenstam & Weiner, 1989). The teeth are prefabricated as an organic matrix by odontoblast cells at the posterior end of the radula, with the overlying epithelial tissue

controlling the subsequent transportation and deposition of ions onto this matrix (Mann et al., 1986; Kim et al., 1989). Once mature, the teeth are progressively abraded and finally lost as a result of feeding (Runham, 1963; Runham & Isarankura, 1966).

In chitons (Mollusca: Polyplacophora), each transverse tooth row bears 17 teeth, including a pair of large major laterals whose cusps are hardened with iron and calcium biominerals. Magnetite (Fe_3O_4) is the principal mineral formed within the posterior cutting face and anterior surface of the tooth cusps, while at later stages of development the tooth core is infilled with either an apatitic calcium phosphate or limonite and lepidocrocite, depending on the species (Kim et al., 1989; Lowenstam & Weiner, 1989; Macey et al., 1994; Lee et al., 2003a, b). Limpets (Mollusca: Patellogastropoda) possess fewer teeth per transverse row than chitons, and utilise the ferric oxide goethite (α-FeOOH) to mineralise their major lateral teeth, along with silica as hydrated amorphous opal ($SiO_2.nH_2O$) and calcium (Lowenstam, 1962; Runham et al., 1969; Mann et al., 1986; Liddiard et al., 2004). As a consequence of this mineralisation, the teeth of chitons and limpets are well suited for rasping hard surfaces, and are commonly found grazing on hard substrata such as limestone where they rake or excavate the surface, ultimately ingesting the rock in order to extract the epi- or endolithic algal components (Steneck & Watling, 1982; Macey et al., 1996; van der Wal et al., 2000).

The rate of radula production has been determined for a limited number of molluscs, with most studies concentrating on prosobranch and pulmonate gastropod species (Runham, 1962, 1963; Runham & Isarankura, 1966; Isarankura & Runham, 1968; Padilla et al., 1996). These studies, which have utilised a number of techniques, have reported radula production rates ranging between 1.0 and 6.4 tooth rows.day^{-1}. Recently, a cold-shock technique was employed to determine the radula production rate (0.36 rows.day^{-1}) of

the chiton *Acanthopleura hirtosa* (Blainville, 1825), (Shaw et al., 2002), which is considerably slower than rates reported previously.

In order to elucidate the relative disparity between the rate determined for *A. hirtosa* (Shaw et al., 2002) and those determined for other molluscs, radula production has been re-examined in *A. hirtosa* and has been investigated in two sympatric iron-mineralising mollusc species, the chiton *Plaxiphora albida* (Blainville, 1825) and the limpet *Patelloida alticostata* (Angas, 1865). These species are key inhabitants of intertidal communities in Western Australia (Black et al., 1979; Black et al., 1988), and have been the focus of numerous studies in relation to tooth biomineralisation (Kim et al., 1989; Macey et al., 1996; Lee et al., 2003a; Liddiard et al., 2004). Further studies on the mineralisation process require a detailed understanding of the demand for elemental precursors during radula development. As such, the quantitative elemental composition of radulae from each species has also been established.

MATERIALS AND METHODS

Radula production rates

All mollusc specimens were collected from intertidal limestone rocks within the Perth metropolitan area of Western Australia (32^{o}S, 116^{o}E). Adult animals, as determined by size, were subjected to a cold-shock treatment (Isarankura & Runham, 1968) within 30 min of collection. This procedure induces a constriction anomaly in the developing radula membrane, the progression of which can be tracked after the subsequent production of new radula material. For *Acanthopleura hirtosa*, the cold-shock procedure followed that described in Shaw et al. (2002), where freshly collected animals were immersed for 48 hours in seawater that had been pre-cooled to 4^{o}C. For *Plaxiphora albida* and *Patelloida alticostata*, the technique was modified to account for species variation in procedure

tolerance. Optimum shock parameters (seawater temperature and duration) were determined to be 4^{o}C for 24 hours and 1^{o}C for 48 hours for *P. albida* and *Pa. alticostata*, respectively (data not shown).

Following the cold-shock, a natural feeding regime was promoted by maintaining animals within an artificial environment approximating that of their natural habitat. This consisted of twin open-air tanks containing limestone rocks that were kept moist and partially submerged in fresh seawater, which was delivered via an overhead reticulation system at a rate of ~6.5 L per min. During the course of each study, air and water temperatures were recorded using minimum/maximum thermometers.

Every two days a single animal was removed from each tank for immediate dissection. Following excision, radulae were cleaned in 2.5% NaOCl before observation under an Olympus SZH10 stereo dissecting microscope, where both the total number of tooth rows and the number of tooth rows occurring posterior to the constriction anomaly were recorded. Radula production rate curves were generated by plotting the number of tooth rows formed against the number of hours that had elapsed between the end of the cold-shock and dissection. As the cold-shock treatment is likely to result in a temporary slowdown of radula production (Shaw et al., 2002), animals in which zero radula production was observed were discounted and the post-shock effect in the remaining animals was accounted for by justifying data points through time zero. The radula production rates calculated for individuals of each species were subsequently compared using regression analysis. The radulae of ten individuals from each species were excised from animals taken straight from the wild for comparison to cold-shocked radulae.

Elemental analysis

The radulae were excised from ten freshly collected specimens of *A. hirtosa*, *P. albida* and *Pa. alticostata* and cleaned using a fine jet of water. The number of tooth rows in each

radula was documented, following which they were dried at 60^{o}C for 12 h, and the sample dry weight recorded. A nitric acid with peroxide digest was then used to dissolve the radulae, followed by quantitative elemental analyses for Fe, Ca, P, S, Mg, Na, Zn, K, Al, Cu and extractable Si using inductively coupled plasma-atomic emission spectroscopy (ICP-AES) (Mc Daniel, 1991). Results were calculated as total μg of each element per sample, which was then converted to μg.g tissue^{-1} using the radula dry weights. The concentrations of elements in the tissues of each species were compared statistically using ANOVA. Daily requirements were estimated by dividing the total μg of each element by the total number of tooth rows and by the radula production rates determined for each species.

RESULTS

Radula production rates

No constrictions were observed in radulae dissected from non cold-shocked animals taken directly from the wild, indicating that constriction anomalies are attributable to the cold-shock and are not a natural part of radula formation. Radula production rates in adult individuals of *Acanthopleura hirtosa*, *Plaxiphora albida* and *Patelloida alticostata* were calculated to be 0.40, 0.36 and 0.51 rows.day^{-1}, respectively (Table 1). Regression analyses demonstrated a high positive fit for individuals within each study, with r^2 values of 0.96 ($y = 0.02x - 3x10^{-5}$), 0.91 ($y = 0.01x + 3x10^{-5}$) and 0.90 ($y = 0.02x + 4x10^{-6}$) for *A. hirtosa*, *P. albida* and *Pa. alticostata*, respectively (Fig. 1). The two chiton species were similar in body length, although *A. hirtosa* possessed a greater number of tooth rows per radula compared to *P. albida*. *Patelloida alticostata* was smaller in body length than either of the chiton species but possessed the greatest number of tooth rows. The temperatures recorded during each study were similar for all species.

Table 1. Data (± 1 SE) for *Acanthopleura hirtosa*, *Plaxiphora albida* and *Patelloida alticostata* maintained within an artificial habitat after a cold-shock treatment.

Species	Average radula production rate (rows.day^{-1})	Average adult size (max length mm)	Average total number of tooth rows	Average seawater temperature (^{o}C)
Acanthopleura hirtosa	0.40 ± 0.01 (*n* = 34)	54 ± 0.6 (*n* = 34)	81 ± 0.8 (*n* = 34)	24 ± 0.3 (*n* = 20)
Plaxiphora albida	0.36 ± 0.01 (*n* = 31)	48 ± 1.7 (*n* = 31)	52 ± 0.8 (*n* = 31)	21 ± 0.1 (*n* = 18)
Patelloida alticostata	0.51 ± 0.02 (*n* = 35)	26 ± 0.5 (*n* = 35)	88 ± 1.0 (*n* = 35)	24 ± 0.4 (*n* = 20)

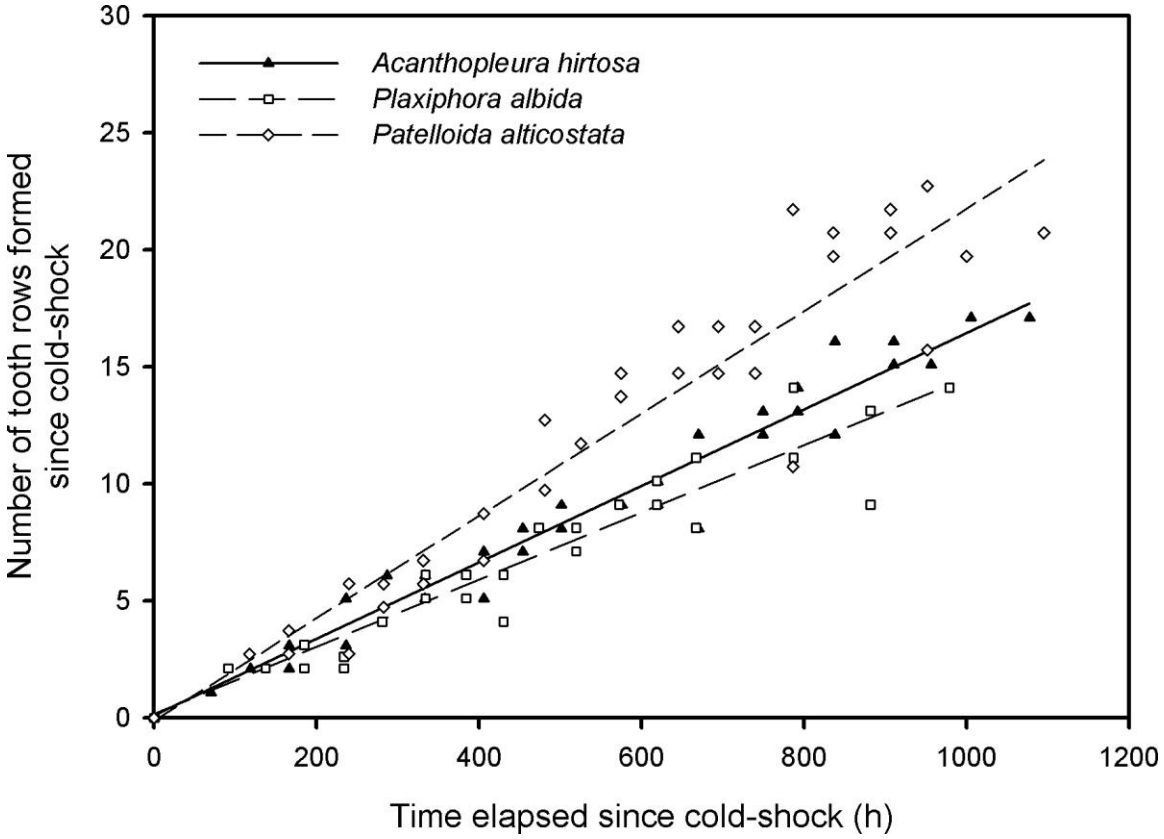

Figure 1. Radula production rates for *Acanthopleura hirtosa*, *Plaxiphora albida* and *Patelloida alticostata*. Points represent the number of tooth rows produced after a cold-shock treatment. Data and regression lines have been justified through time zero to account for post-shock effects.

Elemental analysis

Iron formed the major elemental component in the radulae of each of the three species examined, with those of *A. hirtosa* and *P. albida* containing approximately 88,500 and 98,000 $\mu g.g^{-1}$ of Fe, respectively. That of *Pa. alticostata* contained significantly less Fe at 65,000 $\mu g.g^{-1}$ ($p = 0.03$ and 0.01 for *A. hirtosa* and *P. albida*, respectively, $\alpha = 0.05$) (Table 2). Relative to the two other species, the radula of *A. hirtosa* contained significantly higher concentrations of Ca, P, Mg and Zn ($p < 0.01$, $\alpha = 0.05$ in all cases). Notably, high concentrations of S were detected from all species, although the radula of *Pa. alticostata* contained significantly less than that of the two chitons ($p < 0.01$, $\alpha = 0.05$ in all cases). *Patelloida alticostata* also had significantly higher concentrations of Al and extractable Si than either *A. hirtosa* or *P. albida* ($p < 0.01$, $\alpha = 0.05$ in all cases).

Table 2. Composition and daily requirement of elements for the process of radula formation in *Acanthopleura hirtosa*, *Plaxiphora albida* and *Patelloida alticostata*. BDL = below detectable limits.

Species	***Acanthopleura hirtosa***			***Plaxiphora albida***			***Patelloida alticostata***		
Sample size (*n*)	10			10			10		
Number of tooth rows (± 1 SE)	74 ± 1.1			54 ± 0.7			84 ± 2.0		
Radula dry weight (mg) (± 1 SE)	6.6 ± 0.4			6.5 ± 0.5			1.5 ± 0.1		
Element	$\mu g.g\ tissue^{-1}$	%	$\mu g.day^{-1}$	$\mu g.g\ tissue^{-1}$	%	$\mu g.day^{-1}$	$\mu g.g\ tissue^{-1}$	%	$\mu g.day^{-1}$
Fe	88457	59.2	3.06	98087	86.6	4.12	64731	83.5	0.55
Ca	28304	18.9	1.00	2433	2.1	0.11	1672	2.2	0.01
P	19238	12.9	0.68	5169	4.6	0.22	828	1.1	0.01
Mg	5082	3.4	0.18	1033	0.9	0.05	470	0.6	0.00
S	4395	2.9	0.16	4629	4.1	0.20	3274	4.2	0.03
Na	2003	1.3	0.07	693	0.6	0.03	1324	1.7	0.01
Zn	993	0.7	0.03	101	0.1	0.00	53	0.1	0.00
K	256	0.2	0.01	271	0.2	0.01		BDL	
Al	242	0.2	0.01	252	0.2	0.01	1201	1.5	0.01
Cu	149	0.1	0.01	110	0.1	0.00	62	0.1	0.00
Si	346	0.2	0.01	424	0.4	0.02	3924	5.1	0.03

Note: The nitric acid with peroxide digest cannot fully dissolve Si, and as such the results only provide an indication of the relative extractable Si for each species.

The daily requirements for elements involved in radula synthesis were calculated using the radula production rates determined for each species in the previous section (Table 2). The limpet *Pa. alticostata* was shown to require 0.55 μg Fe.day^{-1}, while *A. hirtosa* and *P. albida* required 3.06 and 4.12 μg Fe.day^{-1} for radula mineralisation. A substantial daily demand for Ca, P, Mg and S was also established, especially in *A. hirtosa*. All remaining elements were typically required in amounts <0.1 μg.day^{-1}.

DISCUSSION

Radula production rates

The radula production rates of 0.40, 0.36 and 0.51 rows per day determined for *Acanthopleura hirtosa*, *Plaxiphora albida* and *Patelloida alticostata* are among the slowest reported to date for any mollusc. Rates have been determined for 21 mollusc species (including the current study), with five being species that incorporate significant amounts of iron into their radula teeth. In a comprehensive study by Isarankura & Runham (1968), radula production rates were determined for eight prosobranch and seven pulmonate gastropod species, with production rates ranging from 1 to 6.4 rows per day, and averaging approximately 3.3 rows per day across all species. Relatively fast radula production rates have also been determined for the prosobranch molluscs *Lacuna vincta* and *L. variegata*, which produce 2.94 and 2.97 rows per day, respectively (Padilla et al., 1996).

A major distinction between the species investigated in the current study, and most of those observed by previous researchers, is that *A. hirtosa*, *P. albida* and *Pa. alticostata* each incorporate iron biominerals into their tooth cusps. The only iron-mineralising species investigated by Isarankura & Runham (1968) was the limpet *Patella vulgata*, which had a replacement rate of ~1.5 rows per day, comparatively slow relative to the remaining species documented in their study. Further evidence for slow rates in iron-mineralising species has

been provided by Nesson (1969), who reported a rate of between 0.4 and 0.8 rows per day for the chiton *Mopalia muscosa*, comparable to the rates determined for the species in the present study.

Research by van der Wal et al. (2000) on the mechanical properties of chiton and limpet teeth demonstrated that tooth hardness was dependent on the relative amounts of mineral and organic matter present in the tooth. As such, the inclusion of iron minerals in the teeth of chitons and limpets acts to prolong the working life of the teeth when feeding on hard substrata such as calcareous limestone (Runham et al., 1969; Bullock, 1989; Lowenstam & Weiner, 1989). The results determined for *A. hirtosa*, *P. albida* and *Pa. alticostata* suggest that the extended functional life of the teeth, attributable to iron-mineralisation, translates to a slower rate of radula replacement.

However, it is acknowledged that numerous factors combine to influence the given radula production rate, therefore making it difficult to make direct comparisons between any particular species. Previous studies have proposed that tooth size and shape, the mode of feeding, the properties of the food source and tooth hardness all contribute to tooth wear qualities (Isarankura & Runham, 1968; Steneck & Watling, 1982; Padilla, 1985; Okoshi & Ishii, 1996). In addition, both Isarankura & Runham (1968) and Padilla et al. (1996) have reported slower rates in larger animals, proposing that this is due to the slower metabolic rates of large individuals compared to small ones. It is likely that rates would be faster in juvenile *A. hirtosa*, *P. albida* or *Pa. alticostata* compared to their adult counterparts, even though size may not be useful for making rate comparisons between adults of various species.

During the course of the study, animals were observed to be feeding, as evidenced by the deposition of faecal pellets and the maintenance of limited algal coverage on the rock near each individual. Although grazing effort, and therefore radula wear and replacement,

may have been influenced by the lack of a tidal system in the tanks, the continual supply of reticulated seawater is likely to have promoted opportunities for feeding rather than reduce them. As such, the rates determined for each of the species examined may be slight overestimates compared to those of animals in the wild. However, given the extremely small tidal amplitudes (Pattiaratchi et al., 1997) and narrow patterns of zonation experienced along the Perth coastline (Black et al., 1979) the rates observed for the chitons and limpet are likely to be representative of those in their natural habitat.

The rate of radula production determined for *A. hirtosa* in the current study was slightly higher compared to the rate determined previously for this species by Shaw et al. (2002) (0.40 rows per day compared with 0.36). Notably, a slightly higher average water temperature was also recorded in the current study (24^{o}C compared to 22^{o}C). Although temperature has been shown to influence radula production rate (see, for example Isarankura & Runham, 1968; Padilla et al., 1996), its effect is likely to be small for animals acclimatised/acclimated within their natural metabolic range. The higher rate observed by Shaw et al. (2002) is likely to be attributable to the correction made to the post cold-shock slowdown of radula production, which has a short-term affect on all animals during the early stages of the study, and which, if not corrected for, will result in a slight depression of the actual rate. This lag effect was acknowledged by Shaw et al. (2002), but not accounted for in the final determination of radula production rate in that paper.

Although they are similar in overall size, the major lateral teeth of *A. hirtosa* are unicuspid, while those of *P. albida* are tricuspid. As these two species are sympatric, it is likely that they are exploiting different niches on the same substratum. This is supported by the composition of their faeces, which contained significantly different amounts of inorganic material, at 88% and 70% for *A. hirtosa* and *P. albida* respectively (Macey et al., 1996). It is possible that *A. hirtosa* is targeting the endolithic algal component of the rock,

whilst *P. albida* targets the epilithic component and, thereby, interspecific differences in tooth structure are balanced out.

Elemental analysis

A number of studies have determined the elemental composition of chiton and limpet radulae (Nesson, 1969; Kim et al., 1986; Okoshi & Ishii, 1996). The concentration of elements, especially iron, determined in these earlier studies compares closely with those established in the present study. A single exception is the radula of *Mopalia muscosa*, which contains 80 μg of iron per tooth row (Nesson, 1969); eight times higher than the value determined for the chitons in the present study. The reasons for the difference are unclear, as *M. muscosa* is similar in body size and radula morphology to *P. albida* (Nesson, 1969).

The difference in the amount of iron in *P. albida* compared to that of *A. hirtosa* is likely due to differences in the distribution of this element within the major lateral teeth of these two species. In *P. albida*, magnetite covers the posterior cutting face of the cusp and coats the anterior tooth surface, thus enveloping the tooth's limonite/lepidocrocite core (Fig. 2). In *A. hirtosa*, the extent of magnetite coverage is primarily limited to the cutting face of the cusp and the apatitic calcium phosphate core region contains no iron (Macey et al., 1996; Lee et al., 2003a). Similarly, the low amount of iron observed in the limpet *Pa. alticostata* is likely to derive from its reliance on the iron oxide goethite with silica in the form of hydrated amorphous opal to strengthen and cushion its teeth (Runham et al., 1969; Lowenstam, 1971; Mann et al., 1986; Liddiard et al., 2004).

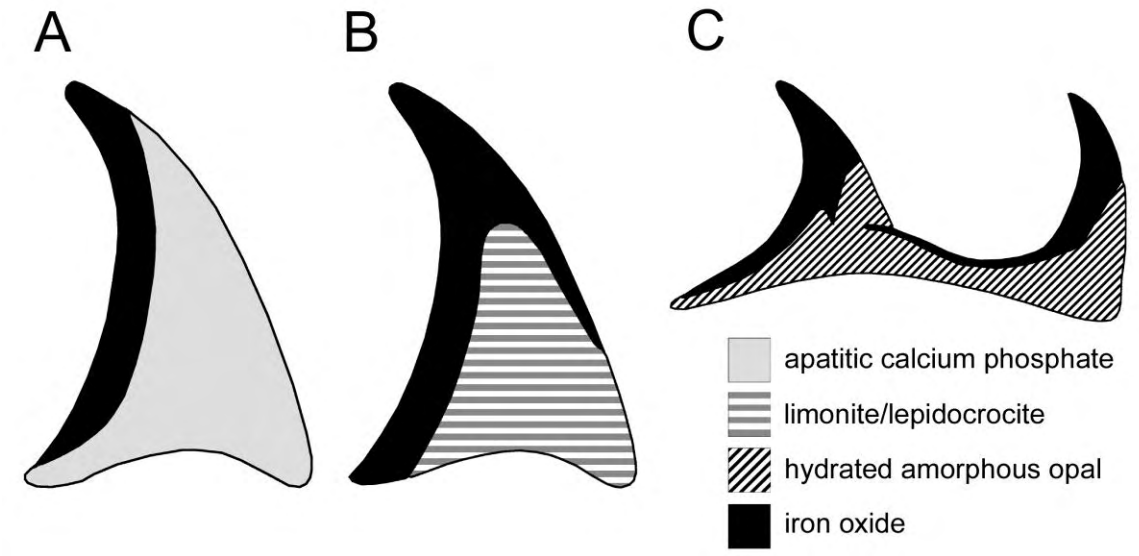

Figure 2. Diagrammatic representation of cross sections through the posterior cutting surface (P) and tooth core, showing the distribution of magnetite in a, *Acanthopleura hirtosa* b, *Plaxiphora albida*, and goethite and silica in c, *Patelloida alticostata*. (adapted from Liddiard et al. (2004))

The process of biomineralisation in chiton and limpet teeth continues to draw interest within the emerging fields of biomimetics and nanotechnology, with the ultimate aim of controlling the formation of nanocomposite structures. One of the remaining objectives in this discipline is to elucidate the mechanisms that control the cellular transport and deposition of ions responsible for tooth mineralisation. Such studies will require an accurate understanding of the demand for elemental precursors in radula mineralisation in order to facilitate accurate dosing with reagents for molecular and immunological studies. In addition, an understanding of the physiological demand for iron in radula synthesis may assist further studies pertaining to the supply of this element, which is likely to be derived from a combination of sources, such as algae, substratum, seawater and even tooth recycling.

Acknowledgements

The authors thank the TAFE Fremantle Maritime Centre for the allocation of space for this study. We are grateful to Garth Maker and Mark Maddern who assisted in animal collections. Special appreciation to Professor Kenji Okoshi and Edward Stockdale for their valuable advice and time. Financial support was provided by an Australian Research Council Discovery Grant. All experiments conducted during the study comply with the Australian Code of Practice for the Care and Use of Animals for Scientific Purposes - 7th Edition 2004.

Literature Cited

Black, R., Fisher, K., Hill, A. & McShane, P., 1979. Physical and biological conditions on a steep intertidal gradient at Rottnest Island, Western Australia. *Australian Journal of Ecology*, **4**, 67-74.

Black, R., Lymbery, A. & Hill, A., 1988. Form and function: size of radular teeth and inorganic content of faeces in a guild of grazing molluscs at Rottnest Island, Western Australia. *Journal of Experimental Marine Biology and Ecology*, **121**, 23-35.

Bullock, R.C., 1989. Mechanical wear of radula denticle caps of *Acanthopleura granulata* (Gmelin, 1791) (Polyplacophora: Chitonidae). *American Malacological Bulletin*, **7**, 13-19.

Isarankura, K. & Runham, N.W., 1968. Studies on the replacement of the gastropod radula. *Malacologia*, **7**, 71-91.

Kim, K.S., Macey, D.J., Webb, J. & Mann, S., 1989. Iron mineralization in the radula teeth of the chiton *Acanthopleura hirtosa*. *Proceedings of the Royal Society London*, **B237**, 335-346.

Kim, K.S., Webb, J., Macey, D.J. & Cohen, D.D., 1986. Compositional changes during biomineralization of the radula of the chiton *Clavarizona hirtosa*. *Journal of Inorganic Biochemistry*, **28**, 337-345.

Lee, A.P., Brooker, L.R., Macey, D.J., Webb, J. & van Bronswijk, W., 2003a. A new biomineral identified in the cores of teeth from the chiton *Plaxiphora albida*. *Journal of Biological and Inorganic Chemistry*, **8**, 256-262.

Lee, A.P., Brooker, L.R., van Bronswijk, W., Macey, D.J. & Webb, J., 2003b. Contribution of Raman Spectroscopy to identification of biominerals present in teeth of *Acanthopleura rehderi*, *Acanthopleura curtisiana*, and *Onithochiton quercinus*. *Biopolymers (Biospectroscopy)*, **72**, 299-301.

Liddiard, K.J., Hockridge, J.G., Macey, D.J., Webb, J. & van Bronswijk, W., 2004. Mineralisation in the teeth of limpets *Patelloida alticostata* and *Scutellastra laticostata* (Mollusca: Patellogastropoda). *Molluscan Research*, **24**, 21-31.

Lowenstam, H.A., 1962. Goethite in radular teeth of recent marine gastropods. *Science*, **137**, 279-280.

Lowenstam, H.A., 1971. Opal precipitation by marine gastropods (Mollusca). *Science*, **171**, 487-490.

Lowenstam, H.A. & Weiner, S., 1989. *On Biomineralization*. Oxford: Oxford University Press.

Macey, D.J., Brooker, L.R., Webb, J. & St. Pierre, T.G., 1996. Structural organization of the cusps of the radular teeth of the chiton *Plaxiphora albida*. *Acta Zoologica*, **77**, 287-294.

Macey, D.J., Webb, J. & Brooker, L.R., 1994. The Structure and Synthesis of Biominerals in Chiton Teeth. *Bulletin de l'Institut Oceanographique*, **14**, 191-197.

Mann, S., Perry, C.C., Webb, J., Luke, B. & Williams, R.J.P., 1986. Structure morphology composition and organization of biogenic minerals in limpet teeth. *Proceedings of the Royal Society London*, **227**, 179-190.

Mc Daniel, W., 1991. Sample preparation procedure for spectrochemical determination of total recoverable elements in biological tissues, Revision 1.0. In *Method 200: 3*, vol. Method 200.3 Ohio: U.S. Environmental Protection Agency.

Nesson, M.H., 1969. *Studies on radula tooth mineralization in the polyplacophora*. PhD thesis, California Institute of Technology, Pasadena, USA.

Okoshi, K. & Ishii, T., 1996. Concentrations of elements in the radular teeth of limpets, chitons and other marine mollusks. *Journal of Marine Biotechnology*, **3**, 252-257.

Padilla, D.K., 1985. Structural resistance of algae to herbivores. *Marine Biology*, **90**, 103-109.

Padilla, D.K., Dittman, D.E., Franz, J. & Sladek, R., 1996. Radula production rates in two species of *Lacuna* Turton (gastropoda: Littorinidae). *Journal of Molluscan Studies*, **62**, 275-280.

Pattiaratchi, C., Hegge, B., Gould, J. & Eliot, I., 1997. Impact of sea-breeze activity on nearshore and foreshore processes in southwestern Australia. *Continental Shelf Research*, **17**, 1539-1560.

Runham, N.W. & Isarankura, K., 1966. Studies on radula replacement. *Malacologia*, **5**, 73.

Runham, N.W., 1962. Rate of replacement of the molluscan radula. *Nature*, **194**, 992-993.

Runham, N.W., 1963. A study of the replacement mechanism of the pulmonate radula. *Quarterly Journal of Microscopial Science*, **104**, 271-277.

Runham, N.W., Thornton, P.R., Shaw, D.A. & Wayte, R.C., 1969. The mineralization and hardness of the radular teeth of the limpet *Patella vulgata* L. *Zeitschrift fur Zellforschung und mikroskopische Anatomie*, **99**, 608-626.

Shaw, J.A., Brooker, L.R. & Macey, D.J., 2002. Radular tooth turnover in the chiton *Acanthopleura hirtosa* (Blainville, 1825) (Mollusca: Polyplacophora). *Molluscan Research*, **22**, 93-99.

Steneck, R.N. & Watling, L., 1982. Feeding capabilities and limitation of herbivorous molluscs: A functional group approach. *Marine Biology*, **68**, 299-319.

van der Wal, P., Giesen, H. & Videler, J., 2000. Radular teeth as models for the improvement of industrial cutting devices. *Materials Science & Engineering C: Biomimetic Materials, Sensors & Systems*, **7**, 129-142.

Appendix B:

Paper submitted to The American Malacological Bulletin: Accepted.

Methods of sample preparation of radula epithelial tissue in chitons (Mollusca: Polyplacophora)

J.A. Shaw, D.J. Macey, P.L. Clode, L.R. Brooker, R.I.Webb, E.J. Stockdale &

R.M. Binks

ABSTRACT

A glutaraldehyde fixative developed for preserving the radula superior epithelium of the adult chiton *Acanthopleura hirtosa* (de Blainville 1825), was used in conjunction with conventional and microwave-assisted sample processing schedules to produce high quality tissue preservation for observation by light and electron microscopy. In addition, high pressure freezing (HPF) and cryosubstitution were used to fix the radula tissue of juvenile specimens. Microwave-assisted fixation was preferred to conventional bench-top techniques due to the superior preservation of fine cell structure together with reduced processing times and chemical exposure. Although restricted to very small (< 200 μm) samples, the quality of juvenile radulae processed by HPF was excellent. The improvements in tissue preservation gained by using microwave and cryo-preservation techniques are therefore critical for obtaining accurate ultrastructural information of the radula in marine molluscs. In particular, these findings highlight additional processing options available for the study of cellular structures in biomineralizing tissues.

INTRODUCTION

The radula has been the focus of numerous studies over many decades, with its intricate and varied design being used to elucidate aspects of molluscan ecology, biology and taxonomy (see for example: Fretter and Graham 1962; Runham 1963;

Steneck and Watling 1982; Padilla 1985; Scheltema 1988; Salvini-Plawen 1990). In addition, the radulae of polyplacophoran and patellid gastropod molluscs have received particular attention as a result of their unique ability to harden their teeth with iron and other biominerals (Mann *et al*. 1986; Lowenstam and Weiner 1989; Webb *et al*. 1989).

The chiton radula represents an excellent example of matrix-mediated biomineralization, where the minerals are formed in a highly organized manner within the framework of an organic matrix (Simkiss and Wilbur 1989; Watabe 1990; Mann 2001; Weiner and Addadi 2002). While considerable progress has been made in elucidating the general structural organization of minerals deposited within the tooth matrix and the sequence in which they are deposited (see for example: Lowenstam 1962; Kim *et al*. 1989; Macey *et al*. 1994; Brooker *et al*. 2006), the precise mechanisms involved in the cellular transport of ions to the tooth cusps are poorly understood. The elemental precursors for biomineralization are thought to be delivered to the teeth by the overlying superior epithelial tissue, which surrounds the cusps during all stages of development (Nesson and Lowenstam 1985) (Figure 1). The superior epithelium and teeth are encapsulated within the radular sheath, the inferior epithelium and the radula membrane; with the whole structure resembling a tube open only along the dorsal surface (Figure 1). Histological investigation of the epithelial tissue is difficult due to the complex composition and structure of the radula, which contains both hard mineralized structures and cartilaginous membranes in close proximity to cellular material.

Chemical fixatives such as glutaraldehyde buffered in filtered seawater are commonly used for preserving marine organisms, where the osmotic pressure of the solution acts to mimic that of the animal, thereby reducing swelling or shrinkage of the tissues (Dykstra and Reuss 2003). However, fixation often gives rise to variations in the ultrastructural morphology of organelles (Hayat 2000), and it is therefore preferable to

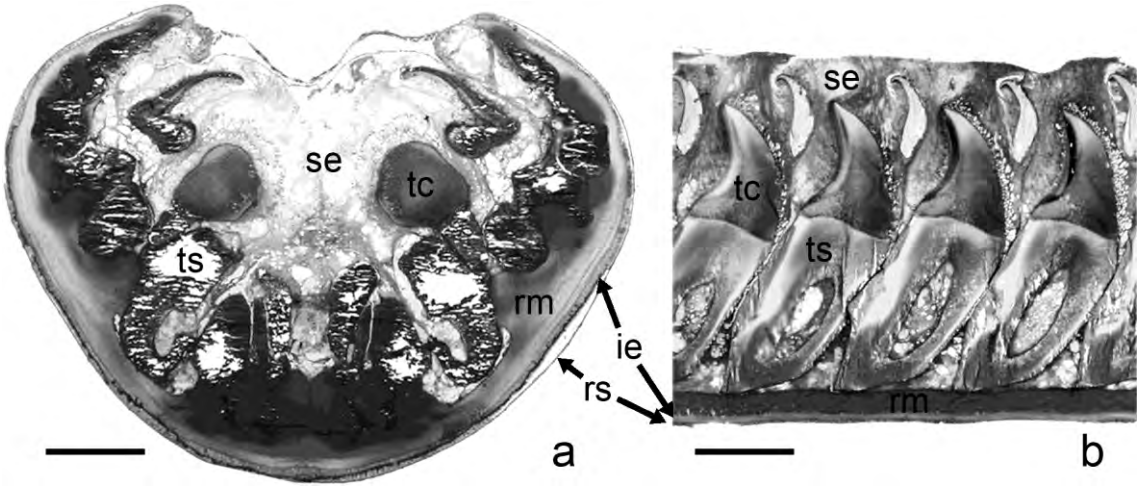

Figure 1. Radula apparatus of the chiton *Acanthopleura hirtosa* (adult) in (a) transverse section and (b) longitudinal section exhibiting various hard and soft tissue components. se = superior epithelium, ie = inferior epithelium, tc = tooth cusp, ts = tooth stylus, rm = radula membrane, rs = radula sheath. Scale bars = 200 μm.

utilize several techniques to acquire true comparative information. Microwave-assisted fixation and cryopreservation techniques (McDonald *et al*. 2007; Webster 2007), which are now common in laboratories worldwide, provide two additional means of obtaining such comparative information. The main advantage afforded by microwave protocols is a dramatic reduction in sample processing times (<4 hours), while at least maintaining, if not improving, fixation quality over conventional methods (see for example: Giberson and Demaree 1999; Laboux *et al*. 2004). Excellent tissue preservation can also be attained using cryopreservation techniques, which aim to achieve vitreous ice formation in samples and thereby prevent ice crystal damage. However, due to difficulties associated with heat dissipation, only very small samples (<200 μm) can be frozen successfully (see for example: Wilson *et al*. 1998; Sawaguchi *et al*. 2005).

In order to improve our current techniques and thus better understand the detailed cellular structure of the superior epithelium in chiton and limpet teeth, we have investigated alternative fixation methods. Determining the precise structure of these

cells will assist in elucidating their function and the mechanisms involved in the transport of ions into the teeth, which remains a fundamental obstacle to our wider understanding of the initial phase of biomineralization. The aim of this current study is thus to compare three fixation methodologies (conventional chemical, microwave-assisted and low temperature), and to present comparative data regarding preservation of the superior epithelial tissues of the chiton *Acanthopleura hirtosa* for both light and electron microscopy.

MATERIALS AND METHODS

Conventional and microwave-assisted chemical fixation and cryofixation techniques were utilized for the preparation of epithelial tissues for light microscopy (LM) or transmission electron microscopy (TEM). Adult and juvenile specimens of the chiton *Acanthopleura hirtosa* (average animal length ~4 cm and ~0.8 cm respectively) were collected from intertidal limestone at Woodman Point within the Perth metropolitan area of Western Australia (Lat. 32^{o}S, Long. 116^{o}E). Incisions were made along both pallial grooves from the anus towards the head, thereby freeing the foot, visceral mass and buccal mass as a single entity from the shell plates and girdle. The visceral mass was then carefully removed to expose the radula sac. Dissections were performed as quickly as possible to reduce the deterioration of radula epithelial tissue.

Preparation of Radulae from Adult Animals

For samples processed using either conventional or microwave-assisted methods, the dissected tissue mass was immediately immersed in a fixative comprised of 2.5% glutaraldehyde buffered in 0.1 M phosphate, with a pH of 7.2 and an osmolarity of 900 mmol.kg^{-1} adjusted using sucrose (buffer A). Following which, the buccal mass and radula was separated from the remainder of the animal and the radula either left whole or cut transversely into three or four segments (the buccal mass was discarded). The tissues were then processed by either conventional bench-top methods or

accelerated microwave-assisted protocols using a Pelco Biowave® fitted with a cold spot and vacuum chamber, according to the specific schedules detailed in Table 1. This included fixation with glutaraldehyde in buffer A, rinsing in buffer A, post fixation in 1% osmium tetroxide (OsO_4) in 0.05 M phosphate buffered saline (buffer B) at 4^{o}C, and a final rinse in buffer B, prior to dehydration through a graded series of acetones, then infiltration and embedding in Spurr's resin. Preparation of radula tissue by high-pressure freezing was not possible for adults due to limitations in sample size, which are restricted to ~200 μm.

Table 1. Conventional and microwave-assisted processing schedules for the radula epithelial tissues of adult *Acanthopleura hirtosa*.

Step	Medium	Concentration %	Conventional times	Microwave times	Microwave wattage (W)
Fixation	glutaraldehyde (buffer A)	2.5*	24 h	2x(2 ^{on}/2 ^{off}/2 ^{on}) (min) (v)	80
Rinse	buffer A		15 min x4	40 sec (v)	250
Post-fixation	OsO_4 (buffer B)	1*	2 h	2x(2 ^{on}/2 ^{off}/2 ^{on}) (min) (v)	80
Rinse	buffer B		15 min x4	40 sec (v)	250
Dehydration	acetone	10, 30, **50***, **75***, **90***, **100***	15 min x2 each	40 sec each (100 x2)	250
Infiltration	Spurr's resin	5, 10, 20, 40, **50**, 60, **75**, 80, **90**, **100***	8-12 h each	3 min each (100 x2) (v)	250
Polymerisation	Spurr's resin	**100***	conventional oven 60^{o}C overnight		

Note: Concentrations in bold represent the microwave schedule, concentrations not in bold represent the conventional schedule, *represents concentrations used in both schedules. (v) = steps undertaken in vacuum, $^{on/off}$ denotes magnetron (irradiation) cycle.

Following polymerization, resin blocks were sectioned for observation at both the LM and TEM level. For LM, 1 μm-thick sections were mounted on glass slides and stained with aqueous 1% Methylene Blue and 1% Azur II (20 sec) prior to imaging on an Olympus BX51 optical microscope fitted with an Olympus DP70 digital camera. For TEM, ~60 nm-thick sections were mounted on copper grids and double stained with uranyl nitrate (single crystal in one drop of 50% methanol) (10 min) followed by Sato's modified lead citrate (10 min) (Hanaichi *et al*. 1986) prior to imaging on a JEOL 2000 TEM at 80 kV.

Preparation of Radulae from Juvenile Animals

Juvenile specimens of *A. hirtosa* were processed using conventional and microwave-assisted methods as for adult radulae, however, schedules were adjusted in order to account for the reduction in tissue size, and samples were embedded in Procure Araldite (formerly Epon Araldite) (Table 2). For cryofixation of juvenile radulae, the immature portion of each radula was removed by cutting transversely approximately 200 μm from the posterior end. Each immature portion was then placed into a 200 μm membrane filled with 20% bovine serum albumin in artificial seawater. These membrane mounted samples were rapidly frozen in a high-pressure freezer (Leica EMPACT 2) prior to cryosubstitution in acetone containing 2% OsO_4 at -85^{o}C for 52 h. Samples were then progressively warmed from -85^{o}C to 20^{o}C over 13 h in a Leica automatic freeze substitution unit prior to being washed in acetone and infiltrated and embedded in Araldite resin. Cryo-prepared sample blocks were polymerized underwater using a Pelco Biowave® microwave at 650 W for 90 min. Conventional, microwave-assisted and cryo-prepared sections were imaged unstained on a JEOL 2100 TEM at 120 kV using a Gatan Orius SC1000 digital camera.

Table 2. Conventional and microwave-assisted processing schedules for the radula epithelial tissues of juvenile *Acanthopleura hirtosa*.

Step	Medium	Concentration %	Conventional times	Microwave times	Microwave wattage (W)
Fixation	glutaraldehyde (buffer A)	2.5*	24 h	2x(2 ^{on}/2 ^{off}/2 ^{on}) (min) (v)	80
Rinse	buffer A		10 min x4	40 sec (v)	250
Post-fixation	OsO_4 (buffer B)	1*	1 h	2x(2 ^{on}/2 ^{off}/2 ^{on}) (min) (v)	80
Rinse	buffer B		10 min x4	40 sec (v)	250
Dehydration	ethanol/acetone$^{(a)}$	**50***, **75***, **90***, **100*, 100**$^{(a)}$, 100$^{(a)}$	10 min each (100 x2)	40 sec each	250
Infiltration	Procure Araldite	5, 20, **50**, 60, **75**, 80, **90**, **100***	4-8 h each	3 min each (100 x2) (v)	250
Polymerisation	Procure Araldite	**100***	conventional oven 60^{o}C overnight		

Note: Concentrations in bold represent the microwave schedule, concentrations not in bold represent the conventional schedule, *represents concentrations used in both schedules. (v) = steps undertaken in vacuum, $^{on/off}$ denotes magnetron (irradiation) cycle, (a) = acetone.

RESULTS AND DISCUSSION

Preservation of Adult Radulae

While glutaraldehyde fixation of radula epithelium was satisfactory at the LM level when conventional bench-top methods were used, microwave-assisted protocols dramatically reduced sample processing times from six days to one hour (Table 1) and resulted in superior ultrastructural preservation at the TEM level. In addition, microwave-assisted protocols increased fixative penetration into the tooth, improving, for example, tissue preservation within the stylus canal (Figure 2), which fixed poorly by conventional methods.

Figure 2. Light micrograph of a longitudinal section through a major lateral tooth from adult *Acanthopleura hirtosa* at row 6 prepared using microwave-assisted protocols. Despite being situated deep within the tooth stylus (ts), the tissues of the stylus canal (sc) are well preserved. se = superior epithelium, tc = tooth cusp. Scale bar = 50 μm.

The endothelial radula sheath layer, recognizable by the presence of ciliated endothelial cells distributed over the entire sheaths surface, remained intact when processed by microwave methods (Figure 1), in contrast to conventional methods where it was often disrupted. It is likely that the shorter sample processing and handling times afforded by microwave fixation reduce the likelihood of damage to this delicate membrane. Both techniques preserved prominent vesicles that line the anterior and posterior surfaces of the tooth cusps (Figure 3). We have found that these vesicles can be either abundant or virtually absent at the same stage of tooth development in different animals. It is currently not known whether these vesicles are natural features of the adult epithelium or artifacts resulting from the fixation process.

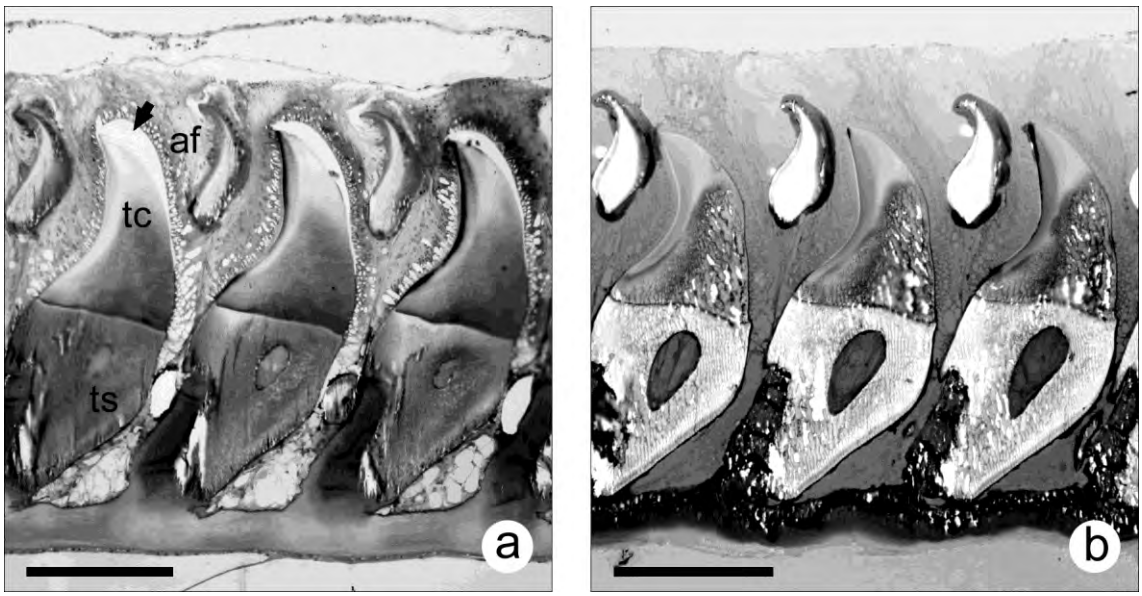

Figure 3. Major lateral tooth rows 12 – 14 from radulae of adult *Acanthopleura hirtosa* prepared using (a) conventional and (b) microwave techniques. Note the separation (arrow) of the superior epithelium from the anterior face (af) of the tooth cusps (tc) in conventionally fixed material and the poor infiltration of resin into the tooth stylus (ts) and cusp in microwave prepared material. Scale bars = 200 μm.

Conventional fixation often resulted in the separation of the superior epithelium from the hard tooth cusps, while in microwave fixed material this artifact was rarely observed (Figure 3). Despite a number of attempts being made to improve resin penetration into the base material using both conventional and microwave-assisted methods, including lower resin concentrations and increased infiltration times, the fibrous appearance of the major lateral tooth cusps and stylus persisted and was indeed far more noticeable in microwave prepared specimens (Figure 3). This is indicative of poor infiltration by the epoxy resin and is a common problem encountered in mollusc species by many researchers (see for example: Nesson and Lowenstam 1985; Mackenstedt and Markel 1987).

Microwave-assisted sample processing resulted in far better preservation of tissue ultrastructure compared to conventional methods. TEM of both conventional and microwave prepared samples revealed the typical arrangement of organelles within the superior epithelium near the cusp surface that are common to chitons, including microvilli, mitochondria, rough and smooth endoplasmic reticulum and abundant, electron dense ferritin siderosomes (Figure 4). However, at higher magnifications it could be clearly seen that samples fixed using the microwave contained numerous granules approximately 60 nm in diameter. These granules, which are likely to be either aggregations of ribosomal material or glycogen, appeared throughout the cytoplasm, particularly near the apical poles of the superior epithelium (Figure 5). These fine structures are either absent or not well preserved in conventional preparations and have not been reported by previous authors (see for example: Nesson and Lowenstam 1985; Kim *et al*. 1989). It is likely that the retention of these structures seen in microwave prepared samples is a direct result of the dramatic reduction in processing time of samples, thereby reducing chemical exposure and the chance of extracting soluble components of the tissue.

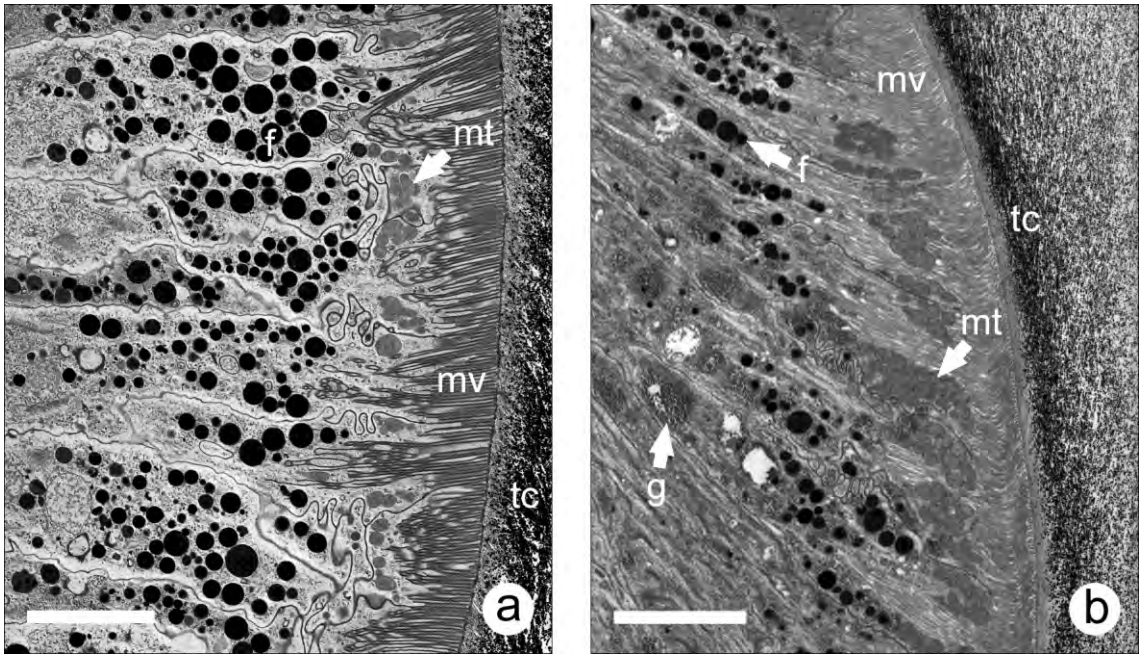

Figure 4. Transmission electron micrographs of the radula superior epithelium abutting the tooth cusp (tc) of (a) conventionally and (b) microwave processed radulae from adult *Acanthopleura hirtosa* at tooth rows 14 and 13 respectively. f = ferritin siderosome, g = granules, mt = mitochondria, mv = microvilli. Scale bars = 5 μm.

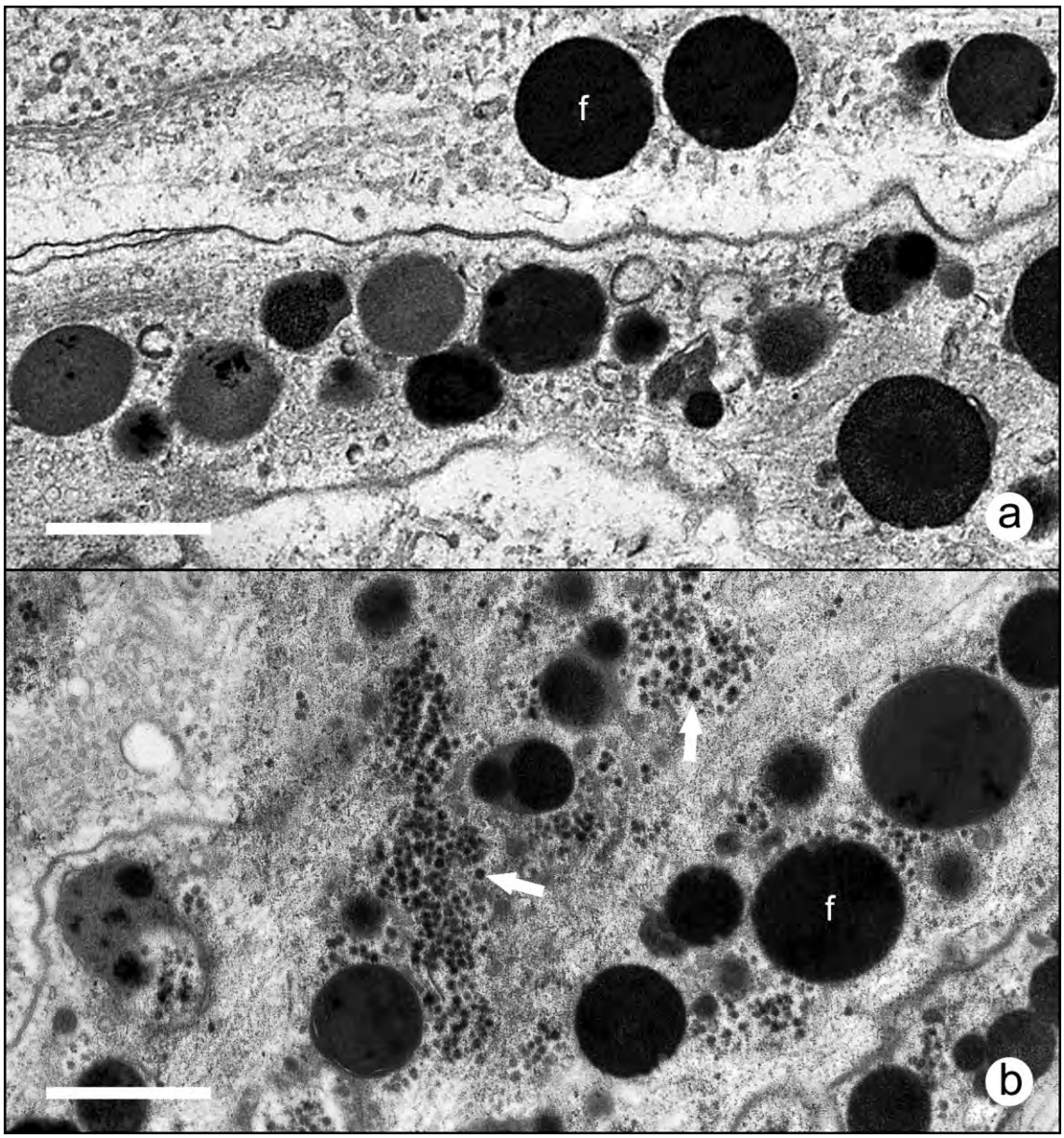

Figure 5. Transmission electron micrograph of (a) conventional and (b) microwave prepared superior epithelium from adult *Acanthopleura hirtosa* showing differences in the preservation of fine structure. Arrows denote aggregations of ribosomal- or glycogen-like structures within the cytoplasm. f = ferritin siderosome. Scale bars = 1 μm.

Preservation of Juvenile Radulae

The type and arrangement of organelles within the apical epithelium of juvenile radulae follows the same characteristic configuration as that described for adult tissue. The quality of tissue preservation of juvenile *Acanthopleura hirtosa* radula epithelium, when using conventional and microwave-assisted methods, was very similar to that observed in adults (Figure 6a and b). While the reduction in sample size is likely to improve fixative penetration in juvenile radulae, the comparable fixation quality between adult and juvenile tissue suggests that size is not a limiting factor. This is evidenced by the absence of ~60 nm granules in conventionally fixed juvenile tissue, which were retained in both adult and juvenile tissue processed in the microwave (Figures 5b and 6b).

With the exception of some slight separation of epithelial tissue from the tooth cusps and bases, high-pressure freezing (HPF) resulted in unsurpassed preservation of juvenile *A. hirtosa* radula tissue (Figure 6c). Nuclei, with well defined chromatin adjacent to the nuclear membrane, mitochondria with well preserved cristae, rough endoplasmic reticulum and Golgi apparatus are clearly represented in the cytoplasm, together with microvilli and ferritin siderosomes (Figure 6c). The ~60 nm granules observed in microwave-assisted preparations were also present in HPF samples (data not shown). Notably, the large vesicles surrounding the tooth cusps in the adult epithelium were also observed in juvenile tissue prepared using conventional and microwave protocols, but were absent in HPF material (data not shown). While variations in ultrastructure may arise from differences in the functional state of the cells at the time of fixation (Hayat 2000), it is more likely that these vesicles are artifacts resulting from glutaraldehyde fixation rather than a natural physiological condition (Bowers and Maser 1988).

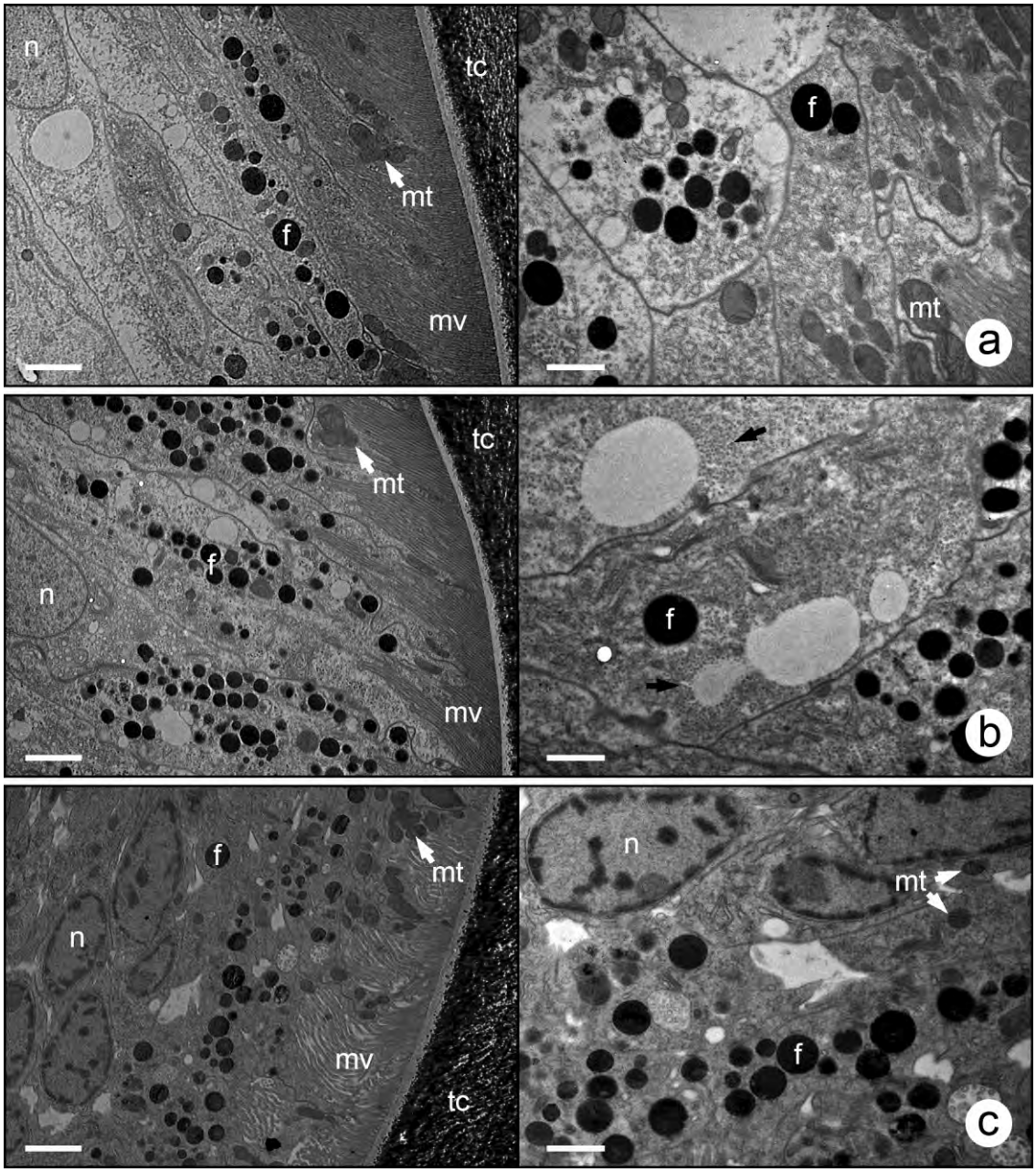

Figure 6. Transmission electron micrographs comparing the preservation of cell ultrastructure in radula epithelium from juvenile specimens of the chiton *Acanthopleura hirtosa* processed using (a) conventional, (b) microwave-assisted and (c) high-pressure freezing protocols. Black arrows denote aggregations of ribosomes/glycogen. f = ferritin siderosome, mv = microvilli, mt = mitochondria, n = nucleus, tc = tooth cusp. Note: all images are taken from the first tooth row after the onset of mineralization in the cusps. Scale bars = (images on left) 2 μm, (images on right) 1 μm.

Despite a slight improvement in resin infiltration using the conventional method, microwave-assisted processing of radula superior epithelium is preferred due to the improved quality of tissue preservation and the vastly reduced time for sample processing. While cryopreservation using HPF results in excellent ultrastructural preservation, it is limited with respect to sample size. As such, only the radulae of juveniles or very small mollusc species can be prepared using this method. In addition, the relative portability and affordability of microwave technology compared to HPF makes it a more realistic option for many laboratories. While each of these new techniques has proven to be suitable for fixation of tissue at the LM level, the improved retention of ultrastructural information gained by using microwave and HPF methods highlights the need for a re-evaluation of fine cell structure in molluscan radulae.

While the ultrastructure of the radula epithelium of chitons and limpets has been well documented (Nesson and Lowenstam 1985; Mann *et al*. 1986; Kim *et al*. 1989; Rinkevich 1993), no studies have been conducted in relation to the development of this tissue as the teeth progress from an unmineralized to a mineralized state, information that is crucial for resolving the cellular basis of biomineralization. In addition, cryo-techniques have recently been used in conjunction with chemical fixation to characterize the organic matrix in limpets, by dramatically reducing artifacts resulting from staining, dehydration and embedding (Sone *et al*. 2007). The high-pressure freezing method outlined in the current study therefore provides a valuable first step in preserving the organic matrix for subsequent cryo-sectioning in a frozen hydrated state. The methods of sample preparation presented here will not only benefit future investigations of the superior epithelium and organic matrix of chitons and limpets, but will also be of use for taxonomic and morphological studies of molluscan radulae in general.

ACKNOWLEDGEMENTS

The authors would like to thank the assistance of Mr. Gordon Thompson at Murdoch University for his advice on histological preparations. This research was carried out using facilities at the Centre for Microscopy, Characterisation and Analysis, at The University of Western Australia, which are supported by University, State and Federal Government funding and the Centre for Microscopy and Microanalysis at the University of Queensland. Financial support was provided by The Australian Research Council (Grant # DP0559858). We also acknowledge the technical, scientific and financial assistance from the NANO-MNRF. All experiments conducted during the study comply with the Australian Code of Practice for the Care and Use of Animals for Scientific Purposes - 7th Edition 2004. Animals were collected under CALM permit # SF005916.

LITERATURE CITED

Bowers, B., and M. Maser. 1988. Artifacts in fixation for transmission electron microscopy. *In*: R.F.E. Crang and K.L. Klomparens, eds., *Artifacts in Biological Electron Microscopy,* Plenum Press, New York. Pp. 13-42

Brooker, L.R., A.P. Lee, D.J. Macey, J. Webb, and W. van Bronswijk. 2006. *In situ* studies of biomineral deposition in the radula teeth of chitons of the suborder Chitonina. *Venus* **65:** 71-80.

Dykstra, M.J. and L.E. Reuss. 2003. *Biological Electron Microscopy : Theory, Techniques, and Troubleshooting.* Kluwer Academic/Plenum Publishers, New York.

Fretter, V. and A. Graham. 1962. *British Prosobranch Molluscs, Their Functional Anatomy and Ecology.* Ray Society, London.

Giberson, R.T. and R.S.J. Demaree. 1999. Mircrowave processing techniques for electron microscopy: a four-hour protocol. *Methods in Molecular Biology* **117:** 145-158.

Hanaichi, T., T. Sato, T. Iwamoto, J. Malavasi-Yamashiro, M. Hoshino, and N. Mizuno. 1986. A Stable Lead by Modification of Sato's Method. *Journal of Electron Microscopy* **35:** 304-306.

Hayat, M.A. 2000. *Principles and Techniques of Electron Microscopy*. Cambridge University Press, Cambridge.

Kim, K.S., D.J. Macey, J. Webb, and S. Mann. 1989. Iron mineralization in the radula teeth of the chiton *Acanthopleura hirtosa*. *Proceedings of the Royal Society London* **B237:** 335-346.

Laboux, O., N. Dion, V. Arana-Chavez, L.-G. Ste-Marie, and A. Nanci. 2004. Microwave Irradiation of Ethanol-fixed Bone Improves Preservation, Reduces Processing Time, and Allows Both Light and Electron Microscopy on the Same Sample. *Journal of Histochemistry and Cytochemistry* **52:** 1267-1275.

Lowenstam, H.A. 1962. Magnetite in denticle capping in recent chitons (Polyplacophora). *Bulletin of the Geological Society of America* **73:** 435-438.

Lowenstam, H.A., and S. Weiner. 1989. *On Biomineralization.* Oxford University Press, Oxford.

Macey, D.J., J. Webb, and L.R. Brooker. 1994. The Structure and Synthesis of Biominerals in Chiton Teeth. *Bulletin de l'Institut Oceanographique* **14:** 191-197.

Mackenstedt, U., and K. Markel. 1987. Experimental and comparative morphology of radula renewal in pulmonates (Mollusca, Gastropoda). *Zoomorphology* **107:** 209-239.

Mann, S. 2001. *Biomineralization, Principals and Concepts in Bioinorganic Materials Chemistry*. Oxford University Press, Oxford.

Mann, S., C.C. Perry, J. Webb, B. Luke, and R.J.P. Williams. 1986. Structure morphology composition and organization of biogenic minerals in limpet teeth. *Proceedings of the Royal Society London* **227:** 179-190.

McDonald, K.L., M. Morphew, P. Verkade, and T. Müller-Reichert. 2007. Recent advances in high-pressure freezing: Equipment and specimen loading methods. *In*: J. Kuo, ed., *Electron Microscopy Methods and Protocols*, Humana Press, Totowa. Pp. 143-173.

Nesson, M.H., and H.A. Lowenstam. 1985. Biomineralization processes of the radula teeth of chitons. *In:* J.L. Kirshvink, D.S. Jones and B.J. MacFadden, eds., *Magnetite biomineralization and magnetoreception in organisms*, Plenum Press, New York. Pp. 333-361.

Padilla, D.K. 1985. Structural resistance of algae to herbivores. *Marine Biology* **90:** 103-109.

Rinkevich, B. 1993. Major primary stages of biomineralization in radula teeth of the limpet *Lottia gigantea*. *Marine Biology* **117:** 269-277.

Runham, N.W. 1963. A study of the replacement mechanism of the pulmonate radula. *Quarterly Journal of Microscopial Science* **104:** 271-277.

Salvini-Plawen, v.L. 1990. Origin, phylogeny and classification of the phylum Mollusca. *Iberus* **9:** 1-33.

Sawaguchi, A., S. Ide, and T. Suganuma. 2005. Application of 10-mm thin stainless foil to a new assembly of the specimen carrier in high-pressure freezing. *Journal of Electron Microscopy* **54:** 143-146.

Scheltema, A.H. 1988. Ancestors and decendents: relationships of the Aplacophora and Polyplacophora. *American Malacological Bulletin* **6:** 57-68.

Simkiss, K., and K.M. Wilbur. 1989. *Biomineralization: Cell Biology and Mineral Deposition.* Academic Press, San Diego.

Sone, E.D., S. Weiner, and L. Addadi. 2007. Biomineralization of limpet teeth: A cryo-TEM study of the organic matrix and the onset of mineral deposition. *Journal of Structural Biology* **158:** 428-444.

Steneck, R.N. and L. Watling. 1982. Feeding capabilities and limitation of herbivorous molluscs: A functional group approach. *Marine Biology* **68:** 299-319.

Watabe, N. 1990. Calcium phospate structures in invertebrates and protozoans. *In:* J. G. Carter, ed., *Skeletal Biomineralization: Patterns, Processes and Evolutionary Trends*, Van Nostrand Reinhold, New York. Pp. 35-44.

Webb, J., D.J. Macey, and S. Mann. 1989. Biomineralization of iron in molluscan teeth. *In*: S. Mann, J. Webb and R.J.P. Williams, eds., *Biomineralization*, VCH Verlagsgesellschaft, Weinheim. Pp. 345-387.

Webster, P. 2007. Microwave-assisted processing and embedding for transmission electron microscopy. *In*: J. Kuo, ed., *Electron Microscopy Methods and Protocols*, Humana Press, Totowa. Pp. 47-65.

Weiner, S., and L. Addadi. 2002. At the Cutting Edge. *Science* **298:** 375-376.

Wilson, M.T., M.A. Farmer, and C.J. Karwoski. 1998. Ultrastructure of the frog retina after high-pressure freezing and freeze substitution. *Journal of Microscopy* **189:** 219-235.

Appendix C:

**Proceedings of the 9th International Symposium on Biomineralization,
(Eds.) Arias, J.L., Fernández, M.S.
Editorial Universitaria, Santiago, Chile, 2007, pp. 187-192.**

The Stylus Canal: A Conduit for the Delivery of Ions to the Mineralizing Tooth Cusps of Chitons?

Jeremy A. Shaw, David J. Macey, Lesley R. Brooker, Peta L. Clode and Edward J. Stockdale

ABSTRACT

The stylus canal is a cell filled cavity that runs the majority of the length of each major lateral tooth base in chitons. Previous studies have focused on the cusps of the major lateral teeth and the superior epithelial tissue that is thought to be responsible for mineralizing them with iron and calcium biominerals. For the first time, a histological study of the stylus canal has revealed that the canal cells contain microvilli and ferritin-like siderosomes, arranged in a similar configuration to those in the columnar epithelial cells abutting the surface of the tooth cusps. In addition, the canal terminates directly below the tooth cusps, placing it in an ideal position to act as a conduit for the delivery of ions to the inside of the cusp. Proof of the existence of an additional ion delivery route has the potential to significantly enhance our understanding of the biomineralization pathways in these animals.

INTRODUCTION

The radula is the principal feeding organ for many mollusc species. It is comprised of an elongated array of transverse tooth rows that are carried forward in a conveyor belt manner (Lowenstam and Weiner, 1989). In chitons (Mollusca: Polyplacophora), each transverse row bears 17 teeth, including a pair of large major laterals, whose cusps are hardened with iron and calcium biominerals. Odontoblast cells prefabricate the teeth

as an organic matrix upon which the various biominerals are formed. The subsequent delivery of ions to the organic matrix is thought to be effected by the overlying superior epithelial tissue that surrounds the teeth at all stages of development. Magnetite (Fe_3O_4) is the principal mineral formed within the posterior cutting face and anterior surface of the tooth cusps, while at later stages of development the tooth core is infilled with either an apatitic calcium phosphate or iron(III) phosphate depending on the species (Lee *et al*., 2003).

Most of the research related to chiton teeth has focused directly on the magnetite bearing cusps and the iron-rich cells that abut their anterior and posterior surfaces (for example, see Kim *et al*., 1989; Wealthall *et al*., 2005). However, located centrally within the tooth base lies a cell filled cavity referred to as the stylus canal (Nesson and Lowenstam, 1985). The cells of this cavity appear to be linked to the superior epithelium, while at their apex they lie in close proximity to the mineralizing tooth cusps. While the existence of the stylus canal has been recognized, no attempts have been made to fully resolve its structure or function. In order to characterize this unique feature, a histological investigation of the stylus canal has been undertaken, using light microscopy and transmission and scanning electron microscopy.

MATERIALS AND METHODS

Specimens of the chiton *Acanthopleura hirtosa* were collected from intertidal limestone at Woodman Point within the Perth metropolitan area of Western Australia (Lat. 32^{o}S, Long. 116^{o}E). Radulae were cleaned with 2% sodium hypochlorite and fixed overnight in 2.5% glutaraldehyde in seawater. They were then dehydrated through a graded series of ethanol followed by amyl acetate, before drying to the critical point of CO_2. Individual teeth were removed from the radula and either left whole or fractured to expose the stylus canal. The teeth and tooth fragments were mounted on aluminum

stubs and gold coated prior to imaging on a Philips XL 20 scanning electron microscope at 10 KeV.

Whole radulae were fixed for 24 hours in 2.5% glutaraldehyde buffered in 0.1 M phosphate at pH 7.2 and adjusted to an osmolarity of 900 mmol/kg using sucrose. Samples were then post-fixed for 2 hours in 0.1 M OsO_4 buffered in phosphate at 900 mmol/kg. Fixed samples were dehydrated through a graded series of acetone before infiltration and embedding in Spurr's resin. Sections for light microscopy were imaged on an Olympus BX51 optical microscope. Sections for transmission electron microscopy were imaged on a Philips CM 100 transmission electron microscope at 80 KeV.

RESULTS

Scanning electron micrographs of the major lateral teeth confirmed the existence of an opening located in the center of the medial surface of the tooth bases (Fig. 1A.). This opening connects to a single cell-filled cavity within the tooth base termed the stylus canal, which is divided into distal and proximal arms. The distal arm of the canal extends toward the tooth cusp for approximately 300 μm, while the proximal arm projects from the opening towards the radula membrane for only 100 μm. The canal is separated from the cusp by 25 μm of tooth base material situated just below the junction zone (Fig. 1B.). Longitudinal sections through the stylus canal illustrate that the canal tissue resembles columnar epithelium (Fig. 1B.). Transmission electron micrographs of the apical region of the canal cells confirm the presence of microvilli, mitochondria and electron dense structures that strongly resemble ferritin siderosomes (Fig. 2A and 2B.).

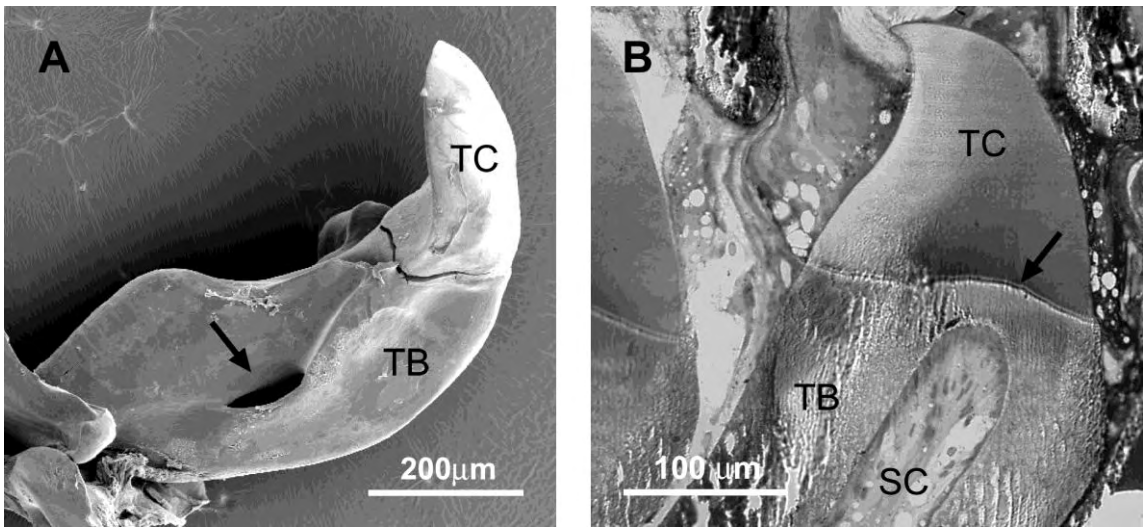

Figure 1. Major lateral tooth of the chiton *Acanthopleura hirtosa*. **A**, Scanning electron micrograph showing the opening of the stylus canal (arrow) on the medial surface of the tooth base. **B**, Light micrograph of a longitudinal section through the cell-filled cavity of the stylus canal (SC), illustrating the columnar configuration of the tissue and its close proximity to the junction zone (arrow). TC = tooth cusp, TB = tooth base

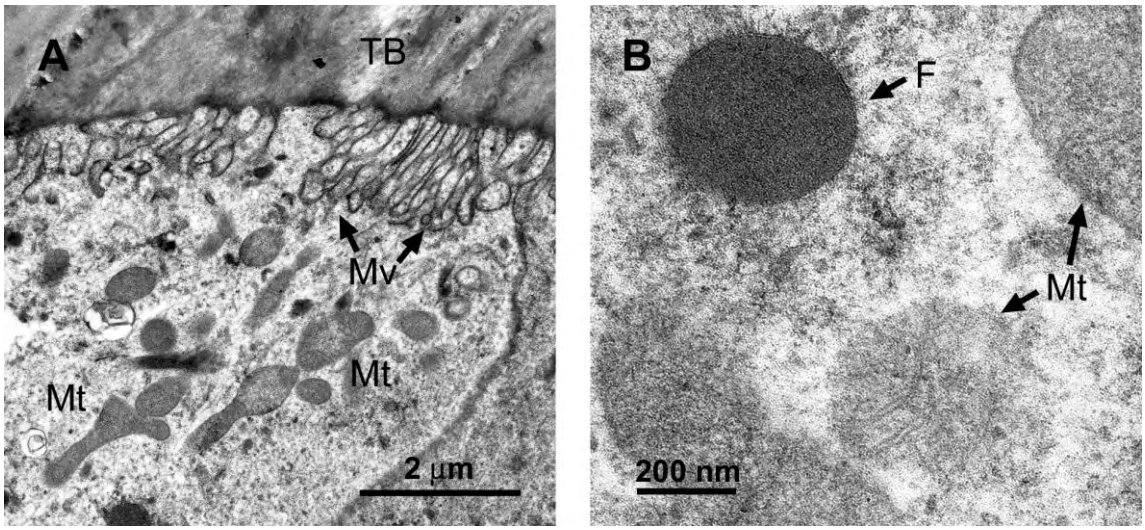

Figure 2. Transmission electron micrographs of the apical region of the stylus canal cells. **A**, Microvilli (Mv) abut the wall of the stylus canal in the region directly below the junction zone. TB = tooth base **B**, Electron dense, membrane bound structures resembling ferritin siderosomes (F) are present within the apical region. Mt = mitochondria

DISCUSSION

For the first time, a detailed histological investigation of the stylus canal has revealed a unique structure that may be involved in the biomineralization of the major lateral tooth cusps of chitons. While the existence of the stylus canal was first acknowledged by Nesson and Lowenstam (1985), no suggestion as to its function was proposed, with subsequent research remaining focused on the superior epithelial tissue surrounding the tooth cusps in order to resolve the cellular processes involved in cusp maturation.

The canal cells are remarkably similar in structure to the superior epithelial cells that abut the surface of the tooth cusps. Both have a columnar configuration and appear to have the same sub-cellular components, especially microvilli and ferritin-like siderosomes. Notably, the microvilli and siderosomes occur at the apex of the canal in close proximity to the junction zone, providing evidence that the canal has a cusp-orientated function.

The findings of this study have revealed that the canal is ideally positioned to act as a conduit for the delivery of ions between the superior epithelium and the tooth cusp. The majority of the stylus canal extends towards the tooth cusp, terminating just below the junction zone, a region that has been shown to be the initial site of ion deposition in chitons (Macey and Brooker, 1996). While analyses of this region indicate that it is high in iron, calcium and phosphorus ions, there is no evidence for mineralization, and it has been proposed that the junction zone may be a reservoir for the dissemination of ions to the mineralizing fronts in the tooth cusp (Brooker *et al*., 2003).

While the exact delivery and deposition processes involved in tooth maturation are unclear, the complex nature of the final mineralized composite suggests that the deposition process is under strict biological control. The superior epithelial cells, which abut the outer surface of the tooth cusps, contain large amounts of ferritin and these

tissues are likely to be of prime importance in the iron mineralization process (Nesson and Lowenstam, 1985; Kim *et al*., 1989). However, as iron mineralization of the tooth cusps progresses, it may become increasingly difficult for ions to pass from the superior epithelium into the core region of the tooth cusp. In addition, this self-limiting deposition may result in a loss of cellular control over the mineralization conditions within the cusps. As such, the stylus canal may act as a subsidiary pathway for the delivery of ions in later stages of mineral deposition, and may also exert some control over conditions within the tooth core. In support of this, Brooker *et al*. (2003) have demonstrated that the deposition of magnetite in the posterior region of the cusp occurs simultaneously on two fronts. This double front strategy suggests that iron may be derived from a source located on the anterior tooth surface or possibly from the stylus canal via the junction zone.

The stylus canal appears to be a structure unique to polyplacophoran molluscs. It has been found in all chiton species examined to date, while an equivalent structure has not been documented in any other molluscan group (for example, see Fretter and Graham, 1962; Hickman, 1977; Messenger and Young, 1999). Indeed, the bases of most gastropod teeth are solid in structure (Hickman, pers. comm., 2006). The canal is present in chiton teeth regardless of the size of the species or their radula teeth. For instance, it is found in small species, such as *Acanthochiton johnstoni*, whose major lateral teeth are approximately 260 μm in length, and in large species, such as *Cryptochiton stelleri*, whose major laterals can reach 1.1 mm in length (unpublished data). Consequently, the presence of the canal does not seem to be dependent on tooth size. Given that the canal is absent from the bases of all remaining non-iron mineralized teeth, irrespective of the species, it would seem likely that a functional relationship exists between the stylus canal and tooth cusp mineralization.

While further research is required to fully elucidate the function of the stylus canal, the findings presented here suggest that the canal is in some way involved in cusp mineralization. This alternate route of ion transport should be taken into consideration during future investigations related to the study of tooth cusp mineralization in chitons.

ACKNOWLEDGMENTS

The authors would like to thank the staff at The Centre for Microscopy and Microanalysis (University of Western Australia) for providing access and technical support, and also Mr. Gordon Thompson at Murdoch University for his advice on histology. Financial support was provided by The Australian Research Council (Grant # DP0559858) and Murdoch University's Division of Science and Engineering. All experiments conducted during the study comply with the Australian Code of Practice for the Care and Use of Animals for Scientific Purposes - 7th Edition 2004.

REFERENCES

Brooker, L.R., Lee, A.P., Macey, D.J., van Bronswijk W., Webb, J. (2003). Multiple-front iron-mineralisation in chiton teeth (*Acanthopleura echinata*: Mollusca: Polyplacophora). Mar. Biol. 142:447-454.

Fretter, V., Graham, A. (1962). British Prosobranch Molluscs, Their Functional Anatomy and Ecology. Ray Society, London, 755 p.

Hickman, C.S. (1977). Integration of electron scan and light imagery in study of molluscan radulae. Veliger 20(1):1-8.

Hickman, C.S. (2006) Department of Integrative Biology, University of California, Berkeley, USA, (Private Communication).

Kim, K.S., Macey, D.J., Webb, J., Mann, S. (1989). Iron mineralization in the radula teeth of the chiton *Acanthopleura hirtosa*. Proc. R. Soc. Lond. B237:335-346.

Lee, A.P., Brooker, L.R., Macey, D.J., Webb, J., van Bronswijk, W. (2003). A new biomineral identified in the cores of teeth from the chiton *Plaxiphora albida*. J. Biol. Inorg. Chem. 8:256-262.

Lowenstam, H.A., Weiner, S. (1989). On Biomineralization. Oxford University Press, Oxford, 324 p.

Macey, D.J., Brooker, L.R. (1996). The junction zone: Initial site of mineralization in radula teeth of the chiton *Cryptoplax striata* (Mollusca: Polyplacophora). J. Morph. 230:33-42.

Messenger, J.B., Young. J.Z. (1999). The radular apparatus of cephalopods. Phil. Trans. R. Soc. Lond. B 354(1380):161-182.

Nesson, M.H., Lowenstam, H.A. (1985). Biomineralization processes of the radula teeth of chitons. *In: MagnetiteBbiomineralization and Magnetoreception in Organisms* (Kirshvink, J.L., Jones, D.S., MacFadden, B.J. eds.) Plenum press, New York, pp. 333-361.

Wealthall, R.J., Brooker, L.R., Macey, D.J., Griffin, B.J. (2005). Fine structure of the mineralized teeth of the chiton *Acanthopleura echinata* (Mollusca: Polyplacophora). J. Morph. 265(2):165-175.

Appendix D:

Published paper

Molluscan Research, 2002, **22**, 93–99

Radula tooth turnover in the chiton *Acanthopleura hirtosa* (Blainville, 1825) (Mollusca: Polyplacophora)

Jeremy A. Shaw[A], *Lesley R. Brooker*[A] *and David J. Macey*[A,B]

[A]Division of Science and Engineering, Murdoch University, Murdoch WA 6150, Australia.
[B]To whom correspondence should be addressed. Email: d.macey@murdoch.edu.au

Abstract

The rate of radula production in the chiton *Acanthopleura hirtosa* (Blainville, 1825) was determined by following structural irregularities induced in the radula using a cold-shock treatment of 4°C for 48 h. In animals treated in this manner and subsequently maintained in an artificial intertidal habitat to ensure, as far as possible, a natural feeding regimen, the rate of radular production was calculated as 0.36 rows per day. This indicates that *A. hirtosa* renews its total radular length (mean 78 rows, SD = 6.5, n = 23) approximately once every 6.5 months, a relatively slow rate when compared with that of other molluscs.

Additional keywords: biomineralisation, cold-shocking, mollusc.

Introduction

The chiton radula consists of a ribbon like series of transverse tooth rows that are produced in a 'conveyor belt' manner (Lowenstam and Weiner 1989) from odontoblasts at the posterior end of the radula sheath (Kaas *et al.* 1998). Depending on the species, each transverse row consists of between 13 and 17 individual teeth. However, the main teeth that are involved in feeding are the prominent, glossy-black second lateral teeth, usually termed the major laterals. These teeth undergo a process of maturation along the length of the radula that involves the incorporation of iron and calcium based minerals onto an organic matrix (Kirschvink and Lowenstam 1979; Kim *et al.* 1989). This imparts to the teeth a unique combination of hardness and resilience, suitable for grazing on hard substrata (Webb *et al.* 1989). The anterior most teeth are worn by abrasion as the animals graze (Bullock 1989) and, as such, replacement appears to be in a state of dynamic equilibrium, where the rate of teeth being shed anteriorly is balanced by their production posteriorly (Runham 1963).

While a number of studies have been conducted in relation to the turnover rate of the molluscan radulae (Runham 1962, 1963; Runham and Isarankura 1966; Isarankura and Runham 1968; Padilla *et al.* 1996;), these have concentrated on gastropods, with a particular emphasis on pulmonates. Isarankura and Runham (1968) have developed a number of methods for studying the turnover rate, ranging from direct counts of teeth found in the faeces of animals, to marking the radula by surgical methods. These investigators also discovered that radula abnormalities occurring in *Helix aspersa* Möller, 1774, due to cold winter conditions, could be induced experimentally by a 'cold-shocking' technique. This method has since been found to be simple and reliable and facilitates the testing of a large number of individuals (Padilla *et al.* 1996).

The ongoing interest in the biomineralisation process in chiton teeth (see, for example, Webb *et al.* 1989; Lee *et al.* 1998, 2000) has led to the need to estimate the rate of tooth turnover, so that the demand for mineral precursors can be ascertained and some estimate of the flux of these elements through the chiton body established. The species used in the

 10.1071/MR02005 1323-5818/02/02093

present study was *Acanthopleura hirtosa* (Blainville, 1825), which is an abundant member of the Western Australian molluscan community. It occurs in the upper intertidal region of coastlines from Albany to Shark Bay (Wells and Bryce 1986) and has proved to be an ideal model for studies of the biomineralisation process (Evans *et al.* 1990, 1992; Macey and Brooker 1996; Macey *et al.* 1996).

Materials and methods

Adult specimens (mean length 37.6 ± 4.8 mm, $n = 36$) of *A. hirtosa* were collected from various sites in the Perth metropolitan area (Lat. 32°S, Long. 116°E) between February and March 2001. To reduce the likelihood of any damage to the specimens during collection, chitons were removed from their home scars by driving a screwdriver into the substratum near the mantle of each specimen. Each animal, along with a portion of the substratum to which it was attached, was levered free of the rock surface, placed in fresh seawater and transported back to the laboratory as quickly as possible.

To minimise the chances of the study altering the natural rate of radula production, all experimental animals were kept in an artificial environment, or 'mesocosm'. This consisted of a large open air tank containing limestone rocks collected from the intertidal region normally occupied by *A. hirtosa*. The rocks were positioned in the tank such that they partially protruded above the water line, providing the chitons with a habitat approximating their natural intertidal environment. In order to keep the exposed rocks moist and to simulate surf spray, the tank was continuously supplied with fresh seawater that was delivered via an overhead reticulation system. No organisms were removed from the rocks, which contained various species of algae, anemones, limpets, barnacles, crabs, polychaetes and other small invertebrate fauna. A number of juvenile and small adult chitons of various other species were also present.

In order to test the viability of the mesocosm as a chiton habitat, it was initially seeded with 21 specimens of *A. hirtosa* collected from the wild in early February and left to reside for a period of 2 months. Ten of these animals were included in the cold-shocking procedure, along with a further 15 collected from the wild in late March. Differentiation of the freshly collected specimens from the control animals was achieved by using a Dremel (Racine, Wisconsin, USA) engraving tool to score lines on either the fourth or fifth valve, respectively. All 25 animals were then subjected to a derivation of the cold-shocking technique of Isarankura and Runham (1968). A constriction was produced in the developing radula membrane by plunging the chitons into seawater prelowered to a temperature of 4°C and maintaining them at that temperature for 48 h. Directly following the cold-shocking procedure, while the animals were in a relaxed and extended state, their lengths were recorded. Two specimens were dissected and their radulae removed in order to provide Day 0 data, whereas all remaining specimens were transferred to the mesocosm, where they attached to the substratum. On subsequent alternate days, at the same time each day (± 2 h), a single specimen was selected at random for dissection. Prior to removal of the radula, chitons were anaesthetised by placing them in a shallow container of fresh tap water, which was then chilled at –1°C for 1 h. Radulae were then dissected out, cleaned using 2.5% sodium hypochlorite and the radula length and total number of transverse rows recorded. Radula constriction was observed and photographed using an Olympus DP10 digital camera, attached to an Olympus SZH10 stereo dissecting microscope, and the number of teeth prior to the position of the constriction was counted and recorded. In order to verify that the constriction anomaly was not a natural construct of the radular ribbon, five chitons were dissected straight from the wild for comparison.

Results

No constrictions were found in the radulae of animals dissected fresh from the field, indicating that the observed deformations were attributable to the cold-shocking procedure rather than being a natural construct of the radula. Only a single animal died in the mesocosm during the initial 2-month viability study. This occurred within a few days of transfer, suggesting that the combined shock of collection and transfer was the cause of death. A further two animals died following the 4°C cold-shocking procedure and transfer to the mesocosm. Animals that survived were assumed to be feeding in a normal manner due to the maintenance of limited algal coverage on the substratum and the deposition of a large number of faecal pellets in the mesocosm. Indeed, following the experimental period,

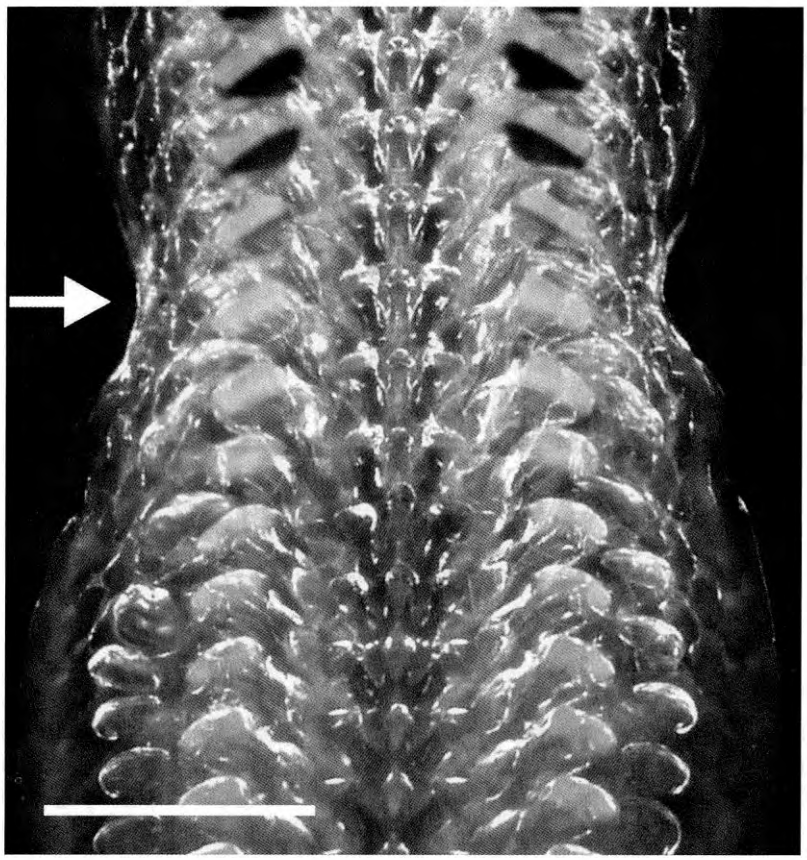

Fig. 1. Constriction (arrow) produced in the radula by placing animals in seawater precooled to a temperature of 4°C and maintaining them at that temperature for 48 h. Scale bar: 1 mm.

some of the smaller chiton species from the mesocosm were found to have spawned, indicating that these chitons, at least, were capable of reproducing while in the system. Preliminary cold-shocking trials at a temperature of –1°C produced 90% mortality, suggesting that this lower temperature is beyond the tolerance limit of this species.

The cold-shocking technique produced an obvious constriction of the radula membrane that could be tracked along the radula in all experimental animals throughout the experimental period (Fig. 1). Whereas some individual variation was seen in tooth turnover rate towards the end of the experimental period, the overall results were very consistent and allowed the calculation of an average rate of tooth turnover of 0.36 rows per day (SD = 0.06, $n = 20$; Fig. 2). Initial determination of the position of the constriction with regard to tooth row number was made difficult by the very low turnover rate, which meant that fractions of tooth rows had to be estimated. However, there does appears to be an initial lag phase, because the mean turnover rate for the first 8 days is only 0.27 rows per day (SD = 0.04, $n = 4$), which could be attributable to recovery from the cold-shocking procedure. Data obtained from animals in the study indicate that the average total number of transverse tooth rows for *A. hirtosa* is 78 (SD = 6.5, $n = 23$). Combining the data for tooth turnover rate and total row number gives a total radula replacement time of approximately 203 days (~6.5 months).

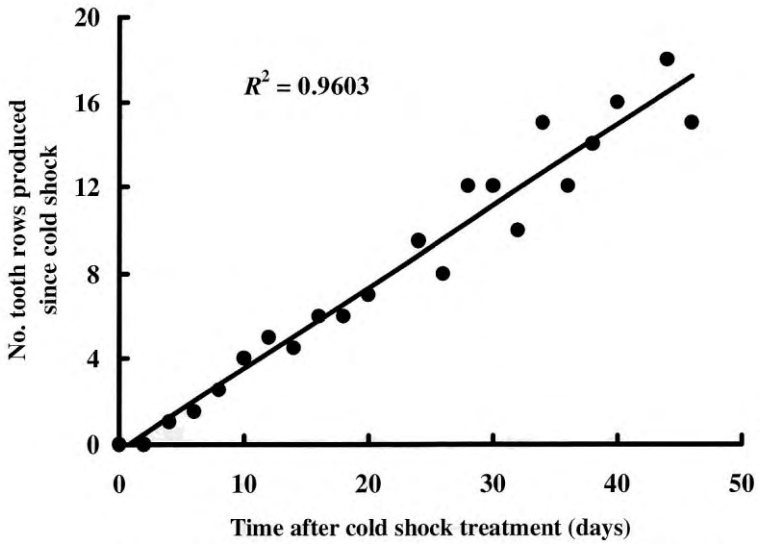

Fig. 2. Number of tooth rows formed after cold shock treatment.

Discussion

This paper reports, for the first time, the use of a cold-shocking method for measuring tooth turnover rate in temperate intertidal chitons, revealing a radula replacement rate of 0.36 rows per day in *A. hirtosa*. A previous study of radula production, using a variety of techniques including cold-shocking, found that radula turnover rates of 15 prosobranch and pulmonate species varied from 1 to 6.4 tooth rows per day (Isarankura and Runham 1968). In a subsequent study of two littorinid species, the cold-shocking technique revealed a calculated turnover rate of approximately 2.95 rows per day (Padilla *et al.* 1996). Isrankura and Runham (1968) found that a number of factors affect tooth turnover rate in gastropods, none more profound than that of ambient temperature, which increased radula production two to threefold in response to incremental rises of 10°C. The Perth region experiences a 'Mediterranean' climate, with average maximum and minimum temperatures of 29 and 18°C, respectively, in summer and 18 and 9°C, respectively, in winter. Local nearshore water temperatures range from 15 to 24°C, from winter to summer, respectively (Pearce *et al.* 1999). The present study was conducted during the months of late summer to early autumn, with the mesocosm at a relatively high water temperature of 22°C, with a variation of less than 1°C overnight. Hence, the production rate of 0.36 rows per day, although low in comparison with the gastropod species of previous studies, is likely to reflect a relatively high turnover rate for *A. hirtosa*. It would be interesting to repeat the study during the winter months to determine whether the radula turnover rate is reduced at a lower temperature. Isarankura and Runham (1968) found that active herbivores have higher rates of radula production than more sluggish or carnivorous forms, indicating that turnover is adapted to the feeding activity of the animal. Although it is difficult to compare the level of feeding intensity between gastropods and *A. hirtosa*, it can be argued that because *A. hirtosa* is an intertidal species that has an intermittent, semidiurnal feeding regimen, it is not an active herbivore for much of each 24 h period. As such, this could account, in part, for its comparatively low turnover rate.

There are several other factors that could affect the wide variation exhibited in the turnover rates of the different molluscs studied, including the physical size of the teeth, their structural design, their resistance to wear and the hardness of the animal's food source. The initial size of the mature teeth, prior to their use in feeding, determines how quickly they will wear away, with smaller teeth becoming functionally ineffective and in need of replacement sooner than larger teeth. Unfortunately, the lack of any data on tooth size in previous studies precludes direct comparison with the chiton teeth in the present study. However, the main teeth used by chitons in feeding, the second laterals, are usually large prominent teeth. In *A. hirtosa*, the cusps of these teeth measure 254 μm high and 247 μm wide (SD = 4.7, 3.9, respectively; $n = 8$). Hence, it may well be that the possession of large cusps affords the chiton a slower rate of tooth wear.

The majority of gastropods in the studies of both Isrankura and Runham (1968) and Padilla *et al.* (1966) were herbivores feeding off seaweeds, soft algae or lettuce. The only species that has a natural feeding strategy similar to that of *A. hirtosa* is *Patella vulgata*. Both species are hard substrate grazers, and although *P. vulgata* was not given a natural substrate to feed off, at approximately 1.5 rows per day it returned one of the lowest radula turnover rates for the gastropods (Isrankura and Runham 1968). This is somewhat contradictory to what would be expected, because it could be assumed that the abrasive, high impact nature of chiton and limpet feeding would actually necessitate a high turnover rate. However, another factor that both these species have in common is the incorporation of hard minerals into their tooth design, which affords them greater resistance to wear. The main working teeth of *A. hirtosa* are hardened with iron oxides, such as magnetite and lepidocrocite (Kim *et al.* 1989; Lee *et al.* 1998), whereas *P. vulgata* incorporates iron and silicon into its teeth (Lowenstam 1962, 1971). As such, it could be suggested that radula turnover in chitons and limpets is slower than that found in other molluscan groups due to the reduced mechanical wear of the teeth afforded by their extensive mineralisation. A further point to consider is that mineralisation is a physiologically expensive process, which necessitates rationalisation of tooth production rates with respect to the total energy allocation of radula manufacture.

The only other published study on radula production rates in the polyplacophora was that performed by Nesson (1969), where the rate of radula replacement for *Mopalia muscosa* (Gould, 1846) was determined by labelling the teeth with ^{59}Fe. In that study, the tooth turnover rate was calculated to be approximately 0.6 rows per day, nearly double that of *A. hirtosa*. However, this is still considerably slower than the rates calculated for the gastropod species, suggesting that the polyplacophora, as a group, may have slower radula production rates than other mollusc groups. Whether this reduced rate can be attributed to their mineralisation process remains to be seen and further research into radula production may provide insights into the tooth hardness–turnover rate association.

The difference in the rates observed between *A. hirtosa* and *M. muscosa* may lie in the differing tooth morphology and feeding regimens of these two species. The working face of the major lateral teeth in chitons varies in structure from a broad chisel-like form (as in the chitonidae) to one to three pronounced cusps (in most other chiton families) (Nesson and Lowenstam 1985). The cusp structure seen in *A. hirtosa* is of the broad unicuspid type (Macey *et al.* 1996), whereas that of *M. muscosa* is of a tricuspid design (Nesson 1969). While no direct comparison has been made between these two species, comparisons of the structural organisation of the cusps of chiton teeth have been made between *A. hirtosa* and *Plaxiphora albida* (de Blainville, 1825), which also has tricuspid teeth (Macey *et al.* 1996). The two cusp designs are used differently with respect to feeding, with the major laterals of

P. albida used in a rake-like manner, whereas those of *A. hirtosa* have a more excavational capacity (Macey *et al.* 1996). From this feeding strategy, it would be expected that the teeth of *A. hirtosa* would be worn away more quickly. The fact that this does not occur may well be attributable to differences in tooth structure at the microcrystalline level.

A number of factors may be responsible for the slight variation seen in rates of tooth row formation for individual specimens of *A. hirtosa*. Isarankura and Runham (1968) found a close correlation between radula replacement and the age of very young specimens of the gastropod *Achatina fulica* (Bowdich, 1822), whereas in older specimens the rate appears to be more closely related to the size of individuals. Although only adult chitons were used in the present study, there was a difference of 16 mm in length between the largest and smallest specimens, so size cannot be ruled out as a factor. Perhaps of greater significance to the individual variation is the effect of temperature on metabolism, because any fluctuations may have slowed or increased radula production over the course of the study. While the ambient temperature of the artificial mesocosm was relatively constant for the experimentation period, and day to day variations would be expected to have a compound effect that should be similar for all chitons in the experiment, the location of individual chitons within the mesocosm may have caused some variation. Because some of the rocks were submerged and others exposed, some chitons may have adopted positions that were sheltered from the elements, whereas others may have been subjected to a more variable range of conditions with regard to temperature and water availability.

Acknowledgments

The authors thank Ken Frankish (TAFE Fremantle Maritime Centre) for the allocation of space for this study. Special appreciation goes to Garth Maker for all the useful insights and ideas during this undertaking and to Dr Mike Van Keulen for the use of various pieces of equipment. Financial support was provided by an Australian Research Council large grant.

References

Bullock, R. C. (1989). Mechanical wear of radular denticle caps of *Acanthopleura granulata* (Gmelin, 1791) (Polyplacophora : Chitonidae). *American Malacological Bulletin* **7**, 13–19.

Evans, L. A., Macey, D. J., and Webb, J. (1990). Characterization and structural organization of the organic matrix of the radula teeth of the chiton *Acanthopleura hirtosa*. *Philosophical Transactions of the Royal Society London* **B329**, 87–96.

Evans, L. A., Macey, D. J., and Webb, J. (1992). Calcium biomineralization in the radula teeth of the chiton, *Acanthoplura hirtosa*. *Calcified Tissue International* **51**, 78–82.

Isarankura, K., and Runham, N. W. (1968). Studies on the replacement of the gastropod radula. *Malacology* **7**, 71–91.

Kaas, P., Jones, A. M., and Gowlett-Holmes, K. L. (1998). Class Polyplacophora: introduction. In 'Mollusca: The Southern Synthesis Part B'. Fauna of Australia. (Eds P. L. Beesley, G. J. B. Ross and A. Wells.) pp. 161–177. (CSIRO Publishing: Melbourne.)

Kim, K.-S., Macey, D. J., Webb, J., and Mann, S. (1989). Iron mineralization in the radula teeth of the chiton *Acanthopleura hirtosa*. *Proceedings of the Royal Society London* **B237**, 335–346.

Kirschvink, J. L., and Lowenstam, H. A. (1979). Mineralization and magnetization of chiton teeth: paleomagnetic, sedimentologic, and biologic implications of organic magnetite. *Earth and Planetary Science Letters* **44**, 193–204.

Lee, A. P., Webb, J., Macey, D. J., van Bronswijk, W., Savarese, A., and De Witt, C. (1998). *In situ* Raman spectroscopic studies of the teeth of the chiton *Acanthopleura hirtosa*. *Journal of Biological Inorganic Chemistry* **3**, 614–619.

Lee, A. P., Brooker, L. R., Macey, D. J., van Bronswijk, W., and Webb, J. (2000). Apatite mineralization in the chiton *Acanthopleura echinata*. *Calcified Tissue International*, **67**, 408–415.

Lowenstam, H. A. (1962). Goethite in radular teeth of recent marine gastropods. *Science* **137**, 279–280.

Lowenstam, H. A. (1971). Opal precipitation by marine gastropods (Mollusca). *Science* **171**, 487–490.

Lowenstam, H. A. and Weiner, S. (1989). 'On Biomineralization.' (Oxford University Press, Oxford.)
Macey, D. J., and Brooker, L. R. (1996). The junction zone: the initial site of mineralization in the radula teeth of the chiton *Cryptoplax striata* (Mollusca : Polyplacophora). *Journal of Morphology* **230**, 33–42.
Macey, D. J., Brooker, L. R., Webb, J., and St Pierre, T. G. (1996). Structural organization of the cusps of the radula teeth of the chiton, *Plaxiphora albida*. *Acta Zoologica* **77**, 287–294.
Nesson, M. H. (1969). 'Studies on Radula Tooth Mineralization in the Polyplacophora.' PhD Thesis. (California Institute of Technology: Pasadena, California, USA.)
Nesson, M. H., and Lowenstam, H. A. (1985). Biomineralization processes of the radula teeth of chitons. In 'Magnetite Biomineralization and Magnetoreception in Organisms'. (Eds J. Kirschvink, D. S. Jones and B. J. Macfadden.) pp. 333–363. (Plenum Press: New York.)
Padilla, D. K., Dittman, D. E., Franz, J., and Sladek, R. (1996). Radular production rates in two species of *Lacuna* Turton (Gastropoda: Littorinidae). *Journal of Molluscan Studies* **62**, 275–280.
Pearce, A. F., Rossbach, M., Tait, M., and Brown, R. (1999). Sea temperature variability off Western Australia 1990 to 1994. *Fisheries Research Report* **111**, 1–45.
Runham, N. W. (1962). Rate of replacement of the molluscan radula. *Nature* **194**, 992–993.
Runham, N. W. (1963). A study of the replacement mechanism of the pulmonate radula. *Quarterly Journal of Microscopian Science* **104**, 271–277.
Runham, N. W., and Isarankura, K. (1966). Studies on radula replacement. *Malacology* **5**, 71–89.
Webb, J., Macey, D. J., and Mann, S. (1989). Biomineralization of iron in molluscan teeth. In 'Biomineralization'. (Eds S. Mann, J. Webb and R. P. J. Williams.) pp. 345–387. (VCH Verlagsgesellschaft: Weinheim.)
Wells, F. E., and Bryce, C. W. (1986). 'Seashells of Western Australia.' (Advance Press: Perth.)